Komatiites of eastern Lapland and their Ni-Cu-PGE potential

M.Sc. Thesis
Henri Höytiä
December 2018
Department of Geosciences and Geography
Faculty of Science

HELSINGIN YLIOPISTO
HELSINGFORS UNIVERSITET
UNIVERSITY OF HELSINKI

Tiedekunta/Osasto Fakultet/Sektion – Faculty		**Laitos/Institution– Department**
Faculty of Science		Department of Geosciences and Geography
Tekijä/Författare – Author Henri Höytiä		
Työn nimi / Arbetets titel – Title Komatiites of Eastern Lapland and their Ni-Cu-PGE potential		
Oppiaine /Läroämne – Subject Geology (petrology and economic geology)		
Työn laji/Arbetets art – Level M.Sc. thesis	**Aika/Datum – Month and year** 12/2018	**Sivumäärä/ Sidoantal – Number of pages** 163

Tiivistelmä/Referat – Abstract

Komatiites are ultramafic rocks produced in high-degree (> 20 %) partial melting of the mantle. They can be emplaced as extrusives and subvolcanic dikes and sills. Komatiitic melts are of high-temperature, low-viscosity, and naturally enriched in base and precious metals, e.g., Ni, Cu, and the platinum group elements (PGE). Consequently, they are able to form komatiites-hosted Ni-Cu-PGE deposits that globally comprise a significant source for base and precious metals. For such ores, the sulfur-undersaturated komatiitic melts need to reach sulfur saturation. This can be achieved by gaining external sulfur from, e.g., sulfide-bearing country rocks. Komatiites are found in Archean to Proterozoic greenstone belts. Due to their age, primary mineral composition and original spatial position of komatiites have been modified by metamorphism, deformation, as well as, erosion. Geochemical studies of assimilation signals, depletion/enrichment in base and precious metals together with volcanological and stratigraphic studies are critical in exploration of komatiite-hosted Ni-Cu-PGE deposits.

The Eastern Lapland Archean domain (ELAD) is a granite-gneiss-greenstone terrain with abundant komatiitic rocks, located in the municipalities of Salla and Savukoski in Northern Finland. It is characterized by amphibolite-facies metamorphism and predominant thrust tectonics, which have destroyed the majority of primary magmatic characteristics in the area.

In this thesis, ore potential of the ELAD komatiites is evaluated on the basis of field observations and samples collected during geological mapping of komatiitic bodies of the area. Studies of thin section petrography, whole-rock geochemistry and mineral chemistry of olivine and spinel have been performed. In addition, previously analyzed whole-rock data provided by the Geological Survey of Finland (GTK) are utilized.

The komatiitic lavas and cumulates of ELAD were derived from parental melts of komatiitic basaltic composition. Cumulates formed from these melts are critical for exploration. They have been interpreted as basal cumulates of thick komatiitic sequences or cumulates of major magma pathways. Furthermore, komatiites crystallized from Cr-undersaturated melts and komatiites showing depletion or enrichment with respect to Ni are found in the area. Both of these features have been attributed to potentially mineralized environments. Also, sulfide-bearing country rocks, which provide a potential source for sulfur, are present. Nevertheless, strong alteration of the ELAD komatiites hampers geochemical interpretations.

Avainsanat – Nyckelord – Keywords
komatiite, komatiite-hosted Ni-Cu-PGE deposits, nickel, nickel exploration, Lapland, Archean, Precambrian, The Eastern Lapland Archean domain, Salla, Savukoski

Säilytyspaikka – Förvaringställe – Where deposited
Helsinki University Library

Muita tietoja – Övriga uppgifter – Additional information
This thesis was done in collaboration with the Geological Survey of Finland (GTK) and the University of Helsinki

HELSINGIN YLIOPISTO
HELSINGFORS UNIVERSITET
UNIVERSITY OF HELSINKI

Tiedekunta/Osasto Fakultet/Sektion – Faculty		Laitos/Institution– Department
Matemaattis-luonnontieteellinen tiedekunta		Geotieteiden ja maantieteen laitos
Tekijä/Författare – Author Henri Höytiä		
Työn nimi / Arbetets titel – Title Itä-Lapin komatiitit ja niiden Ni-Cu-PGE malmipotentiaali		
Oppiaine /Läroämne – Subject Geologia (petrologia ja taloudellinen geologia)		
Työn laji/Arbetets art – Level Pro gradu	**Aika/Datum – Month and year** 12/2018	**Sivumäärä/ Sidoantal – Number of pages** 163

Tiivistelmä/Referat – Abstract

Komatiitit ovat ultramafisia kiviä, jotka ovat syntyneet vaipan korkean asteen osittaisen sulamisprosessin seurauksena. Purkautessaan ne muodostavat extrusiiveja ja puolipinnallisia juonia ja sillejä. Luonteenomaista komatiittisille sulille ovat korkea purkauslämpötila ja matala viskositeetti. Lisäksi ne ovat rikastuneet mm. nikkelistä, kuparista ja platinaryhmän alkuaineista (PGE). Komatiittien yhteyteen liittyy maailmanlaajuisesti taloudellisesti merkittäviä ortomagmaattisia Ni-Cu-PGE esiintymiä. Malmien synnyn kannalta komatiittinen sula vaatii kyllästymistä rikin suhteen, mikä voidaan saavuttaa esimerkiksi assimiloimalla rikkipitoisia sivukiviä. Komatiitteja esiintyy arkeeisilla ja paleoproterotsooisilla vihreäkivivyöhykkeillä. Iästään johtuen niiden mineraalikoostus ja asema ovat muuttuneet metamorfoosin, deformaation ja eroosion seurauksena, mikä asettaa haasteita tutkimiselle. Malminetsinnällisesti assimilaation osoittaminen, metallien rikastuminen/köyhtyminen sekä komatiittisten muodostumien vulkanologiset ja stratigrafiset tutkimukset ovat kriittisiä.

Itä-Lapin arkeeinen vyöhyke sijaitsee Pohjois-Suomessa Sallan ja Savukosken kuntien alueella. Alueella esiintyy runsaasti komatiitteja. Aluetta kuvastavat amfiboliittifasieksen metamorfoosi ja hallitsevat ylityöntörakenteet. Niistä johtuen alueen komatiittien primäärit piirteet ovat lähes täysin tuhoutuneet.

Tässä pro gradussa Itä-Lapin komatiittien malmipotentiaalia tarkastellaan kartoitustöissä tehtyjen havaintojen ja kerättyjen näytteiden avulla. Näytteistä on tehty ohuthiepetrografian, kokokivigeokemian sekä oliviinin ja spinellin mineraalikemian tutkimuksia. Näiden lisäksi tarkastelussa hyödynnetään Geologian tutkimuskeskukselta (GTK) saatuja aineistoja, jotka sisältävät kokokivianalyysejä Itä-Lapin aiemmista tutkimuksista.

Itä-Lapin komatiittiset laavat ja kumulaatit ovat syntyneet kantasulista, joiden on tulkittu olleen koostumukseltaan komatiittista basalttia. Malminmuodostuksen kannalta kriittisiä ovat kantasulista syntyneet kumulaatit, joiden on tulkittu edustavan MgO-rikkaita paksujen laavapatjojen/tulokanavien kumulaatteja. Lisäksi tutkimusalueella havaitaan mineraalipotentiaalisia kromin suhteen alikylläisestä sulasta syntyneitä komatiitteja ja komatiitteja, jotka ovat rikastuneet tai köyhtyneet nikkelin suhteen. Alueella esiintyy myös sulfidirikkaita sivukiviä potentiaalisina rikkilähteinä. Itä-Lapin komatiittien voimakas muuttuminen kuitenkin hankaloittaa geokemian tulkintoja.

Avainsanat – Nyckelord – Keywords
komatiitti, komattiitiset Ni-Cu-PGE malmit, nikkeli, malminetsintä, Lappi, Itä-Lapin arkeeinen vyöhyke, arkeeinen aioni, prekambri, Salla, Savukoski

Säilytyspaikka – Förvaringställe – Where deposited
Helsingin yliopiston kirjasto

Muita tietoja – Övriga uppgifter – Additional information
Tämä työ on toteutettu yhteistyössä Geologian tutkimuskeskuksen (GTK) ja Helsingin yliopiston kanssa.

TABLE OF CONTENTS

1. INTRODUCTION

Komatiites are ultramafic volcanic rocks with distinctive geochemical compositon (e.g., high abundances of MgO, Ni, and Cr) and physical properties (high-temperature and low-viscosity lavas) (e.g., Hill et al. 1995, Barnes 2006, Arndt et al. 2008). They are well-known for hosting economically significant Ni-Cu-platinum group element (PGE) sulfide deposits (e.g., Barnes 2006, Lesher & Barnes 2008, Konnunaho et al. 2015) and recording information of Archean mantle dynamics and composition, which reflect chemical and thermal evolution of the Earth (e.g., Grove and Parman 2004, Arndt et al. 2008). The majority of komatiites are old and generally yield ages from the Archean (ca. 3.2–2.5 Ga) to the early Proterozoic (> 1.9 Ga), although also Phanerozoic komatiites have been described from a few locations (Echeverría 1980, Hanski et al. 2004). Initially, komatiites were introduced to the scientific literature by the Viljoen brothers (Viljoen & Viljoen 1969a, b), who studied previously undescribed ultramafic lavas and their structures, and textures in the Komati River Valley in Barberton greenstone belt, South Africa, in the late 1960's. Typically found in greenstone belts (ancient rifting environments located in cratonic areas), komatiites are rare as a rock type but nowadays found in all continents (Arndt et al. 2008). Classical occurrences of komatiites and komatiite-hosted Ni-Cu-PGE are found in, e.g., Canada (Pyke et al. 1973), Western Australia (Barnes 2006), as well as, in Fennoscandia (Barnes & Often 1992, Konnunaho et al. 2015). Komatiite-hosted Ni-Cu-PGE (platinum group elements) deposits are an important source of metals globally and comprise approximately 20% of Ni sulfide resources (± by-products, i.e. Cu, Co, and PGE) worldwide (Mudd & Jowitt 2014). Basically, the deposits can be divided to primary orthomagmatic sulfide deposits and laterite deposits, formed by deep weathering of komatiitic cumulates (Lesher & Barnes 2008). This thesis focuses only on the orthomagmatic deposits.

Finland hosts abundant komatiitic rocks, particularly in the eastern and northern parts of the country (e.g., Hanski et al. 2001, Lehtonen 2016). Also, several relatively small komatiitic Ni-Cu-PGE deposits have been discovered in these terrains (Konnunaho 2016). However, the potential to find more is intriguing (e.g., Makkonen et al. 2017). The study area of this thesis, The Eastern Lapland Archean domain (ELAD), is a relatively vaguely known area of granitoid complexes and supracrustal sequences, with abundant komatiitic rocks, located in eastern parts of Northern Finland (Piirainen et al. 1985,

Juopperi 1994, Sorjonen-Ward & Luukkonen 2005). The nature of komatiites of ELAD and their affinity to ore-forming processes has not yet been systematically studied regionally. The area has been subjected to medium to high-grade metamorphism in upper amphibolite facies conditions (Virransalo 1985, Kivisaari 2008, Hölttä & Heilimo 2017), as well as, remoulded by predominant thrust tectonics (Papunen et al. 1997). Therefore, the rocks of ELAD are characterized by metamorphic mineral compositions and lack of primary structures, and hence have poorly constrained stratigraphy, which evidently generates challenges for exploration of komatiite-hosted Ni-Cu-PGE deposits. Although economic Ni-Cu-PGE remain undiscovered in the area at present, active mineral exploration studies have been conducted on the komatiitic sequences from the 1970's to 2010's (e.g., Papunen et al. 1977, Piirainen et al. 1985, Papunen et al. 1997, Iljina, 2003 & 2009). Recently, also a small PGE-Ni mineralization was located from the area (Heikura et al. 2010).

In this thesis, the results of a collaborative project regarding origin, exploration potential, and metallogeny of komatiitic suites of ELAD by the Geological Survey of Finland (GTK) and the University of Helsinki (Haapala et al. 2018) are presented in terms of ore potential. The project comprised a targeted mapping program conducted on the komatiitic bodies of ELAD during the summers of 2017 and 2018. A comprehensive data set of whole-rock geochemistry, mineral chemistry, and isotope chemistry, in addition to thin sections, of the ELAD komatiites was collected during these studies. In addition to this thesis, two other M.Sc. dissertations are being prepared simultaneously (Haapala, in preparation & Tepsell 2018). Using preceding whole-rock geochemistry data provided by GTK and data gathered during this project, ore potential of komatiites of ELAD is examined. Globally it has been demonstrated that if there are no direct observations of sulfide-bearing komatiites, indirect insights to the ore potential of seemingly barren komatiite sequences can be outlined with the help of whole-rock geochemistry and mineral chemistry (e.g., Naldrett et al. 1984, Lesher et al. 2001, Barnes et al. 2004, Barnes 2006, Lesher & Barnes 2008, Le Vaillant et al. 2016, Makkonen et al. 2017). By using these tools, vectoring towards potentially mineralized environments is attempted.

2. KOMATIITES

Komatiites can be emplaced as extrusions, dikes, sills, and/or subvolcanic intrusions. However, many scientists hold on to the view of their principally extrusive character. Komatiites are naturally rich in elements such as Mg, Ni, and Cr, some also in PGE, and contain low abundances of elements such as Si, Al and Ti. In the official IUGS recommendations a komatiite is defined as a high-Mg volcanic rock with 52 % > SiO_2 > 30 %, MgO > 18 %, (NaO_2 + K_2O) < 2 % and TiO_2 < 1 % (Le Bas 2000, Le Maitre et al. 2002) (Figure 1). Markedly, the IUGS classification is based on mobile elements such as the alkalis and SiO_2, which limits its use for highly metamorphozed komatiites. Hence, komatiitic rocks can be also classified by their MgO and TiO_2 contents to komatiites (MgO > 18 % and TiO_2 < 1 %) and komatiitic basalts (MgO < 18 % and TiO_2 < 1 %) (Arndt et al. 2008). Rocks, which can be by spatial, petrological, or geochemical criteria

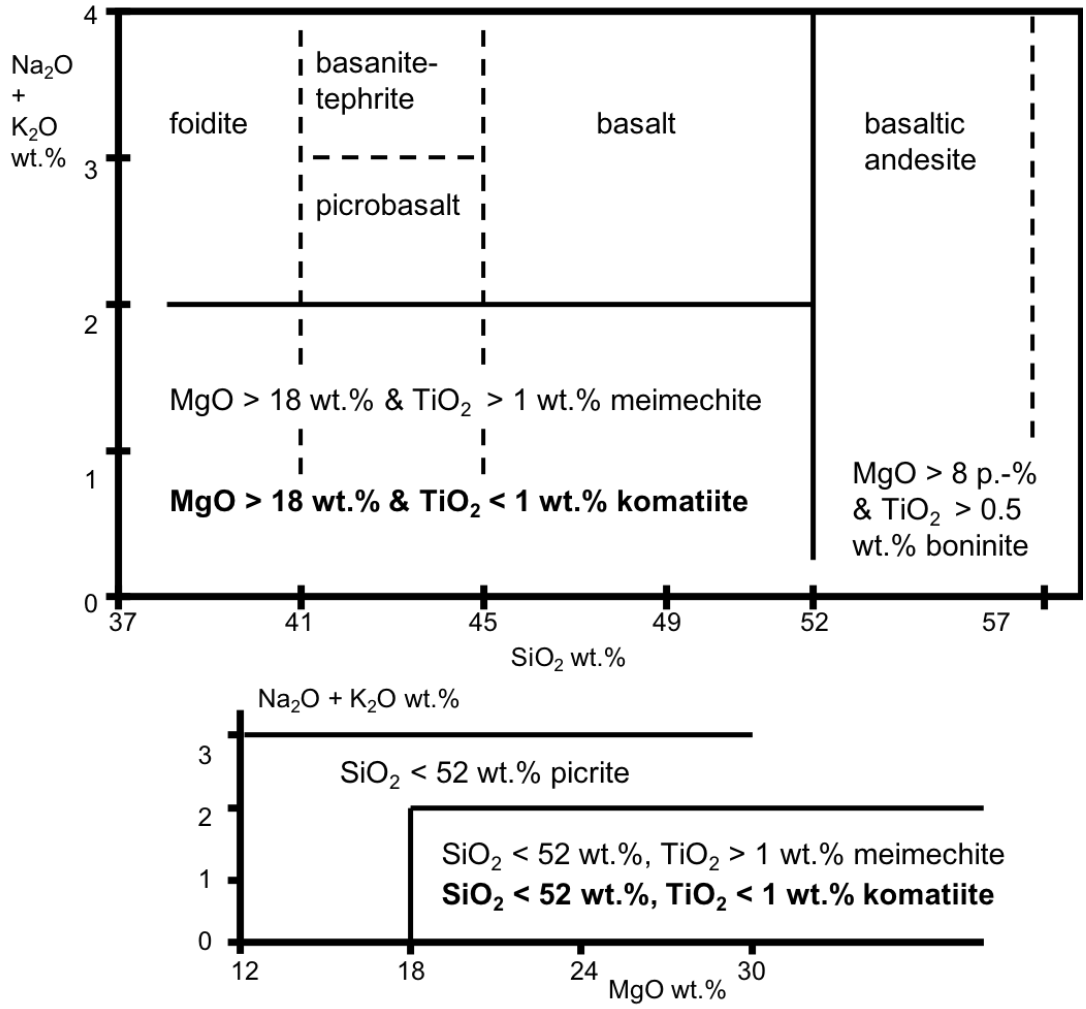

Figure 1. Definition of komatiite in total alkali-silica (TAS) diagram of mafic and ultramafic volcanic rocks (upper) and in diagram of high-MgO volcanic rocks (lower). After LeMaitre et al. (2002) & Le Bas (2000).

linked to komatiites are referred to with the prefix “komatiitic” (Arndt & Nisbet 1982, Arndt et al. 2008). Kerr and Arndt (2001) have also emphasized that real komatiites should display characteristic textural features such as spinifex (bladed and acicular olivine, and/or pyroxene crystals in fine-grained matrix, e.g., Nesbitt 1971). However, spinifex-like undercooling textures are not only restricted to komatiites, as they have been also found in other types of high-Mg lavas, e.g., picrites and high-Mg basalts (e.g., Hanski 1992, Lowrey et al. 2017).

2.1 Komatiite petrology

Komatiites represent primitive mantle melts and require high degree partial melting of the mantle (up to 50 %) (Nesbitt & Sun 1976, Sun & Nesbitt 1978, Hertzberg 1992). The formation of komatiites has generally been attributed to mantle plume upwelling and related volcanism in a variety of geodynamic settings mainly during the Archean and early Proterozoic (Brooks & Hart 1974, Nisbet & Walker 1982, Campbell et al. 1989, Arndt et al. 2008). However, the Archean geodynamic settings may not be comparable to modern ones and the nature of the Archean mantle, besides its high heat flux, is not understood in detail (Grove & Parman 2004, Arndt et al. 2008). Consequently, a hydrous komatiite model, where volatiles in the mantle source would render komatiite formation without the presence of a mantle plume, have been suggested by some authors (e.g., Brooks & Hart 1974, Allégre 1982, Grove & Parman 2004). Nevertheless, due to reduced heat flux of the mantle from the Archean to the present day, komatiites are not generally formed in modern geodynamic settings, as extremely high degree partial melts cannot be produced from the mantle anymore. This can also be observed in the decrease of MgO contents of komatiites as a function of time (e.g., Nisbet et al. 1982, Arndt et al. 2008).
As for physical characteristics, komatiites are exceptional rocks. The estimated eruption temperatures for komatiitic melts range from 1400°C to 1650°C (Huppert & Sparks 1985, Arndt et al. 2008 In addition, komatiitic melts are of low viscosity (ca. 0.1–0.75 Pa·s) comparable to that of water, which allowed them to flow rapidly and turbulently over vast areas (Hill et al. 1995, Hill 2001, Arndt et al. 2008). Together these features produced a strong thermoerosional force and gave komatiites a high capability to assimilate their country rocks (e.g., Hill et al. 1995).

2.1.1 Structures and textures

Komatiites form a variety of distinctive textures and structures. Generally, they are classified as lavas, including their intrusive counterparts (lava in this case is a non-accurate term, as komatiites also display intrusive emplacement mechanisms) and rare pyroclastic variants. Lavas form either undifferentiated and/or to some extent differentiated beds, which can be observed by the existence of cumulates and evolved mafic compositions. Cumulates are formed by flow differentiation, which stacks and collects heavier crystals (e.g., olivine), and under turbulent conditions bursts the leftover melt away from interspace between the crystals to form ad-, meso- and/or orthocumulates (Wager et al. 1960, Hill et al. 1995, Arndt et al. 2008). Skeletal, platy, bladed, acicular and dendritic olivine, and/or pyroxene textures known as spinifex and harrisite, in contrast, form in calm or stagnant parts of the flow, where high thermal gradient has produced undercooled and diffusive conditions, which allowed the crystals to come in contact with each other and grow abnormally large (e.g., Nesbitt 1971, Donaldson 1982, Shore & Fowler 1999, Faure et al. 2006). Harrisite usually forms larger and regular column-like crystals, whereas spinifex is often smaller, sometimes randomly ordered, and displays acicular and dendritic forms. Furthermore, spinifex is usually formed in the upper parts of the flows, whereas harrisite is found mostly in the basal parts (Hill et al. 1995). Pyroclastic komatiites, which may form, e.g., due to phreatomagmatic eruptions, have been described for instance from the Central Lapland greenstone belt (CLGB) (Saverikko 1985).

The primary mineral composition of komatiites is largely dominated by olivine and minor clinopyroxene (± chromite), the latter of which form the main intercumulus phases in komatiitic cumulates (Barnes et al. 1995, Arndt et al. 2008). Primary magmatic orthopyroxene in komatiites is rare and often reflects the effect of contamination by silicic crust (Barnes 2006, Arndt et al. 2008). Because of the Archean to Proterozoic age of komatiites, however, most of them have undergone post-magmatic modification. Therefore, they today appear as varying serpentine-amphibole-chlorite-talc-carbonate-metamorphic olivine-bearing rocks and schists, in which primary magmatic minerals and features have not always been preserved (e.g., Jolly 1982, Beswick 1982, Aitken & Echeverría 1984, Barnes 2006, Arndt et al. 2008).

Based on examples from the Western Australia, komatiite lava sequences can be separated to regime, facies, and subfacies of flows, where different textures and structures are formed at different conditions (see Hill et al. 1995, Hill 2001, Barnes 2006) (Figure 2). A well differentiated lava flow is shown in Figure 3, albeit not all komatiite sequences are differentiated or display the ideal assemblage of regimes, facies, or subfacies (e.g., Barnes 2006, Arndt et al. 2008). Komatiitic bodies are seldom a result of a single large eruption but rather consist of a number of flows emplaced by a variety of extrusive and intrusive mechanisms (Hill 2001, Barnes 2006, Arndt et al. 2008). Generally, komatiite flows tend to form lava conduits or channels, through which large volumes of komatiite magma percolates and forms thick dunitic cumulate units. Komatiite flows typically get thinner and less cumulate-dominated further away from the conduit, like in distal and marginal parts where the current gets slower, sets and cools (Hill 2001, Barnes 2006).

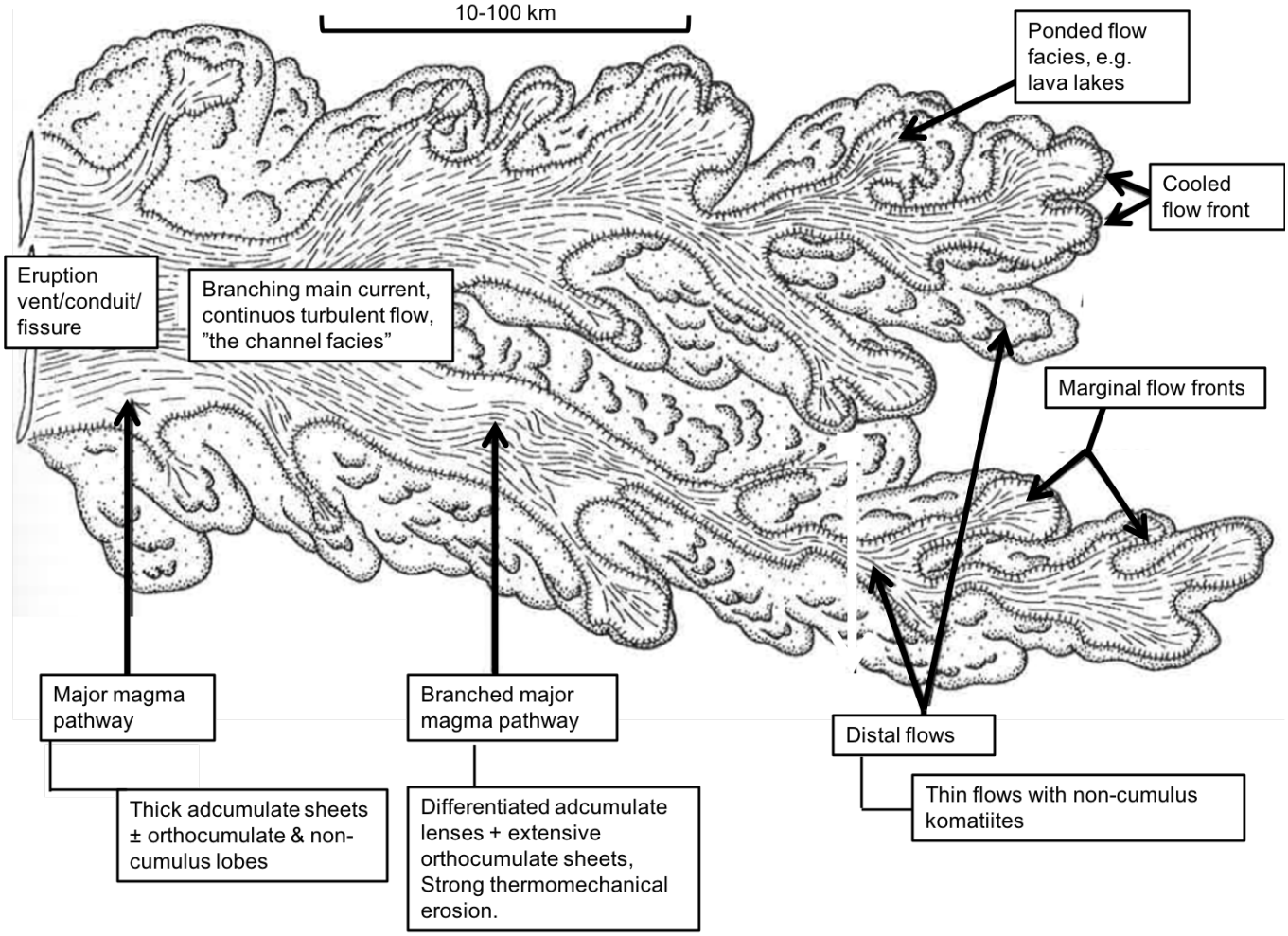

Figure 2. Schematic illustration of an extrusive komatiite flow with several different flow facies and their subfacies with typical textural and structural features marked. Modified after Hill (2001) and Barnes (2006).

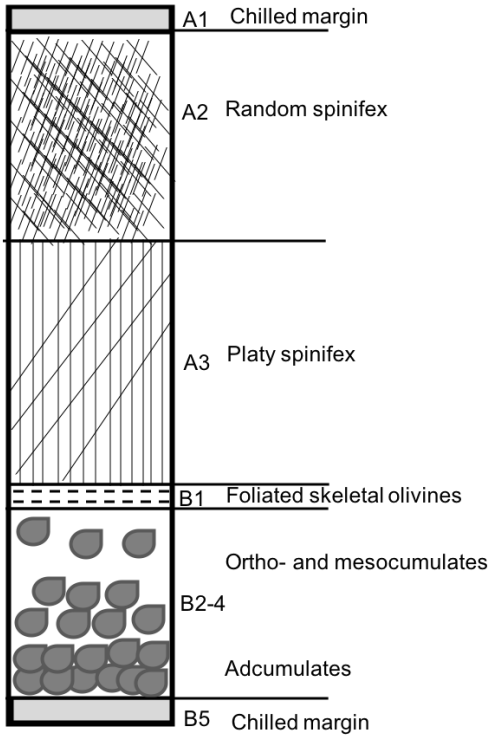

Figure 3. An ideally differentiated komatiite lava sequence with all A- (spinifex zones) and B-zones (cumulate zones) present. Modified after Pyke et al. (1973) and Faure et al. (2006).

2.1.2 Geochemical diversity and petrogenetic types of komatiites

Originally, Viljoen and Viljoen (1969a, 1969b) recognized two different types of komatiites based on whole-rock composition: peridotitic komatiites (PK) with MgO > 15 wt.% and basaltic komatiites (BK) with MgO < 15 wt.%. Furthermore, a genetic relation between the two was based on high (ca. 1.5) CaO/Al_2O_3, which the Viljoens thought to be a defining feature for all komatiitic melts. However, Arndt (1977) noted that CaO/Al_2O_3 alone was quite inconclusive, as Ca is often mobile during post-magmatic processes. This led to a new approach by Nesbitt et al. (1979), who divided komatiites to aluminum-depleted (ADK) and aluminum undepleted (AUK) types. The ADKs are characterized by high CaO/Al_2O_3, low (< 15) Al_2O_3/TiO_2, and in terms of rare eart elements (REE), by elevated MREE/HREE (middle REE/high REE) patterns (Gd/Yb > 1). The AUKs, on the other hand, have only slightly elevated CaO/Al_2O_3 (ca. 1), chondritic (ca. 20) Al_2O_3/TiO_2, and flat MREE/HREE patterns (Gd/Yb ca. 1). This classification also took a stand on the petrogenesis of different types of komatiites: ADKs were considered lower degree partial melts (ca. 30%) derived from deeper in the mantle, where garnet was present in the residual phase due to its stability in high pressure (> 8

GPa). AUKs, in turn, were thought to be higher degree partial melts (up to 50%) and left behind only a residue of olivine due to lower pressure (ca. 5 GPa) of melting in the upper levels of the mantle (Nesbitt et al. 1979, Hertzberg & Ohtani 1988, Hertzberg 1992). Arndt et al. (2008) found the classification of Nesbitt et al. (1979) confusing and preferred to use a classification based on geochemistry of four classic komatiite locations: Barberton-type (i.e. the ADK-type), Munro-type (i.e. the AUK-type), Karasjok-type (Ti-enriched komatiites, TEK, Barnes & Often 1990) and Gorgona-type (Al-enriched komatiites, AEK, Jahn et al. 1982). This classification reflects the evolution of komatiitic melts and their formation environments over time (Table 1).

Table 1. Classification of komatiites by Arndt et al. (2008). For comparison, respective classifications of these groups to aluminum-depleted komatiite (ADK), aluminum undepleted komatiite (AUK), aluminum-enriched komatiite (AEK), and titanium-enriched komatiite (TEK) are also presented.

	BARBERTON-TYPE	**MUNRO-TYPE**	**KARASJOK-TYPE**	**GORGONA-TYPE**
Type*	ADK	AUK	TEK (AUK)	AEK (AUK)
Al_2O_3/TiO_2	low (10-15)	chondritic (~20)	low (10-15)	high (> 20)
(Gd/Yb)N	high (ca. 1.5)	chondritic (ca. 1)	high (ca. 1.5)	chondritic (ca. 1)
Age at type location	Archean, ~ 3.5 Ga	Archean, ~ 2.7 Ga	Paleoproterozoic, ~ 2.4 Ga	Phanerozoic, ~ 90 Ma
Type location	Barberton greenstone belt, South Africa	Abitibi greenstone belt, Canada	Karasjok greenstone belt, Norway	Gorgona Islands, Colombia

*(Nesbitt et al. 1979, Jahn et al. 1982, Barnes & Often 1990)

To illustrate the characteristic Ti enrichment of Paleoproterozoic komatiites, Hanski (1992) developed an [Al_2O_3] vs. [TiO_2] mole proportion diagram (Figure 4). The diagram uses only primary olivine compositions to eliminate the effect of fractionation and accumulation during crystallization, as well as secondary modification by metamorphism and hydrothermal processes allowing comparison between all high-MgO melts. The variations in molecular Ti and Al abundances allowed Hanski (1992) and Hanski et al.

(2001) to constrain different source and depth for komatiites with similar Al_2O_3/TiO_2: Titanium enrichment represents low degree partial melting and/or fertile source, whereas Al depletion implies a high-pressure source. Nevertheless, Sossi et al. (2016) emphasize that absolute Al content of primary magma composition at a given MgO content provides a more sensitive indicator of the source pressure than the traditional Al_2O_3/TiO_2 and/or Gd/Yb, both of which require information abot the degree of partial melting, which is usually obtained from Mg# or MgO content of the parental magma. According to Sossi et al. (2016), the degree of partial melting at a given pressure defines the petrogenetic type of a komatiite, and consequently would favor production of either AUKs or ADKs depending on the degree of partial melting at a given pressure. Therefore, both types may originate from a single mantle plume. Hypothetically, ADKs would form at the cooler edges of the plume, whereas AUKs would originate from the hotter plume head and tail. Furthermore, Sossi et al. (2016) suggest a new classification by Al content to low-Al, medium-Al, and high-Al komatiites, which would more accurately estimate the source pressure and depth (Figure 5). All in all, use of Al_2O_3/MgO and Al_2O_3/TiO_2 together would give more credible estimates of both the depth and degree of partial melting of different types of komatiites than using only either of them.

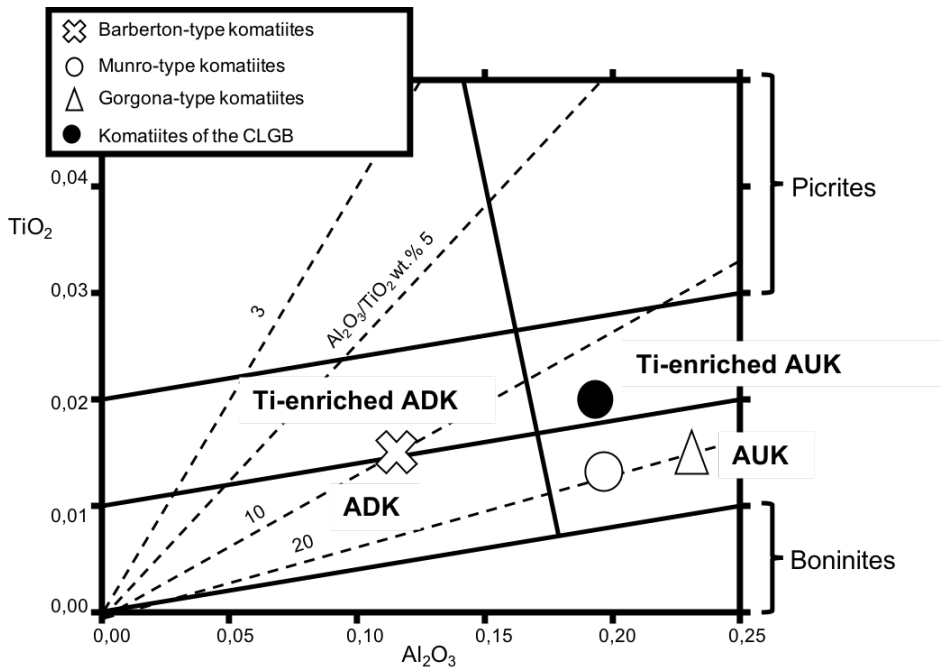

Figure 4. $[Al_2O_3]$ vs. $[TiO_2]$ mole proportion diagram by Hanski (1992) with Arndt et al. (2008) komatiite types plotted. The clear difference between Archean Al-depleted (Barberton-type) and Al undepleted (Munro-type) komatiites, as well as, Ti enrichment related to Paleoproterozoic komatiites, and Al enrichment related to Phanerozoic komatiites are illustrated. Also, borders are drawn to distinguish higher Ti picrites and lower Ti boninites from komatiites. The high-Ti meimechites are not presented in this Figure. Dashed lines represent Al_2O_3/TiO_2 ratios. The mole proportions are calculated with equations: $[Al_2O_3] = Al_2O_3/(2/3*MgO–FeO)$ and $[TiO_2] = TiO_2/(2/3*MgO–FeO)$, with iron as Fe^{2+} (c.f. Hanski 1992). Modified after Arndt et al. (2008).

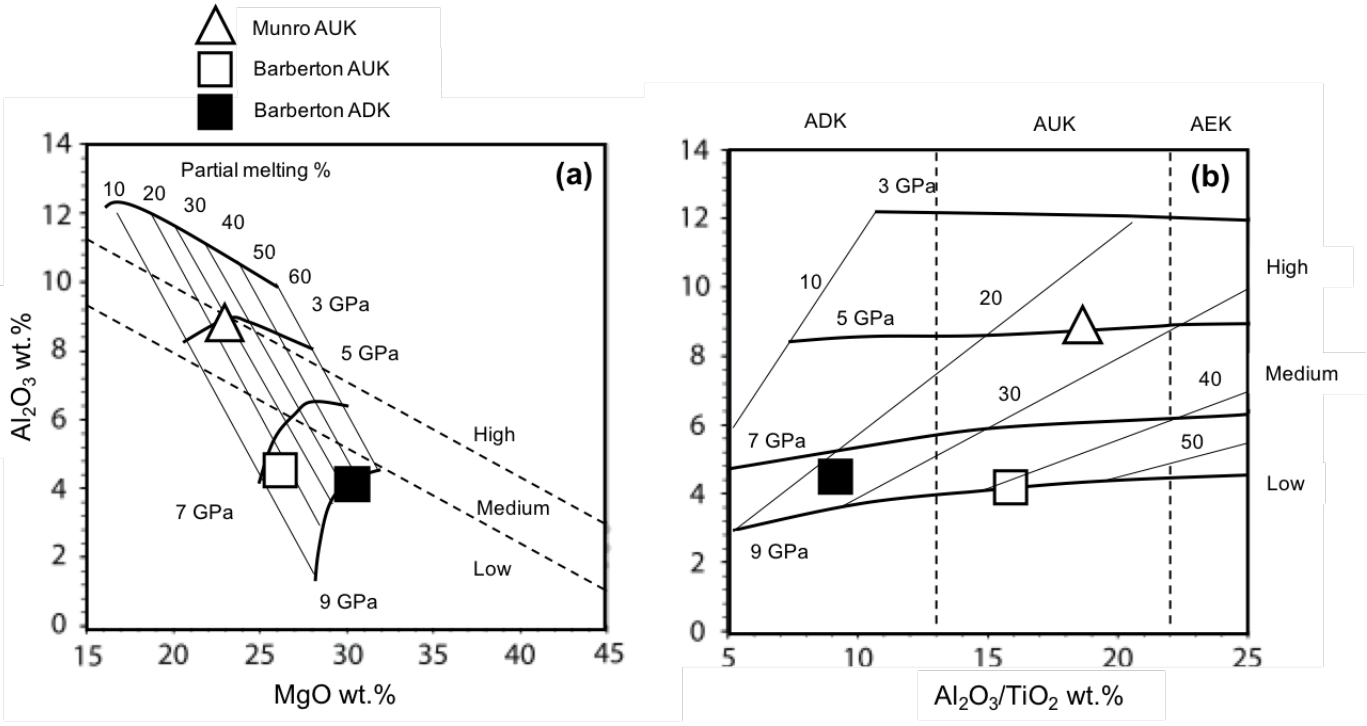

Figure 5. Komatiite classification suggested by Sossi et al. (2016) based on absolute Al contents at a given MgO content. Munro- and Barberton-type komatiites are plotted to underline the benefits of the new classification. Al_2O_3 and MgO stand as sensitive indicators of source pressure and degree of partial melting, respectively. (a) The classes of low-Al, medium-Al and high-Al komatiites are defined by olivine fractionation trends (olivine-control lines). (b) The Sossi et al. (2016) classification and complementary nature of using Al_2O_3/TiO_2. In this diagram the curves are calculated by 25 wt.% of MgO. The diagram illustrates the depletion paradox, as the Barberton AUK komatiites (and some other AUKs, too) are actually depleted with respect to primitive mantle in terms of major and trace element abundances. Modified after Sossi et al. (2016).

2.2 Komatiite-hosted Ni-Cu-PGE deposits

Komatiite-hosted Ni-Cu-PGE deposits are an important source of base (Ni, Cu, Co) and precious (PGE) metals. They hold approximately 20 % of total magmatic Ni sulfide resources in the world (Mudd & Jowitt 2014). Discoveries of several Ni-Cu-PGE ore bodies in, e.g., greenstone belts of Canada (e.g., Naldrett 1966) and Australia (e.g., Ross & Hopkins 1975) in the 1960's and following scientific recognition of their komatiitic origin led to an intensive research on komatiitic rocks with simultaneous exploration boom in the areas they were located (Arndt et al. 2008). Events of global komatiite-hosted Ni-Cu-PGE deposit formation (ca. 2.95, 2.7, and 1.9 Ga) coincide with elevated mantle plume activity and crustal growth and, furthermore, correspond to peaks in abundance of banded iron formations (BIF), sulfidic deep-sea sediments, and volcanogenic massive sulfide (VMS) deposits (Bekker et al. 2009).

2.2.1 *Classification of the deposits*

Excluding the age and/or nature of emplacement of komatiite-hosted Ni-Cu-PGE deposits, they can be classified in a simple manner on the basis of the style of mineralization (Lesher & Keays 2002, Lesher & Barnes 2008). Four types are recognized: magmatic massive sulfides at the contacts and base of komatiite cumulate body (I), magmatic disseminated sulfides associated within cumulate body (II), contact zone stratiform reef-type magmatic sulfides enriched in PGE, typically found in the contact zones of differentiated cumulate body (III), and magmatic sulfides modified by post-magmatic processes or tectonic movements, often found in country rocks close to komatiites or within faults and shear zones (IV) (Barnes 2006, Lesher & Barnes 2008). In many cases, however, two or more types characterize a single deposit (Barnes 2006, Arndt et al. 2008). Furthermore, regardless of the mineralization style, metal contents in different deposits vary (e.g., Barnes 2006). Classical deposits, such as the Kambalda Ni-(Cu) deposit (e.g., Lesher 1989) in Western Australia contain economic amounts of Ni with minor Cu and Co, and typically are poor in PGE. In contrast, deposits such as the Raglan Ni-Cu-PGE deposit (Barnes et al. 1982) in Canada are economic in terms of Ni but also have significant amounts of Cu and PGE. Moreover, in rare cases (usually type III deposits) PGE form the main, in most cases uneconomic, mineralization, as in Boston Creek in Canada (Stone et al. 1993) or in Lomalampi in Finland (Törmänen et al. 2016). Basically, ores associated with high-MgO komatiites are typically rich in Ni-(±Cu), whereas ores associated with less magnesian komatiites such as komatiitic basalts tend to be enriched in Ni, but also significantly enriched in Cu-Co-PGE (Barnes 2006, Lesher & Barnes 2008).

2.2.2 Ore genesis

The key factors for the formation of sulfide ores associated with komatiites are: 1) naturally high abundances of Ni-Cu-PGE in komatiitic melts, 2) sulfur undersaturation of komatiitic melts, i.e. the high capability of komatiitic melts to dissolve external sulfur, 3) the unusual physical ability of komatiitic melts to erode and assimilate country rocks, and hence gain external sulfur and 4) post-magmatic modification of magmatic ores, which may enhance enrichment of base and precious metals (e.g., Barnes 2006, Lesher & Barnes 2008, Konnunaho 2016). Significant deposits are usually found in ad- to mesocumulate

units that represent major magma pathways (e.g., Robb 2005, Lesher & Barnes 2008, Fiorentini et al. 2010a, Barnes & Fiorentini 2012).

As komatiites are high-degree partial melts (> 20 %) of the mantle they consume great amounts of olivine and naturally incorporate large amounts of elements from their mantle sources, including Ni, Cu, Co, Cr, and PGE, as well as, S. Due to the high degree of melting, komatiitic melts are capable of dissolving a lot more sulfur than they naturally gain from the mantle (S is incompatible during mantle melting, so its abundance decreases in the partial melt when the degree of melting increases), which means that they are undersaturated in terms of major sulfur-bearing phases (e.g., Robb 2005, Lesher & Barnes 2008). Consequently, in a komatiitic system, externally added sulfur and/or considerable amounts of magma production are needed to reach sulfide saturation and sulfide–silicate immiscibility, where a sulfide melt fraction is physically separated from the silicate magma. Especially, sulfide saturation during early stages of fractionation has been attributed to economic Ni-Cu-PGE deposits, as the majority of Ni has not yet been consumed by olivine crystallization and formation of early sulfide fractions self-enhances production of more sulfides from the magma (Ripley & Li 2013, Barnes et al. 2016). Highlighting the early saturation hypothesis, it has been demonstrated that S undersatured high-Mg magmas become even more-undersaturated during their adiabatic ascent below the crust (Mavrogenes & O'Neill 1999, Ariskin et al. 2013). However, disseminated ores can also form during later stages of fractionation (e.g., Lesher & Barnes 2008), which would promote for chalcophile elements (e.g. Ni) having an effect on sulfur concentration at sulfide saturation (SCSS), also when their concentrations are decreased in the high-Mg melt (Ariskin et al. 2013). In practice, external sulfur can be gained by, e.g., assimilation of sulfide-bearing country rocks by thermomechanical erosion. Furthermore, in order to form an economic ore deposit accumulation of sulfide fractions to specific zone(s) is required (Lesher et al. 2001, Lesher & Barnes 2008).

Partitioning of the ore-forming elements between silicate and sulfide phases controls the distribution of these elements and, consequently, formation of ores. According to equation 1, concentration of an element in the immiscible sulfide melt can be estimated by the silicate/sulfide mass ratio known as the R-factor. For example, Ni, Cu, and Co show high, and Pt and Pd extremely high partitioning into the sulfide liquid phase due to their chalcophile tendencies (Table 2). Therefore, these elements have a strong affinity to

the sulfide phase, when an immiscible sulfide liquid is segregated. In contrast to other elements mentionaed before, Ni behaves in a lithophile way during mantle melting, therefore, being strongly controlled by olivine fractionation if the sulfide phase is not present. In addition to high D-values (sulfide–silicate partition coefficient) for critical elements, formation of an ore deposit demands interaction between sulfide melt and an adequate volume of silicate magma to concentrate as much elements from the silicate phase to the sulfide phase as possible. For Ni, this is possible under low R-factor, due to its naturally high concentration in the parental magma, whereas Pt and Pd as trace elements with very low concentrations (5–10 ppb) in the mantle, generally, demand high R-factor to be able to equilibrate with considerable amount of silicate magma. Basically, PGE content alone is a good indicator of the R-factor. In general, komatiite-hosted deposits are formed under low to moderate R-factors (ca. 100–1000) and theoretically, massive sulfide (Type I) deposits form under lower R-factor than disseminated (Type II) deposits.

$$\mathbf{(1)} \qquad \mathbf{C_{sul} = C_{sil}D(R + 1)/(R + D)}$$

where C_{sul} is the concentration of an element in the sulfide phase, C_{sil} is the original concentration of the element in the silicate magma, D is sulfide–silicate partition coefficient, which tells how strongly an element has an affinity to sulfide or silicate liquid and R is mass ratio of between silicate and sulfide melt (C_{sil}/ C_{sul}). After Campbell and Naldrett 1979.

Table 2. Sulfide–silicate partition coefficients (D) for ore-forming elements in komatiitic systems. Modified after Robb (2005).

	Ni	Cu	Co	Pt	Pd
High-MgO komatiite (27 % MgO)	100	250–3000	40	10^4–10^5	10^4–10^5
Low-MgO komatiite (19 % MgO)	175	250–2000	60	10^4–10^5	10^4–10^5

2.2.3 Post-magmatic modification of Ni-Cu-PGE ores

Komatiite-hosted Ni-Cu-PGE deposits have commonly been exposed to post-magmatic modification of varying degree. However, the effect of metamorphism, post-magmatic alteration and regional tectonic deformation to komatiitic ores is not always unambiguous

and much remain to be understood, as many characteristic modifications are often specific to a single deposit or area (e.g., Barnes et al. 2016). In general, disseminated ores that lack strong buffer capability, are more vulnerable to post-magmatic alteration than massive ores, which, in turn, are more susceptible to tectonic remobilization due to their extremely ductile nature (e.g., Stone & Archibald 2004, Barnes 2006, Barnes et al. 2016). Post-magmatic alteration (serpentinization, carbonatization, oxidation, desulfurization etc.) may modify the original primary sulfides and end up in a secondary upgrade of the metal tenor by, e.g, producing more Ni-rich secondary sulfides such as millerite. As for sulfides, for example Barnes et al. (2009) and Konnunaho et al. (2013) have demonstrated that a strong talc-carbonate alteration (CO_2 metasomatism) and/or serpentinization may oxidize the primary Fe sulfide assemblages, release S and Ni from them, and replace the original assemblage by secondary magnetite-pyrite assemblage in a process known as desulfurization. The released S then enhances Ni release from olivine and may form secondary Ni sulfide assemblages (e.g., millerite), which under favorable conditions may precipitate and lead to an upgrade of the ore tenor. In many cases the secondary upgrade forms the bulk of an economic deposit (Barnes 2006).

The physical weakness of sulfides makes them liable to localized stress and strain, which may control the ore deposit geometry in highly deformed areas. Progressive folding and shearing are capable of remobilizing and concentrating massive sulfide ores into low-strain areas such as fold hinges or shear-induced strain shadow zones (Stone & Archibald 2004, Duuring et al. 2010, Barnes et al. 2016). Furthermore, disseminated and massive ores may be passively thickened by folds (Duuring et al. 2010).

Characteristic to tectonic remobilization caused by shearing are so called *durchbewenung* breccias (translates to breccia formed by movement), where rounded silicate fragments are accommodated into a matrix of less competent sulfides (e.g., McCutcheon 2011, Barnes et al. 2016). Notably, komatiite-hosted Ni-Cu-PGE can form at several kilometers depth in the crust and may not be as susceptible to rapid crustal movements, weathering, and erosion as ores formed on the surface. In some cases, a deposit may be detectable only if erosion and tectonic processes have brought it closer to surface (Barnes et al. 2016).

2.2.4 Komatiitic Ni-Cu-PGE in Finland

Several komatiite-hosted Ni-Cu-PGE deposits are found in Finland (see Makkonen et al. 2017, see fig. 3 in it). A recent review of the Finnish komatiitic Ni-Cu-PGE deposits given by Konnunaho (2016) divides them to Archean komatiites (ca. 2.94–2.75, Lehtonen 2016) of eastern and NW-Finland, and two episodes of Paleoproterozoic komatiite magmatism (2.5–2.4 Ga and ca. 2.06 Ga, Hanski & Huhma 2005) in the Central Lapland Greenstone belt (CLGB). Also, two major groups of komatiite-hosted Ni-Cu-PGE deposits are recogzined on the baisis of metal content (Table 3): 1) Ni-(Cu-PGE) deposits (Cu and PGE-enriched Ni deposits as in the Raglan area) and 2) Ni-(Cu) deposits (classical Ni-rich deposits as in the Kambalda area) found in both Archean and Paleoproterozoic terranes (Konnunaho et al. 2015). In addition, there is the Paleoproterozoic and unusual PGE(-Cu-Ni) deposit of Lomalampi (Törmänen et al. 2016). Curiously, the recently (2009) discovered world-class Sakatti Cu-Ni-PGE deposit also links to komatiitic magmatism of CLGB (Brownscombe et al. 2015, Makkonen et al. 2017). On the basis of the mineralization style classification, the Finnish deposits are mainly of the disseminated Type II although massive sulfides (type I) are found in, e.g., the Hietaharju, Peura-aho, Tainiovaara, and Hotinvaara deposits. Many of the deposits are subjected to post-magmatic modification, such as the Vaara deposit (types IV and V) and rather represent mixtures several types (Konnunaho et al. 2013, Konnunaho et al. 2015). The Finnish deposits comprise both, high-Mg and low-Mg parental melts and, in addition, represent a variety of magma types although mainly AUK (Konnunaho et al. 2015, Konnunaho 2016, Makkonen et al. 2017).

The Finnish komatiite-hosted Ni-Cu-PGE deposits are principally associated with MgO-rich cumulates crystallized from Cr-undersaturated melts (Konnunaho et al. 2015, Konnunaho 2016). Also, mass-independent fractionation in multiple sulfur stable isotope systematics (see Bekker et al. 2009) has revealed importance of externally gained sulfur for the ore formation in the Finnish komatiite Ni-Cu-PGE deposits (Konnunaho et al. 2013, Konnunaho 2016).

Table 3. Characteristics of selected Finnish komatiite-hosted Ni-Cu-PGE deposits. Data are from Konnunaho (2016), Makkonen et al. (2017), Brownscombe et al. (2015), and Konnunaho et al. (2015). Table modified after Konnunaho (2016). SGB = the Suomussalmi greenstone belt, Ind. = individual, CLGB = the Central Lapland greenstone belt and RC = the Rommaeno complex.

Deposit	Location	Age	Magma type, Al_2O_3/TiO_2	Parental melt MgO wt.%	Metal association	Mineralization type
Vaara	SGB	Archean	AUK (19)	19 ± 3.8	Ni-(Cu-PGE)	II
Hietaharju	SGB	Archean	AUK (15)	10.5 ± 2.6	Ni-(Cu-PGE)	II, (I)
Peura-aho	SGB	Archean	AUK (15)	9.3 ± 3	Ni-(Cu-PGE)	II, IV-V, (I)
Tainiovaara	Ind. body	Archean	AUK (23)	15.0 ± 1.5	Ni-(Cu-PGE)	II, (I)
Lomalampi	CLGB	Paleoproterozoic	AUK (15)	15.0 ± 6	PGE-(Ni-Cu)	II
Hotinvaara	CLGB	Paleoproterozoic	AUK (34)	unknown	Ni-(Cu)	II, (IV-V, I)
Ruossakero	RC	Archean	Ti-depleted (46)	30.0 ± 3	Ni-(Cu)	II
Sarvisoaivi	RC	Archean	Ti-depleted (37)	19.0 ± 5.6	Ni-(Cu)	II
Sakatti	CLGB	Paleoproterozoic	unknown	19 ± 0	Cu-Ni-PGE	II, I

3. EXPLORATION OF KOMATIITIC NI-CU-PGE DEPOSITS

Recognition of prospective areas and environments in terms of komatiite-hosted Ni-Cu-PGE ores can be outlined in five suggestive rules: I) presence of major magma pathways in the komatiite sequence (or presence of high-Mg magmatism in the first place), II) presence of sulfide-bearing country rocks, III) detecting signs of sulfide saturation and segregation, IV) detecting signs of contamination, and V) determining structural control and/or present erosion level of the komatiitic sequence (Brand 1999, Barnes et al. 2004, Lesher & Barnes 2008, Barnes et al. 2016). Practically, thick cumulate units are more prospective than thinner lava flows. Nevertheless, different techniques work in different areas and scales, and in general, there is no absolute method to explore komatiites worldwide (Barnes et al. 2004, Barnes 2006, Konnunaho 2016, Le Vaillant et al. 2016).

Geophysical methods, e.g., magnetic and electromagnetic surveys are important in locating potential areas, particularly in metamorphic terrains (e.g., Le Vaillant et al. 2016), due to magnetite formation in serpentinization, which makes metamorphosed komatiites visible as positive anomalies on magnetic maps. However, magnetite is not formed during, e.g., CO_2-metasomatism. Furthermore, deformation and post-magmatic alteration may limit the use of traditional geochemical signals in detecting contamination and/or sulfide segregation (e.g., Jahn et al. 1980, Gruau et al. 1992, Barnes et al. 2004,

Le Vaillant et al. 2016). Consequently, when applied to practice, locating major magma pathways in metamorphosed, deformed and poorly exposed terrains, assessing adequate sulfur sources, and constraining the effect of the post-magmatic modification to komatiite geochemistry regionally become essential for exploration of komatiite-hosted Ni-Cu-PGE deposits.

3.1 Using whole-rock geochemistry

Whole-rock geochemistry can be used in defining the prospective long-term high-volume magma pathways in a komatiitic sequence, as well as, tracing sulfide segregation and contamination signals (e.g., Leshet et al. 2001, Barnes et al. 2004, Arndt et al. 2008). However, under appropiate conditions basically any element may behave in a mobile manner and interpretations of whole-rock geochemistry should always be considered case-specifically. Based on a generalized view acquired from komatiite studies, major elements Mg, Si, Fe, and Al and trace elements such as Ni, Co, Ti, Zr, Cr, and PGE should preserve their magmatic values during alteration and metamorphism (Barnes 2006, Arndt et al. 2008). However, this is obviously case-dependent and for example Mg, Fe, Si, as well as Ni, modified during serpentinization (e.g., Jahn et al. 1980). Alkali and alkaline earth elements (Cs, Rb, K, Na and Ba, Sr, Ca, Eu^{2+}) and chalcophile elements such as S, Au, Cu, Zn, and Pb easily form complexes with metamorphic and hydrothermal fluid and behave in a mobile manner during alteration (e.g., Lesher et al. 2001, Le Vaillant et al. 2016). Also, light rare earth elements (LREE) may be mobilized by CO_2-dominant fluids (Gruau et al. 1992, Lesher et al. 2001). Moreover, Le Vaillant et al. (2016) argue based on recent studies of Ni, Pd, and Pt behavior in hydrothermal fluids that these may also be mobile during post-magmatic modification.

3.1.1 Locating major magma pathways

Major magma pathways are typically found where high-MgO cumulates are the most abudant (e.g., Barnes 2006, Arndt et al. 2008). Chromium is very useful for evaluation of them, as it reflects variations in temperature and oxygen fugacity (fO_2) of the melt (e.g., Barnes 1998). In this case, however, parental melt compositions must be considered, as the reduced komatiitic melts become more oxidized with decreasing MgO content

(Barnes 1998, Barnes 2006). Therefore, parental melts of cumulate sequences should always be considered, as cumulates formed from high-MgO komatiitic melts that are typically Cr-undersaturated and critical for Ni-Cu-PGE ores, whereas cumulates of low-MgO komatiitic and komatiitic basaltic parental melts are often initially Cr-saturated (e.g., Barnes 1998, Lesher et al. 2001, Barnes 2006, Barnes & Fiorentini 2012, Konnunaho 2016). This makes the use of Cr-saturation for latter two inefficient. However, in komatiitic sequences formed from low-MgO komatiitic and komatiitic basaltic parental, cumulates with Cr-undersaturated compositions may be formed directly after eruption as temperature and fO_2 conditions may delay crystallization of chromite. Furthermore, Barnes & Fiorentini (2012) have emphasized that komatiitic olivine cumulates lacking cumulus chromite, regardless of Cr-saturation of the parental magma, are commonly found within mineralized units. These features promote the use of, e.g., Ni vs. Cr and Cr vs. MgO in identification of prospective magmatic environments (e.g., Brand 1999, Barnes & Fiorentini 2012).

3.1.2 Sulfide segregation

The strong partitioning of Ni and PGE into immiscible sulfide phase during sulfide segregation and the associated depletion of these elements in barren komatiitic cumulates have been widely connected to mineralized komatiites (e.g., Naldrett et al. 1984, Brand 1999, Lesher et al. 2001, Barnes 2006). Sequences in which both depletion and enrichment of Ni and PGE are observed are the most critical for Ni-Cu-PGE ores (e.g, Naldrett et al. 1984). Particularly, large whole-rock data sets are useful in detecting depletion (e.g., Naldrett et al. 1984, Lesher et al. 2001). The depletion may not be as detectable at high R-factor as at low R-factor, because the relative level of depletion may not have been strong enough to produce the halos, given the high mass fraction of the magma (e.g., Barnes 2006, Fiorentini et al. 2010a). Especially, PGE depletion is basically only detectable in komatiitic sequences, where silicate/sulfide ratios (R factor) are low (Fiorentini et al. 2010a). Also, the depth, where the possible segregation occurred should be considered, as sometimes although the depletion is present, sulfide segregation may have occurred at depths out of reach. Nevertheless, tracing marks of sulfur segregation is not unambiguous and in a scientific sense, globally conclusive characteristics have not been discovered. Moreover, many explanations are interpretative and rather arouse

controversy on a global scale, as after an ore deposit has already been discovered conclusions are much easier to draw.

3.1.3 Contamination

In light of global trends, an economic Ni-Cu-PGE deposit demands external sulfur, which is highlights the importance of contamination of komatiites by sulfur-bearing country rocks (Lesher et al. 2001, Bekker et al. 2009, Ripley & Li 2013). Contamination can be directly detected in the field by occurrence of xenoliths and/or hybrid rock types, but in lack of these, trace element geochemistry (e.g., Lesher et al. 2001) and stable sulfur isotope systematics (Bekker et al. 2009) become important. According to Lesher et al. (2001), high-degree partial melts derived from primitive mantle are magmatically depleted in terms of highly incompatible lithophile elements (HILE). The HILE elements are strongly enriched in the crust, and hence high U, Th, and LREE (La, Ce, Pr, Nd, Sm) abundances in komatiites are indicative of involvement of crustal components in the system. Also, comparison between the HILE and moderately incompatible elements (MILE), e.g., heavy REE (HREE: Gd, Tb, Dy, Ho, Er, Tm, Yb, and Lu), Zr, and Y, are useful in detecting contamination marks. Compared to the HILE, the MILE are enriched in komatiitic systems and in the upper crust. Furhermore, negative anomalies of the high-field strength elements (HFSE, particularly Nb, Ta, and Ti) also reflect potential crustal contamination, as the crust is generally enriched in Si but depleted in Nb, Ta, and Ti with respect to other incompatible elements (Lesher et al. 2001, Barnes et al. 2016). In addition, the upper crust is less enriched HFSE than in MILE (Lesher et al. 2001). Therefore, ratios of, e.g., La/Yb, Th/Yb, La/Sm, Zr/Ti, and Zr/Y can be used in tracing marks of contamination in komatiitic systems (Lesher et al. 2001, Barnes et al. 2004). However, discriminating between contamination and alteration is ambiguous as REE may be affected by post-magmatic alteration (Jahn et al. 1980, Barnes et al. 2004). In addition to incompatible elements, Bekker et al. (2009) have shown that due to absence of the ozone in the Archean atmosphere, Archean metasedimentary rocks display mass-independent fractionation of ^{33}S and ^{34}S isotopes in contrast to mantle derived magmas, which strictly display mass-dependent fractionation. Therefore, utilization of , e.g., S, Fe and Cu isotopes provide a powerful tool in tracing the assimilation of external sulfur in komatiitic melts. Fiorentini et al. (2010b) and Ripley and Li (2013) have demonstrated that addition of external sulfur during contamination is not a necessity to make an ore

deposit, especially, if magma volumes are remarkably high and sulfur saturation occurred early on several stages. However, their models are theoretical and more connected to small-scale disseminated ores.

3.2 Using mineral chemistry

As in the case of whole-rock geochemistry, concentrations of base metals in different minerals (e.g., olivine, pyroxene, and spinel) can be utilized in tracing sulfide segregation and contamination indicators. Element exchange between the main phases, e.g., olivine, Cr-spinels, and possible sulfide phase in komatiites may result in similar depletion halos and/or enriched concentrations of base metals in minerals as in whole-rock compositions. Everything is, however, condition-dependent: Ni, e.g., is compatible with all the mentioned minerals under appropriate circumstances (e.g., Li et al. 2008). Also, discriminating between secondary and primary minerals becomes crucial, as metamorphic mineral assemblages naturally are inappropiate for tracing magmatic events.

3.2.1 Olivine chemistry

Only magmatic olivine compositions can be used in tracing sulfide segregation and contamination events (e.g., Li et al. 2004, Li et al. 2007). As olivine represents the primary silicate liquidus phase in komatiitic systems, it is a sensitive indicator of parental magma composition and magmatic processes it underwent. Consequently, partition coefficients of base metals between sulfide liquid and silicate liquid can be utilized. For example, Brenan (2003) has concluded by experimental studies of olivine-sulfide phase equilibria that nickel partitions even more strongly to sulfide liquid than olivine if a Ni-rich sulfide liquid is already present. This would indicate Ni-poor olivine to be indicative of economic mass of sulfide liquid. However, subsolidus element exchange may level the Ni distribution between the olivine and sulfide phases and leave behind no marks of Ni depletion in olivine, although a high-Ni sulfide phase was present (Barnes et al. 2013). Also, komatiite melt needs to reach sulfide saturation early enough, before fractionation of olivine has consumed the majority of Ni in the system. As for depletion, systems, where sulfide segregation occurred early on may experience a relatively more rapid Ni decrease

in relation to olivine forsterite contents than systems where segregation did not take place (Li et al. 2007). However, during, e.g., serpentinization Ni released from olivines is shared between serpentine, magnetite, and possible sulfides, hence making metamorphic olivine depleted in nickel. Similar behavior is also observed in the case of iron, which leads to increased Fo contents in metamorphic olivines (Blais & Auvray 1990).

3.2.2 Spinel chemistry

Several studies have demonstrated the use of oxides (e.g., magnetite, chromium magnetite, and chromite) as tracers for Ni-Cu-PGE deposits (e.g., Barnes et al. 1996, Barnes & Roeder 2001, Dupuis & Beaudoin 2011, Dare et al. 2012, Dare et al. 2014, Boutroy et al. 2014). Magnetite and chromite are both very common accessory minerals in komatiitic rocks and their chemical composition is controlled by the conditions they formed in (e.g., temperature, fO_2, and Fe and Ni contents of the magma). Therefore, they show distinct fingerprints when formed at margins of a Ni-Cu-PGE deposit (Barnes & Roeder 2001, Dare et al. 2014, Boutroy et al. 2014). Furthermore, magnetite and chromite are relatively refractory and resistant to alteration and weathering compared to other high-temperature primary minerals like olivine (Barnes & Roeder 2001, Boutroy et al. 2014). Chromite is often magmatic, whereas magnetite is found in both magmatic and secondary forms (Barnes 1998, Dupuis & Beaudoin 2011). Secondary magnetite often replaces Fe sulfides and forms rims around chromite (Barnes 1998, Dupuis & Beaudoin 2011, Boutroy et al. 2014, Dare et al. 2014).

Formerly, Zn-rich chromite was attributed to mineralized komatiites (e.g., Groves et al. 1977). However, rather than reflecting igneous compositions, the relatively mobile Zn released from surrounding country rocks during metamorphism can be concentrated to the cores of magmatic chromites by diffusion-induced element exchange, as magnetite rim is formed (Barnes et al. 1996, Barnes 2000, Lesher et al. 2001). On the other hand, Barnes et al. (1996) have emphasized the use of Co contents relative to MgO a suitable discrimination method between chromites derived from sulfide-bearing and barren rocks. As for recently developed techniques, Dare et al. (2012), Boutroy et al. (2014), and Dare et al. (2014) have demonstrated that primary oxides crystallizing simultaneously with early (Fe-rich) sulfide liquid are higher in lithophile elements (e.g., Ti, V, and Cr are up

to 2 wt.%) than oxides crystallizing together with the residual liquid (Cu-rich). Chalcophile element (e.g., Ni, Co, Zn, Sn, and Mo) concentrations in magnetite are dependent on their concentration in the sulfide liquid and co-crystallizing sulfide. Use of lithophile and chalcophile elements is efficient, as partitioning of lithophile elements in a komatiitic system, where a sulfide liquid is segregated is mainly controlled by magnetite formation. Hence, evolution of the sulfide liquid can be outline by lithophile and chalcophile element abundances in magnetite (Dare et al. 2014, Boutroy et al. 2014). Features outlined above are also valid for chromite, as magnetite that has crystallized from an ultramafic parental magma is rare (e.g., Boutroy et al. 2014). Secondary magnetite, in turn, is depleted in most trace elements including Ni, Mn, V, Ti, Al, and Cr but enriched in Si and Mg. Magnetite that replaces sulfides or chromite often has elevated Cr contents (Boutroy et al. 2014, Dare et al. 2014). Hence, different compositions in secondary and primary magnetite create a useful tool for exploration, with the help of which discrimination between mineralized and barren rocks is possible (Boutroy et al. 2014).

4. STUDY AREA

The study area is located in the municipalities of Savukoski and Salla in Eastern Lapland in Northern Finland (Figure 6). In geological literature, the area is also referred to as "the eastern Lapland block of gneissose granites and gneisses and the Tuntsa-Savukoski supracrustal formation" (Mikkola 1941), "the Tuntsa terrane" (Sorjonen-Ward & Luukkonen 2005) and "the Kemihaara Complex and the Tuntsa Suite" (Makkonen et al. 2017). However, in this study the term "The Eastern Lapland Archean domain" (ELAD) adopted from Juopperi (1994) and Juopperi and Vaasjoki (2001) is used to avoid confusion between the names of the lithotectonic units in the area and the area itself.

4.1 Regional geology of the Eastern Lapland Archean domain

The first bedrock studies in ELAD were recorded by Mikkola (1936) during the making of the extensive 1:400 000 Muonio-Sodankylä-Tuntsajoki geological map of the Finnish Lapland (Mikkola 1941). Subsequent lithotectonic and lithological descriptions by other authors (e.g., Papunen et al. 1977, Juopperi 1994, Juopperi & Vaasjoki 2001, Sorjonen-

Ward & Luukkonen 2005) are at least to some extent based on his groundbreaking work. Geologically, ELAD belongs to the northeastern part of the Fennoscandian shield (see Hölttä et al. 2012: fig. 1; Slabunov et al. 2006a: fig. 2). It is bordered by the Paleoproterozoic Lapland granulite belt (LGB) in the north and by the Paleoproterozoic schists of the Central Lapland greenstone gelt (CLGB) in the south and the west. All lithological units of ELAD continue to Russia, where they "grade" into Archean gneisses of the Belomorian mobile belt (BMB) (Juopperi 1994, Juopperi & Vaasjoki 2001, Sorjonen-Ward & Luukkonen 2005, Slabunov et al. 2006b). Therefore, some authors consider ELAD tectonically as a part of the Belomorian province (Gaál & Gorbatschev 1987, Slabunov et al. 2006), while some authors classify it as a part of the Karelian province (Hölttä et al. 2012, see fig. 1 & Slabunov et al. 2006a, see fig. 2). All lithological contacts between ELAD and the surrounding Paleoproterozoic belts (LGB and CLGB) are strongly tectonized (Sorjonen-Ward & Luukkonen 2005, Nironen 2017).

ELAD domain comprises a gneiss-granite-greenstone belt association of high- to medium-grade metamorphic gneisses and supracrustal volcano-sedimentary sequences, including abundant komatiitic rocks (Figure 6) (Mikkola 1941, Juopperi 1994, Sorjonen-Ward & Luukonen 2005). By lithotectonic means, three granitoid complexes and two supracrustal belts are recognized: 1) the Kemihaara-Vintilänkaira granitoid complex (KVGC), 2) the Tulppio metavolcanic belt (TVB), 3) the Ahmatunturi granitoid complex (AGC), 4) the Tuntsa metasedimentary belt (TSB) and 5) the Naruska granitoid complex (NGC) (Mikkola 1941, Juopperi 1994, Sorjonen-Ward & Luukkonen 2005). All of these units are principally Archean in age, ranging ca. 2.9–2.5 Ga (Juopperi & Vaasjoki 2001). Later Paleoproterozoic intrusions and dykes in the area record ages from ca. 2.5 to 1.9 Ga (Juopperi & Vaasjoki 2001, Huhma et al. 2018). However, age(s) of the komatiitic sequences of ELAD are not known in detail – they have been mainly interpreted based on ambiguous relationships to adjacent granitoids. Due to high- to medium-grade metamorphism in the upper amphibolite facies conditions (Virransalo 1985, Slabunov et al. 2006a, Kivisaari 2008, Hölttä & Heilimo 2017) and predominant thrust from the southwest (Virransalo 1985, Koistinen 1987a, 1987b, Papunen et al. 1997) the rocks of ELAD are characterized by metamorphic mineral assemblages, lack of primary structures and textures, and poorly constrained stratigraphy (Juopperi 1994, Juopperi & Vaasjoki 2001, Sorjonen-Ward & Luukkonen 2005). Remote location, poor exposure, and tough

terrain render the area as being amongst the geologically most vaguely known terrains in Finland.

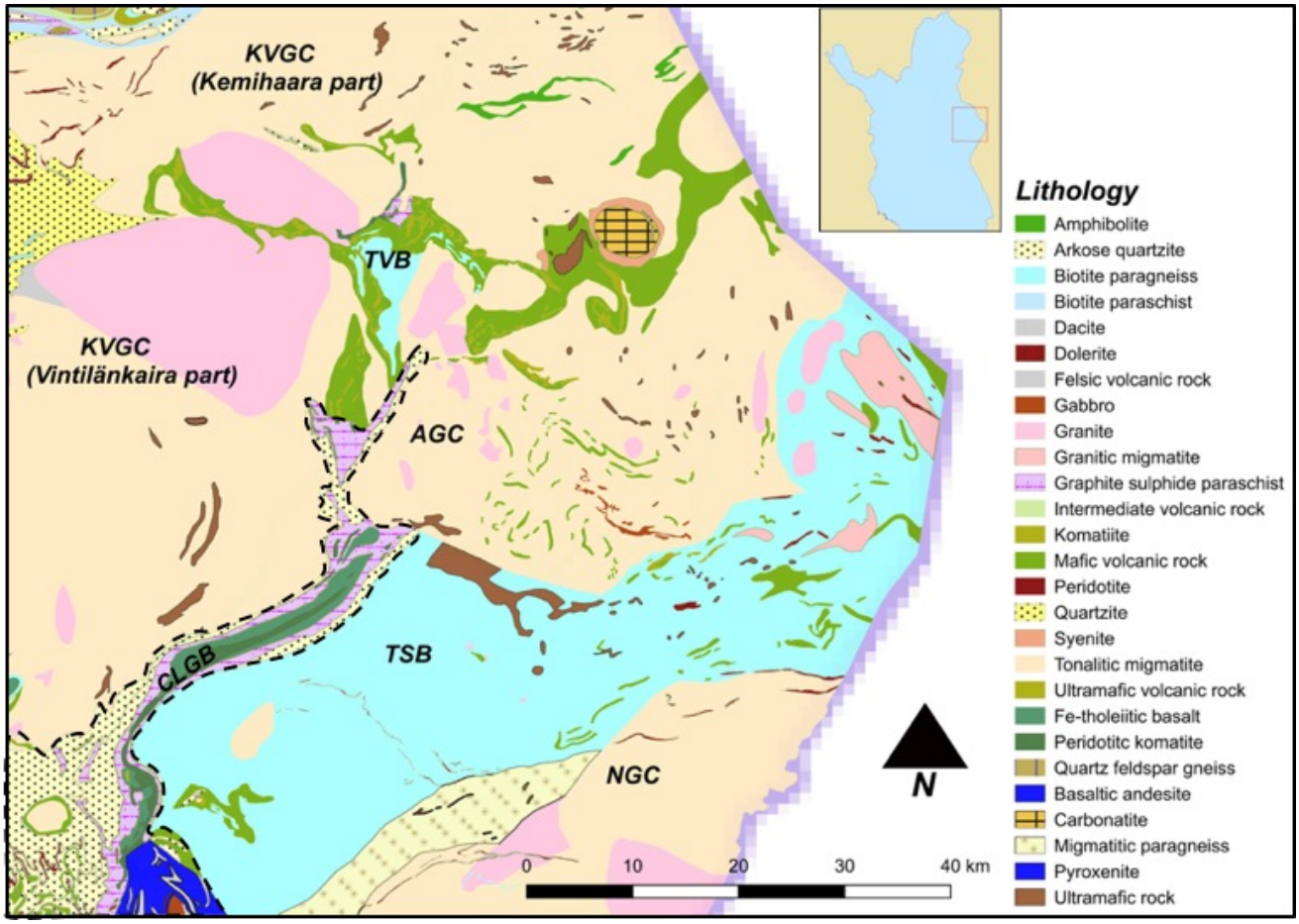

Figure 6. Geological map of The Eastern Lapland Archean domain modified after Digi KP – Bedrock map of Finland. The interpreted Archean-Paleoproterozoic boundary is marked with the dashed black line. All rocks shown in the legend are metamorphic. Abbreviations: KVGC = Kemihaara-Vintilänkaira granitoid complex, TVB = Tulppio metavolcanic belt, AGC = Ahmatunturi granitoid complex, TSB = Tuntsa metasedimentary belt, NGC = Naruska granitoid complex & CLGB = Central Lapland greenstone belt.

4.2 Granitoid complexes

The granitoid complexes of ELAD consist of tonalitic-trondhjemitic-granodioritic (TTG) to granitic gneisses with minor gneiss and amphibolite intercalations, all of which are typically cut by younger granitic and/or syenitic intrusions (Mikkola 1941, Juopperi 1994, Juopperi & Vaasjoki 2001, Sorjonen-Ward & Luukkonen 2005).

4.2.1 Kemihaara-Vintilänkaira granitoid complex

The Kemihaara-Vintilänkaira granitoid complex (KVGC) is the northernmost and the least studied of the granitoid complexes (see Figure 6). In terms of aerogeophysical data, two separate parts are recognized: the Kemihaara (northern) and the Vintilänkaira (southern) (Juopperi 1994, Juopperi & Vaasjoki 2001). Ultramafic bodies in the area are abundant but relatively scattered and small in size (Papunen 1976). Juopperi (1994) and Juopperi & Vaasjoki (2001) have considered the bodies as remnants of the Tulppio metavolcanic belt.

The northern Kemihaara part of the complex consists of foliated and banded magnetite-bearing granite gneisses, which Mikkola (1941) called "mylonitic" due to their distinctive textural features in comparison to other granitoids of ELAD. Juopperi (1994) considered these rocks as migmatized tonalitic gneisses as they are found in close proximity to the Lapland granulite belt. The southern Vintilänkaira part is mainly composed of tonalitic gneisses that are crosscut and migmatized by younger granites and pegmatites (Mikkola 1941, Juopperi 1994). Ultramafic bodies are not known from there. Two zircon U-Pb age determinations constrain an age span of 2832±6 Ma to 2805±4 for the Kemihaara gneisses, which is probably also attributable to the Vintilänkaira gneisses that have not been dated. In addition, KVGC hosts two age groups of younger granites with age span from 2.5 to 1.9 Ga. Notably, the Marjavaara syenite, located in the contact zone of KVGC and TVB, crosscuts TVB volcanic rocks, and yields a U-Pb zircon age of 2795±20 Ma (Juopperi & Vaasjoki 2001). On the other hand, the contact zone between KVGC and TVB is tectonized (Papunen et al. 1997). Another peculiarity in KVGC is the Sokli carbonatite (ca. 355 Ma in age, Vartiainen & Wolley 1974) that hosts significant phosphate (± Nb-Ta-rare earth element (REE)) resources (e.g., Vartiainen 1980).

4.2.2 Ahmatunturi granitoid complex

The Ahmatunturi granitoid complex (AGC), located between TVB and TSB (see Figure 6), consists of moderately and unevenly magnetite-bearing tonalitic gneisses (Mikkola 1941, Juopperi 1994). Several ultramafic bodies are located in the northern parts of the complex in addition to one large body in the southwestern parts. Also, in the proximity of the Ahmatunturi fell, some of the gneisses contain relicts of mafic-intermediate

igneous rocks but their relation to the Tulppio metavolcanic rocks is not known (Juopperi 1994, Juopperi & Vaasjoki 2001). Granites in the area display a variety of textural types, some of which are formed in association with the migmatized granite gneisses, while others are typically found together with banded tonalitic hornblende-gneisses (Mikkola 1941, Juopperi 1994). According to Juopperi & Vaasjoki (2001), the gneisses are Archean in age (2.9–2.8 Ga), although the analytical results are somewhat discordant. The contact zone between AGC and TVB is probably intrusive (Juopperi 1994), and at least partially tectonized, whereas the contact between AGC and TSB is strongly tectonized and characterized by hornblende-bearing gneisses (Mikkola 1941, Juopperi 1994, Juopperi & Vaasjoki 2001). Curiously, the Suurkovanselkä alkalisyenite, located in the contact zone of AGC and TVB cross-cuts the Tulppio metavolcanic rocks and yields a discordant titanite age of 2683±1 Ma (Juopperi & Vaasjoki 2001).

4.2.3 Naruska granitoid complex

The Naruska granitoid complex (NGC) is the southernmost of the granitoids complexes and bordered by TSB in the north and Paleoproterozoic schists of CLGB in the south and the west (see Figure 6). The principal rock types are granitic to tonalitic gneisses, which in places contain abundant relicts of metasedimentary and metavolcanic rocks (Mikkola 1941, Juopperi 1994). Komatiites have not been found in NGC. Granitic gneisses are most probably migmatized counterparts of the older tonalitic gneisses (Juopperi 1994, Juopperi & Vaasjoki 2001). The tonalitic-granitic gneisses of NGC span ages between 2744±25 and 2702±5 Ma (Juopperi & Vaasjoki 2001), which sets them in the same age group with the Belomorian orthogneisses (Bogdanova & Bibikova 1993), as well as, most of the other Archean granitoids in Finland (Hölttä et al. 2012). The contact between NGC and TSB is ambiguous: the strongly migmatized rocks within show gradational, tectonic and intrusive features (Mikkola 1941, Juopperi & Vaasjoki 2001). Based on gradational contact features and the span of U-Pb zircon ages, Juopperi and Vaasjoki (2001) suggested that NGC and TSB represent the same lithotectonic unit with NGC being a deeper erosional section. On the other hand, Sorjonen-Ward and Luukkonen (2005) saw the results of U-Pb zircon age determinations as evidence of protracted evolution in the granitic magmatism of NGC.

4.3 Supracrustal belts

Two supracrustal E-W trending volcanic-sedimentary sequences are recognized in ELAD: the Tulppio metavolcanic belt (TVB), mainly composed of metavolcanic rocks with minor metasedimentary rocks, and the Tuntsa metasedimentary belt (TSB) that hosts metamorphosed sedimentary rocks and minor metavolcanic rocks (Mikkola 1941, Juopperi 1994).

4.3.1 Tulppio metavolcanic belt

The Tulppio metavolcanic belt (TVB), also known as the Tulppio greenstone belt (e.g., Maier et al. 2013), is the northernmost of the supracrustal belts, and located in between KVGC and AGC (see Figure 6). The main rock types in the area are olivine-serpentine-dominated and tremolite-chlorite-dominated rocks together with hornblende-dominated amphibolites. Also, minor occurrences of quartz-feldspar schists, Al-rich paragneisses, black schists, and quartzites are present (Kauniskangas 1987, Juopperi 1994).

The rock assemblage of TVB shows a geochemical association of volcanic rocks ranging from ultramafic to rhyolitic in composition (Juopperi 1994, Papunen et al. 1997, Heikura et al. 2010). However, intermediate compositions are only found in a couple of locations (Kauniskangas 1987, Heikura et al. 2010). The volcanic rocks are recognized as komatiitic cumulates (olivine/serpentine-dominated rocks), komatiitic lavas (tremolite-chlorite-dominated rocks), submarine Fe- and Mg-tholeiites (amphibolites), and rhyolitic felsic volcanic rocks (quartz-feldspar schists) (Papunen 1977, Kauniskangas 1987, Juopperi 1994, Papunen et al. 1997, Sorjonen-Ward & Luukkonen 2005). The komatiitic rocks often contain interlayers of amphibole- and/or graphite-bearing aluminous schists, and sulfide- and quartz-bearing cherty rocks, which are regarded as sedimentary-volcanoclastic sequences (Juopperi 1994, Juopperi & Vaasjoki 2001, Sorjonen-Ward & Luukkonen 2005). Based on komatiite petrography, Virransalo (1985) has estimated temperatures up to ca. 700°C and pressures around 4 kbar for peak metamorphic conditions in the Tulppio belt.

The age of TVB volcanic rocks is obscure: many authors consider them Archean (Mikkola 1941, Juopperi 1994, Sorjonen-Ward & Luukkonen 2005, Törmänen et al. 2009, Makkonen et al. 2017) but many admit that, in the view of rather deficient age data and unknown relations to adjacent rocks, some of them might as well be Paleoproterozoic. Virransalo (1985), Piirainen et al. (1985), and Kauniskangas (1987) called The TVB rocks as the Tulppio-group and divided them into several formations to constrain the lithostratigraphy. However, Juopperi (1994) and Juopperi and Vaasjoki (2001) argued that lithostratigraphic classification of the TVB rocks is difficult as the area is relatively poorly exposed, and no primary structures are present in the strongly deformed rocks. The challenges in lithostratigraphy of TVB can also be underlined by dissenting opinions among the above-mentioned authors (see Virransalo 1985, see fig. 8 and Kauniskangas 1987, see fig. 2), as well as Papunen et al. (1997, see fig. 15). The contacts between TVB and the surrounding granitoids are interpreted as intrusive (the granitoids intrude TVB) and partially tectonized (Juopperi & Vaasjoki 2001).

4.3.2 Tuntsa metasedimentary belt

The Tuntsa metasedimentary belt (TSB) is the southernmost of the supracrustal belts (see Figure 6). Mikkola (1941) called the area the Tuntsa-Savukoski supracrustal formation as it extends from the Savukoski village to the Russian border (Tuntsa area) and continues to the Belomorian in the east. TSB is bordered by NGC in the south, AGC in the north, and the Paleoproterozoic schists of CLGB in the west (Juopperi 1994, Sorjonen-Ward & Luukonen 2005, Hölttä & Heilimo 2017).

The belt is mainly composed of quartz-feldspar gneisses, mica paragneisses and their migmatized equivalents (Mikkola 1941, Juopperi 1994, Sorjonen-Ward & Luukkonen 2005). Also, the largest komatiitic cumulate body in ELAD (the Värriöjoki body), in addition to abundant smaller bodies towards the east, is located in TSB. Some of the smaller bodies correspond geochemically to The TVB komatiites (Juopperi 1994). According to Juopperi (1994) the gneisses in the area are interpreted as turbiditic greywackes derived from a typical late Archean ca. 2.9–2.8 Ga granitoid-tholeiitic crust, constraining an age span for the deposition of TSB. Minor rock types in TSB include metasedimentary rocks such as quartzites, as well as, (tourmaline-bearing) pegmatites

and felsic dykes. All of the minor rock types were deformed in the same main event with the paragneisses (Juopperi 1983, Juopperi 1994, Juopperi & Vaasjoki 2001). The stratigraphy within the unit has been interpreted based on a polymictic conglomerate from the Nuolusvaara hill described in detail by Juopperi & Veki (1988). TSB is intruded by two ca. 2.46–2.45 Ga Paleoproterozoic mafic intrusions Peuratunturi and Koulumaoiva that are characterized by olivine-bearing gabbroic cumulates with well-preserved primary magmatic features (Huhma et al. 2018). In addition, another similar intrusion, Jäkäläharjut (Torolehto), is located close to the contact zone of AGC and TSB (Iljina 2003).

During the Proterozoic, TSB was affected by the westwards strengthening Barrovian-type amphibolite facies metamorphism with peak conditions at T = ca. 680°C and P = 10–12 kbar (Kivisaari 2008, Hölttä & Heilimo 2017), which destroyed the majority of the primary structures and recrystallized the sedimentary rocks to monotonous equigranular migmatized gneisses and augen-gneisses (Juopperi 1994, Juopperi & Vaasjoki 2001, Kivisaari 2008). The predominant structural feature in TSB is a penetrative foliation with almost horizontal dips to NW-SE (Kivisaari 2008, Hölttä & Heilimo 2017) that is comparable to the Lopian Chupa-deformation stage in the Belomorian (Stenar 1972, Bogdanova & Bibikova 1993). In contrast to the diverse contact zone between TSB and NGC described in section 4.2.3, observations of the contact features between TSB and AGC, as well as, between TSB and CLGB are non-existent (Juopperi & Veki 1988, Juopperi & Vaasjoki 2001).

5. KOMATIITES OF THE EASTERN LAPLAND ARCHEAN DOMAIN

ELAD hosts several occurrences of komatiitic rocks ranging in size from small bodies to large continuous sequences, such as the Tulppio greenstone belt (Figure 7) (Mikkola 1941, Papunen et al. 1977, Papunen et al. 1997, Törmänen et al. 2009). Due to ubiquituous serpentinization, most of the komatiitic rocks are magnetic and easily recognized on aeromagnetic maps (Figure 8). However, also non-magnetic talc-carbonate altered komatiites are present (see Figures 7 & 8). In view of the current geological map of ELAD (see Digi KP -Bedrock of Finland), many komatiitic bodies have been drawn after

magnetic anomalies without direct observations. Komatiites have so far been found within all lithotectonic units except for NGC. Most of the komatiitic bodies and formations are concentrated in or in the close proximity to TVB. Several bodies and smaller occurrences are, however, found scattered across KVGC, AGC, and TSB (Mikkola 1941, Törmänen et al. 2009, Nironen 2017).

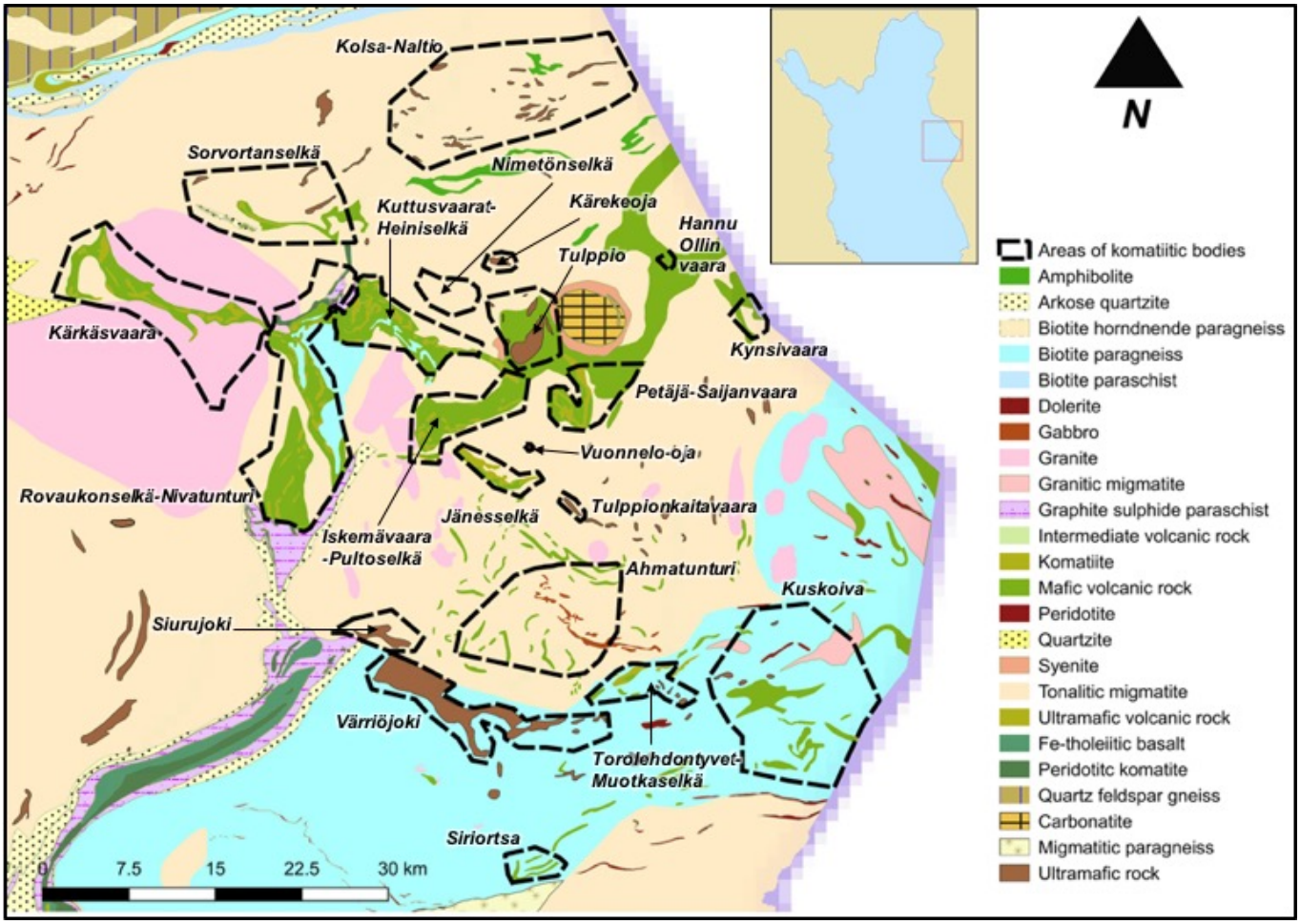

Figure 7. Komatiitic bodies of The Eastern Lapland Archean domain outlined by target areas and names presented in chapter 5. The bedrock map from DigiKP – Bedrock Map of Finland. The rock types in the legend are all metamorphic.

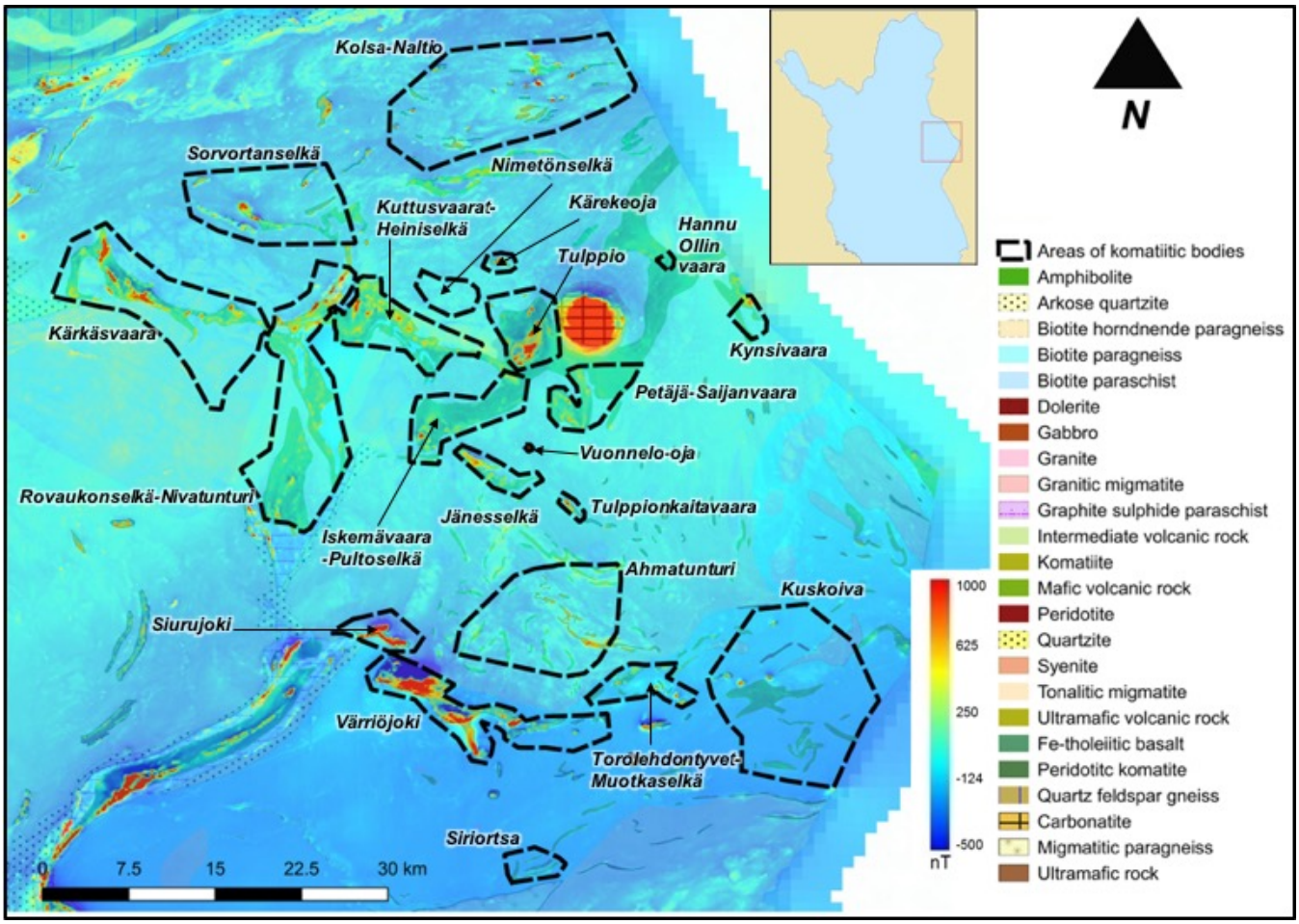

Figure 8. Komatiitic bodies of The Eastern Lapland Archean domain outlined by target areas and names presented in chapter 5 shown on magnetic map from GTK's open database. On the bottom is the bedrock map from DigiKP – Bedrock Map of Finland. The rock types in the legend are all metamorphic.

As suggested by several authors (e.g., Papunen 1977, Piirainen et al. 1985, Juopperi 1994, Papunen et al. 1997, Sorjonen-Ward & Luukkonen 2005, Törmänen et al. 2009, Maier et al. 2013), the komatiites of ELAD represent metamorphosed and variably differentiated lava flows (± cumulate sequences). Notably, according Vuollo (1986) and Törmänen et al. (2009) some of the komatiitic rocks have a possible intrusive nature. However, interpretations on emplacement environment are only based on geochemical and petrograhical evidence, and thus ambiguous. Nevertheless, komatiitic sequences, where only the cumulate-dominant B-zones are preserved, exist thorough ELAD, whereas sequences, where the non-cumulate-dominant A-zones are mostly present in TVB. The cumulate rocks are typically olivine/serpentine-dominated rocks, whereas the non-cumulate rocks display tremolite-chlorite-talc-dominated mineral assemblages. Juopperi (1994) has classified all of the volcanic rocks within ELAD to belong to TVB association. However, as outlined above, without precise geochronological information, primary magmatic structures, and rigorous observations of crosscutting relations to adjacent rocks,

the komatiites of ELAD may well represent several stages of magmatism (Mikkola 1941, Juopperi 1994, Papunen et al. 1997, Sorjonen-Ward and Luukkonen 2005, Törmänen et al. 2009, Makkonen et al. 2017, Huhma et al. 2018). Analogue for such an interpretation can be found in the Archean Kuhmo-Suomussalmi-Tipasjärvi greenstone belt (Lehtonen 2016). Therefore, in this thesis the komatiitic rocks are treated in the order of their geographic location within the lithotectonic units. More information of the ages, isotopic signatures, and petrological differences of the komatiites of ELAD can be found from Haapala (in preparation) and Tepsell (2018).

5.1 Previous Ni-Cu-PGE studies and exploration activities

The komatiites of ELAD have been in the focus of research and exploration for decades. Detailed depictions of the conducted actions and interesting findings are included in the areal descriptions in sections 5.2, 5.3, 5.4 and 5.5.

First studies after Mikkola's (1941) regional mapping to study the ore potential of the ultramafic rocks in ELAD, was the work conducted by the University of Turku and the Geological Survey of Finland in the late 1970's in the framework of the Lapland Nickel project (Papunen 1976, Papunen et al. 1977, Idman 1980). Their findings led to an intense exploration activity by Rautaruukki Oy and Lapin Malmi Oy in the late 1970's and early 1980's, as they carried out a variety of targeted studies in the komatiitic bodies of TVB and AGC, as well as in the Värriöjoki komatiitic body in TSB (e.g., Tukiainen & Mattila 1979, Mattila 1980, Nuutilainen 1980a, 1980b, Vuotovesi 1983a, 1983b, Roos 1983, Vuotovesi 1984). The University of Oulu project on Archean areas in the 1980's was the first profound approach towards understanding the nature of the ELAD komatiites (Piirainen et al. 1985). This project led to the first detailed studies in the form of three M.Sc. theses concerning the petrology, geochemistry, origin, metamorphism and stratigraphy of the Tulppio belt komatiites (Peltoniemi 1984, Virransalo 1985, Kauniskangas 1987). Simultaneously, Vuollo (1986) studied the geology of the Värriöjoki body in his M.Sc. thesis in co-operation with Lapin Malmi Oy. In addition, Outokumpu Oy, in co-operation with Rautaruukki Oy and Lapin Malmi Oy, performed preliminary studies on selected komatiitic bodies in TVB during the late 1980's (Koistinen 1987a, b, Sandberg & Karttunen 1988).

During GTK's extensive Lapland Volcanite project in 1984–1989 some detailed studies were also carried out in ELAD, although the project mainly focused on CLGB volcanic rocks (Juopperi 1988, Lehtonen et al. 1998). The majority of present knowledge of the ELAD komatiites was achieved in GTK's projects "Archean bedrock in the Eastern Lapland" (1992–1994) and "Archean schist belts in the Eastern Lapland and their exploration potential" (1994–1996) led by Heikki Juopperi (Juopperi 1994, Juopperi & Vaasjoki 2001). During these projects a geological background for ELAD was fully established and analogues to similar Archean greenstone terrains in Canada and West-Australia were considered. In 1996–1997, the University of Turku in co-operation with Outokumpu Oy, conducted a detailed mapping program in TVB and its surroundings (Papunen et al. 1997). The results of their research gave new insights into geochemistry, petrology, and stratigraphy of the ELAD komatiites. Subsequently to their work, Outokumpu Oy re-examined the Kuttusvaarat area in TVB in 1997–1998 (Lahtinen 2003).

In 1996–1999, 1996–2002 and 2000–2003 GTK studied ELAD within their "Archean terranes in the northern Finland I", "Layered Igneous Complexes in the northern Finland I" and "Archean terranes in the northern Finland II" projects (Juopperi 2002, Iljina 2003, Juopperi 2005, respectively). However, the focus of these projects was steered towards other prospective areas in Finland and ELAD was left to minor role. Between 2002–2009 and within the "Ore resources of mafic igneous rocks in the Northern Finland" project (Iljina 2009), GTK's main research in ELAD was focused on the Värriöjoki and Tulppio bodies and the Kuttusvaarat-Heiniselkä area komatiites.

5.2 Komatiites within the Kemihaara-Vintilänkaira granitoid complex

KVGC comprises two main groups of komatiitic bodies: the Sorvortanselkä and the Kolsa-Naltio (Figures 7 & 8). In addition, a poorly exposed Kärekeoja body is present in the SE part of the complex. Presence of komatiitic rocks in there has been confirmed on the basis of local boulders (Papunen et al. 1997). The Sorvortanselkä bodies are the only ones drilled. Many of the ultramafic occurrences (see DigiKP – Bedrock of Finland) within KVGC lack direct bedrock observations. The eastern part of the area mostly belongs to the Urho Kekkonen National Park.

5.2.1 Sorvortanselkä komatiites

The Sorvortanselkä area located in the Kemihaara Wilderness Nature Conservation (Natura 2000) area includes three confirmed komatiitic bodies (Figure 7). Two of the bodies are located right on the N side of the Uittipiekantunturi fell and the third, small body is found in the N side of the Karhanavaara hill. The bodies are mainly surrounded by granite gneisses and minor quartzites and their connection to each other is not known (Tukiainen & Mattila 1979, DigiKP – Bedrock of Finland). The southernmost body is not exposed, whereas the largest middle body and the Karhanavaara body are well exposed. According to Mattila (1979), the middle body mainly consists of serpentine-amphibole-chlorite-bearing ultramafic rocks and hornblende-plagioclase-quartz-bearing mafic rocks. The southern body is composed of strongly altered serpentine-talc-carbonate rock and mafic rocks similar to the middle body, some of which have a weak chalcopyrite dissemination. The thickness of till in the area ranges from 2 to 16 meters (Sandberg & Karttunen 1988).

During studies by Rautaruukki Oy in 1978–1979, several mineralization-indicative features were found in the area (Tukiainen & Mattila 1979, Mattila 1979). Consequently, four diamond drill holes (DDH, 520 m in total) were drilled to the conductive anomalies in the southern and middle bodies in 1979 (Mattila 1979, Nuutilainen 1980b). Explanation for the conductive anomalies were pyrrhotite-pyrite-bearing intercalations in the middle body and the physical state of the ultramafic rocks (abundant hydrous minerals) in the southern body.

5.2.2 Kolsa-Naltio komatiites

The Kolsa-Naltio area comprises SSW-NNE trending group of separate komatiitic bodies in the eastern part of KVGC (Figure 7). The westernmost bodies are found close to the Kemijoki River (Saarisuvanto and Seitainaapa), whereas the eastern bodies are scattered in the proximity of the Naltiotunturi fell and the Iso Kolsanmurusta hill. The bodies are relatively small, from a few tens of meters up to a few km in diameter and consist of relatively well-preserved serpentinized dunites, comparable to the less altered Tulppio body in TVB (Idman 1980). Curiously, Papunen (1976) has located weak pentlandite-

heazlewoodite dissemination (1–5 mm in diameter) in serpentinite boulders of the Seitainaapa body. The Uura-aapa bog conservation area (Natura 2000) covers the eastern part of the area and all the western Kolsa-Naltio bodies are located in the Urho Kekkonen National Park.

5.3 Komatiites within the Tulppio metavolcanic belt

TVB comprises the largest continuous sequence of komatiitic rocks in ELAD. Komatiitic occurrences in the area are in this thesis divided into seven groups on the basis of location and previous targeted studies and exploration activity. All targets are presented in figures 7 and 8.

5.3.1 Kärkäsvaara komatiites

The Kärkäsvaara area comprises the westernmost parts of TVB (Figure 7 & 8) and is among the least studied areas within the belt. The area contains several positive magnetic anomalies suggestive of ultramafic rocks, most of which, however, are not exposed as ultramafic rocks. The largest magnetic anomaly (and the largest ultramafic body) in the area is the Kärkäsvaara body itself, which according to Papunen (1976) consists of olivine serpentinites and serpentine-chlorite rocks. The body is approximately 2.5 x 1 km in area, one of the largest in ELAD. Other exposed bodies are the relatively small occurrences located to the west of the Kivihaaranmurusta hill and to the south from the Suksenrovat hills. These bodies share macroscopically similar rock types with the Kärkäsvaara body. Also, the second largest positive magnetic anomaly and the westernmost occurrence in the area, the Kappervaarat body, is sparsely exposed with a few local olivine-amphibole-pyroxene rock boulders found mainly in the southern part of the magnetic anomaly (Papunen 1976).

5.3.2 Rovaukonselkä-Nivatunturi komatiites

The Rovaukonselkä-Nivatunturi area comprises a ca. 20 km long and ca. 4 km wide almost N-S trending zone within TVB (Figures 7 & 8). Komatiites are more abundant in the northern Nivatunturi part, whereas Mg-tholeiitic rocks and komatiitic basalts dominate the volcanic sequence in the Rovaukonselkä area (Kauniskangas 1987). There,

a rock association of ultramafic to felsic volcanic rocks together with predominant migmatized paragneisses, which have quartzite and hornblende gneiss intercalations is dominant (Virransalo 1985, Kauniskangas 1987, Juopperi 1988). Ultramafic rocks in the Rovaukonselkä area are rare. The Rovaukonselkä rocks and the Paleoproterozoic Savukoski marine sediments of CLGB in the south are separated by an unconformity, which marks the border between the Archean and the Paleoproterozoic in the Eastern Lapland (Virransalo 1985, Kauniskangas 1987). The Nivatunturi area contains most of the positive magnetic anomalies in the area. It has several occurrences of komatiites, of which the largest is ca. 50–100 m wide and ca. 3.5 km long. The rocks are typically olivine-amphibole-pyroxene rocks. They are better preserved in the western parts of the area, whereas serpentine and chlorite contents increase towards the east (Papunen 1976). The rocks are often foliated (Papunen 1976) and display isoclinal folding (Virransalo 1985). The northeasternmost part of the area (Ketunkuivat) is not exposed at all, although it hosts several positive magnetic anomalies (Papunen 1976, Vihreäpuu 2001).

5.3.3 Kuttusvaarat-Heiniselkä komatiites

The Kuttusvaarat-Heiniselkä area comprises a WNW-ESE-trending and ca. 12 km long and 2–5 km wide zone within the middle parts of TVB (Figures 7 & 8). The area constitutes a rock association of tremolite-serpentine rocks (komatiites), chlorite-tremolite-antophyllite rocks (komatiitic basalts) and chlorite-actinolite rocks (Mg-tholeiites), together with abundant mica paragneisses and heterogeneous felsic sulfidic volcanic/sedimentary rocks (Tukiainen & Mattila 1979, Juopperi 1988, Piirainen et al. 1985, Papunen et al. 1997, Heikura et al. 2009). In addition, minor occurrences of sulfide-bearing black schists, quartzites and skarns (possibly hydrothermally altered ultramafics) have been observed, especially in the Johdejänkä area, to the west of the Kuttusvaarat hills (Juopperi 1988, Lahtinen 2003, Heikura et al. 2009). In the vicinity of the Kuttusvaarat hills komatiites form large uniform bodies and become small shreds enclosed within paragneisses and tholeiitic rocks towards the east in the Kontioselkä-Jolvikkoselkä-Heiniselkä area (Juopperi 1988, Papunen et al. 1997). Papunen et al. (1997) argued that komatiites in the area may represent at least two separate age groups, as some of the komatiites have similar geochemical signatures with the Paleoproterozoic komatiites of CLGB. On the other hand, some of the komatiites are clearly comparable

to the typical Archean komatiites of TVB. Kauniskangas (1987) visioned that the Kuttusvaarat-Heiniselkä komatiitic rocks erupted in an oceanic rift valley related to a back-arc basin environment close to the continental margin.

Since 1975, when Hannu Idman discovered a Ni sulfide-bearing ultramafic boulder (185B-HPI-75: 0.34 wt.% Ni, 0.16 wt.% S) in the Kuttusoja area (Papunen 1976), the Kuttusvaarat-Heiniselkä area has been a key area of interest in terms of mineral exploration. Rautaruukki Oy, Lapin Malmi Oy and GTK carried out intensive studies in the area in late 1970's and 1980's but komatiites with similarly elevated Ni contents as the Idman's sample were not found. In addition, many potential conductive anomalies were found to be caused by sulfide-bearing mica gneiss intercalations within the komatiitic lava beds in drillings (Mattila 1979, Vuotovesi 1983b, Juopperi 1988). However, in 1987, a few tens of cm thick massive pyrrhotite-rich zone (0.55 wt.% Ni and 19.1 wt.% S) was found in the Kontioselkä area (DDH R3). In 1996, Ni-rich boulders were found (286-1-JEV-97: 0.76 wt.% Ni, 0.82 wt.% S) in the Kuttusoja area (Papunen et al. 1997), which resulted in a comprehensive drilling program by Outokumpu Oy (altogether 19 DDH). Elevated nickel contents (up to 0.3%) assayed in sulfide-bearing komatiites were, however, considered metamorphic in origin (Lahtinen 2003). Aiming to locate possible continuations of the massive Ni-rich zone in the Kontioselkä area and to study the Kuttusoja area in detail, GTK drilled 10 DDHs (in total 1188.8 meters) to the Kuttusvaarat-Heiniselkä area in 2006–2009 (Heikura et al. 2009). The best intersections were a 16.5-meter thick (108.15–124.65 m) zone of 0.062 ppm Pd+Pt, including a 1.5-meter thick zone with 0.193 ppm Pd+Pt (DDH R129) and two meters of 0.32 wt.% Ni (DDH R117), both in the Kuttusoja area. Continuation of the massive pyrrhotite rock in Kontioselkä was not located.

5.3.4 Tulppio komatiitic body

The Tulppio komatiitic body (or the Tulppio dunite) is located in the eastern part of TVB, on the western side of the Sokli carbonatite (Figures 7 & 8). It is the second largest komatiitic body in ELAD with a surface area of ca. 5x2 km^2 and depth of ca. 2 km (Papunen et al. 1997, Heikura et al. 2010, Makkonen et al. 2017). The body consists of two komatiitic bodies bordered by Mg-tholeiitic volcanic rocks and metasedimentary

schists: the main body and a smaller Kiimaselkä satellite body in the north (Papunen et al. 1997, Heikura et al. 2010). According to DigiKP - Bedrock Map of Finland, there are also other small satellite bodies in the N-NW, which, however, have not been confirmed by drilling or bedrock mapping but have been drawn to the bedrock map based on positive aeromagnetic anomalies. The main body has a relatively fresh, non-deformed core, composed of metamorphic olivine rock (komatiitic adcumulate) that is bordered by varying tremolite-serpentine-talc-chlorite-carbonate-olivine-bearing rocks (komatiites and komatiitic basalts) and minor mafic-intermediate volcanic rocks, which are possible differentiates of the komatiitic parental magma (Papunen et al. 1977, Papunen et al. 1997, Heikura et al. 2010). However, also gabbroic dykes not related to komatiitic magmatism are found (Heikura et al. 2010). Papunen et al. (1997) and Heikura et al. (2010) considered the mainly body as a lava conduit/channel through which large volumes of komatiitic magma have percolated. Heikura et al. (2010) have obtained a komatiitic parental melt (23 wt.% MgO) for the Tulppio body, which is consistent with the recent results by Haapala (in preparation), who calculated a low-MgO komatiitic parental melt of 17.8 wt.% MgO for the Tulppio succession. In contrast, Maier et al. (2013) proposed a magnesian basaltic parental magma (corresponding to the term "komatiitic basaltic parental magma" in this thesis) for the Tulppio body. Notably, the main body is characterized by somewhat intense quartz veining, which reflects the effect of serpentinization (SiO_2 release from olivines) and indicates that the alteration took place at relatively low depths (Papunen et al. 1977). The Kiimaselkä body consists of similar rocks as the main body (Papunen et al. 1997, Heikura et al. 2010).

In 2005–2009, GTK drilled 24 holes to the Tulppio and the Kiimaselkä bodies (20 to the main body and four to the Kiimaselkä body, in total 2322 meters) and located two PGE-Ni mineralized zones in the main body (Heikura et al. 2010). The eastern mineralization was intersected by drill holes R309 and R316, with a 4-meter thick zone (38.50–42.50 m) of 0.28 wt.% Ni and 0.36 wt.% S and a 6-meter thick zone (91.25–97.25 m) with 0.25 ppm Pd+Pt, 0.14 wt.% Ni and 1.1 wt.% S, respectively. The other mineralized zone was located in the middle of main body and was intersected by several drill holes (R319–320, R323 and R325–326). The best intersections were a 3-meter thick zone (71.90–74.90 m) with 1.1 ppm Pd+Pt, 0.49 wt.% Ni and 0.39 wt.% S in DDH R320 and a 24-meter thick zone (26.50–50.50 m) with 0.11 ppm Pd+Pt, 0.33 wt.% Ni and 0.15 wt.% S in DDH R325. This mineralized zone also has a surface outcrop (29.4-VIHU-06: 0.53 wt.% Ni,

58 ppb Pt, 174 ppb Pd and 0.29 wt.% S). Due to the proximity of the Sokli mining concession, GTK studies in Tulppio were ceased in 2009 and it is not known whether these mineralized zones are spatially connected to each other or not (Heikura et al. 2010). The bedrock of the area is poorly exposed in general, hence the intensive drilling.

5.3.5 Iskemävaara-Pultoselkä komatiites

The Iskemävaara-Pultoselkä area comprises an approximately 20 km long, SW-trending "finger" in TVB, located south from the main Tulppio body (Figures 7 & 8). Lithological assemblage of the area comprises abundant tholeiitic lavas (actinolite-chlorite rocks), with enclosed shreds of komatiitic meso-orthocumulates (tremolite-serpentine rocks and serpentinites). The komatiitic shreds have a clear SW-NE trend and sharp contacts to the tholeiites. The tholeiitic lavas are bordered by Al-mica gneisses in the north and the AGC granitoids in the south (Juopperi 1988, Papunen et al. 1997). Papunen et al. (1997) considers the area to represent a deeper erosional section of the southern Jänesselkä body as the majority of the komatiites are cumulates.

In 1979, a Mo-bearing pyrrhotite-diopside-skarn sample found in the western parts of the area known as Tunturimännikkö aroused Rautaruukki Oy's interest, when they were carrying out a variety of studies in the area. Provenance of the sample was located to a 200–300 m wide tremolite rock sequence within the AGC granitoids. In the same studies, xenoliths of metasedimentary rocks were found in the ultramafic shreds (Tukiainen & Mattila 1979). In 1979–1985, Lapin Malmi Oy conducted studies in the proximity of the Kiimavaarat hills and drilled three DDHs (482 m in total) to a conductive body on the northern slope of the Kiimavaarat hills. However, mainly layers of acidic-basic volcanic/tuffitic rocks with pyrrhotite-rich intercalations of mica gneiss without enrichment in base metals were intersected. Lastly, within the studies in the Kuttusvaarat-Heiniselkä area in 2006–2009, GTK also performed studies in the Iskemävaara area (Heikura et al. 2009) and located Au-Cu-Ag-enriched zones in the contact zones of tholeiitic rocks and komatiites. However, no further studies were conducted.

5.3.6 Petäjä-Saijanvaara komatiites

The Petäjä-Saijanvaara area comprises another south-trending "finger" in TVB, on the southern side of the Sokli carbonatite (Figure 7 & 8). The area has abundant tremolite-serpentine and talc-tremolite-serpentine rocks that represent komatiitic orto- to mesocumulates (Papunen 1976, Papunen et al. 1997). Pyrrhotite dissemination is common, especially in the proximity of the northernmost magnetic anomaly. Also, Mg-tholeiites are found, mainly in the northern parts of the area (Papunen et al. 1997). Törmänen et al. (2009) have noted that the area represents an extrusive komatiitic environment composed of differentiated lava flows. Basically, profound mineral exploration has not been conducted in the area.

5.3.7 Komatiites in the eastern part of the Tulppio belt

Komatiites are rare in the eastern parts of TVB (Figures 7 & 8). The only "major" occurrence is located in the Kynsivaara area, where ca. 600x100-m sized continuous outcrop of heterogeneous ultramafic rock with regular but weak pyrrhotite-pentlandite dissemination is exposed (Papunen 1976). The area is located in the restricted border zone between Finland and Russia. In the Suurkovanselkä area, east from the Petäjä-Saijanvaara area, amphibolites (Mg-tholeiites) and minor gabbroic rocks are well exposed, but the area lacks komatiites. A minor, but beautifully folded komatiite outcrop is located at the northern side of the Hannu Ollin Vaara hill in the northeastern side of the Sokli carbonatite.

5.4 Komatiites within the Ahmatunturi granitoid complex

Komatiites in AGC are restricted to only a few locations (see Figures 7 & 8). The largest occurrence is the Jänesselkä body, located in the northern parts of AGC, only ca. 3 km south from TVB. The body is considered a southern extension of TVB volcanics (Juopperi 1994, Papunen et al. 1997). Smaller komatiitic bodies of Vuonnelo-oja and Tulppionkaitavaara are located on the eastern side of Jänesselkä. In the southern parts of the area, a relatively large Siurujoki body is located close to the contact zones of AGC, CLGB and TSB. In addition, the Ahmatunturi fell area in the southern parts of AGC

countains small (a few tens of meters in diameter) and strongly deformed komatiitic shreds.

5.4.1 Jänesselkä komatiitic body

The bedrock in the Jänesselkä area, especially in the northern parts of the body, is well exposed and characterized by strongly magnetic tremolite-(actinolite)-chlorite rocks, which become more schistose close to contact zones with the surrounding granitoids, and minor quartzites (Mikkola 1941, Papunen et al. 1997).

In contrast to other komatiitic bodies in ELAD, the Jänesselkä body lacks very high-Mg cumulates and is mainly composed of meso-orthocumulates, as well as non-cumulus rocks. Also, evolved pyroxenitic and gabbroic differentiates are present in Jänesselkä (Virransalo 1985, Papunen et al. 1997). Because of the continuous rock association from ultramafic rocks to gabbros, Peltoniemi (1984) originally considered the Jänesselkä body as a gabbro-wehrlite intrusion. On the other hand, Piirainen et al. (1985) and Papunen et al. (1997) have classified the Jänesselkä rocks as Archean komatiites and their mafic differentiates. Their idea is supported by a lava lake environment/emplacement of a subvolcanic intrusion, where the differentiates (cumulates and pyroxenitic-gabbroic rocks) were produced under calm conditions. Based on the rock association, relatively low MgO content compared to komatiites in TVB and relatively lower degree of metamorphism in greenschist facies, Piirainen et al. (1985) sets the Jänesselkä body stratigraphically to uppermost parts of TVB. Haapala (in preparation) has calculated a low-Ti basaltic parental magma (MgO 6.6 wt.%, TiO_2 < 1 wt.%) for the Jänesselkä body. Tepsell (2018) obtained a ca. 2.45 Ga age for the body by U-Pb zircon dating.

In 1987, GTK excavated an exploration trench (040/LVP-87) to the southern part of the complex aiming to reveal contact relations between the ultramafic rocks and the surrounding heterogeneous granite gneisses (Juopperi 1988). Unfortunately, the trench only revealed deformed gneiss, amphibolite and ultramafic rock alternating as layers and clear conclusions from the contact features could not be made. So far, profound exploration has not been conducted in the Jänesselkä area.

5.4.2 Other komatiitic bodies in the Ahmatunturi granitoid complex

The Siurujoki komatiitic body, located in the southwestern parts of AGC is the second largest body within the unit (Figures 7 & 8). The body is located close to two tectonic unconformities: contacts between AGC and TSB, and between AGC and the Paleoporterozoic schists of CLGB. Northern parts of the area belong to the Kaarrerämiä-Kellovuotso bog conservation area. According to the DigiKP - Bedrock map of Finland, the body consists of olivine/serpentine-dominated rocks, which have been classified as peridotites by Papunen (1976). Although no spatial relationship to the Värriöjoki body has been discovered, the Siurujoki body may be connected to Värriöjoki magmatism (Koistinen 1987b).

On the northeastern side of the Jänesselkä body is a relatively small (200x300 m) komatiitic body known as Vuonnelo-oja (Figures 7 & 8). Serpentine-olivine rock of the body is fairly homogeneous and located on a small but strong positive magnetic anomaly (Papunen et al. 1997). In 1996, exploration company Glenmore Highlands Inc. drilled one hole (JÄÄ-073-001, 50.30 m) to the body but found only homogeneous ultramafic rock with varying grain size. The drilling was stopped after a biotite-rich quartzite was intersected at the end of the hole at 48.60 m (Davies 1996).

Approximately 5 km on the southeastern side of the Jänesselkä complex, is located the Tulppionkaitavaara hill, which hosts a well-exposed ca. 800x200 m area of komatiitic rocks (Figure 7). The occurrence is marked by two strong positive magnetic anomalies (Figure 8). The rocks are homogeneous olivine-amphibole-serpentine-chlorite rocks that are partly schistose, but generally barren in terms of sulfides (Papunen 1976).

Scattered and minor occurrences of komatiites are found on the southern side of the Ahmatunturi fell (Figure 7). The characterizing feature in the area is that the outcrops consist of non-magnetic talc-chlorite schists that are enclosed in the surrounding granitoids with sharp contacts. The outcrops are hard to locate, as they are not characterized by strong positive magnetic anomalies (Figure 8).

5.5 Komatiites within the Tuntsa metasedimentary belt

Compared to the ubiquitous metasedimentary rocks, komatiites are not abundant rocks in TSB (see figures 7 & 8). Except for the Värriöjoki komatiitic complex, komatiite occurrences are rather scattered and generally less than 2 km^2 in area. However, after TVB, TSB hosts the most voluminous komatiite magmatism in the study area.

5.5.1 Värriöjoki komatiitic body

The Värriöjoki komatiitic body is located in the southern part of ELAD, in the vicinity of the contact zone of AGC and TSB (figures 7 & 8). It is the largest ultramafic body in the study area and also one of the largest in Finland with approximately 26 m^3 of estimated volume (Lahti et al. 2007, Törmänen et al. 2007). The body consists of four spatially connected blocks: the Värriöjoki block (the main block), the Liessijoki block, the Venehaara block and the Leppäselkä block (Törmänen et al. 2007, Lahti et al. 2007). Also, the abundant small ultramafic bodies located towards the east may possibly be spatially connected to the Värriöjoki complex (Koistinen 1987b). The blocks, except for the Leppäselkä block, are relatively well exposed, even though the terrain in the area is largely boggy and crosscut by the Värriöjoki and Siurujoki river systems. The majority of the main block is located within the Kaarrerämiä-Kellovuotso bog conservation area (Natura 2000). According to Lahti et al. (2007), the depth dimensions for each of the blocks are: the Värriöjoki block 2400 m (in the western parts only < 300 m, though), the Liessijoki block 1500 m, the Venehaara block 1300 m, and for the Leppäselkä only 130 meters.

Lithologically, all blocks consist of medium- to coarse-grained, homogeneous and massive dunitic adcumulate cores, in which, in contrast to the majority of the komatiitic rocks in ELAD, relict magmatic textures are still present. Towards the edges serpentine ± chlorite ± talc-carbonate alteration becomes gradually predominant (Roos 1983, Vuollo 1986, Törmänen et al. 2007). Within the dunitic core of the main body, Vuollo (1986) also highlights minor wehrlite (olivine + clinopyroxene) zones, which microscopically correspond to the dunites but are macroscopically and geochemically different from them.

Ultramafic amphibole-chlorite rocks and mafic gabbroic rocks are found as narrow zones within the serpentinites close to the contact zones (Vuollo 1986, Törmänen et al. 2007). The age of the Värriöjoki body is obscure. Peltoniemi (1984) and Piirainen et al. (1985) considered it as Paleoproterozoic base cumulates of a gabbro-wehrlite association intrusion, which originated from a picritic parental magma. Their idea was supported by Virransalo's (1985) observation that the emplacement of the intrusion caused a contact metamorphic aureole marked by rare occurrences of saussuritic feldspar and chlorite in the surrounding paragneisses. However, according to Vuollo's (1986) comprehensive petrographic and geochemical studies from the main block, the Värriöjoki body rather represents a feeder channel for Paleoproterozoic komatiites. Vuollo (1986) and Haapala (in preparation) have calculated a komatiitic (19.9 wt.% MgO) and komatiitic basaltic parental magmas (12 wt.%) for the body, respectively. In recent studies, the body has been attributed to Archean komatiitic magmatism, because it shares similar geochemistry with the Archean komatiites in the Russian Karelia and Eastern Finland (Juopperi 1994, Törmänen et al. 2009, Makkonen et al. 2017). According to Huhma et al. (2018), Sm-Nd isotope studies imply a major Archean component present in the Värriöjoki system and based on geological setting, a correlation with early Paleoroterozoic ca. 2.44 Ga magmatism should be considered.

During the first drillings of the Värriöjoki komatiitic body by Lapin Malmi in 1982–1983 nine diamond drill holes (567 m in total) were drilled to the main body (Roos 1983). As indicated by previous till sampling (Vuotovesi 1983a), the body was found to be Ni-rich but S-poor, which reflects the affinity of nickel rather to silicates than sulfides. Sulfides were located mainly in the highly altered parts close to the contact zone. However, the studies of Lapin Malmi Oy led to discovery of a small laterite-type Ni-mineralization (Vuotovesi 1984). According to Vuollo (1986) this preglacial regolith is not more than 0.65 m thick and contains up to 2.9 wt.% Ni. However, the Ni-Cr-Co-Zn-enriched layers are usually very thin (< 0.1 m) and discontinuous. Between 2002–2006, GTK investigated the whole Värriöjoki body with detailed geophysical surveys (Lahti et al. 2007) and a 26-DDH drilling program (in total 3209 m) (Törmänen et al. 2007). Similar observations with the studies of Lapin Malmi Oy were again recorded: the body has potential in terms of Ni-Cu-PGE ores, but sulfide-bearing zones are restricted to the altered rocks in the contact zone. Given the size of the body and the present drilling density, the body remains

poorly studied, and discoveries of disseminated ores and/or deep massive ores are still possible (Lahti et al. 2007, Makkonen et al. 2017).

5.5.2 Other komatiitic bodies in the Tuntsa belt

In contrast to the common greenish tremolite-chlorite ± talc rocks that are relatively abundant in TVB, most of the TSB komatiites are olivine-serpentine rocks that represent komatiitic meso-adcumulates, macroscopically comparable to the Tulppio body komatiites. These occurrences are relatively small "plugs", found, e.g., at the Torolehdontyvet hill, on the N-side of Auerma-aapa (place known as Pirunkirkko), on the NW-side of the Kuskoiva fell, at the Veneenvetojänkä bog, at the Venehaaranaapa bog, on the NW-side of the Auermavaara hill and on the SE-side of the Juntterivaara hill (Figures 7 & 8). The occurrences are not more than 1 km^2 in area. Some of the bodies, such as the Juntterivaara body, have lesser ultramafic chlorite-tremolite rocks close to the edges. The rarer amphibole-chlorite-talc-dominated komatiites are found in the southeastern part of Muotkaselkä (possibly connected to the Torolehdontyvet rocks), at the Moukavaara hill, on the northwestern side of the Kuskoivanpahka hill, on the top of the Takkaselkätunturi fell (the "Takka" of the fell), and on the southern side of the Siriortsa hill, which has well-exposed sharp contacts to surrounding paragneiss (figure 7). Typically, these areas also contain abundant mafic volcanic rocks (amphibolites) except for the Moukavaara komatiite occurrence (see DigiKP – Bedrock Map of Finland).

6. MATERIALS AND METHODS

The materials used in this study include re-examined data from the previous studies conducted in ELAD as well as data collected during the new studies conducted within the collaborative research project on the origin, exploration potential, and metallogeny of komatiitic suites of eastern Lapland by GTK and the University of Helsinki (Haapala et al. 2018). Whole-rock geochemistry of komatiitic rocks and mineral chemistry of olivine and spinel are used to assess the Ni-Cu-PGE potential of ELAD. All geochemistry plots have been produced with the help of R programming language-based software Geochemical Data Toolkit (GCDKit, Janoušek et al. 2006).

6.1 Preceding data and data processing

The preceding data set comprises 1781 whole-rock major element analyses (including selected trace elements) and 646 trace element analyses (including trace elements and REE) of a variety of rocks types. Also, polished thin sections from the Värriöjoki and the Tulppio bodies were received for reference materials. The geochemistry data was received in two separate data set combinations. The first, includes data from various projects from 1970's to 2000's obtained from GTK archive, and the other contains data from the University of Turku (UTU) and Outokumpu Oy (OKU) project conducted in 1996–1997 (Papunen et al. 1997). Only the GTK data set included trace element and REE data, as these studies were not performed in the UTU-OKU project. As for the analytical techniques, almost all element concentrations have been determined using X-ray diffraction (XRF) technique. Although the laboratory used for the analyses is dependant on the project, the XRF methods used in Finnish laboratories (e.g., Labtium's 175X used in this project, see section 6.1.8) have been developed on the basis of Rautaruukki Oy's (Raahe laboratory) XRF-methods, which were widely used in the 1980's projects (T. Halkoaho, personal communication). More detailed descriptions on analytical methods of each preceding project data are given in sections 6.1.1–6.1.7.

As for the data processing, the data representing komatiitic rocks was separated from the geochemistry data by rock type name and geochemical criteria of MgO > 10 wt.% and TiO_2 < 1 wt.% (both volatile-free). Also, analyses that fit the above criteria but lacked location (coordinates) or were from the Peuratunturi, Koulumaoiva, or Jäkäläharjut Paleoproterozoic intrusions, were removed from the komatiite data set. Analyses with trace element and REE data were separated from the sorted komatiite data set. From these analyses, samples analyzed before the year 2000 and/or samples, with insufficient data (i.e. more than five of the elements between La-Lu were blank or marked 0) were removed. Consequently, 1135 whole-rock analyses of the preceding data sets represent komatiitic rocks, of which 368 also have appropiate trace element and REE data.

6.1.1 Lapland Nickel project data, University of Turku

In total, 51 samples in the final processed data set were gathered during the Lapland Nickel project (Papunen 1976, Papunen et al. 1977). All samples are grab samples and have been collected in 1975-1976. Samples were analyzed in the Australian Commonwealth Scientific and Industrial Research Organisation (CSIRO) laboratory in Western Australia using the XRF method. Analyzed elements and oxides are are SiO_2, TiO_2, Al_2O_3, $Fe_2O_3^{tot}$, MnO, MgO, CaO, Na_2O, K_2O, P_2O_5, Ba, Ce, Cl, Cr, Co, Cu, Ga, La, Ni, Nb, Pb, S, Sr, V, Y, Zn, and Zr. REE analyses were not performed in this project.

6.1.2 Archean areas project data, University of Oulu

In total, 69 analyses in the final processed data set are from the University of Oulu (OU) project on the Archean areas of Finland (Piirainen et al. 1985). All samples are grab samples and have been collected between 1981-1985. Samples are analyzed in Rautaruukki Oy's laboratory in Raahe using the XRF method X402. Concentrations of SiO_2, TiO_2, Al_2O_3, $Fe_2O_3^{tot}$, MnO, MgO, CaO, Na_2O, K_2O, P_2O_5, Cr, S, Cl, V, Co, Ni, Cu, Zn, As, Rb, Sr, Zr, Mo, and Sn were measured. REE analyses performed in this project are not included in the final REE data set, as they were analyzed before the year 2000.

6.1.3 Värriöjoki data, Lapin Malmi Oy

In total, 70 analyses in the final processed data set are Lapin Malmi Oy's data from the Värriöjoki body published in J. Vuollo's M.Sc. thesis (Vuollo 1986). All samples were collected by minidrill in 1983. Sample length was 0.3 m and they were analyzed in Rautaruukki Oy's laboratory in Raahe by XRF-method X402. Concentrations of SiO_2, TiO_2, Al_2O_3, $Fe_2O_3^{tot}$, MnO, MgO, CaO, Na_2O, K_2O, P_2O_5, Cr, S, Ni, Cu, Zn, Rb, and Sr were measured. Also, FeO contents were obtained separately by titration (Vuollo 1986).

6.1.4 Lapland Volcanite project data, GTK

In total, 116 analyses in the final processed data set were collected during GTK's Lapland Volcanite project in 1987–1988 (Manninen et al. 1988, Lehtonen et al. 1997). Samples

include drill core samples (n = 54) and exploration trench samples (n = 59), as well as, three grab samples. The exploration trench samples were analysed in 1987, drill core and grab samples in 1988. All samples were analyzed using XRF-method A5 in the Rautaruukki Oy's Raahe laboratory. Results included oxides and elements SiO_2, Al_2O_3, MgO, CaO, K_2O, Na_2O, P, S, Fe, Ti, V, Cr, Mn, Cu, Ni, Zn, Sr, Zr, and Ba. Also, some samples include data analyzed by instrumental neutron activation analysis (INAA) method E, in the laboratory of Technical Research Centre of Finland (VTT) in Espoo (As, Rb, Mo, Sn, Au, La & Sm).

6.1.5 Archean bedrock in Eastern Lapland-project data, GTK

Two samples in the final processed data set were collected during this project. Both samples are grab samples and they were analyzed using XRF-method in GTK's laboratory in Espoo. The method was based on the Rautaruukki Oy's Raahe laboratory method A5. Concentrations of SiO_2, TiO_2, Al_2O_3, $Fe_2O_3^{tot}$, MnO, MgO, CaO, Na_2O, K_2O, P_2O_5, Cr, S, Cl, V, Co, Ni, Cu, Zn, As, Rb, Sr, and Zr were received.

6.1.6 Data from 1996–1997 studies, University of Turku & Outokumpu Oy

In total, 108 analyses in the final processed data set were performed during this project. All samples are grab samples and were analyzed using XRF-method at the laboratory of the Technical Research Centre of Finland (VTT) (in 1996 the laboratory was owned by Outokumpu Research Oy) laboratory in Outokumpu. The method was based Rautaruukki Oy's X402 and A5 methods. Concentrations of SiO_2, TiO_2, Al_2O_3, FeO^{tot}, MnO, MgO, CaO, Na_2O, K_2O, Cr_2O_3, P_2O_5, Ni, Co, Cu, Zn, S, Cr, As, Ba, Cl, Rb, Sr, V, Y, Zr, La, Ce, Pb, Sb, Bi, Nb, Sn, W, Th, U, Cs, and Ta were detected for most of the samples. Separate REE analyses were not performed.

6.1.7 Layered igneous complexes in Northern Finland project data, GTK

In total, 388 of the all samples in the final processed data set were analyzed during this project. In addition, 250 of all samples in the final processed Trace element and REE data set derive from this project. All samples are grab samples and were analyzed in GTK's

laboratories using XRF method. The methodology is similar to method 176X used in Labtium Oy today (see section 6.1.8). REE were analysed by ICP-MS in GTK's laboratories. The methodology is similar to Labtium Oy's method 308M.

6.1.8 Ore potential of mafic igneous rocks in Northern Finland-project data, GTK

In total, 331 analyses of major element and 115 analyses of trace element and REE data in the final processed data set derive from this project. Altogether 200 of the major element analyses and 76 of the REE analyses are from drill core. The rest are grab samples. The samples were analysed in Labtium Oy's laboratories by XRF (method 175X) for major elements Pb-fire assay (method 704P) for PGE and Au, carbon analyzer combustion (method 811l) for C, and HF–$HClO_4$ Digestion and Li-metaborate-Na-perborate fusion (method 308M) for the REE.

6.2 New studies and data

Studies on the new samples were conducted during GTK and the University of Helsinki research collaboration project were performed in 6/2017–9/2018. Altogether 56 polished thin sections, 74 major element analyses, 25 REE analyses and 310 mineral chemistry analyses were produced to study The ELAD komatiites. Similar discrimination criteria are applied for the new data as for the preceding data.

6.2.1 Geological mapping of the komatiitic bodies

Bedrock mapping of the komatiitic bodies in the summers of 2017 and 2018 was performed by a field team of three M.Sc. students: Pieti Haapala (PSHA), Henri Höytiä (HMHO) and Johanna Tepsell (JHTE). Positive magnetic anomalies were the main targets of the mapping program, particularly the ones with a poor record of geological and geochemical data were investigated. In addition, non-magnetic extensions of the known bodies in the vicinity of the magnetic anomalies were mapped in search of new komatiite occurrences. Before the mapping, field visits were made to areas with a relatively high amount of pre-existing data, e.g., Kuttusvaarat, Tulppio, and Värriöjoki.

In total, 162 bedrock observations were recorded, and 161 new rock samples collected, mostly from locations not included in the previous databases.

6.2.2 Thin sections

All 56 thin sections were produced (Appendix 1) either in Thin Section Lab in France (http://www.thinsectionlab.com/index.html) or in GTK's thin section lab in Kuopio. Samples were prepared by the research team at the University of Helsinki by sawing approximately 25 mm x 35 mm x 15 mm pieces of unaltered rock, which were then stored individually in resealable plastic baga and sent to the chosen laboratories. In 2017, 30 thin sections were made in the Thin Section Lab and 12 thin sections, all from the Jänesselkä body, in GTK. Furthermore in 2018, 10 thin sections were produced in the Thin Section Lab, and four in GTK.

6.2.3 Major element and REE geochemistry

In total, 70 whole-rock XRF analyses and 25 REE analyses were performed from collected bedrock samples (Appendix 2) and are included in the final processed data set used in this thesis. All samples were analyzed in Labtium Oy.

Samples were sawed according to lab guidelines by the research team at the University of Helsinki. Weathered crust was removed, and only relatively "fresh" parts, with minor alteration and/or fracturing were chosen for analysis. Samples were stored individually in resealable plastic bags before they were sent to the laboratory. All major element analyses and selected trce element analyses were performed by XRF (method 176X; automated pressed powder pellets with add-ons). Pt, Pd, and Au were obtained by Pb-fire assay (method 705P) with inductively coupled plasma optical emission spectrometry (ICP-OES). Carbon was determined by carbon analyzer combustion technique (method 811L). Further descriptions of the analysis methods and detection limits are available at the Labtium Oy website (https://www.labtium.fi/en/our-services/exploration-and-mining/)

To test the quality of the REE data, the first 10 REE analyses were analyzed from the same powder in two separate labs. In Labtium laboratory, method 308M (ICP-MS by HF–

$HClO_4$ Digestion and Li-metaborate-Na-perborate fusion) was used, and in ALS laboratory the samples were analyzed using ICP-MS Lithium Borate Fusion (ME-MS81) technique. A closer description of the latter can be found on the ALS website (http://www.alsglobal.com/services-and-products/geochemistry/geochemistry-testing-and-analysis/whole-rock-analysis-and-lithogeochemistry). The ALS data turned out to be incoherent and of relatively poor precision (partly due to excessively low detection limits) compared to the Labtium data (Figure 9). Therefore, Labtium Oy was decided to be the principal laboratory for the REE analyses during this project. All REE data presented in this thesis is have been analyzed in Labtium Oy.

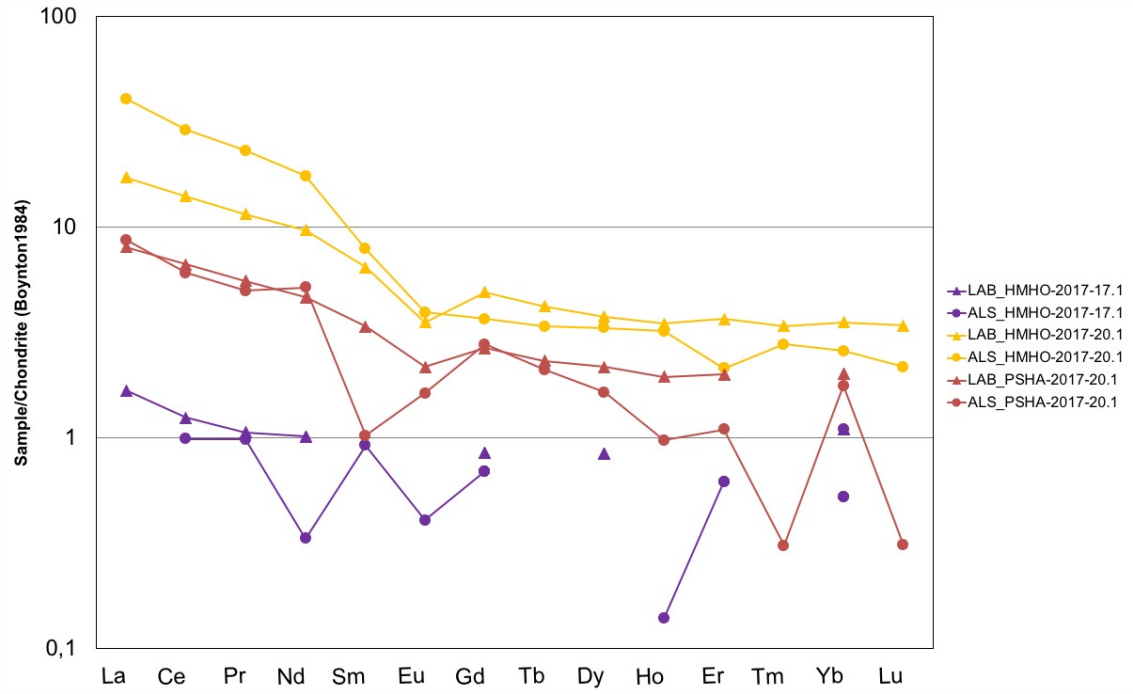

Figure 9. Comparison of the quality of the REE data obtained from Labtium (triangles) and ALS (circles) laboratories. Both laboratories analyzed data from same rock powder of each sample. The ALS data is moreincoherent and less precise, possibly due to excessively low detection limits and differences in methodology, compared to the Labtium data. The Labtium data forms clear largely unspiked trends in the chondrite-normalized REE diagram as normal rocks should. The gaps in the lines mean a value below detection limit.

6.2.4 Mineral chemistry

In order to constrain the exploration potential of the komatiites of ELAD, mineral chemistry of Cr-spinels and olivine was determined. Representative minerals from 10 polished thin sections from different locations (Table 4) were analyzed with electron probe microanalyzer Cameca SX 100 in GTK's laboratory in Espoo (http://en.gtk.fi/research/infrastructure/researchlaboratory/electronoptics.html). Before

the analysis, thin sections were washed with acetone and coated with carbon in JEOL JEE-420 vacuum evaporator. In total, 194 analysis points from 38 individual grains of Cr-spinel were analysed using 15kV accelerating voltage, 40 nA beam current and 5 µm beam diameter. In order to observe the geochemical effect of possible heterogeneities such as zoning, the grains were analyzed systematically with 1–10 analysis points from the core to the grain boundary. Furthermore, 116 analysis points from 59 individual grains of olivine were analysed using 20 kV accelerating voltage with 60 nA beam current and 1 µm beam diameter. Most of the olivines were measured twice to monitor data quality. Concentrations of SiO_2, CaO, FeO, Cr_2O_3, Al_2O_3, MgO, ZnO, V_2O_3, TiO_2, MnO, and NiO were measured from the Cr-spinels and SiO_2, MgO, CaO, FeO, Al_2O_3, K_2O, CoO, MnO, Cr_2O_3, and NiO were measured from the olivines. Standardization was done on samples using the laboratory's in-house standards.

Table 4. Polished thin sections analyzed with electron probe microanalyzer (EPMA) in GTK's laboratory, Espoo. Olivines were analyzed from all thin sections, chromites and Cr-rich magnetites in all but two.

Thin section ID	Location	Cr-spinel	Olivine
4723-2008-R0318-15.70	Tulppio	X	X
4723-2008-R0318-26.75	Tulppio	X	X
HMHO-2017-11.1	Vuonnelo-oja	X	X
HMHO-2017-20.1	Jänesselkä	X	X
PSHA-2017-26.1	Jänesselkä	X	X
PSHA-2017-14.1	Pirunkirkko	X	X
PSHA-2017-32.1	Torolehdontyvet		X
HMHO-2017-39.1	Värriojoki, Venehaara	X	X
PSHA-2017-36.1	Auermavaara		X
JHTE-2017-25.2	Värriojoki, Venehaara	X	X
JHTE-2017-10.1	Sorvortanselkä	X	X
HMHO-2017-17.1	Heiniselkä	X	X

7. RESULTS

7.1 Geological mapping of the komatiitic bodies

In addition to finding new outcrops in formerly explored areas, previously unrecorded komatiite occurrences were found in a number of places (Figures 10 & 11). Although in the current official bedrock map of the Eastern Lapland Archean domain (see DigiKP – Bedrock Map of Finland) almost all areas with positive magnetic anomalies are marked as ultramafic rocks or ultramafic and mafic volcanic rocks, they were not found in many of those places. Consequently, many positive magnetic anomalies are caused by magnetite-bearing gneisses (Figures 10 & 11). In general, strong and rounded positive anomalies seem to represent ultramafic rocks, whereas strong to weak streak-like anomalies, which often have faded edges, are more likely caused by magnetite-bearing granitoids.

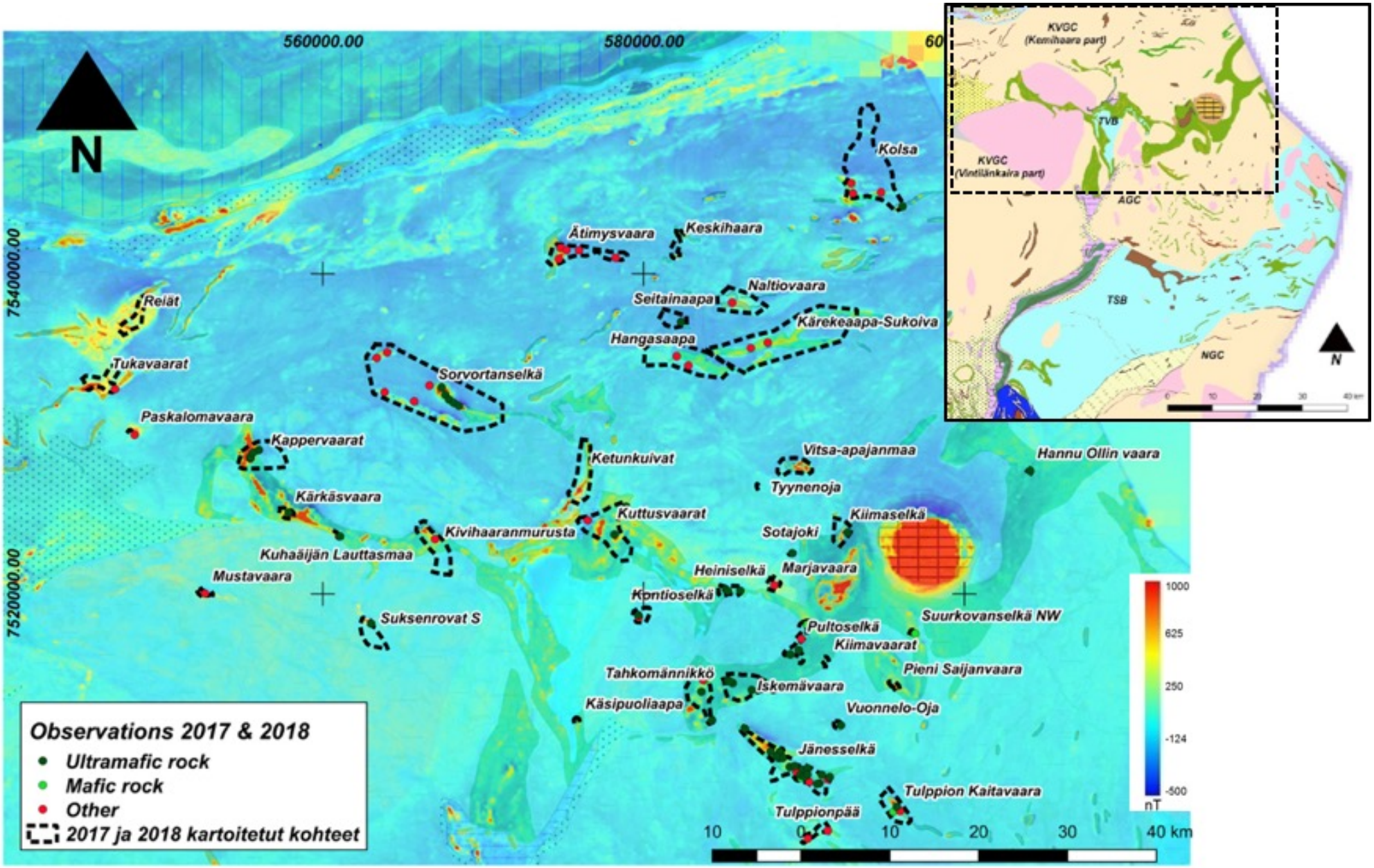

Figure 10. Mapped areas in the northern parts of the Eastern Lapland Archean domain. Simplified lithology of each observation is categorized in different colors. The GTK's national magnetic map is used on the background.

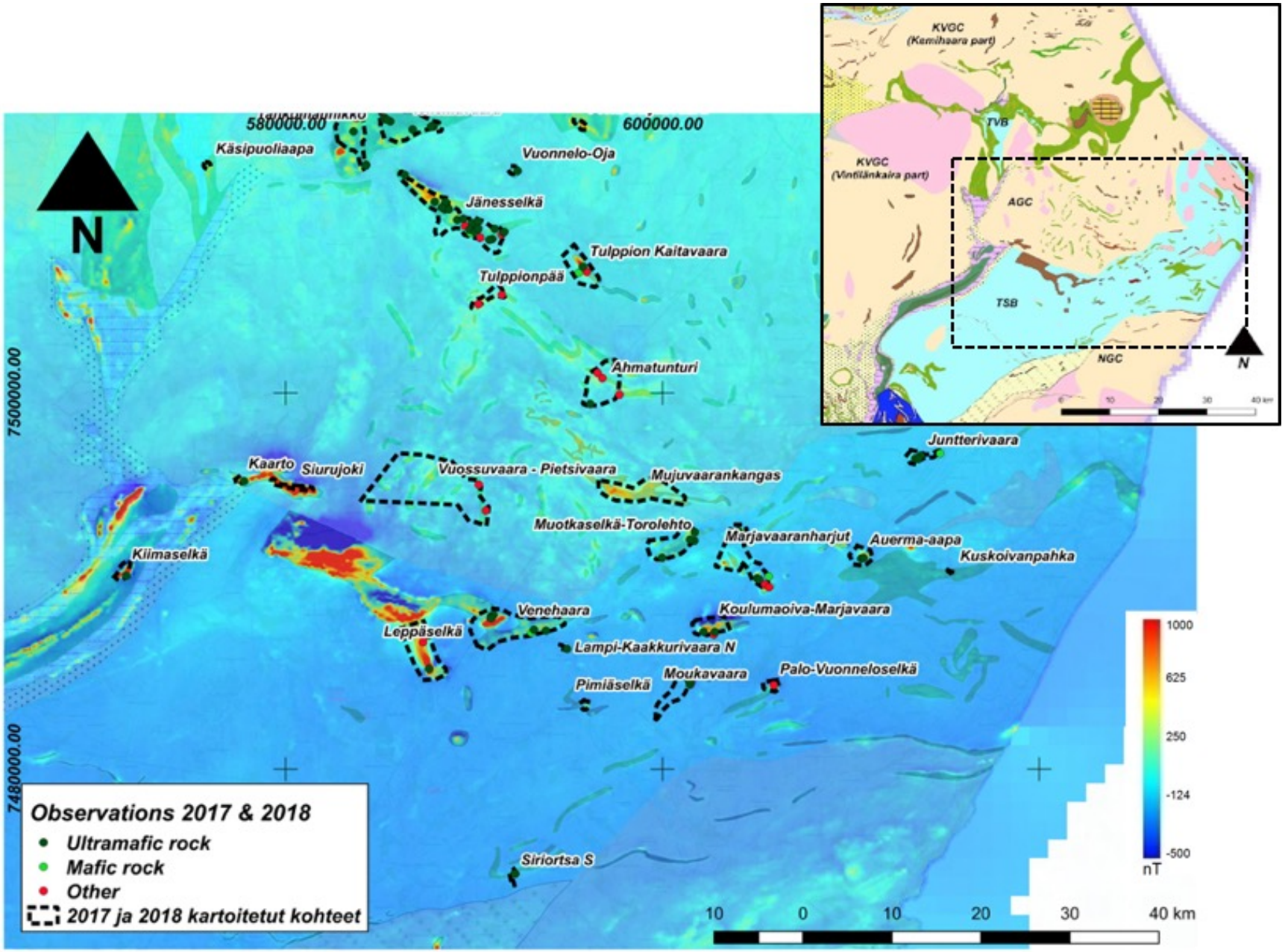

Figure 11. Mapped areas in the southern parts of the Eastern Lapland Archean domain. Simplified lithology of each observation is categorized in different colors. The GTK's national magnetic map is used on the background.

7.1.1 Macroscopic characterization of the komatiites

Komatiites of ELAD can be macroscopically divided into three types: 1) olivine- and serpentine-dominated rocks, which represent komatiitic olivine cumulates, 2) tremolite-dominated rocks, which represent low-MgO komatiitic cumulates and non-cumulate rocks, and 3) chlorite-dominated rocks, which represent low-MgO komatiites and komatiitic basalts. Furthermore, black amphibole (hornblende) and/or plagioclase typically appear in mafic rocks (amphibolites and gabbros). However, the types overlap, as many rocks have only minor olivine and variably amounts of serpentine, tremolite, chlorite and talc. Mostly, metamorphic and deformation features such as folding and penetrative foliation(s) are the dominant textures and structures found in the outcrops (Figure 12). Macroscopically visible magmatic textures were only found in the outcrops of the Värriöjoki komatiitic body (Figure 13).

The olivine-serpentine rocks have brown to grey weathering surfaces, which typically display characteristics patterns, e.g., “elephant skin” pattern (Figure 14) and/or spheroidal weathering (Figure 15). Rarely, metamorphic growth of coarse olivine has produced jackstraw textures (Figure 16), which are found in a few locations in TVB including the Iskemävaara, Kiimavaarat and Tulppio targets. As peculiarities, an olivine-serpentine-dominated rock from the Sorvortanselkä area (JHTE-2017-10) contains rectangular talc-rich “fragments” (Figure 17), and another from the Siurujoki body (JHTE-2018-4) contains metamorphic banding composed of coarse olivine-dominated layers and fine serpentine-dominated layers (Figure 18).

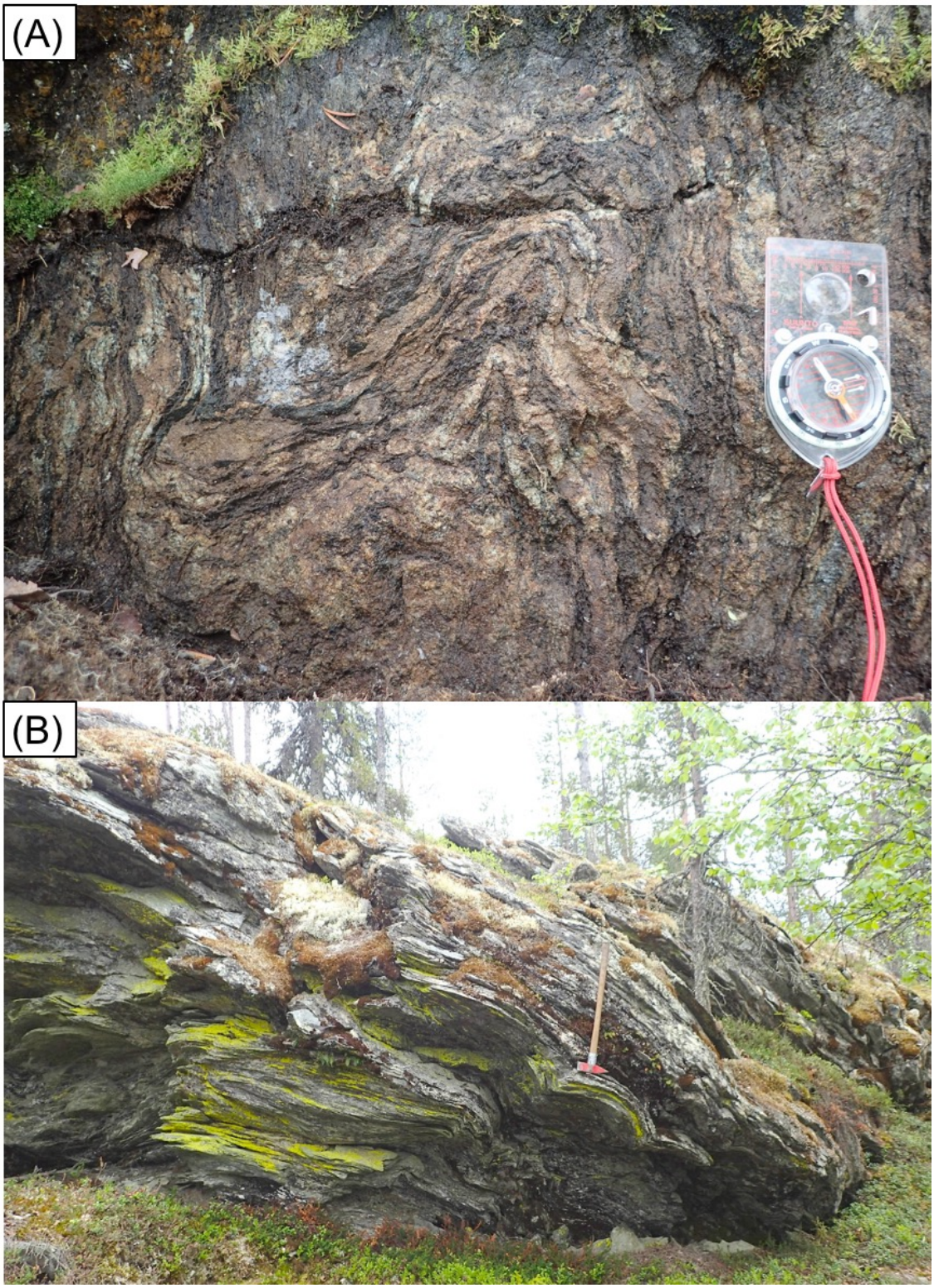

Figure 12. Tight folding in a tremolite-serpentine rock from Hannu Ollin vaara (PSHA-2017-42) in the eastern part of TVB (A). Gentle folding in a chlorite-tremolite schist (PSHA-2017-27) from the Jänesselkä body in AGC (B). Compass (ca. 15 cm) and Rock hammer (90 cm) for scale.

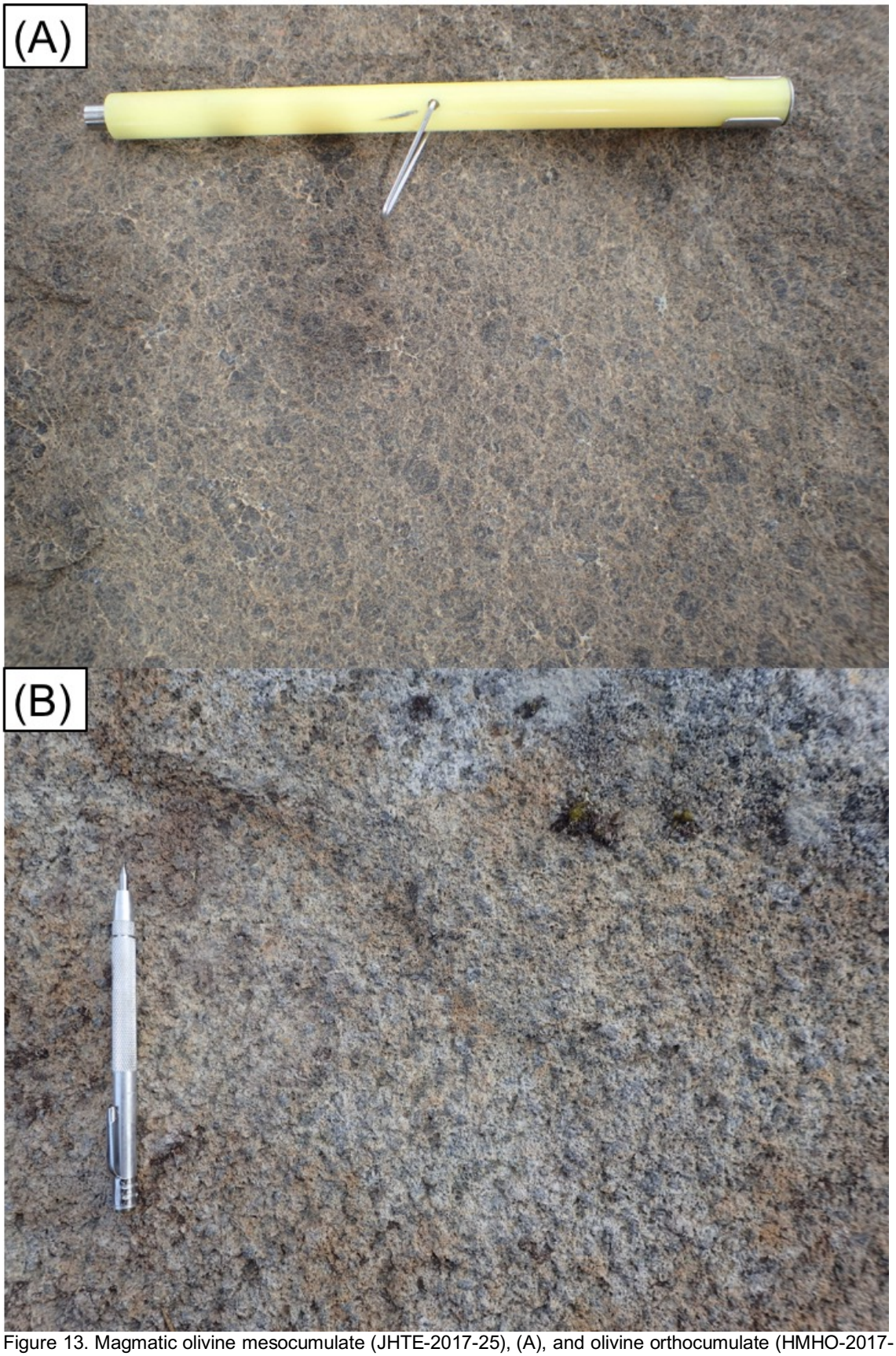

Figure 13. Magmatic olivine mesocumulate (JHTE-2017-25), (A), and olivine orthocumulate (HMHO-2017-38), (B), from the Venehaara block, Värriöjoki komatiitic body. A magnetic pen and a scratcher (both ca. 15 cm in length) for scale.

Figure 14. Schistose elephant-skin weathering pattern in serpentinite (JHTE-2017-18) from the Juntterivaara komatiitic body, Tuntsa belt. Rock hammer (ca. 90 cm in length) for scale.

Figure 15. Spheroidal weathering patterns in serpentinite (HMHO-2017-19.1) from Heiniselkä and tremolite-serpentine rock (HMHO-2018-14) from Kärkäsvaara, Tulppio belt. Rock hammer (ca. 90 cm in lenght) for scale.

Figure 16. Metamorphic jackstraw olivine texture (large “fingers” of serpentinized pseudomorphic olivine) in serpentine-olivine rock (PSHA-2017-7) from Iskemävaara, Tulppio belt. Pen (ca. 13 cm in length) for scale.

Figure 17. Talc-dominated “fragments” on weathering surface of serpentinite (JHTE-2017-10) from the middle body of Sorvortanselkä. Rock hammer (ca. 90 cm in length) for scale.

Figure 18. Metamorphic banding in the Siurujoki body. The red box highlights the location of the lower close-up photo, where discontinuity in the banding is clearly seen in the area marked by black dashed box. Grey layers are serpentine-dominated, whereas brown layers consist of large crystals of metamorphic olivine. The brown layers become unorganized and olivine crystals scatter in the discontinuity area. Ol = olivine. Rock hammer (ca. 90 cm in length) and pen (ca. 13 cm in lenght) for scale.

The tremolite-dominated rocks typically dark greenish to grey weathering surfaces and are easy to recognize because of prevalent acicular tremolite (Figure 19). In some rocks, tremolite comprises most of the rock and forms lepidoblastic textures (Figure 20). Towards chlorite-dominated compositions, komatiites usually become schistose and penetrative foliation is the most dominant feature (Figure 21).

Figure 19. A typical tremolite rock from Kuha Äijän Lauttasmaa (PSHA-2018-9, western part of TVB). The acicular tremolites of a few mm to ca. 2 cm in length along the C-axis can be easily seen by naked eye. Length of the mag pen is ca. 15 cm.

Figure 20. Lepidoblastic tremolite rock (HMHO-2017-47) from the Iskemävaara area, Tulppio belt. Compass (ca. 15 cm in length) for scale.

Figure 21. A talc-chlorite-tremolite schist (HMHO-2017-43) from the Ahmatunturi area. Typical penetrative foliation and some folding are present. Length of the scale box is 5 cm.

7.2 Petrography

Rock types and mineral assemblages in ELAD are metamorphosed and secondary, apart from a couple of exceptions. As preserved cumulate textures have been found in thin sections from the Kolsa area (KVGC), the Tulppio body (TVB) (see Heikura et al. 2010), and the Värriöjoki body (TSB), they can be added to the rock type division outlined in section 6.1.2 as olivine cumulates. Almost all rocks consist of varying amounts of four main minerals: olivine (magmatic or metamorphic), serpentine, tremolite, and chlorite. Magnetitized chromite is the most common oxide, but magnetite and ilmenite are also often present. Sulfides are not rare in komatiitic rocks of ELAD, but their abundance is usually scarce (< 1 %) and grains are small in size (< 200 μm). Weak sulfide dissemination was found in some of the thin sections. Sulfides are present as multiphase grains, in which several different sulfide phases are present. Also, intergrowths with magnetite are present, which reflect desulfurization reactions, where the primary sulfide is replaced by magnetite.

7.2.1 Olivine cumulates

Texturally, four thin sections represent olivine cumulates. One (HMHO-2018-5.1) is from Lakijänkä in the Kolsa-Naltio area in KVGC and other three (JHTE-2017-25.1, JHTE-2017-25.2 and HMHO-2017-39.1) are from the Venehaara block of the Värriöjoki body in TSB. Olivine in these rocks is most likely magmatic. Sulfides were not discovered in these rocks. Sample HMHO-2018-5.1 is a bimodal olivine adcumulate (< 10% of intercumulus material, Barnes 2006) (Figure 22). Olivine is fresh, relatively non-altered and the texture is magmatic. Textural bimodality of the olivine indicates several stages of crystallization. In addition to olivine, cotectic chromite, and secondary magnetite (or magnetitized chromite), as well as, minor serpentine in grain boundaries, are present. Samples JHTE-2017-25.2 and HMHO-2017-39.1 represent magmatic bimodal olivine adcumulates (Figure 23). In these rocks, however, minor clinopyroxene is also present as a cumulus phase as twinned subhedral crystals, which display pale greenish pleochroism. In places serpentine seams crosscut olivine grains. Cotectic chromite and secondary magnetite that replaces chromite, are abundant. Chromite typically has magnetite rims. JHTE-2017-25.2, in contrast to HMHO-2017-39.1, has abundant tremolite in between the grain boundaries. In plane-polarized light, olivines are covered in brownish Fe-pigment, which illustrates the effect of oxidation during dry metamorphism in these rocks. JHTE-2017-25.1 is otherwise similar but a bit more sheared version of JHTE-2017-25.2, which can be seen as decreased grain size (Figure 24).

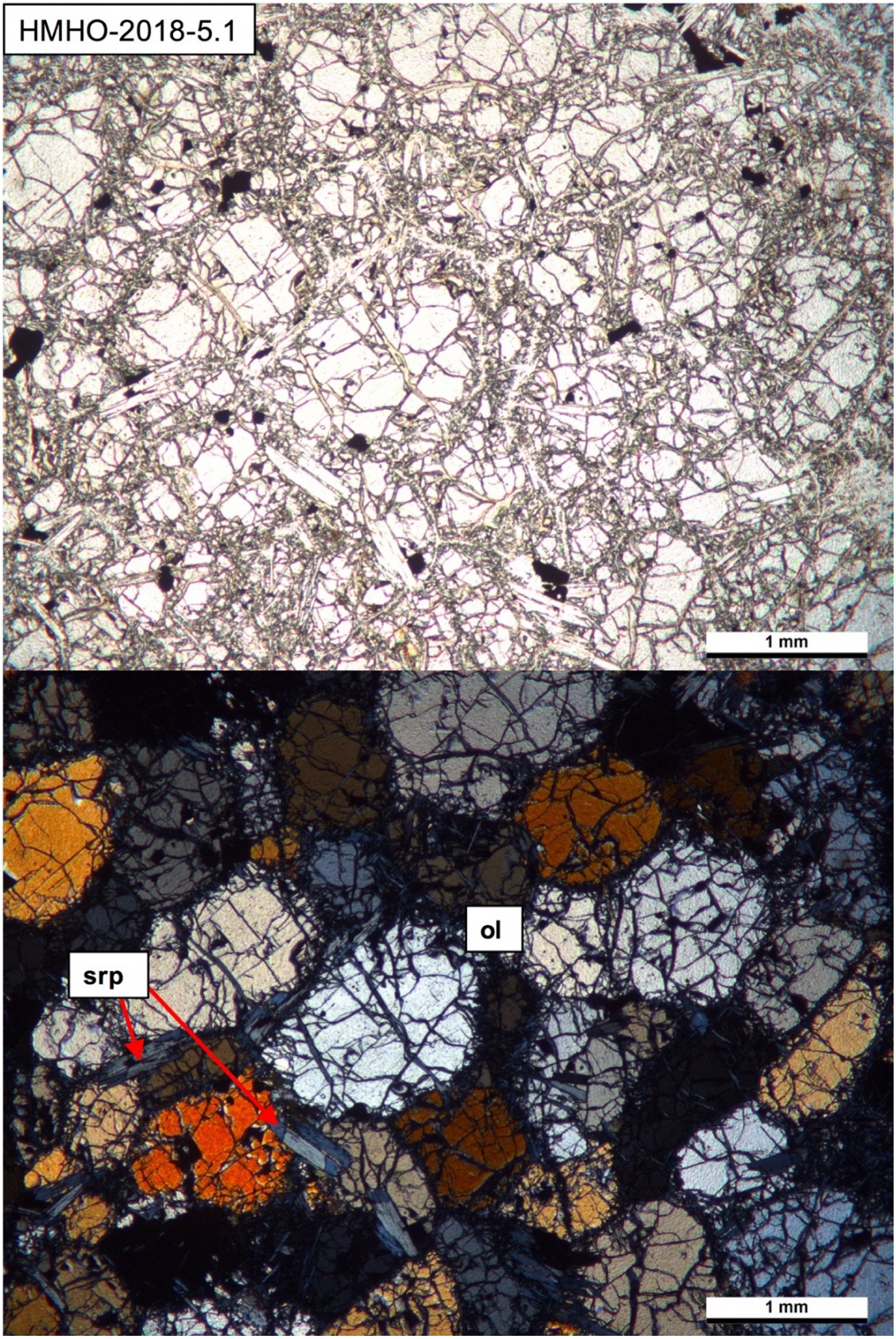

Figure 22. Photomicrograph of bimodal olivine adcumulate from Lakijänkä (HMHO-2018-5.1) in the Kolsa area. Opaque grains are chromites and magnetites, chromite often has magnetite rims. Dark/blueish mush on the olivine grain boundaries is serpentine. Upper image in plane-polarized light, lower in cross-polarized light. Abbreviations: ol = olivine, srp = serpentine.

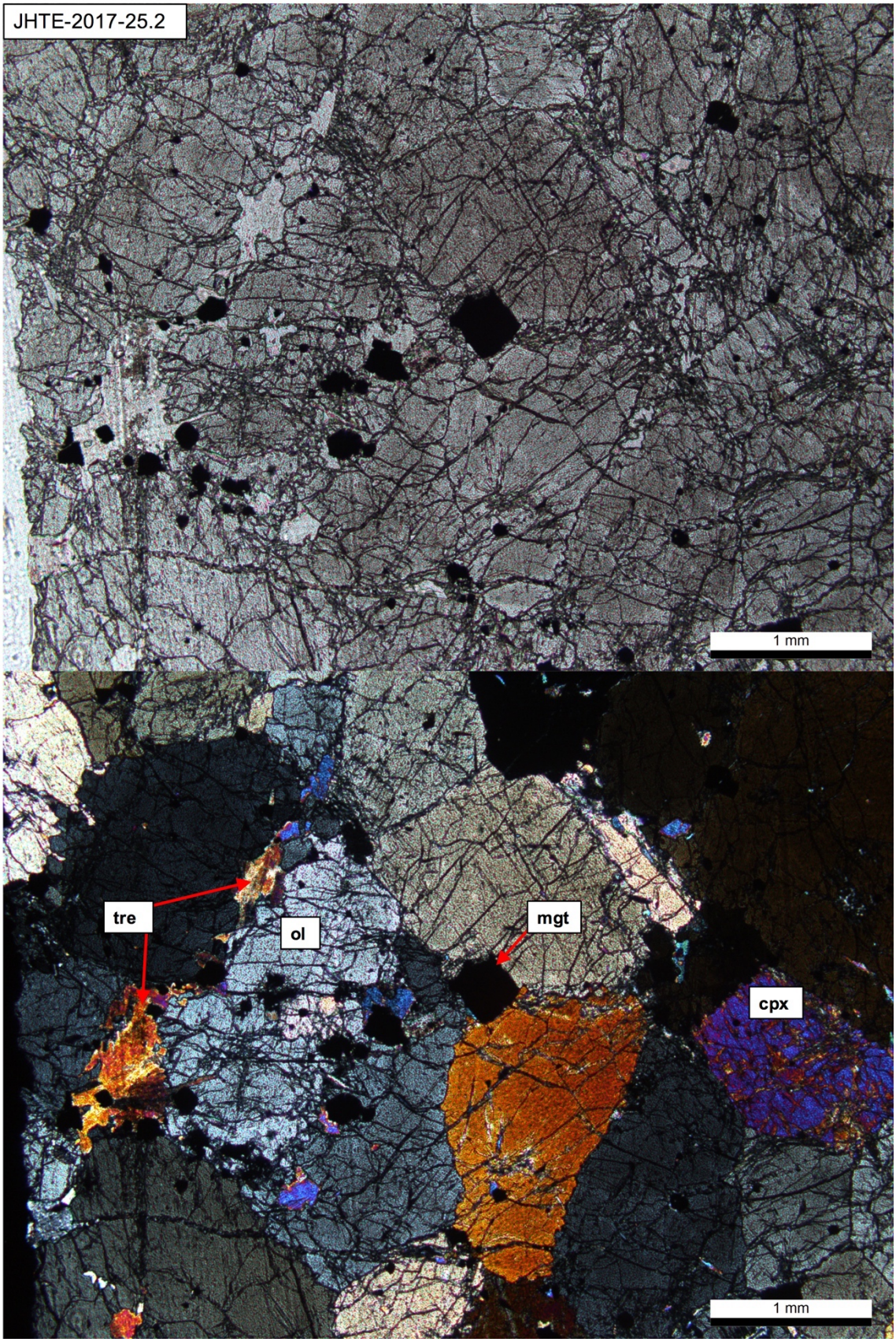

Figure 23. Photomicrograph of bimodal olivine±clinopyroxene adcumulate (JHTE-2017-25.2) from the Venehaara block, Värriöjoki komatiitic body, in TSB. Opaque grains are magnetite and chromite, the latter typically with magnetite rims. Olivine is darkened by Fe-oxidation. Upper image in plane-polarized light, lower in cross-polarized light. Abbreviations: ol = olivine, cpx = clinopyroxene, srp = serpentine, tre = tremolite, mgt = magnetite.

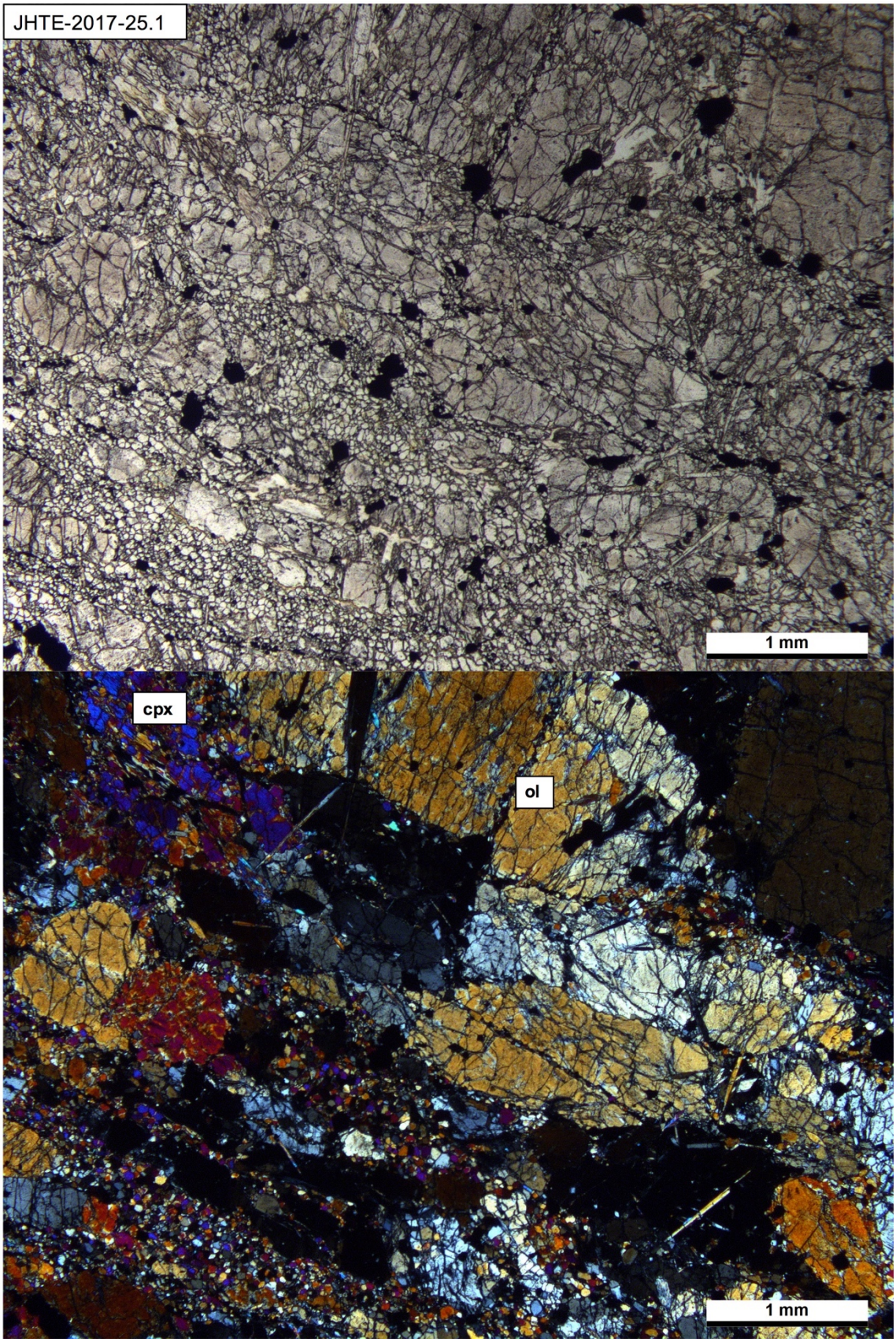

Figure 24. Photomicrograph of bimodal olivine±clinopyroxene adcumulate (JHTE-2017-25.1) from the Venehaara block, Värriöjoki komatiitic body, in TSB. This is a sheared counterpart of the sample JHTE-2017-25.2 (previous figure). Abbreviations: ol = olivine, cpx = clinopyroxene. Upper image in plane-polarized light, lower in cross-polarized light. Abbreviations: ol = olivine, cpx = clinopyroxene.

7.2.2 Olivine/serpentine-dominated rocks

These rocks are diverse and the amounts of olivine, serpentine, and tremolite vary in the mineral assemblage.

As for the olivine-dominated rocks, HMHO-2017-17.1 from the Heiniselkä area and PSHA-2017-7.1 from the Iskemävaara, both from TVB, are composed of large metamorphic crystals of olivine, with only minor serpentine and tremolite (Figure 25). The latter also displays macroscopic jackstraw-texture, with serpentinized olivine pseudomorphs, which is not easily recognized in thin section due to large grain size (several cm).

Most of the rocks in this category have abundant serpentine and tremolite with only minor olivine. For example, JHTE-2017-10.1 from the middle body of Sorvortanselkä is a tremolite-olivine-serpentine rock, where greyish serpentine mush and acicular tremolite crystals dominate (Figure 26). Tremolite seems to have grown on other phases and represents late crystallization in the metamorphic paragenesis. Olivine is found as broken, relatively large grains, which are strongly serpentinized. Accessory talc is also present. Another example is HMHO-2017-1.1 from the Iskemävaara area, where both serpentine and tremolite are abundant but broken small olivine is still present (Figure 27). Olivine in this rock has brownish yellow brucite in their grain boundaries, which can be seen in plane-polarized light.

Curiously, some of the rocks have relict cumulate textures, in which serpentine seams crosscut altered olivine phenocrysts, e.g., PSHA-2017-14.1 & -16.1 (Figure 28) from Pirunkirkko, JHTE-2017-18.1 from Juntterivaara (both from TSB) and HMHO-2017-11.1 from Vuonnelo-oja (AGC) represent these. Texturally these rocks are ortho- and mesocumulates, with serpentine and tremolite found as secondary intercumulus phases.

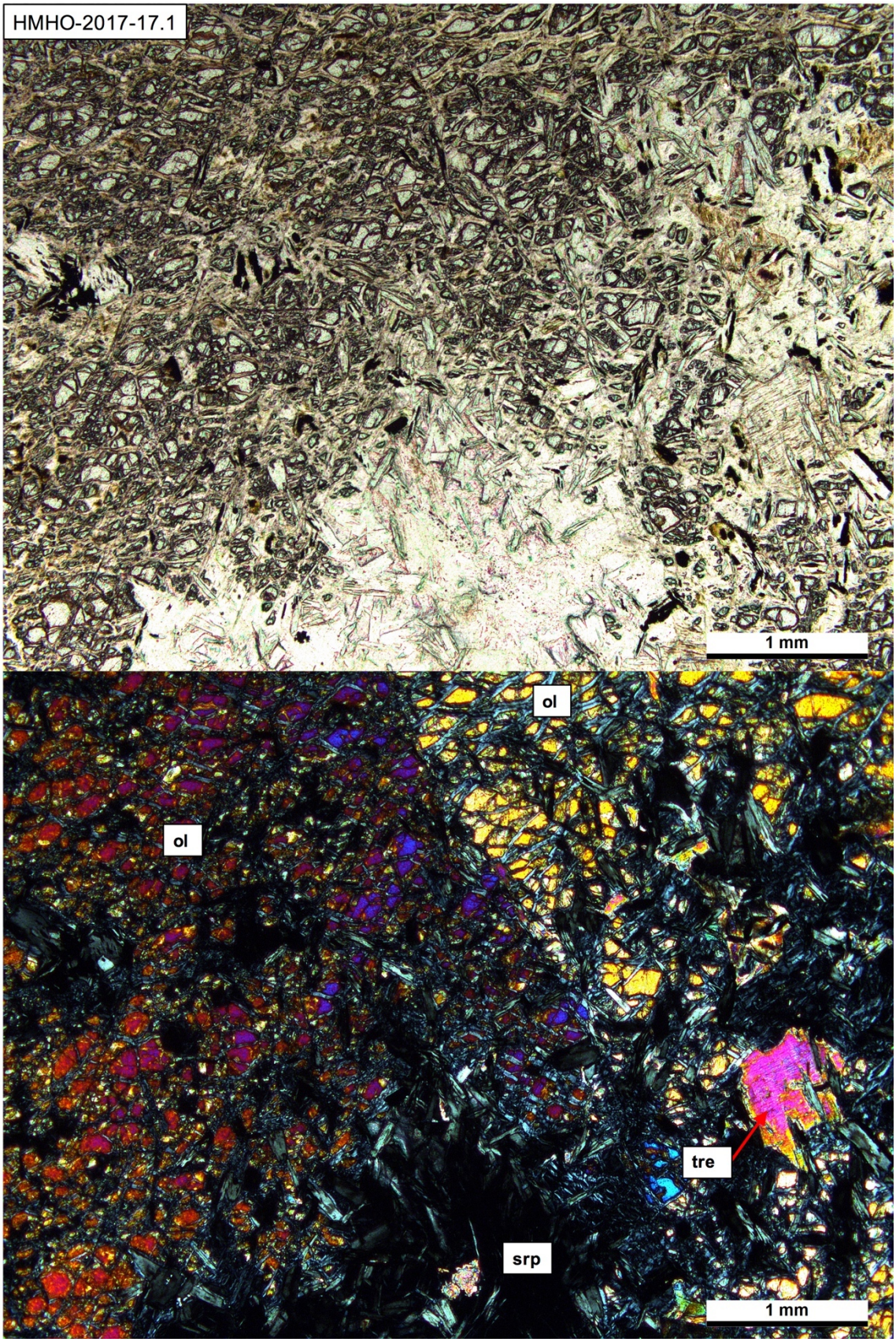

Figure 25. Photomicrograph of olivine rock (HMHO-2017-17.1) from the Heiniselkä area. The rock is characterized by large metamorphic olivine, with only minor serpentine and tremolite. Upper image in plane-polarized light, lower in cross-polarized light. Abbreviations: ol = olivine, srp = serpentine, tre = tremolite.

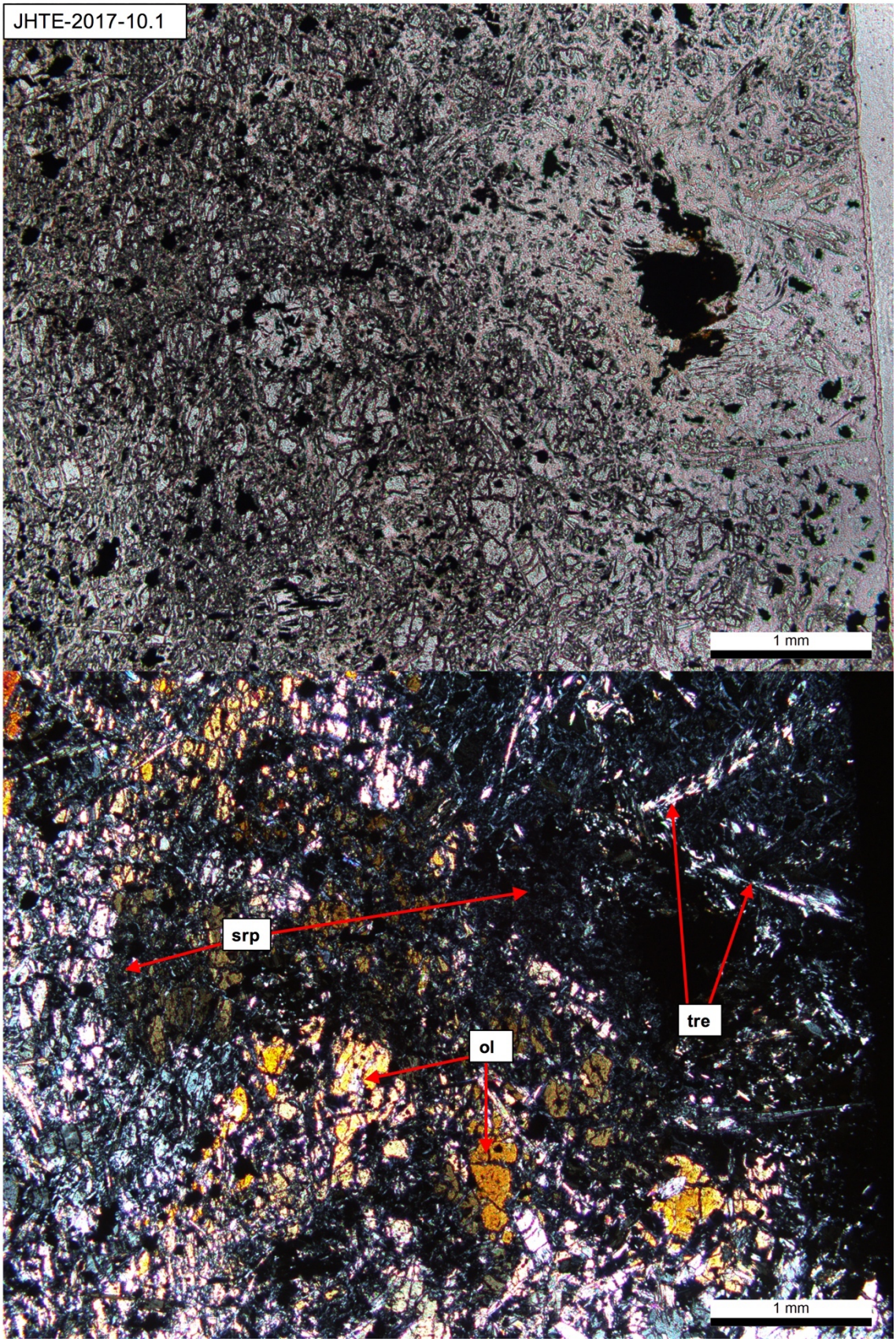

Figure 26. Photomicrograph of a tremolite-olivine-serpentine rock (JHTE-2017-10.1) from the middle body of Sorvortanselkä. Large olivine grain has been altered to serpentine. Tremolite seems to have grown on these phases, representing a late metamorphic crystallization in the paragenesis. Upper image in plane-polarized light, lower in cross-polarized light. Abbreviations: ol = olivine, srp = serpentine, tre = tremolite.

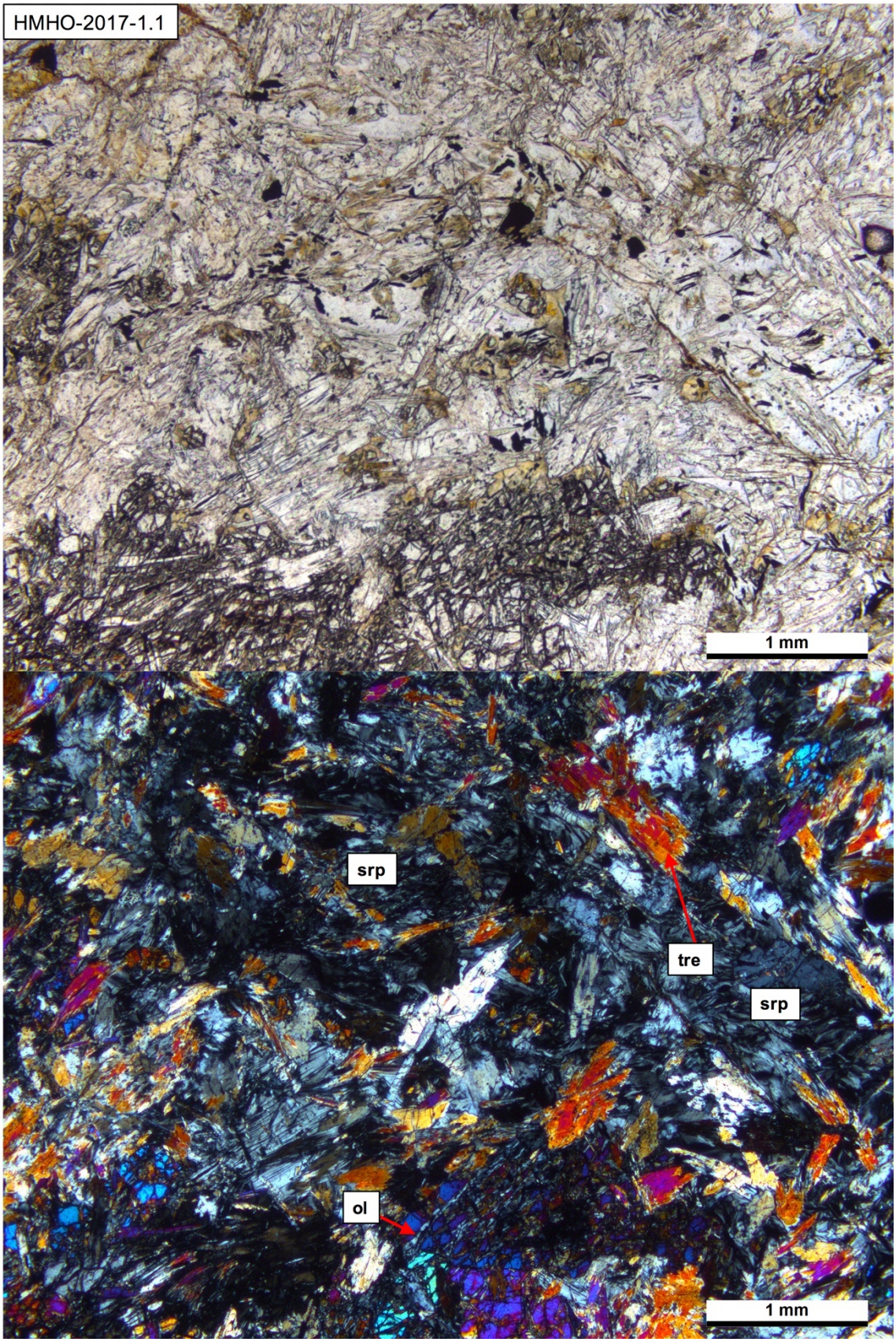

Figure 27. Photomicrograph of olivine-tremolite-serpentine rock (HMHO-2017-1.1) from the Iskemävaara area, Tulppio belt. Tremolite and serpentine are both abundant and olivine is present as relatively small and broken crystals. Yellowish brucite is visible in plane-polarized light. Upper image in plane-polarized light, lower in cross-polarized light. Abbreviations: ol = olivine, srp = serpentine, tre = tremolite.

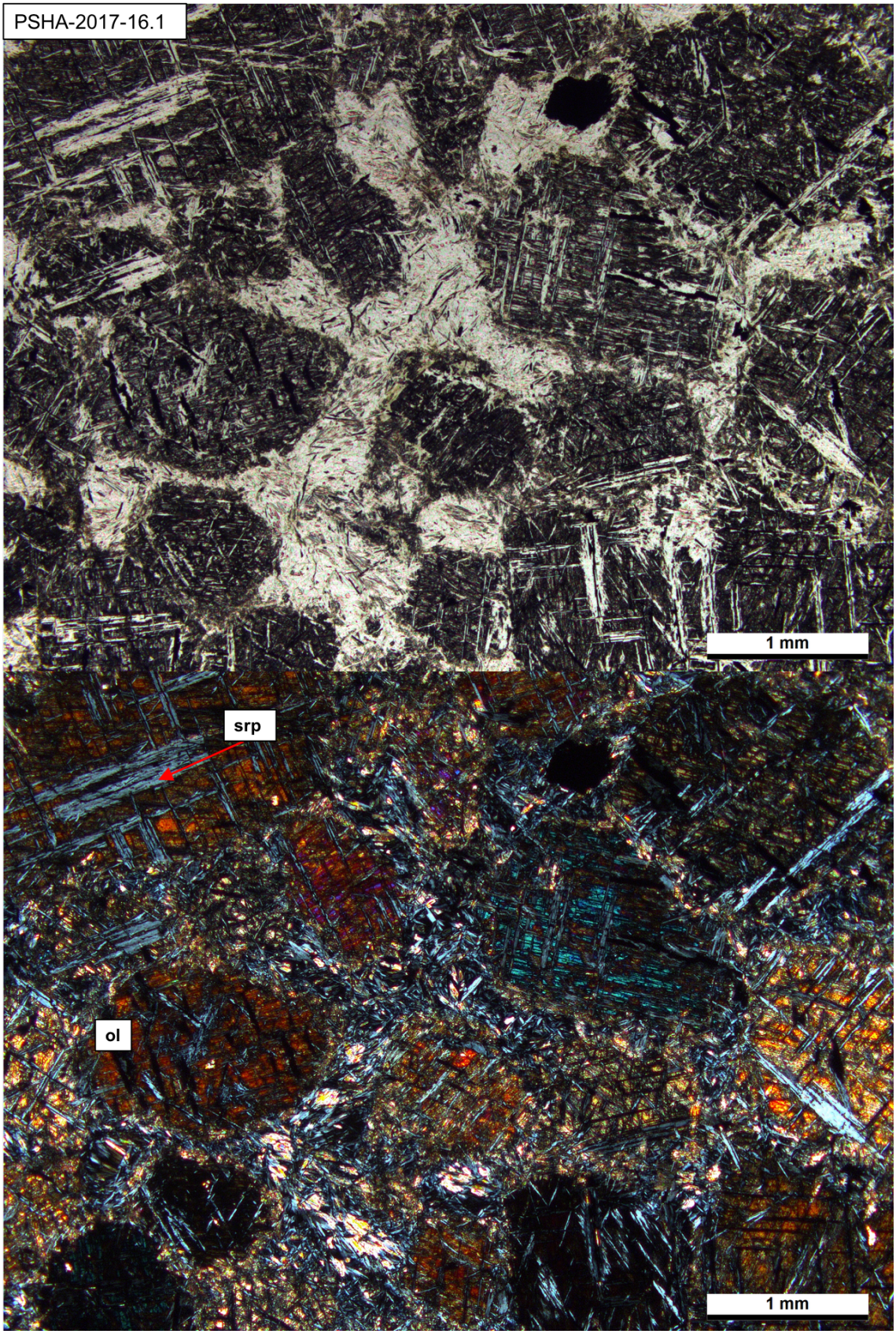

Figure 28. Photomicrograph of a relict olivine orthocumulate (PSHA-2017-16.1) from Pirunkirkko, Tuntsa belt. Olivine grains are crosscut by light bluish serpentine seams. Intercumulus material consists of secondary serpentine + tremolite. Upper image in plane-polarized light, lower in cross-polarized light. Abbreviations: ol = olivine, srp = serpentine.

7.2.3 Tremolite-dominated rocks

Tremolite-dominated rocks are the most common in ELAD. Typically, these rocks lack olivine (although it may be present as an accessory phase) and are composed of varying amount of tremolite, serpentine and chlorite. Also, talc is abundant in some rocks. Opaque minerals are typically magnetite (magnetized chromite) but also ilmenite has been observed.

PSHA-2017-24.2 is a chlorite-serpentine-tremolite rock from Jänesselkä body that shows the typical characteristics of this category (Figure 29). Tremolite is brownish orange, acicular, and forms bundles. Distinguishing between serpentine and chlorite is not always unambiguous in these rocks, albeit chlorite sometimes has greenish pleochroism as in this sample. JHTE-2017-8.1 is a talc-tremolite-serpentine rock and represents a similar type but with abundant talc (Figure 30). Towards the chlorite-dominated rocks serpentine content typically decreases, which is shown by serpentine-chlorite-tremolite schist (JHTE-2017-17.1) from the Juntterivaara body in TSB (Figure 31).

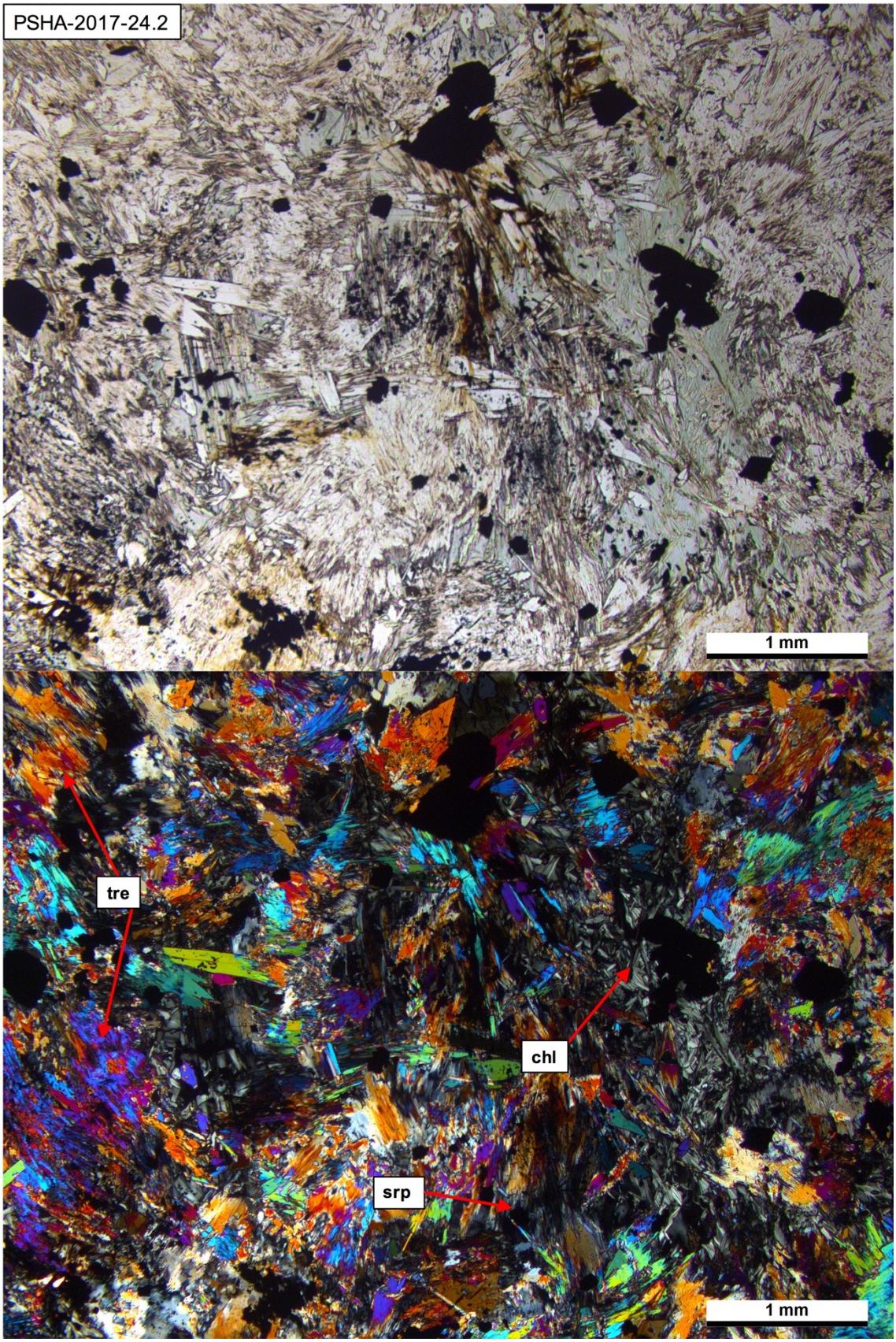

Figure 29. Photomicrograph of chlorite-serpentine-tremolite rock (PSHA-2017-24.2) from the Jänesselkä komatiitic body. The mineral composition of this rock is mainly dominated by brownish orange and acicular tremolite. Serpentine and chlorite are distinguished from each other by the green pleochroism displayed by the latter. Upper image in plane-polarized light, lower in cross-polarized light. Abbreviations: srp = serpentine, tre = tremolite, chl = chlorite.

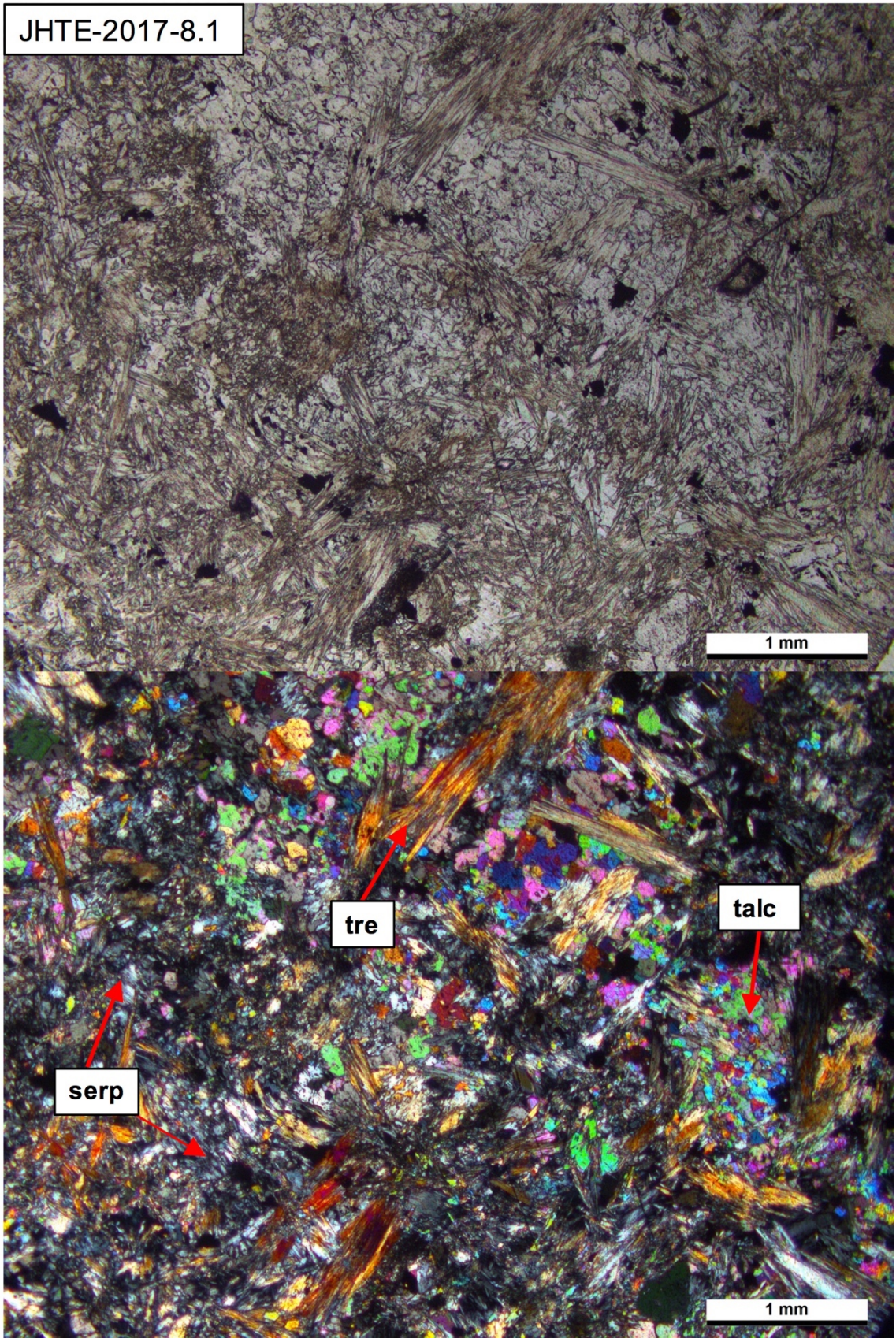

Figure 30. Photomicrograph of talc-tremolite-serpentine rock (JHTE-2017-8.1) from the middle body of Sorvortanselkä. Abundant talc seems to have replaced serpentine. Upper image in plane-polarized light, lower in cross-polarized light. Abbreviations: srp = serpentine, tre = tremolite.

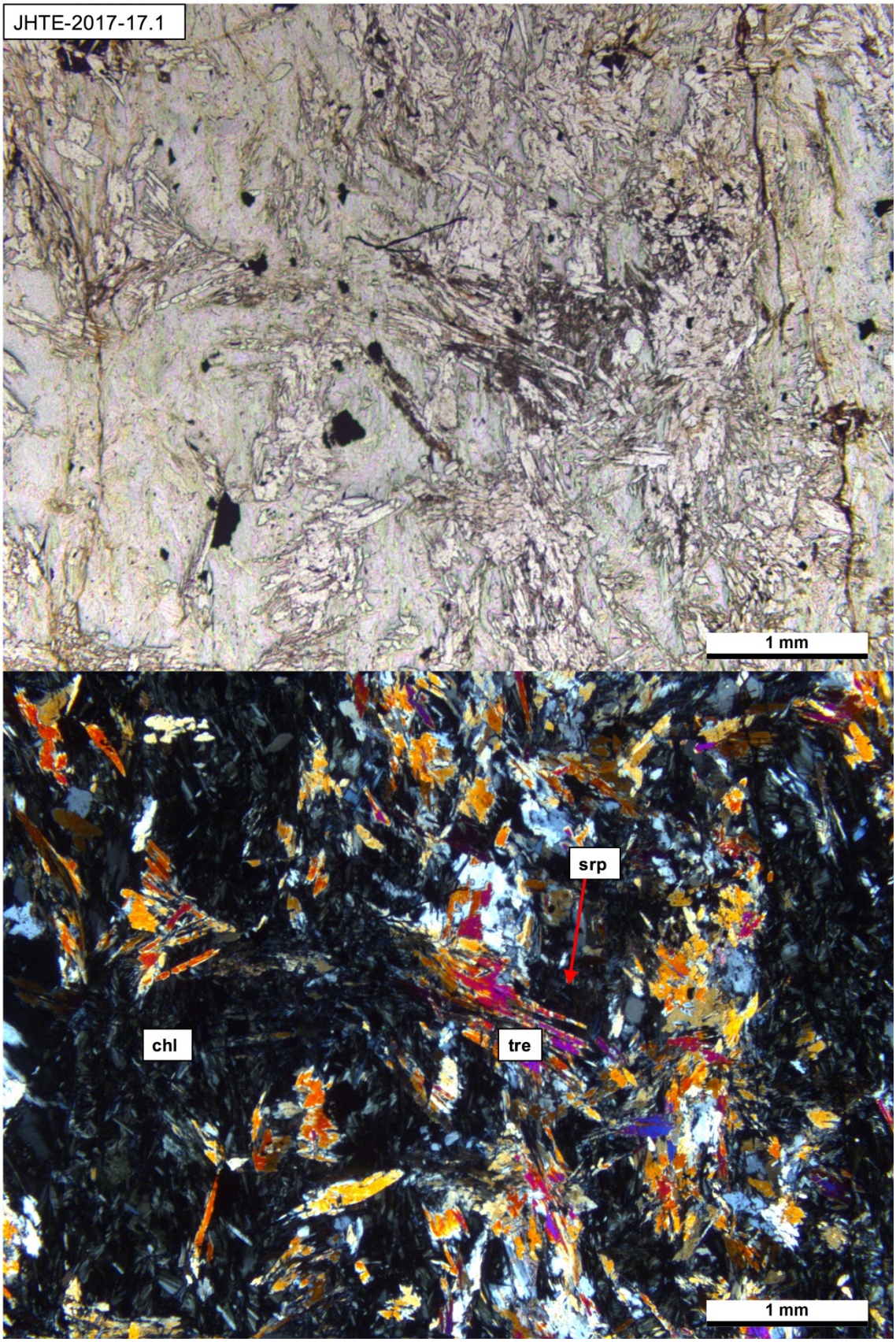

Figure 31. Photomicrograph of serpentine-chlorite-tremolite rock (JHTE-2017-17.1) from the Juntterivaara body, Tuntsa belt. Serpentine and chlorite can be distinguished in the plane-polarized image, in which chlorite shows greenish pleochroism. Upper image in plane-polarized light, lower in cross-polarized light. Abbreviations: srp = serpentine, tre = tremolite, chl = chlorite.

7.2.4 Chlorite-dominated rocks

Chlorite-dominated rocks are usually higly schistose. These schists typically also contain considerable amount of tremolite, which highlights the overlap of classification between the tremolite-dominated and the chlorite-dominated rocks. Some chlorite-dominated high-MgO rocks also contain olivine, whereas in lower MgO rocks only chlorite is present. Most of the chlorite-dominated rocks are found in the Jänesselkä komatiitic body and in the komatiitic bodies of TSB.

JHTE-2017-28.1 from Siriortsa, TSB, is a talc-tremolite-chlorite rock, characterized by penetrative foliation and characteristics of both chlorite-dominated and tremolite-dominated rocks (Figure 32). HMHO-2017-20.1 from the Jänesselkä body is an olivine-bearing chlorite-dominated rock, in which olivine is found as porphyroblasts, and chlorite, together with tremolite forms the fine-grained matrix (Figure 33). HMHO-2017-24.1 from the Jänesselkä complex is a rather evident chlorite rock, with large chlorite porphyroblasts and chlorite-dominated matrix (Figure 34).

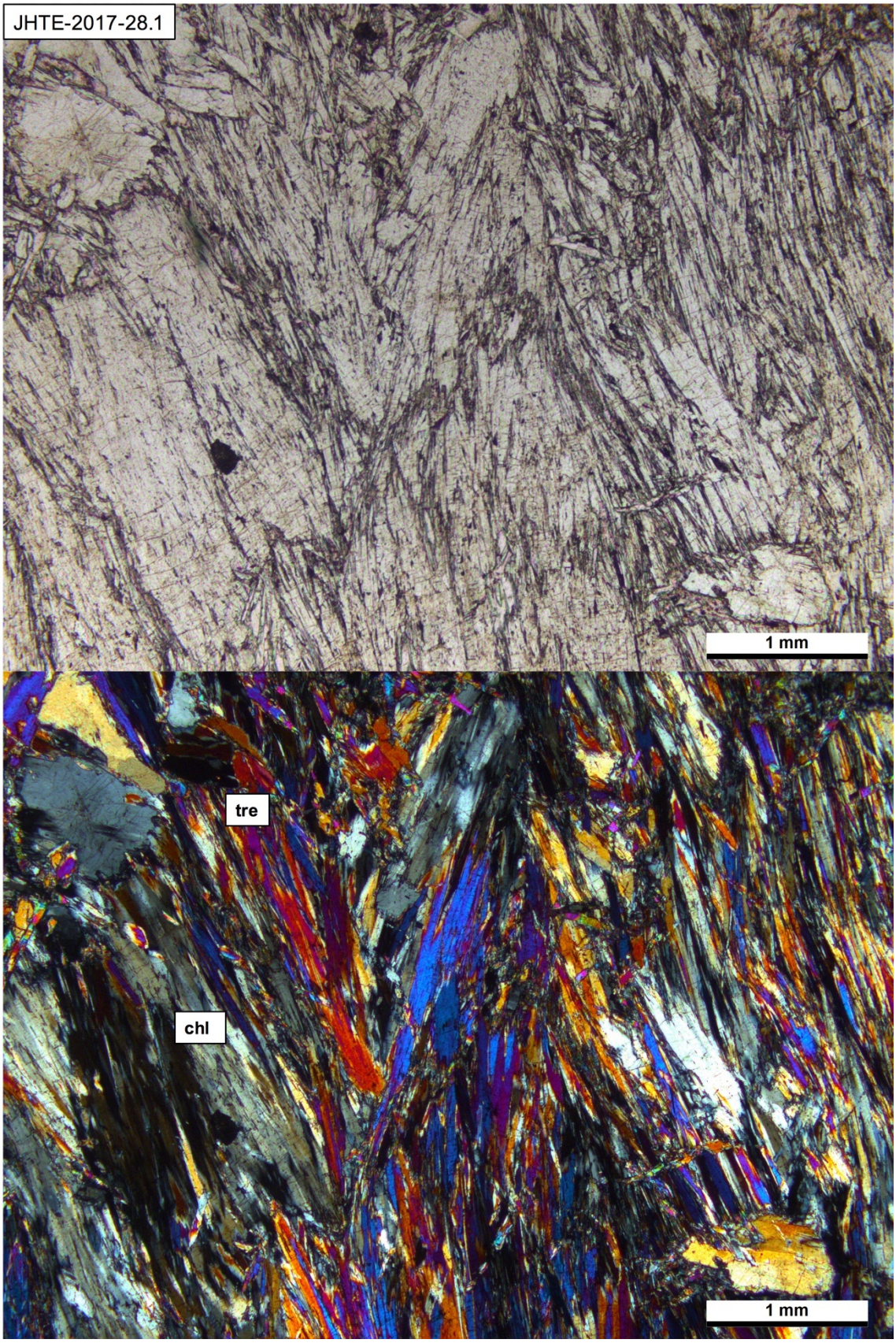

Figure 32. Photomicrograph of chlorite-tremolite rock (JHTE-2017-28.1) from Siriortsa, Tuntsa belt. Paragenesis largely consists of coarse-grained colorful tremolite and grey chlorite. Upper image in plane-polarized light, lower in cross-polarized light. Abbreviations: chl = chlorite, tre = tremolite.

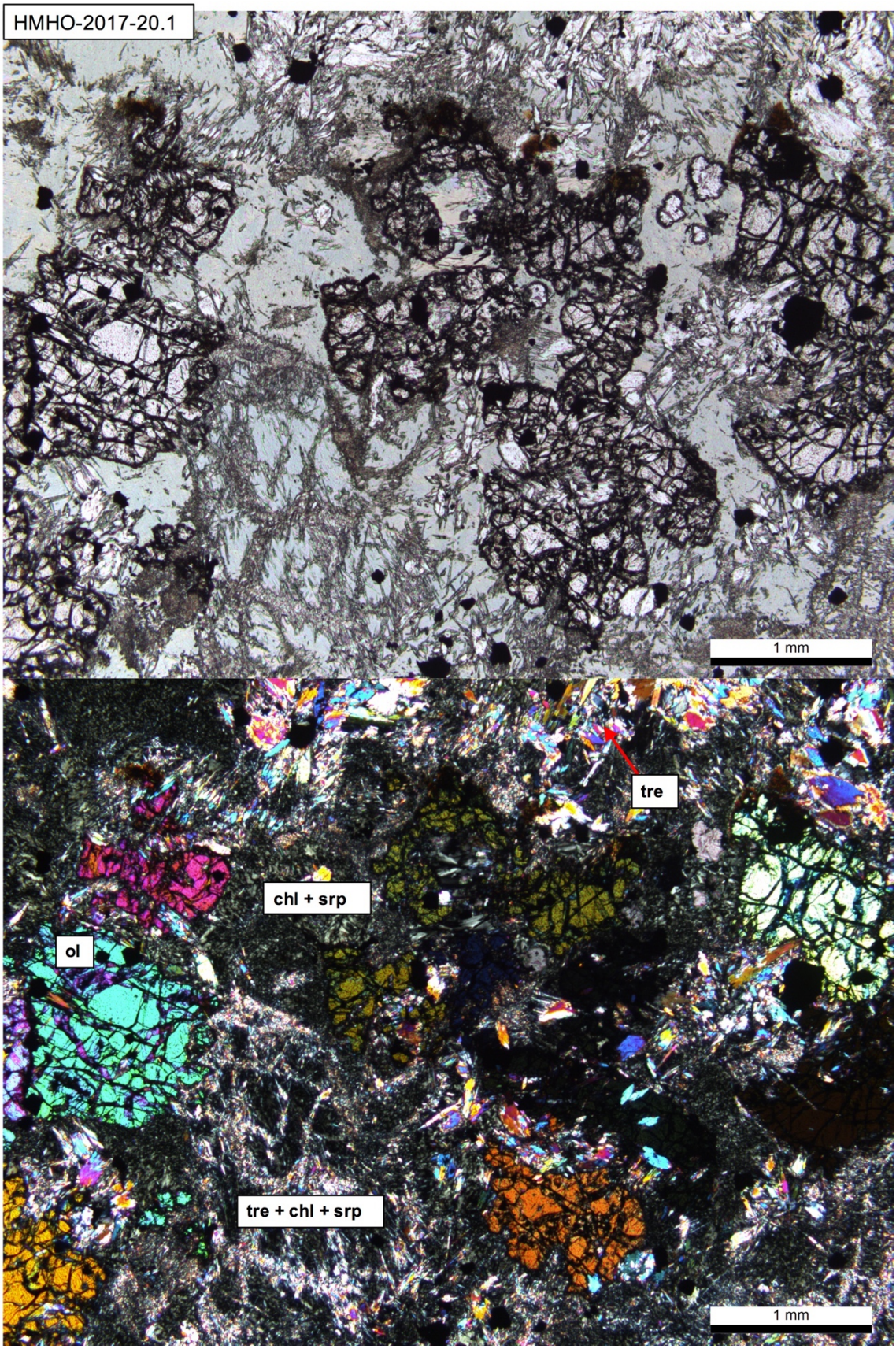

Figure 33. Photomicrograph of olivine-tremolite-chlorite rock (HMHO-2017-20.1) from the Jänesselkä komatiitic body. Olivine is present as porphyroblasts and also chlorite and tremolite porphyroblasts are present. Serpentine-tremolite-chlorite assemblage forms the matrix. Upper image in plane-polarized light, lower in cross-polarized light. Abbreviations: chl = chlorite, tre = tremolite, srp = serpentine, ol = olivine.

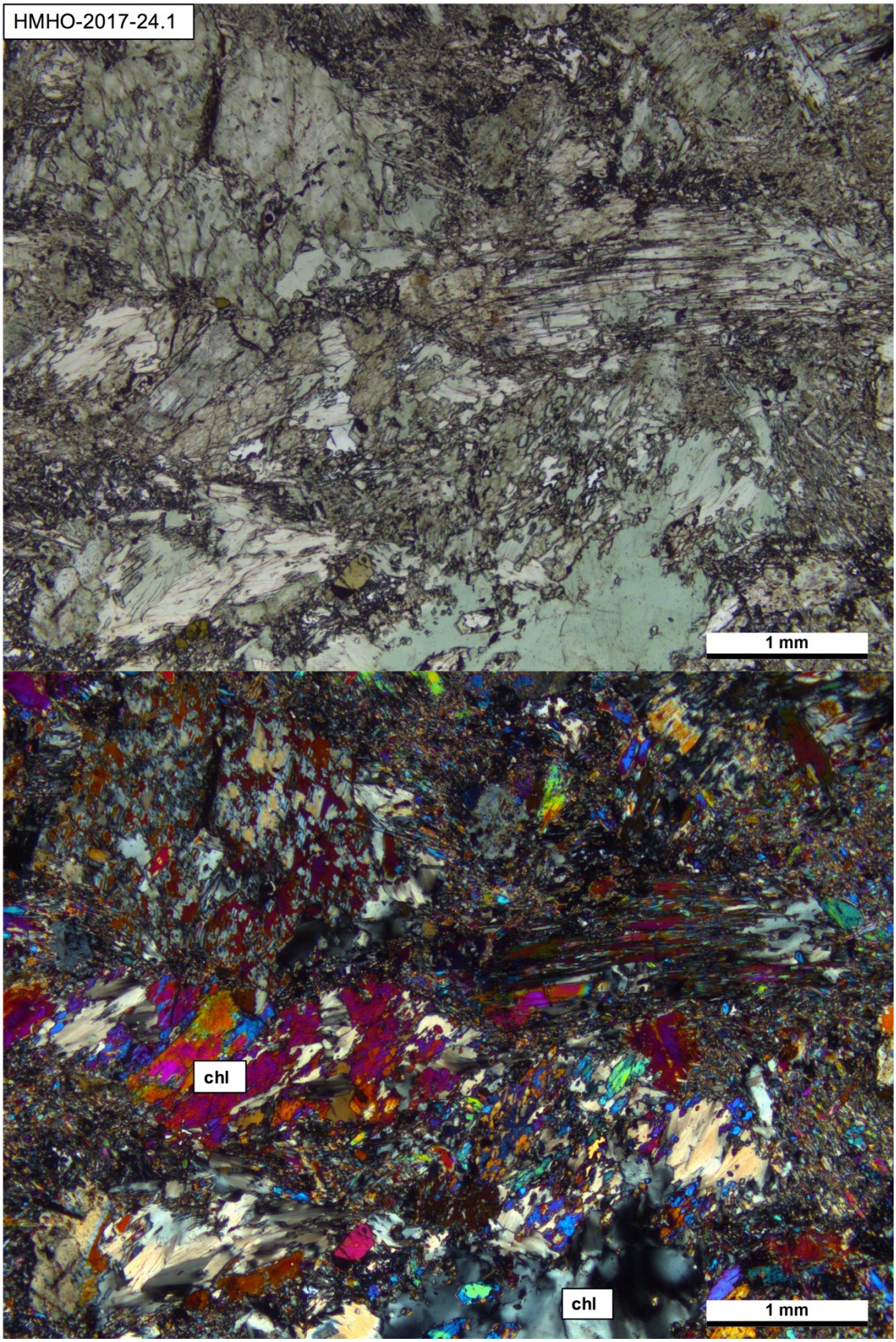

Figure 34. Photomicrograph of chlorite rock (HMHO-2017-24.1) from the Jänesselkä komatiitic body. Chlorite is present as porphyroblasts and in fine-grained matrix. Chlorite clearly replaces an unknown mineral (pyroxene?). Upper image in plane-polarized light, lower in cross-polarized light. Abbreviations: chl = chlorite.

7.2.5 Sulfides

In total, 18/52 of the studied thin sections contain sulfides. Textural types range from traces of small grains to weak and pervasive disseminations (Table 5). Sulfides are often found together with secondary magnetite. Grains consisting of several different sulfide phases, however, are also present. Pyrite and pyrrhotite are the most common sulfides in the komatiites of ELAD, but also pentlandite and chalcopyrite are present in minor quantities. Intergrowths of magnetite, pentlandite, and minor pyrite are common. The grain size of the sulfides is generally around 200–500 μm but also macroscopic sulfides are present.

Table 5. Thin sections, where sulfides were found under reflective light microscope. Trace means one or two individual sulfide grains, Scarce stands for 2–5 individual grains, "weak dissemination" means more than 5 sulfide grains and "pervasive dissemination" means sulfides are found throughout the thin section. Abbreviations: ol = olivine, tre = tremolite, tc = talc, srp = serpentine, hb = hornblende, plg = plagioclase, Py = pyrite, Po = pyrrhotite, Cpy = chalcopyrite, Apy = arsenopyrite, diss. = dissemination.

Thin section ID	Rock type	Target	Sulfide texture	Sulfides
HMHO-2017-11.1	srp-tre-ol rock	Vuonnelo-oja	Trace	Cpy, Po, Py, Pn
HMHO-2017-13.1	ol-tc-srp-tre rock	Tulppionkaitavaara	Weak diss., with mgt	Cpy
HMHO-2017-45.1	ol-tre rock	Moukavaara	Trace, with mgt	Py, Pn
HMHO-2017-46.1	ol-srp-tre rock	Moukavaara	Pervasive diss.	Py, Po, Cpy
HMHO-2018-4.1	hb-plg-qt rock	Petajä-Saijanvaara	Weak diss.	Po, Py, Pn Cpy
JHTE-2017-10.1	tc-tre-ol-srp rock	Sorvortanselka	Scarce, with mgt	Py, Pn
JHTE-2017-18.1	ol-tc-srp rock	Kuskoiva	Trace	Cpy, Py
JHTE-2017-8.1	tc-tre-serp rock	Sorvortanselkä	Pervasive diss.	Py, Po, Cpy, Apy
PS_vaara_1	tre-ol rock	Petajä-Saijanvaara	Pervasive diss.	Py, Po, Pn
PSHA-2017-15.1	ol-tc-srp-tre rock	Kuskoiva	Scarce, with mgt	Py, Pn, Cpy
PSHA-2017-18.1	chl-tre rock	Jänesselkä	Trace, with mgt	Po
PSHA-2017-20.1	tre-chl rock	Jänesselkä	Pervasive diss.	Po, Py, Cpy
PSHA-2017-24.2	chl-srp-tre rock	Jänesselkä	Pervasive diss., with mgt	Py, Po
PSHA-2017-29.1	ol-srp rock	Sorvortanselkä	Weak diss.	Py, Cpy
PSHA-2017-32.2	srp-tre rock	Torolehdontyvet	Weak diss., with mgt	Py, Pn
PSHA-2017-33.2	ol-srp-tre rock	Torolehdontyvet	Pervasive diss., with mgt	Py, Pn, Cpy
PSHA-2017-40.1	ol-srp-chl-tre rock	Torolehdontyvet	Pervasive diss., with mgt	Py, Pn, Cpy
PSHA-2017-42.1	ol-srp-chl-tre rock	Hannu Ollin vaara	Scarce, with mgt	Po, Cpy

As an example, JHTE-2017-8.1 talc-serpentine-tremolite rock from the middle body of Sorvortanselkä (KVGC) has a weak pervasive dissemination of pyrite and pyrrhotite with

minor chalcopyrite and arsenopyrite (Figure 35). Sulfides are found in association with magnetite and as individual grains composed of several different sulfide phases. In contrast, another komatiite from the Sorvortanselkä middle body, a tremolite-olivine-serpentine rock (JHTE-2017-10.1), contains intergrowths of pentlandite and magnetite, which represents oxidation of a primary sulfide by secondary magnetite (Figure 36). An olivine-serpentine-tremolite rock (HMHO-2017-46.1) from the small Moukavaara body (Tuntsa belt), contains a thorough dissemination of pyrite-pyrrhotite-chalcopyrite (Figure 37). Similar dissemination is also observed in tremolite-chlorite rock (PSHA-2017-20.1) from the Jänesselkä komatiitic body (AGC) (Figure 38).

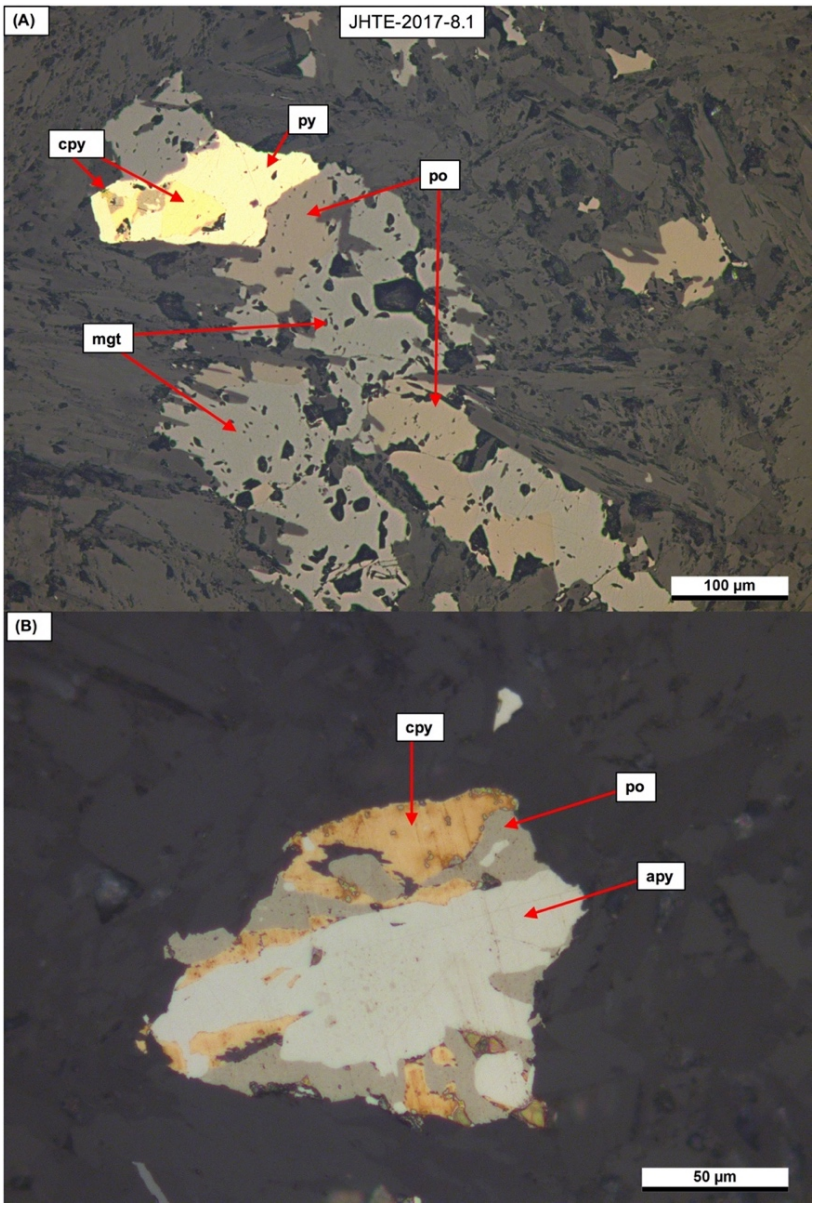

Figure 35. Photomicrograph under reflective lightof sulfides in talc-serpentine-tremolite rock (JHTE-2017-8.1) from the middle body of Sorvortanselkä. Sulfides are present as larger grains together with magnetite (A) and as smaller individual multisulfide alloys (B). Abbreviations: py = pyrite, po = pyrrhotite, cpy = chalcopyrite, apy = arsenopyrite, mgt = magnetite.

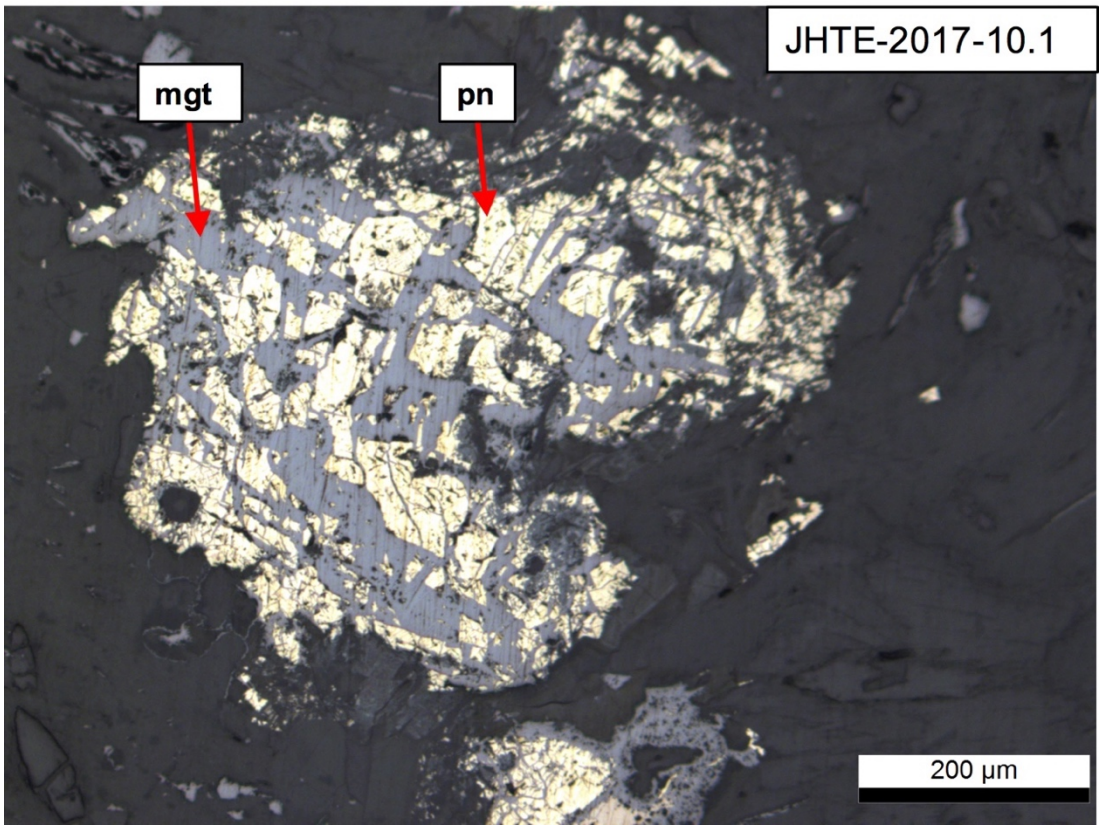

Figure 36. Photomicrograph under reflective light of an oxidized pentlandite grain that is replaced by magnetite in tremolite-olivine-serpentine rock (JHTE-2017-10.1) from the middle body of Sorvortanselkä, Tulppio belt. pn = pentlandite, mgt = magnetite.

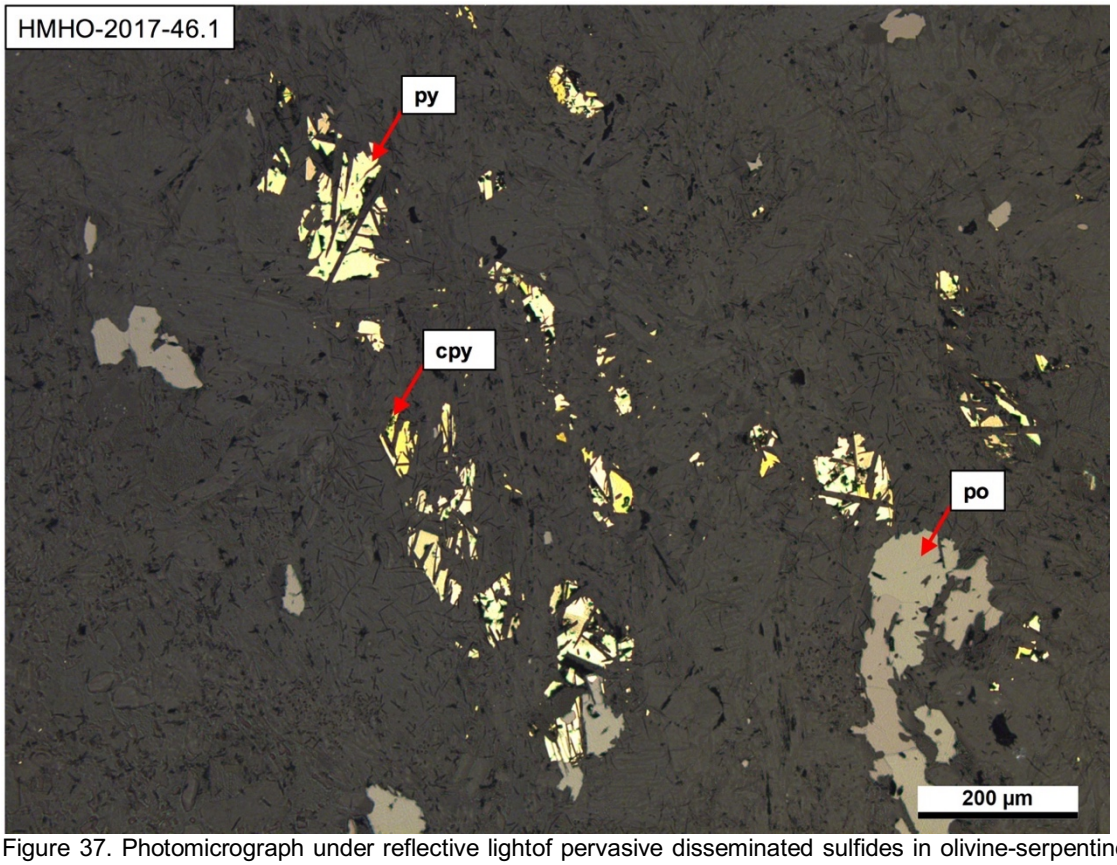

Figure 37. Photomicrograph under reflective lightof pervasive disseminated sulfides in olivine-serpentine-tremolite rock (HMHO-2017-46.1) from the Moukavaara komatiitic body, Tuntsa belt. py = pyrite, po = pyrrhotite, cpy = chalcopyrite.

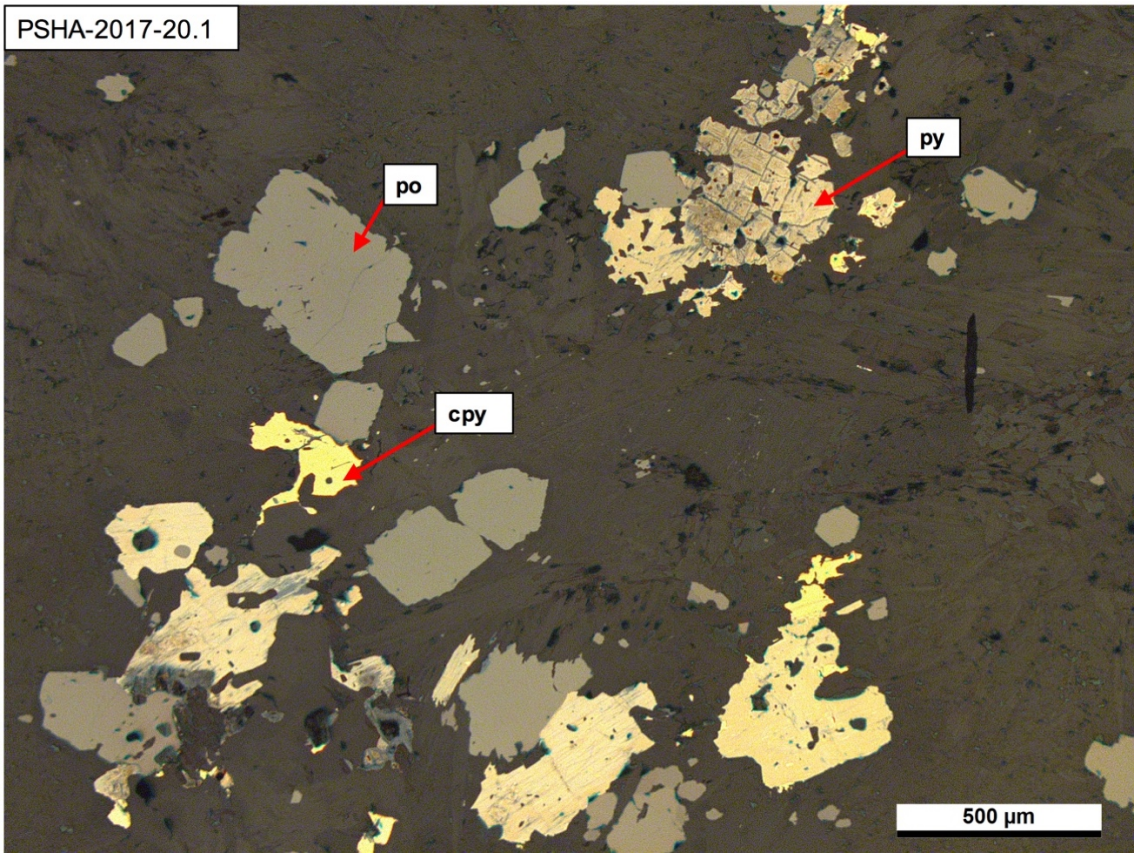

Figure 38. Photomicrograph under reflective lightof pervasive disseminated sulfides in tremolite-chlorite rock (PSHA-2017-20.1) from the Jänesselkä body. Abbreviations: py = pyrite, po = pyrrhotite, cpy = chalcopyrite.

7.3 Geochemistry

In this chapter, the combined and processed data set (see chapter 6) is utilized and plotted according to the lithological unit, defined by the geographical location of each komatiitic body. Furthermore, to constrain komatiite lithofacies, the rocks are divided into cumulates (representing the B-zone), non-cumulus rocks (reprenting liquid compositions and the A-zone) and komatiitic basalts, based on geochemistry (see Makkonen et al. 2017). This division obeys the geochemical criteria as follows: MgO > 28 wt.% = komatiitic cumulates, 28 wt.% > MgO > 18 wt.% = non-cumulus komatiites and MgO < 18 wt.% komatiitic basalts. However, it is important to note that this categorization is not straightforward, as ELAD most possibly hosts cumulates formed from both komatiitic and komatiitic basaltic parental melts. All major element oxides have been normalized to 100 wt.% volatile-free.

7.3.1 Major element geochemistry

Most of The ELAD komatiites are of the AUK-type with Al_2O_3/TiO_2 of 17-30 (Figure 39). Two groups are recognized: TVB and KVGC komatiites have slightly higher Al_2O_3/TiO_2 (> 25) compared to TSB and AGC komatiites, which plot around 18–20. Also, two groups of ADK-type komatiites are present: one with $Al_2O_3/TiO_2 < 10$ and the other with Al_2O_3/TiO_2 10-14. The ADK komatiites are mostly present in TVB. In Al_2O_3/TiO_2-mole proportion diagram (Hanski 1992), most of ELAD data plots close the ADK-AUK division and correspond to Munro-type komatiites. However, in TSB some samples plot in the Ti-enriched AUK field. Also, majority of the Tulppio belt's ADK-type komatiites, actually, plot clearly to the Ti-enriched ADK field. However, also Ti-depleted samples that correspond to boninitic composition are found.

The MgO contents of The ELAD komatiites span from 10 wt.% up to 50 wt.% (Figure 40). The highest MgO contents are found in TSB, TVB and KVGC. TVB, however, contains the whole series of compositions ranging from komatiitic basalt to komatiitic cumulates (MgO 10–50 wt.%). KVGC is characterized by lack of non-cumulus compositions and shows distribution of MgO-contents into two groups with 10–18 and 25–50 wt.%. TSB, on the other hand, lacks komatiitic basalt compositions and has MgO-contents mainly between 25–50 wt.%. The AGC komatiites make their own group with most of the compositions plotting at 25–32 (max. 40) wt.% MgO. SiO_2 contents of The ELAD komatiites largely range between 40–50 wt.%, but scatter is evident in samples having MgO compositions of 18–32 wt.%, particularly in TVB and TSB.

The alkalis (Na_2O & K_2O) show large scatter in all lithotectonic units at MgO contents of 22–50 wt.% but comprise a weak trend at lower MgO contents. In contrast, Al_2O_3, TiO_2 (Figure 41) and CaO show good negative correlation with MgO, especially when it comes to high (> 25 wt.%) MgO contents. However, they scatter at lower MgO contents. Especially in TVB, the scatter is abundant at MgO contents below 35 wt.% and scatter, particularly with TiO_2 at lower MgO contents (< 25 wt.%) is evident. In the other lithotectonic units, olivine fractionation seems to principally control the contents of Al_2O_3, TiO_2 and CaO at a given MgO as they show linear negative correlation.

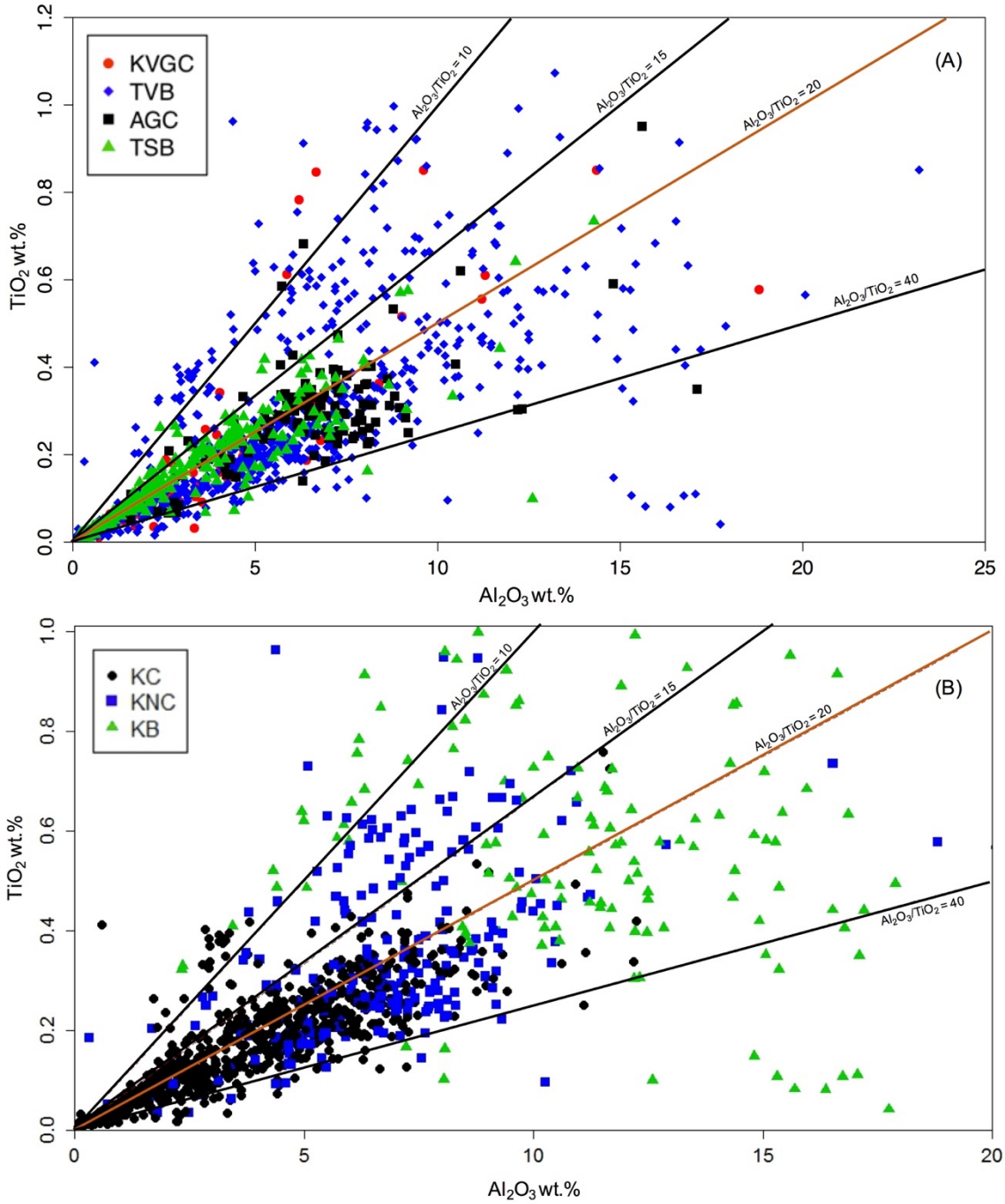

Figure 39. Al_2O_3 vs. TiO_2-diagram of the ELAD komatiites. The reference lines represent Al_2O_3/TiO_2 of 10, 15, 20 and 40. The orange line stands for chondritic value (Al_2O_3/TiO_2 = 20). (A) Samples are categorized on the basis the lithotectonic unit: KVGC (Kemihaara-Vintilänkaira granitoid complex), TVB (Tulppio metavolcanic belt), AGC (Ahmatunturi granitoid complex) and TSB (Tuntsa metasedimentary belt). (B) samples categorized by komatiitic lithofacies: KC = komatiitic cumulate, KNC = komatiitic non-cumulate, and KB = komatiitic basalt.

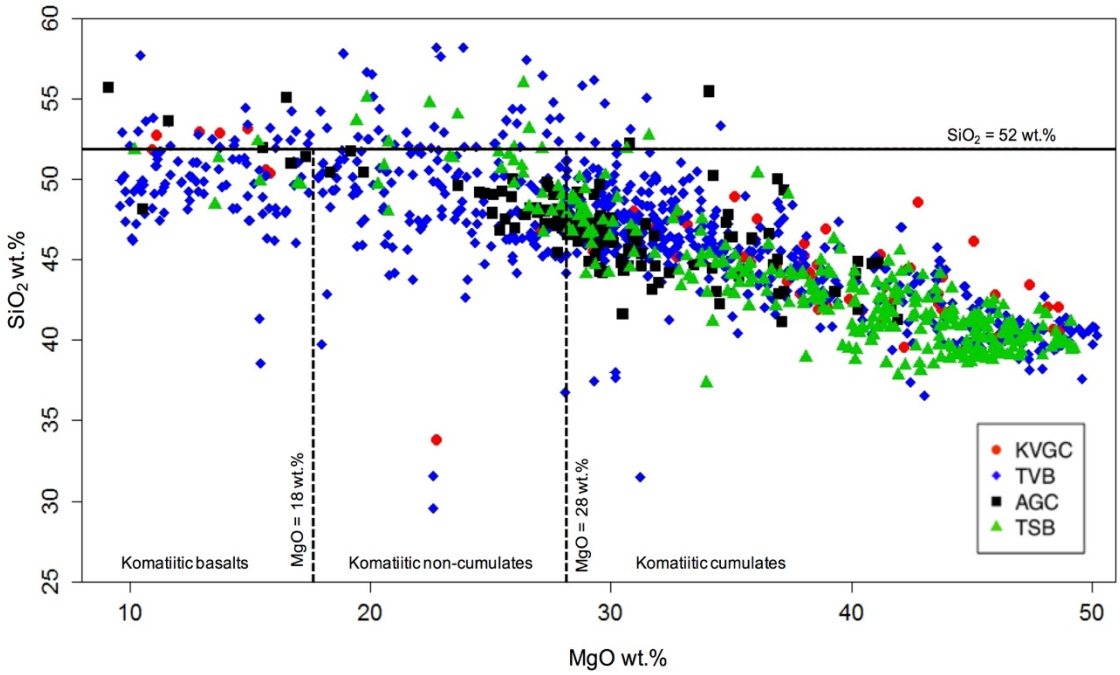

Figure 40. MgO vs. SiO_2-diagram of the ELAD komatiites categorized on the basis of the lithotectonic unit. The solid black line represents the IUGS 52 wt.% SiO_2 upper limit for komatiites (see Le Bas 2000, Le Maitre et al. 2002). The dashed black lines mark the divide to komatiitic basalts, non-cumulus komatiites and cumulates by the MgO content.

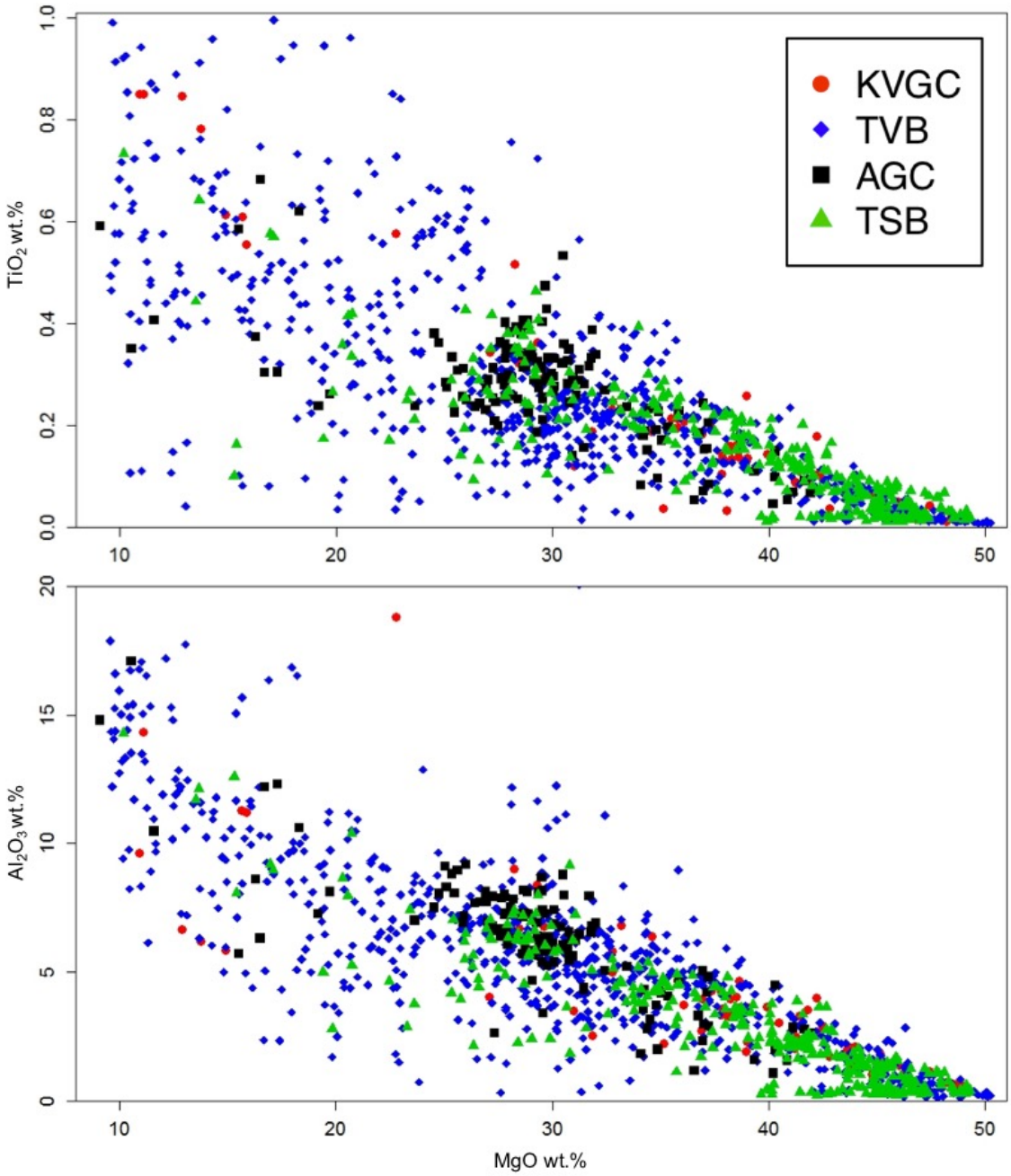

Figure 41. MgO vs. TiO_2 (upper), MgO vs. Al_2O_3 (lower) plots of The ELAD komatiites categorized on the basis of the lithotectonic unit. Both Al_2O_3 and TiO_2 show good correlation at higher MgO contents (MgO > 25 wt.%) but scatter in lower MgO contents, especially in TVB. Abbreviations: KVGC (the Kemihaara-Vintilänkaira granitoid complex), TVB (the Tulppio metavolcanic belt), AGC (the Ahmatunturi granitoid complex) and TSB (the Tuntsa metasedimentary belt)

7.4 Whole-rock geochemistry applied to Ni-Cu-PGE potential

Behavior of chalcophile elements (e.g., Ni and PGE) and Cr, in addition to contamination signals such as enriched LREE, are globally regarded as potential indicators for Ni-Cu-PGE sulfide ores (e.g., Brand 1999, Lesher & Barnes 2009, Fiorentini et al. 2010a, Barnes

& Fiorentini 2012, Konnunaho 2016). Presence of these positive signals allows drawing of indirect conclusions of possible ore-forming processes, even though direct observations of mineralized rocks are limited. In the next sections these features are considered for each lithotectonic unit in light of geochemistry.

7.4.1 The Kemihaara-Vintilänkaira granitoid complex komatiites

The Kemihaara-Vintilänkaira granitoid complex hosts three studied targets: Sorvortanselkä, Kolsa-Naltio and Kärekeoja (Figure 42). In total, 62 samples in the final processed data set represent these targets (Table 6).

Table 6. Distribution of samples between the studied targets in the Kemihaara-Vintilänkaira granitoid complex.

Target	Samples (with REE data)	Cumulates	Non-cumulates	Komatiitic basalts
Kolsa-Naltio	33 (15)	19	1	4
Kärekeoja	24 (20)	24	0	0
Sorvortanselkä	5 (2)	4	1	0
In total	62 (37)	47	2	4

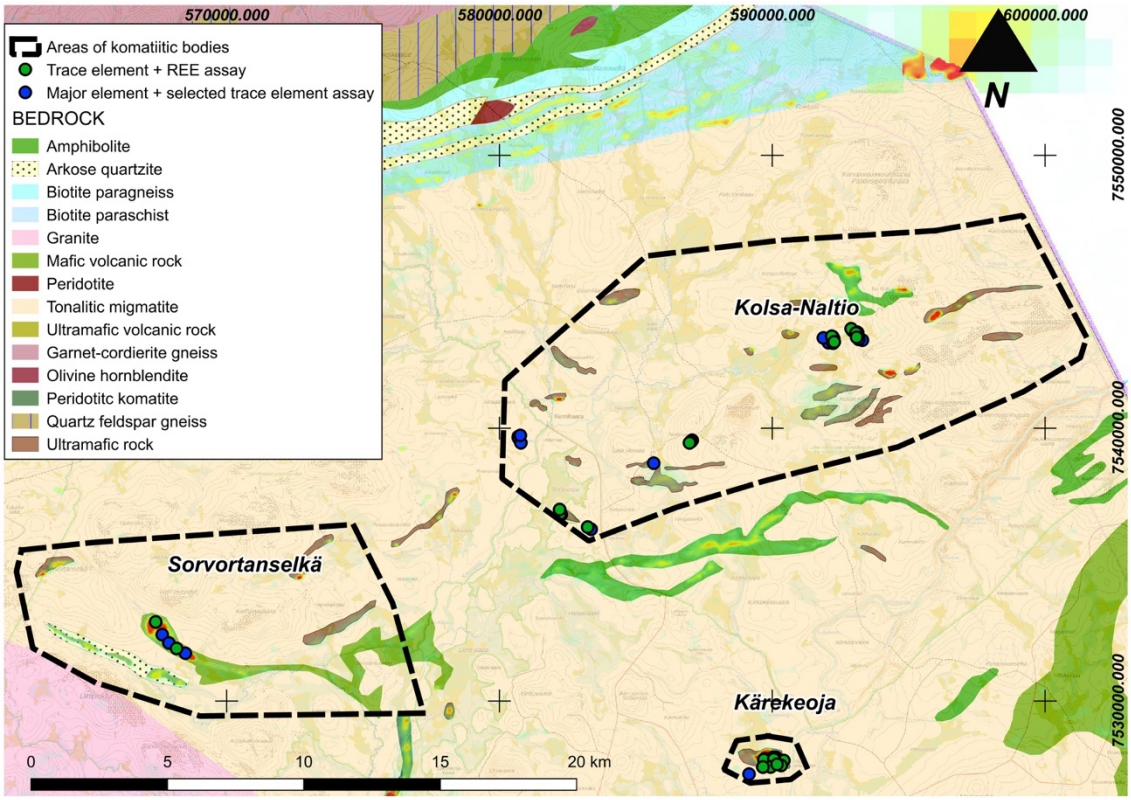

Figure 42. Major (and XRF trace) element and REE assays performed from the komatiites of the Kemihaara-Vintilänkaira granitoid complex.

To briefly elaborate the major element chemistry of KVGC presented in section 7.3., Al_2O_3/TiO_2 in KVGC are ca. 25–30 present in the Kärekeoja and Kolsa-Naltio targets, and lower Al_2O_3/TiO_2 ca. 15 values are found in the Sorvortanselkä target. MgO contents are the highest at Kolsa-Naltio (mostly > 40 wt.%), Kärekeoja plots around 35–40 wt.% and Sorvortanselkä ranges 30–40 wt.%. Additionally, the Kärekeoja body also contains a group of komatiitic basalts.

Ni contents plot mostly between 1500-3000 ppm in all targets, the Kolsa-Naltio being the only one with more than 3000 ppm. Median Ni contents are around 2000 ppm for the Kärekeoja body (max. 2670 ppm), 2800 ppm for Kolsa-Naltio komatiitic bodies (max. 3488 ppm), and 1600 ppm for the Sorvortanselkä middle body, (max. 2510 ppm). Ni depletion is modest in all targets in general (Figure 43). The Kolsa-Naltio and Sorvortanselkä bodies have the widest scatter in Ni contents and plot on the both sides of the Ni-undepletion model line (see Naldrett et al. 1984, Makkonen et al. 2017) and show the strongest Ni depletion. The Kärekeoja komatiites, on the other hand, follow the model line and show only slight depletion. Furthermore, potentially enriched samples plotting above the model line are few. As for other chalcophile elements, Cu abundances in these

rocks are generally low, < 100 ppm. PGE (Pt and Pd) are generally low (< 10 ppb = below detection limits) for all targets, albeit elevated contents from 10 to 55 ppb are sporadically found. The Kärekeoja body hosts the most PGE-anomalous samples: 187.1-PTMO-02 (55 ppb) and 190.1-PTMO-02 (17 ppb). Also, some elevated PGE (Pt+Pd) were detected from the Sorvortanselkä (JHTE-2017-7.1, 26 ppb and JHTE-2017-10.1, 16 ppb) and Kolsa-Naltio (2-PIH-05, 23 ppb of Pd and 140.1-PTMO-02, 12 ppb) targets.

High-MgO komatiites produced by chromite-undersaturated melts are observed mainly in Kolsa-Naltio and in lesser in Kärekeoja and Sorvortanselkä (Figure 44). Only one sample from Sorvortanselkä (JHTE-2017-7.1) plots to the prospective field (the purple circle in the figure 43). Most of the komatiites from KVGC follow cotectic crystallization of olivine and chromite. In the Ni vs. Cr plot (Figure 45) samples from the Kolsa-Naltio bodies plot towards the mineralized komatiite trend (see Brand 1999), but the Ni-abundances are relatively low, around 3000–3500 ppm. The Sorvortanselkä and Kärekeoja komatiites plot to the olivine cumulate and komatiite liquid fields in the diagram. However, the varying Ni contents at similar Cr contents are noteworthy.

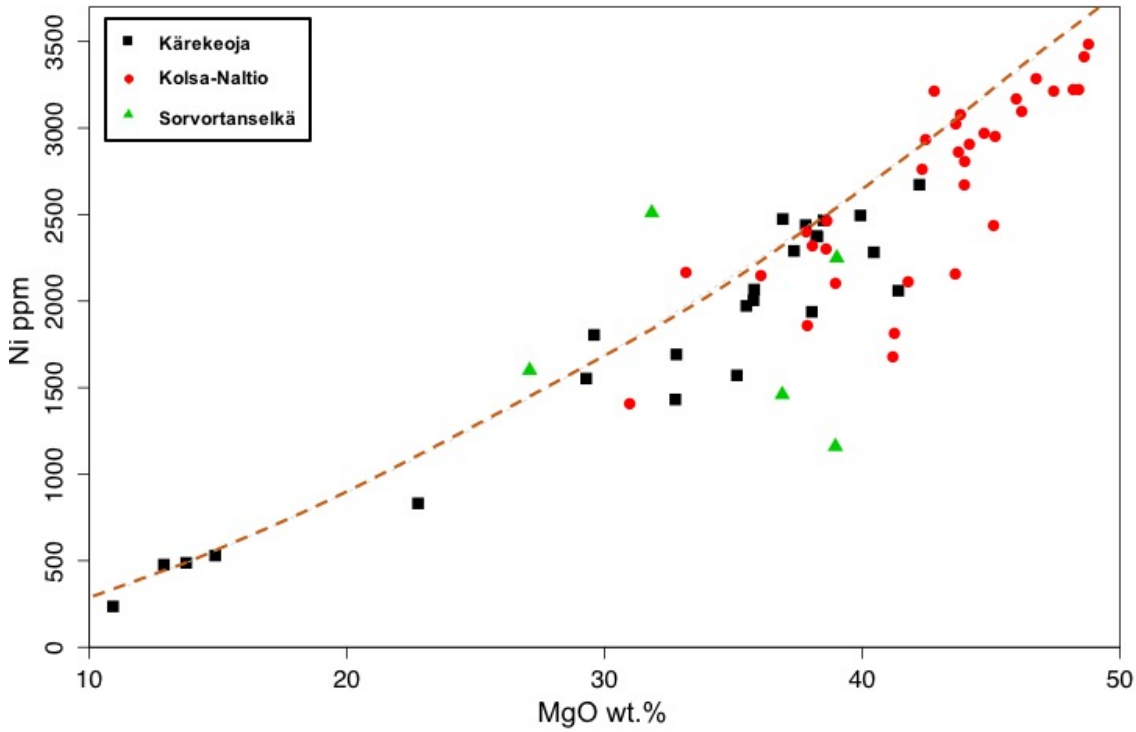

Figure 43. MgO vs. Ni plot of the Kemihaara-Vintilänkaira komatiites. Samples plotting above the Ni-undepletion model line can be considered Ni-enriched, and those plotting below it can be considered Ni-depleted. The Ni-undepletion model line after Naldrett et al. 1984 and Makkonen et al. 2017.

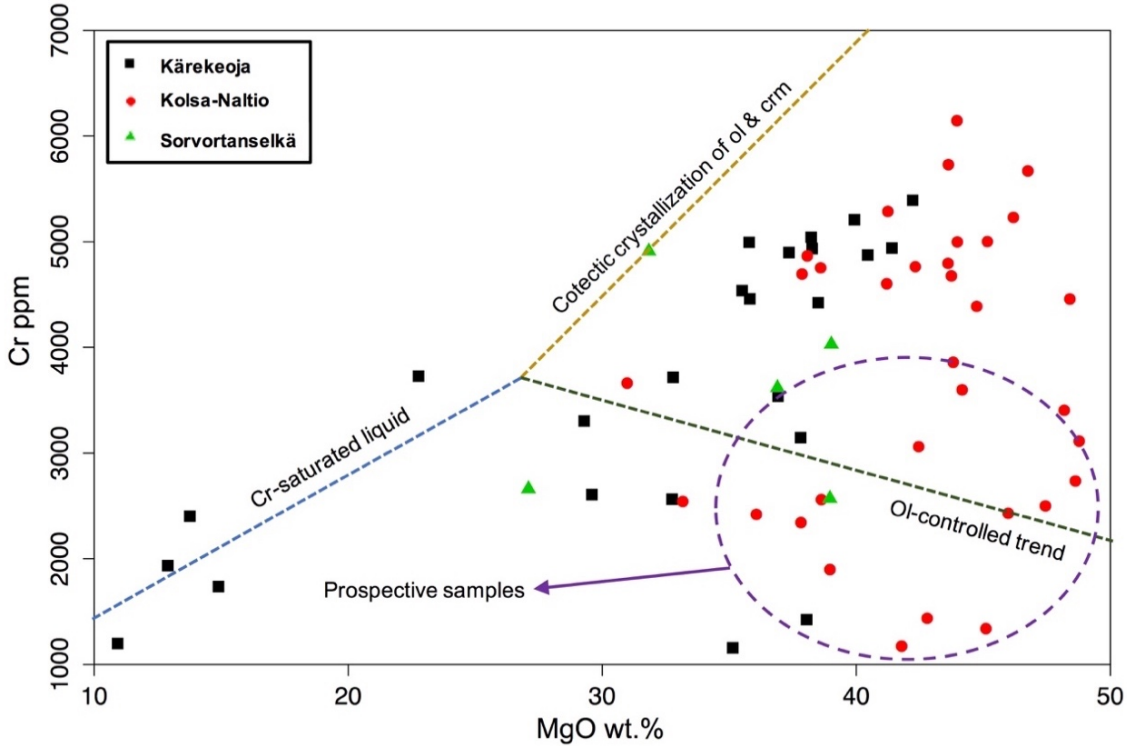

Figure 44. MgO vs. Cr plot of the Kemihaara-Vintilänkaira komatiites. Globally, prospective samples plot in or in the proximity of the purple circle. Blue dashed line represents Cr-saturated liquid, in which solubility is controlled by chromite solubility (the low-MgO rocks). Yellow dashed line represents cotectic crystallization of chromite and olivine from Cr-saturated melt. Green dashed line represents olivine-controlled trend (olivine-liquid mixing, Cr-undersaturated melt), in which crystallization is controlled by olivine. Globally most of the komatiites plot in between the cotectic and ol-controlled trends. Lines after Barnes & Fiorentini (2012), prospective sample field after Konnunaho (2016). Ol = olivine, crm = chromite.

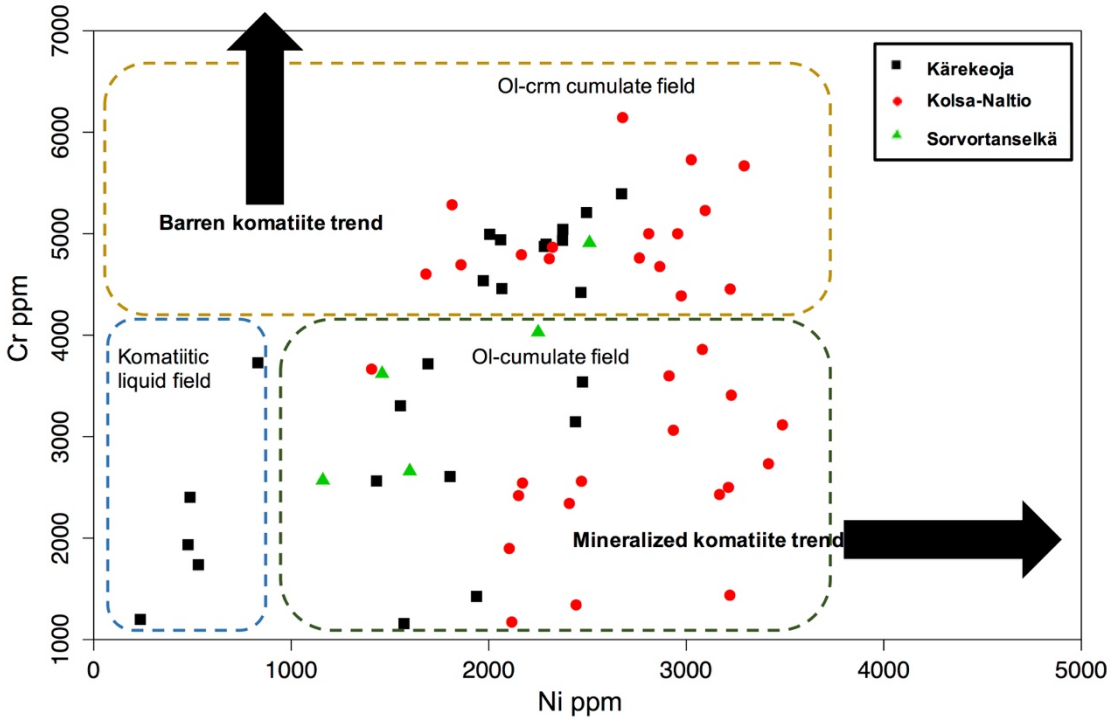

Figure 45. Ni vs. Cr plot of the Kemihaara-Vintilänkaira komatiites. Samples with low Cr and high Ni represent mineralized komatiite trend, along which Ni sulfide abundance increases. Samples with high Cr and low to moderate Ni represent the barren komatiite trend, where ol-crm cumulates are produced and Ni typically partitions into silicates. The dashed fields represent theoretical ol-crm cumulates (yellow), ol-cumulates

(green) and non-cumulus komatiites (blue). Trends and fields after Brand (1999). Ol = olivine, crm = chromite.

Sulfur contents in KVGC are mainly low and median S content in KVGC is ca. 115 ppm. Potentially mineralized (> 2500 ppm of S) samples are absent (Figure 46). Furthermore, there is no clear correlation of high Ni, high Cu, or high Pt+Pd samples with respect to S, although the highest sulfur contents (> 400 ppm) are in rocks with 2000–2500 ppm Ni. Nickel is most likely adhered to silicates.

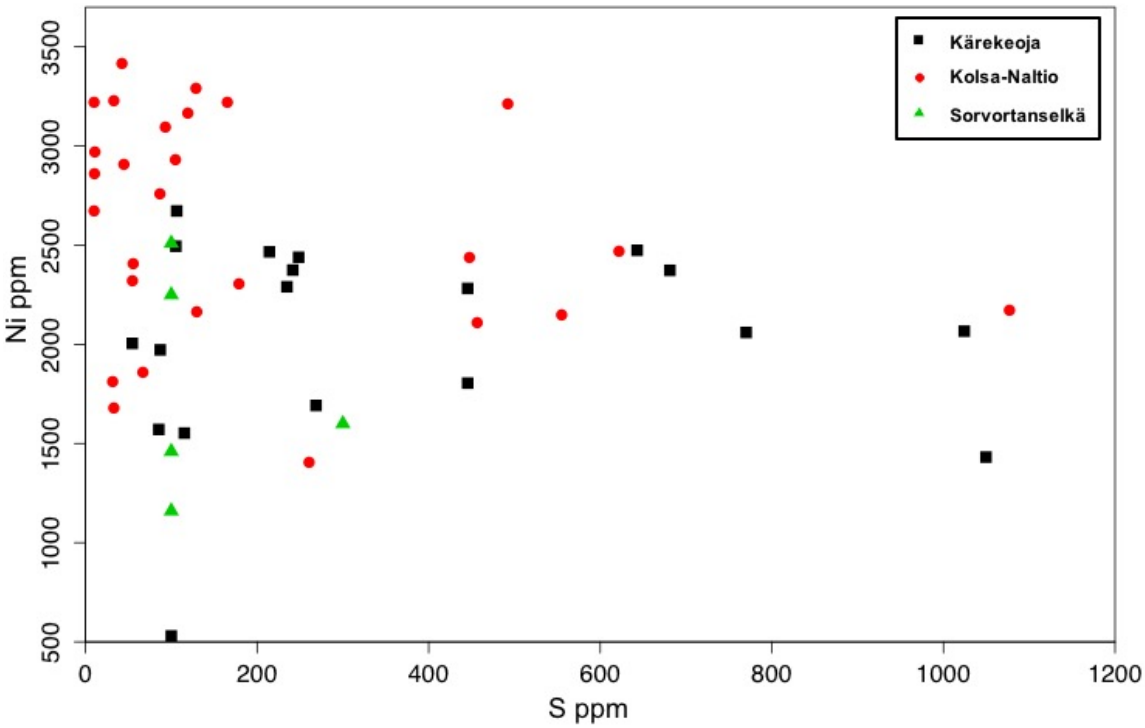

Figure 46. S vs. Ni plot of the Kemihaara-Vintilänkaira komatiites. Sulfur contents are generally low and potentially mineralized (> 2500 ppm of S) samples are absent.

REE-patterns of KVGC targets are varying. The Kärekeoja body has a few clearly LREE-enriched patterns, but the majority of the komatiitic cumulates have flat, patterns corresponding to primitive mantle composition (Figure 47A). The Kolsa-Naltio patterns are somewhat tangled (Figure 47B): both depleted and enriched REE compositions are present making the patterns sawtooth-like. This may also partly be the result of low analytical precision and accuracy at very low concentrations of REE, which typical to komatiitic cumulates. Moreover, the few patterns with enriched LREE are not related to a certain body in the Kolsa-Naltio area. From Sorvortanselkä, only two samples were analyzed for REE (Figure 47C). One sample has clearly elevated LREE with a negative Eu anomaly and flat HREE, while the other has a relatively flat pattern. All targets are characterized by normalized $(Gd/Yb)_N$ ($_N$ = normalized value) median values of ca. 1,

which corresponds to C1 chondrite value. On the other hand, in normalized $(La/Sm)_N$ median values there is scatter, as the Kärekeoja and Sorvortanselkä bodies have values around 1.6 (enriched), while the Kolsa-Naltio bodies exhibit values close to 1 (chondritic) (Figure 48). In theory, komatiites contaminated with with crustal contamination should be enriched in highly incompatible REE (e.g., La & Sm) compared to moderately incompatible REE (e.g., Gd & Yb).

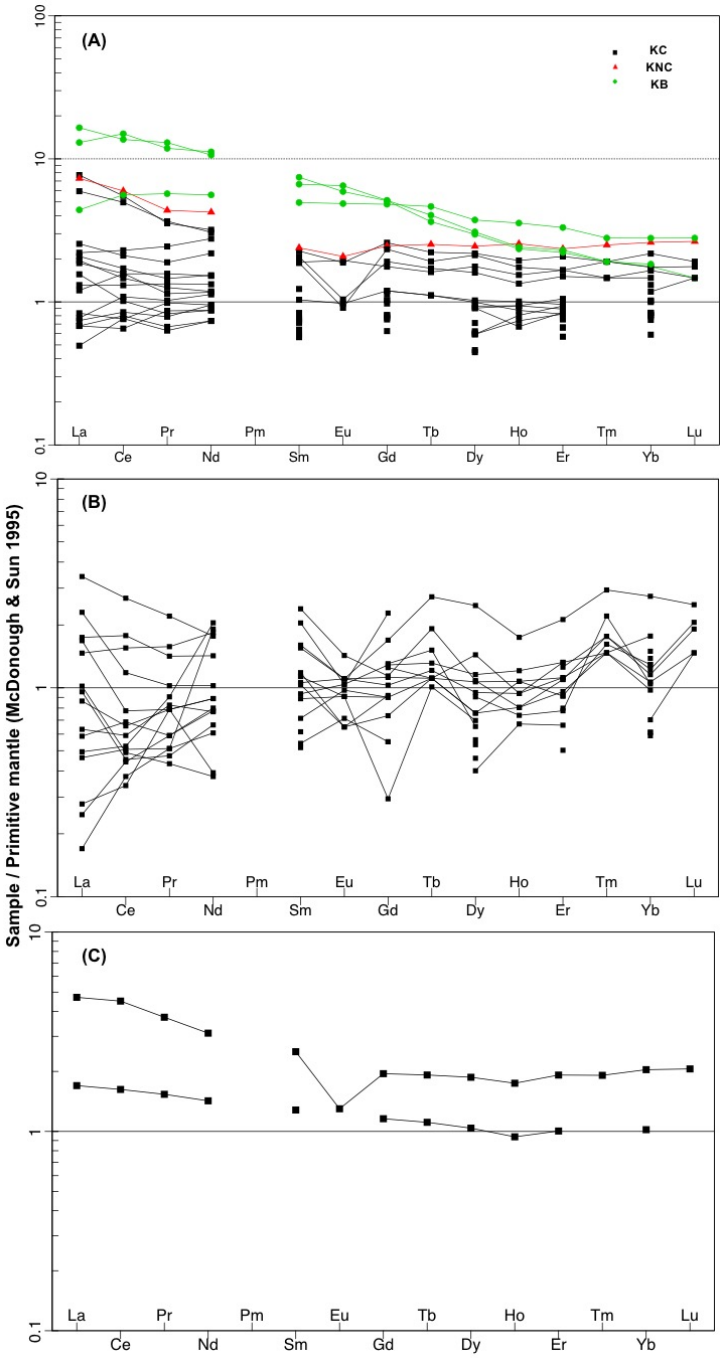

Figure 47. REE-patterns of the Kemihaara-Vintilänkaira komatiites normalized to primitive mantle (Bulk Silicate Earth) after McDonough & Sun (1995). Gaps mean values below detection limit, Pm is an unstable element and was not determined. (A) Kärekeoja, (B) Kolsa-Naltio, (C) Sorvortanselkä. KC = komatiitic cumulate (MgO > 28 wt.%), KNC = komatiitic non-cumulate (28 < MgO > 18 wt.%), KB = komatiitic basalt (MgO < 18 wt.%).

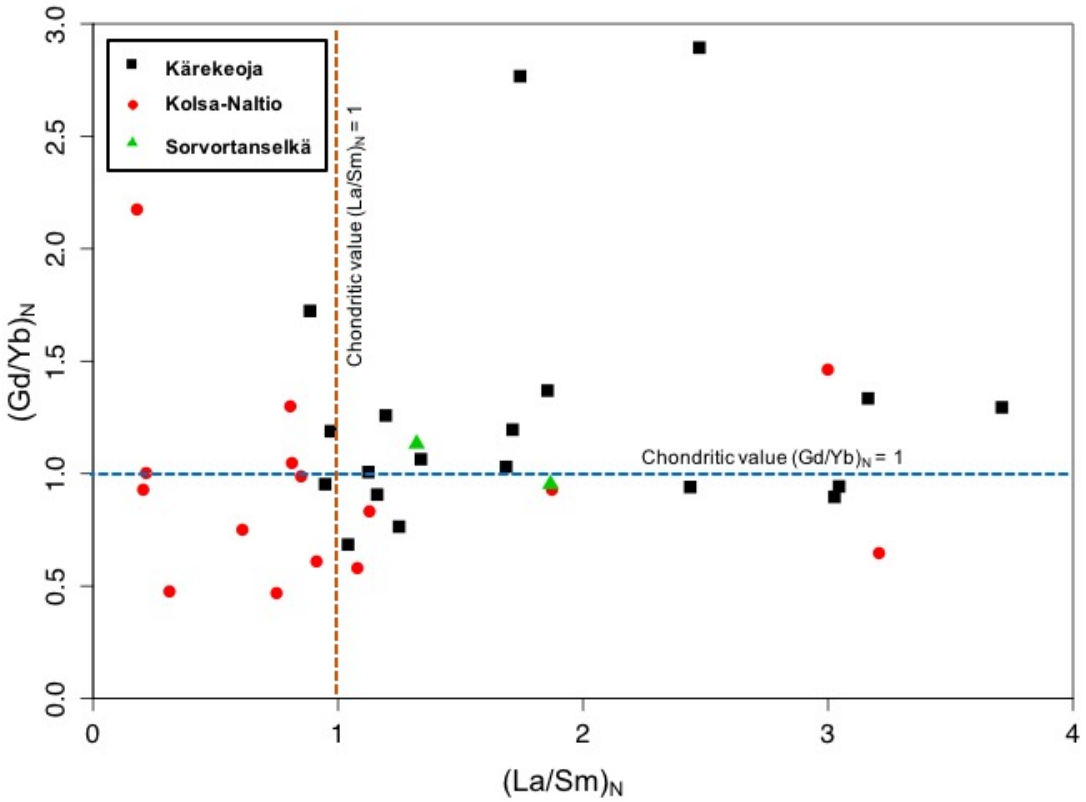

Figure 48. $(La/Sm)_N$ vs. $(Gd/Yb)_N$ plot of the Kemihaara-Vintilänkaira komatiites. Enrichment in $(La/Sm)_N$ relative to $(Gd/Yb)_N$ have been in theory attributed to crustal contamination. Normalization values from REE C1 chondrite (McDonough & Sun 1995).

7.4.2 The Tulppio metavolcanic belt komatiites

The Tulppio metavolcanic belt hosts seven studied targets: Kärkäsvaara, Rovaukonselkä-Nivatunturi, Kuttusvaarat-Heiniselkä, Tulppio, Iskemävaara-Pultoselkä, Petäjä-Saijanvaara, and TVB east (Hannu Ollin vaara + Kynsivaara) (Figure 49). In total, these targets comprise 680 analyses in the combined data set (Table 7).

Table 7. Distribution of samples between the studied targets in the Tulppio metavolcanic belt.

Target	Samples (with REE data)	Cumulates	Non-cumulates	Komatiitic basalts
Kärkäsvaara	26 (21)	21	5	0
Rovaukonselkä-Nivatunturi	56 (30)	7	30	19
Kuttusvaarat-Heiniselkä	249 (51)	116	83	50
Tulppio	119 (20)	107	4	8
Iskemävaara-Pultoselkä	132 (51)	88	24	20
Petäjä-Saijanvaara	91 (35)	69	15	7
TVB east	7 (0)	7	0	0
In total	680 (208)	415	161	104

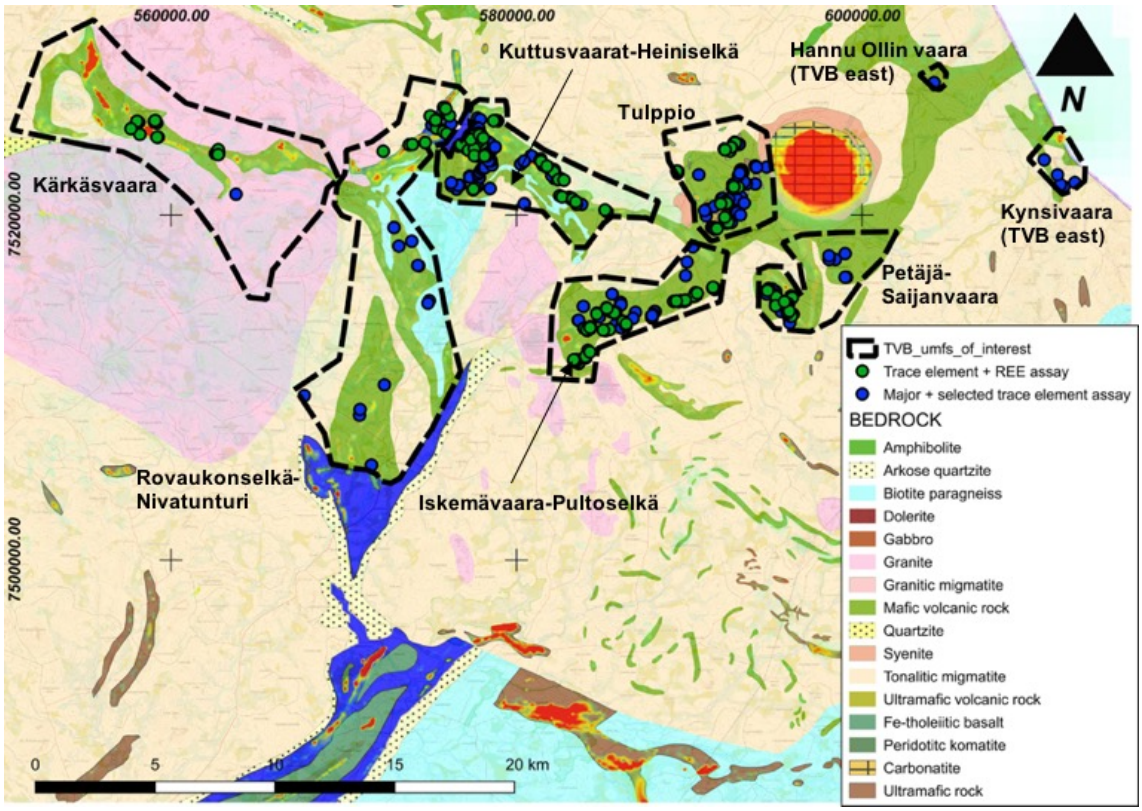

Figure 49. Major element and REE-assays performed from the komatiites of the Tulppio metavolcanic belt.

To briefly elaborate the major element geochemistry of TVB presented in section 7.3: Al_2O_3/TiO_2 make up two distinct trends of komatiites with ratios 10–15, concentrated to the Petäjä-Saijanvaara, Kuttusvaarat-Heiniselkä, and Rovaukonselkä-Nivatunturi areas, and komatiites with ratios 20–35 present in all targets including the three forementioned. As for MgO contents, komatiitic basalts and non-cumulus komatiites are abundant particularly in the Rovaukonselkä-Nivatunturi, Kuttusvaarat-Heiniselkä, and Iskemävaara-Pultoselkä areas. Cumulates with relatively lower MgO contents (30–40 MgO wt.%) are abundant in the Kärkäsvaara and Petäjä-Saijanvaara and TVB east areas, and the high-MgO cumulates (> 40 wt.% MgO) are concentrated in the Tulppio and Petäjä-Saijanvaara areas.

Nickel contents in TVB association range regionally in a similar manner as the MgO contents: the Rovaukonselkä-Nivatunturi has the lowest Ni contents (ca. 500–1500 ppm) and the Petäjä-Saijanvaara, Kärkäsvaara, Iskemävaara-Pultoselkä and TVB east areas have around 1500–2500 ppm of Ni. The highest Ni contents (2500–4000 ppm) are found in the Tulppio body, but also the Iskemävaara-Pultoselkä and Petäjä-Saijanvaara targets have contents exceeding 3000 ppm of Ni. The Kuttusvaarat-Heiniselkä is a site of interest

regarding Ni, as it has very varying Ni contents from 500 to 4000 ppm. In addition, mineralized samples from the Tulppio (VIHU-2006-29.4 and VIHU-2006-29.2) and Kuttusoja areas (284-1-JEV-97 and 286-1-JEV-97) have Ni contents between 4000 and 8000 ppm. Depleted, as well as enriched, Ni contents are observed in several targets in TVB (Figure 50). The strongest scatter is observed in the Tulppio. Minor scatter is also present in the Petäjä-Saijanvaara and Kuttusvaarat-Heiniselkä areas. Other targets plot mainly in the vicinity of the model line. As for the other chalcophile elements, Cu contents in TVB are generally low (< 100 ppm). However, the most anomalous Cu contents (with 600-800 ppm Cu) in ELAD are found in komatiitic basalts in the proximity of the Kuttusvaarat hills. PGE (Pt+Pd) are generally between 10–20 ppb and higher concetrations (> 50 ppb) are mainly located in the Tulppio body.

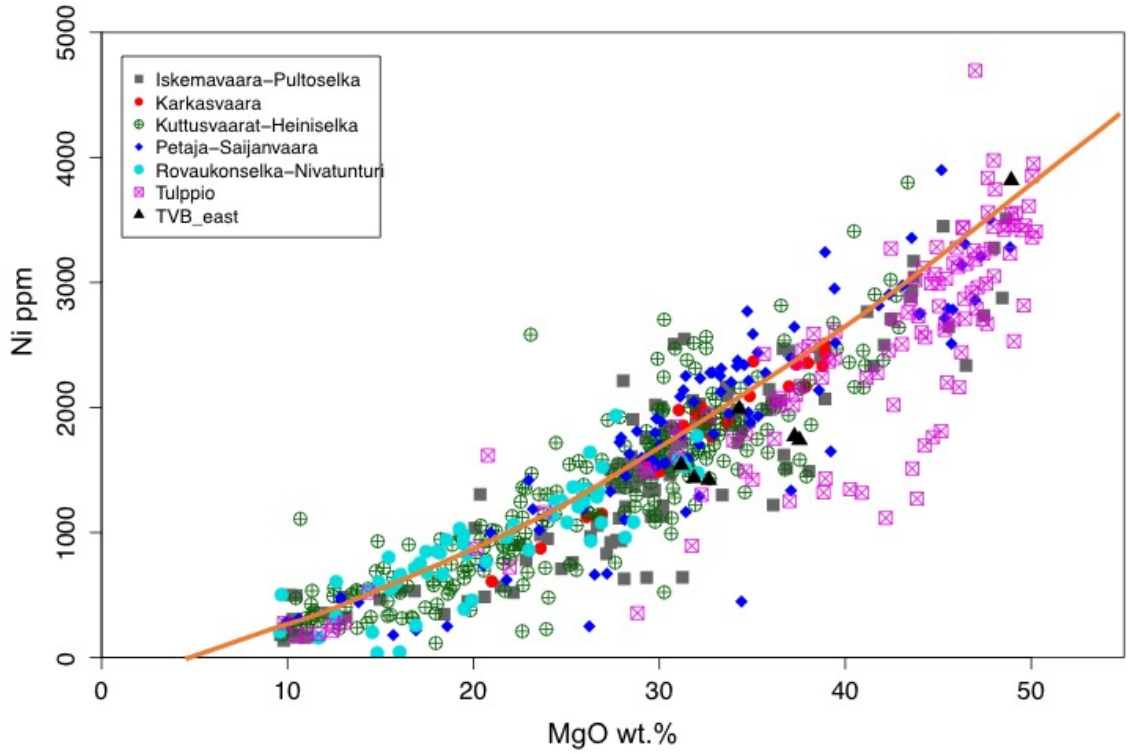

Figure 50. MgO vs. Ni plot of the Tulppio metavolcanic belt komatiites. Samples plotting above the Ni-undepletion model line can be considered Ni-enriched, and those plotting below it can be considered Ni-depleted. The Ni-undepletion model line after Naldrett et al. 1984 and Makkonen et al. 2017.

High-MgO komatiites produced from Cr-undersaturated melts are observed in the Tulppio, Petäjä-Saijanvaara, and Kuttusvaarat-Heiniselkä targets (Figure 51). Also, minor samples from the Iskemävaara-Pultoselkä target plot to the prospective field. Referring, to Maier et al. (2013) calculations of Tulppio's parental magma being a high-Mg basalt (Cr-saturated) in composition, most of The TVB komatiites represent differentiates from it. Interestingly, however, the Tulppio body has very Cr-rich (> 8000

ppm) and Cr-poor (< 2000 ppm) samples at similar MgO contents. The Kuttusvaarat-Heiniselkä area, except for a few scattered Cr-rich samples, rather comprises a trend in between chromite-saturated melt and olivine-controlled (Cr-undersaturated melt) crystallization. The effect of crystallizing cumulates with low Cr contents together with presence of Ni-mineralized samples in Tulppio and Kuttusvaarat-Heiniselkä can be also be seen in Ni vs. Cr–plot, where they plot towards the "mineralized komatiite"-trend (Figure 52).

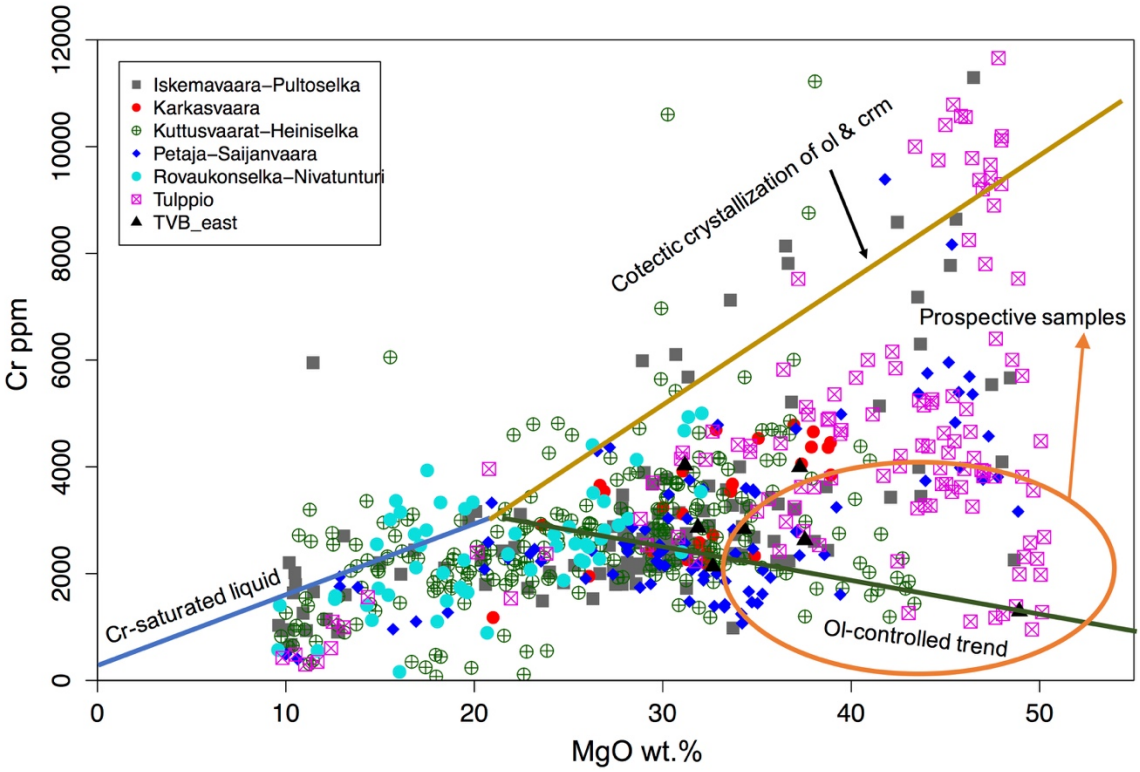

Figure 51. MgO vs. Cr plot of the Tulppio metavolcanic belt komatiites. Globally, prospective samples plot in or in the proximity of the purple circle. Blue dashed line represents Cr-saturated liquid, in which solubility is controlled by chromite solubility (the low-MgO rocks). Yellow dashed line represents cotectic crystallization of chromite and olivine from Cr-saturated melt. Green dashed line represents olivine-controlled trend (olivine-liquid mixing, Cr-undersaturated melt), in which crystallization is controlled by olivine. Globally, most of the komatiites plot in between the cotectic and ol-controlled trends. Lines after Barnes & Fiorentini (2012), prospective sample field after Konnunaho (2016). Ol = olivine, crm = chromite.

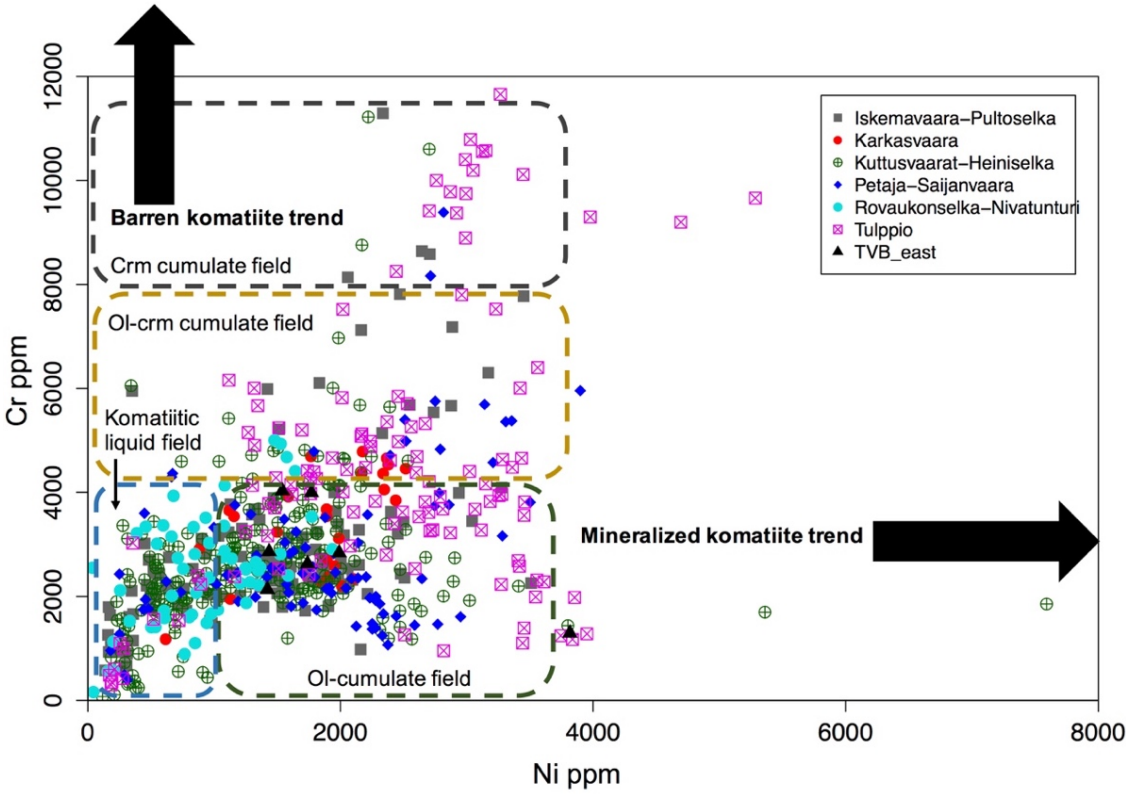

Figure 52. Ni vs. Cr plot of the Tulppio metavolcanic belt komatiites. Samples with low Cr and high Ni represent mineralized komatiite trend, along which Ni sulfide abundance increases. Samples with high Cr and low to moderate Ni represent the barren komatiite trend, where ol-crm cumulates are produced and Ni typically partitions into silicates. The dashed fields represent theoretical ol-crm cumulates (yellow), ol-cumulates (green) and non-cumulus komatiites (blue). Trends and fields after Brand (1999). Ol = olivine, crm = chromite.

Within ELAD, TVB has relatively high S contents (up to 9000 ppm), although majority are below 1500 ppm. Weakly mineralized samples with more than 2500 ppm of S are found mainly in the Rovaukonselkä-Nivatunturi, Petäjä-Saijanvaara, and Iskemävaara-Pultoselkä areas. Minor anomalous contents are also observed in the Tulppio and Kuttusvaarat-Heiniselkä areas. However, the general trend in terms of samples with relatively high S (> 2000 ppm), is that they correspond to relatively low Ni, Cu, and PGE contents, except for the mineralized samples in Tulppio and Kuttusvaarat, which comprise a slightly ascending trend with respect to S (Figure 53).

REE patterns of TVB show LREE enrichment in all areas. In the Iskemävaara-Pultoselkä area, the patterns are relatively flat, with concentrations up to two times primitive mantle values and characterized by relatively high La compared to other LREE (Figure 54). Also, negative Eu-anomalies are present, mainly in komatiitic cumulates. In the Kärkäsvaara area, similar features to Iskemävaara-Pultoselkä are observed, although the enrichment in La relative to other LREE and negative Eu- anomalies are not as strong, and the patterns

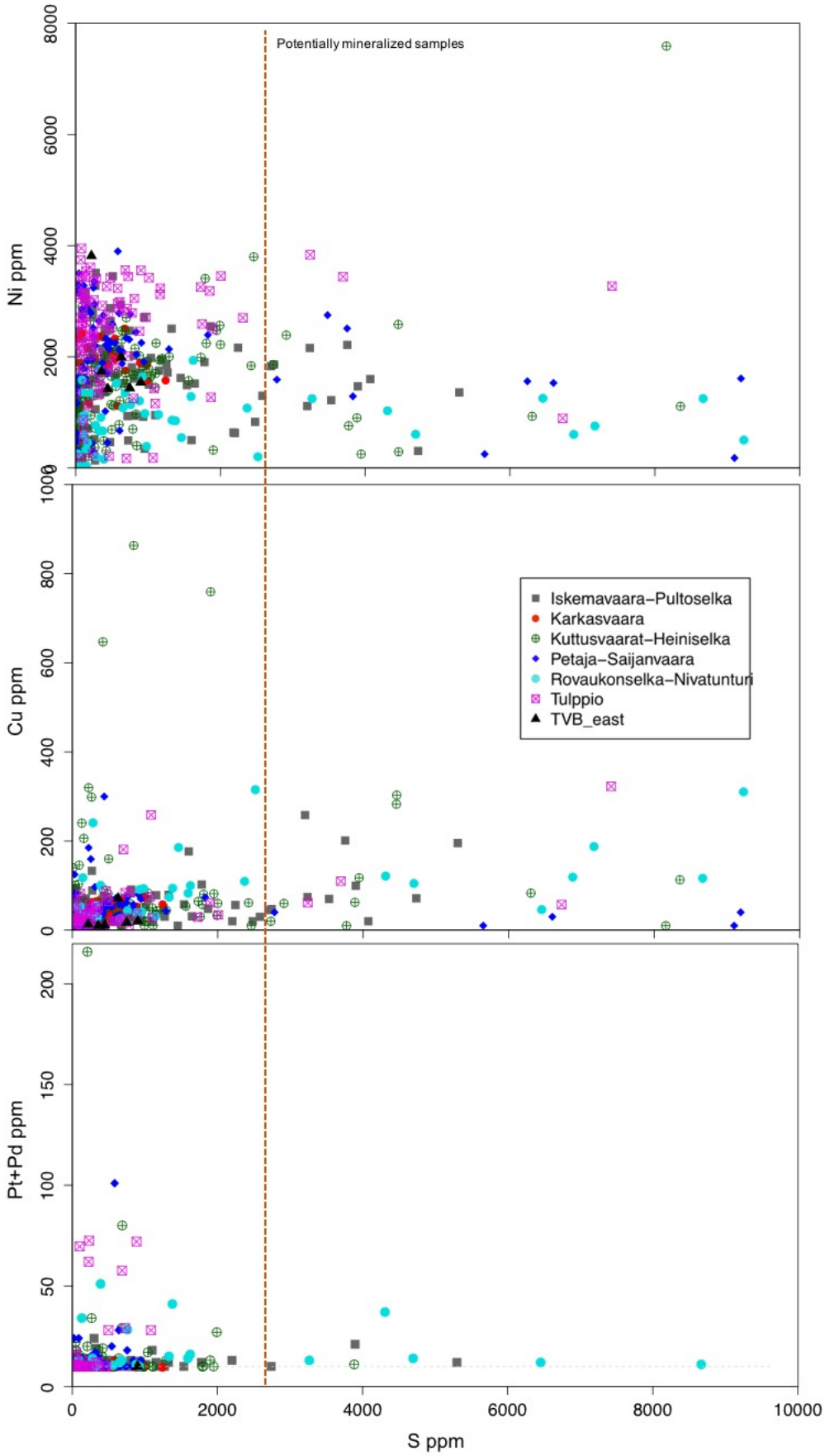

Figure 53. S vs. Ni, S vs. Cu, and S vs. Pt+Pd plots of the Tulppio metavolcanic belt komatiites. In general, the Ni, Cu and PGE contents corresponds to low S contents, except for some likely mineralized samples from the Tulppio and Kuttusvaarat-Heiniselkä targets.

are flatter (Figure 55). The Kuttusvaarat-Heiniselkä is characterized by a notable enrichment of LREE (up to 11 times primitive mantle values) and negative Eu-anomalies, especially in komatiitic cumulate compositons (Figure 56). The patterns of the Petäjä-Saijanvaara and Rovaukonselkä-Nivatunturi area (Figures 57 & 58) are similar to the Kuttusvaarat-Heiniselkä patterns but lack relative LREE enrichment. Therefore, their patterns are flatter with the exception of the negative Eu-anomalies. Contrary to the Eu-anomalies in komatiitic cumulates, in Rovaukonselkä-Nivatunturi they exist mainly in non-cumulate rocks. Notably, the Rovaukonselkä-Nivatunturi also has a group of komatiites showing LREE-depleted patterns, which are comparable to the "hump-shaped" patterns of The CLGB komatiites (Hanski et al. 2001). In Tulppio, both down-sloping and enriched LREE patterns and flat, almost chondritic patterns are present (Figure 59). Furthermore, median $(La/Sm)_N$ for the targets vary from < 1 in the Petäjä-Saijanvaara and Rovaukonselkä-Nivatunturi areas, to ca. 1 in Tulppio and to ca. 1.2 in all other targets, displaying relatively chondritic ratios. Median $(Gd/Yb)_N$ ratios are similar, close to 1, except for the Kuttusvaarat-Heiniselkä (ca. 1.2) and Rovaukonselkä-Nivatunturi (1.4) areas (Figure 60). Interestingly, the Kuttusvaarat-Heiniselkä target has a clear $(La/Sm)_N$-enriched group.

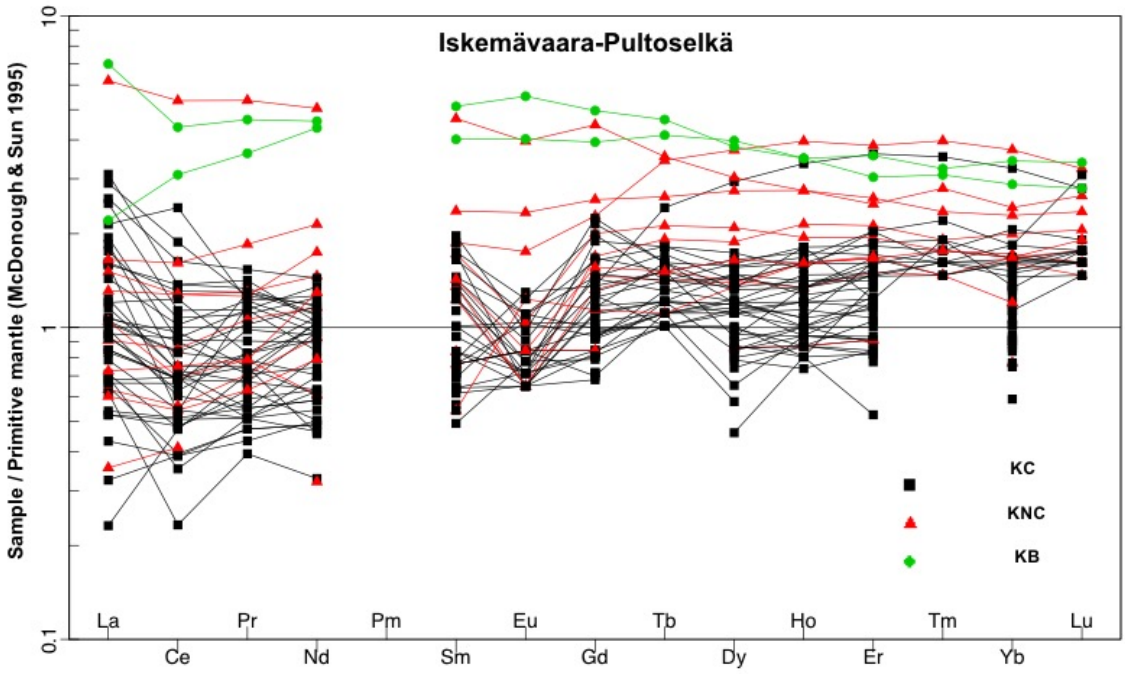

Figure 54. REE-patterns of the Iskemävaara-Pultoselkä area komatiites normalized to primitive mantle (Bulk Silicate Earth) after McDonough & Sun (1995). Gaps mean values below detection limit, Pm is an unstable element and was not determined. KC = komatiitic cumulate (MgO > 28 wt.%), KNC = komatiitic non-cumulate (28 < MgO > 18 wt.%), KB = komatiitic basalt (MgO < 18 wt.%).

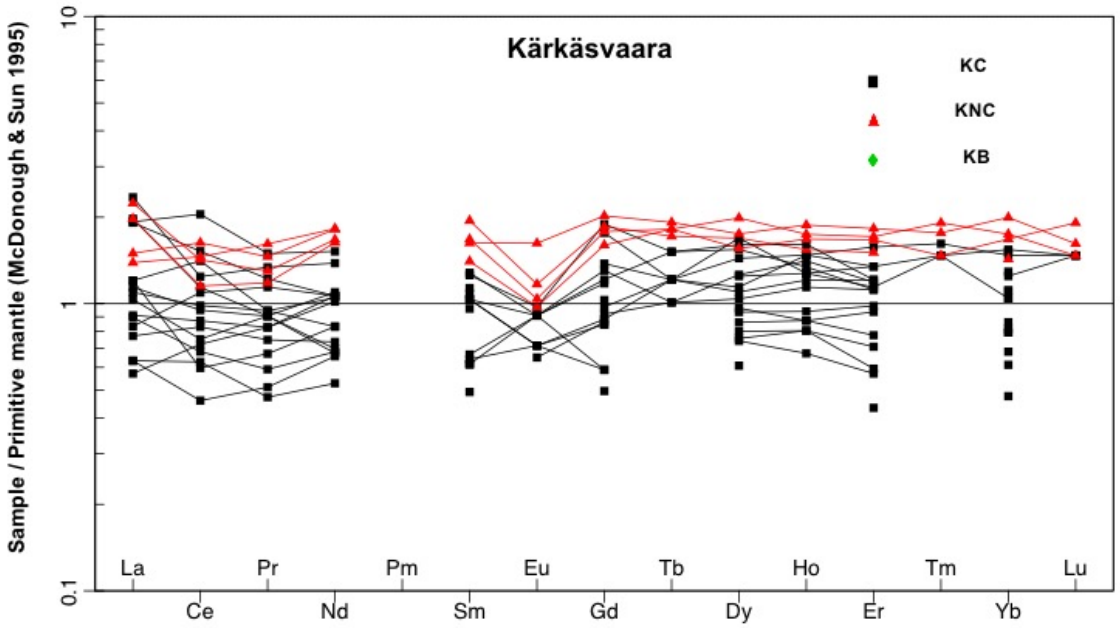

Figure 55. REE-patterns of the Kärkäsvaara area komatiites normalized to primitive mantle (Bulk Silicate Earth) after McDonough & Sun (1995). Gaps mean values below detection limit, Pm is an unstable element and was not determined. KC = komatiitic cumulate (MgO > 28 wt.%), KNC = komatiitic non-cumulate (28 < MgO > 18 wt.%), KB = komatiitic basalt (MgO < 18 wt.%).

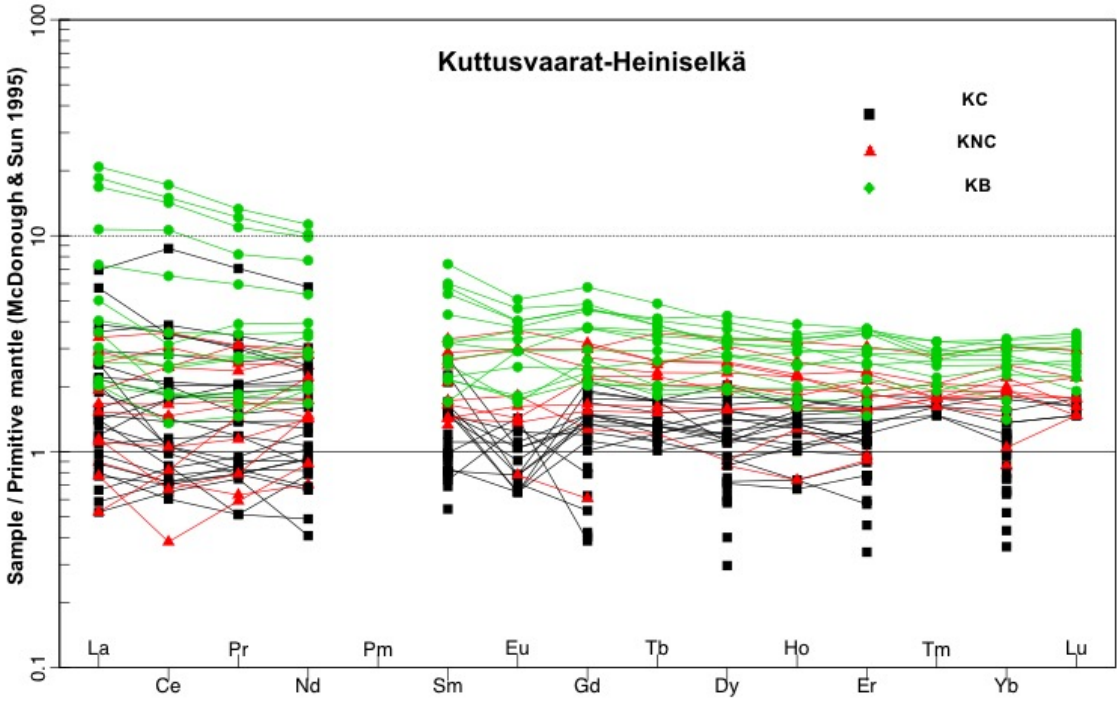

Figure 56. REE-patterns of the Kuttusvaarat-Heiniselkä area komatiites normalized to primitive mantle (Bulk Silicate Earth) after McDonough & Sun (1995). Gaps mean values below detection limit, Pm is an unstable element and was not determined. KC = komatiitic cumulate (MgO > 28 wt.%), KNC = komatiitic non-cumulate (28 < MgO > 18 wt.%), KB = komatiitic basalt (MgO < 18 wt.%).

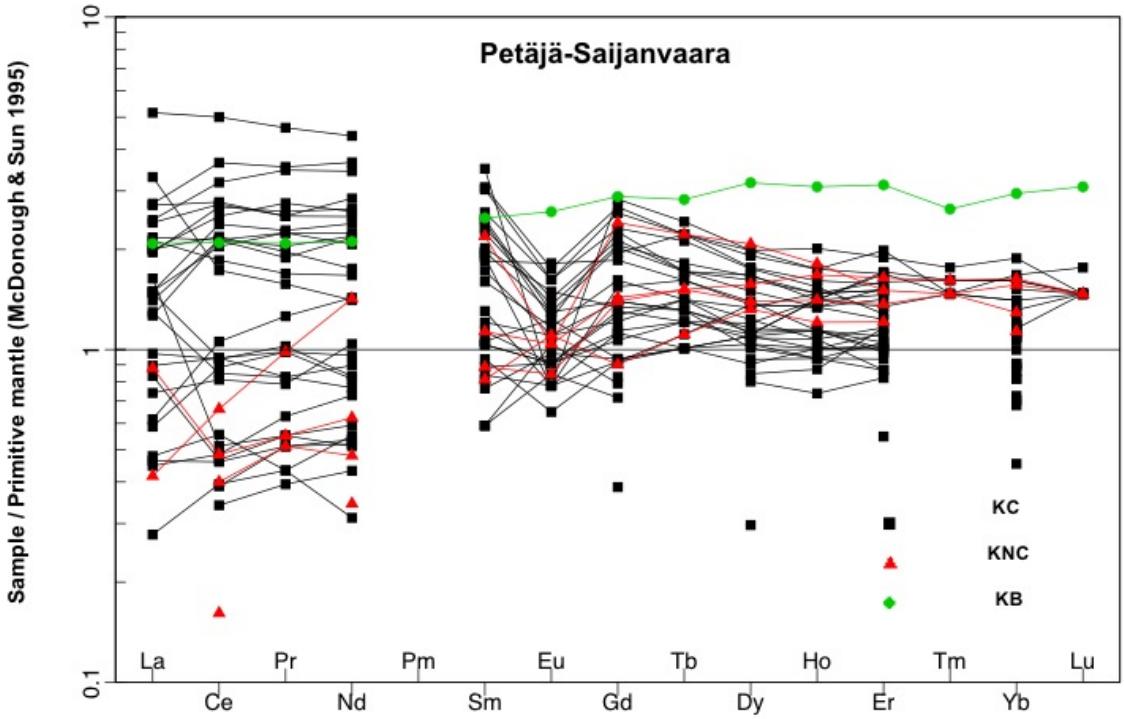

Figure 57. REE-patterns of the Petäjä-Saijanvaara area komatiites normalized to primitive mantle (Bulk Silicate Earth) after McDonough & Sun (1995). Gaps mean values below detection limit, Pm is an unstable element and was not determined. KC = komatiitic cumulate (MgO > 28 wt.%), KNC = komatiitic non-cumulate (28 < MgO > 18 wt.%), KB = komatiitic basalt (MgO < 18 wt.%).

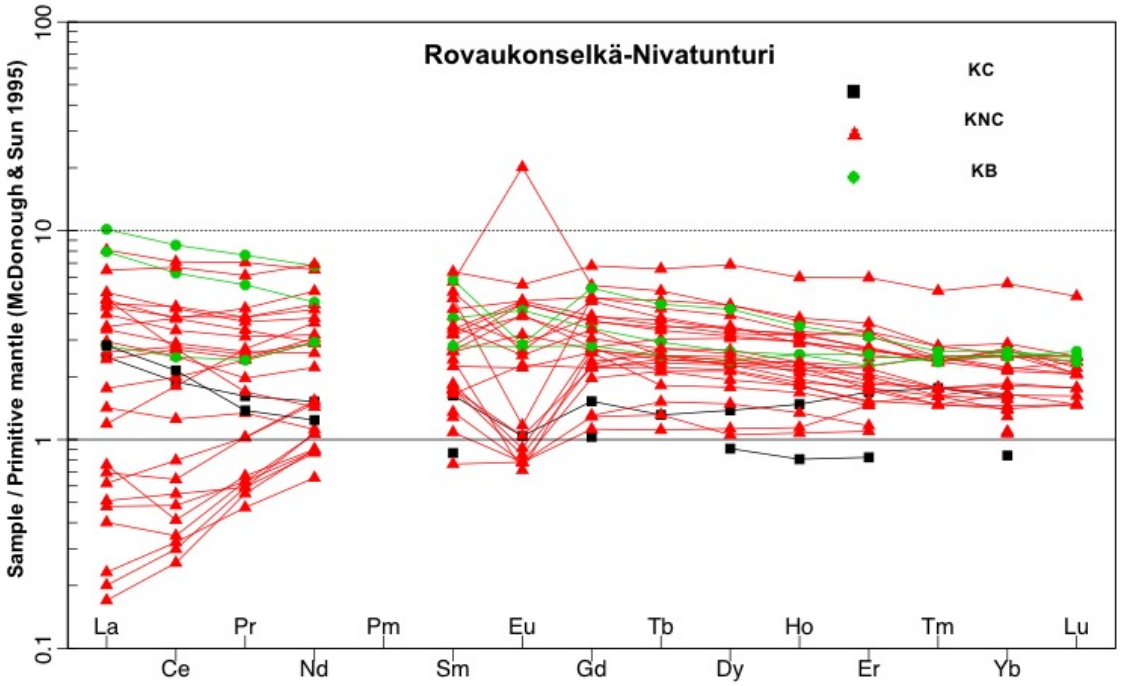

Figure 58. REE-patterns of the Rovaukonselkä-Nivatunturi area komatiites normalized to primitive mantle (Bulk Silicate Earth) after McDonough & Sun (1995). Gaps mean values below detection limit, Pm is an unstable element and was not determined. KC = komatiitic cumulate (MgO > 28 wt.%), KNC = komatiitic non-cumulate (28 < MgO > 18 wt.%), KB = komatiitic basalt (MgO < 18 wt.%).

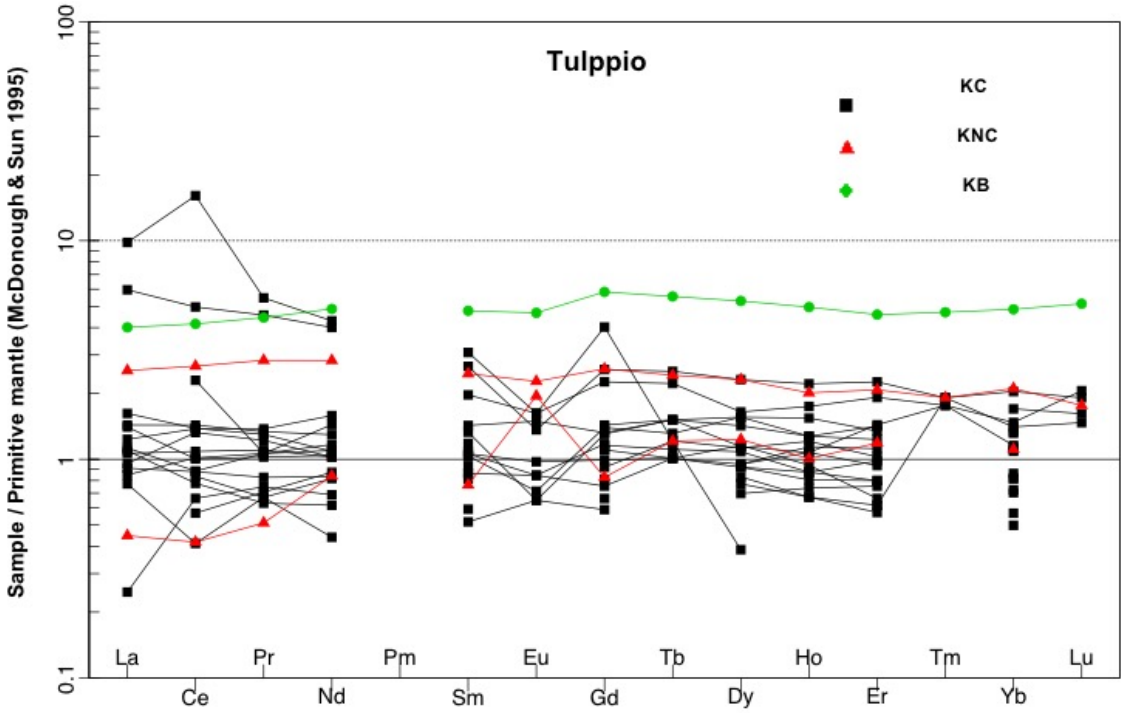

Figure 59. REE-patterns of the Tulppio area komatiites normalized to primitive mantle (Bulk Silicate Earth) after McDonough & Sun (1995). Gaps mean values below detection limit, Pm is an unstable element and was not determined. KC = komatiitic cumulate (MgO > 28 wt.%), KNC = komatiitic non-cumulate (28 < MgO > 18 wt.%), KB = komatiitic basalt (MgO < 18 wt.%).

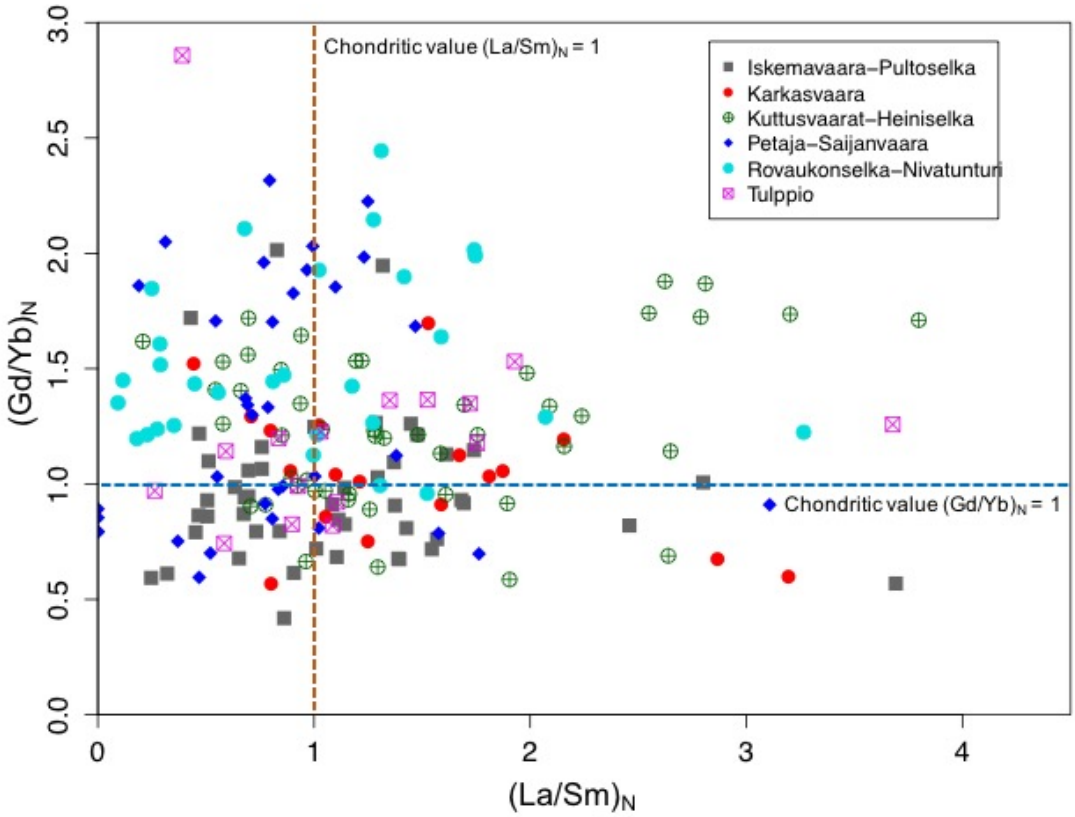

Figure 60. $(La/Sm)_N$ vs. $(Gd/Yb)_N$ plot of the Tulppio belt komatiites. Enrichment in $(La/Sm)_N$ relative to $(Gd/Yb)_N$ have been in theory attributed to crustal contamination. Normalization values from REE C1 chondrite (McDonough & Sun 1995).

7.4.3 The Ahmatunturi granitoid complex komatiites

AGC hosts four studied targets: Jänesselkä, Siurujoki, Tulppionkaitavaara and Vuonnelo-oja (Figure 61). In total, they comprise 124 samples in the combined data set (Table 8).

Table 8. Distribution of samples between the studied targets in the Ahmatunturi granitoid complex.

Target	Samples (with REE data)	Cumulates	Non-cumulates	Komatiitic basalts
Jänesselkä	78 (40)	42	32	4
Siurujoki	22 (0)	21	1	0
Tulppionkaitavaara	15 (13)	14	0	1
Vuonnelo-oja	9 (5)	9	0	0
In total	124 (58)	86	33	5

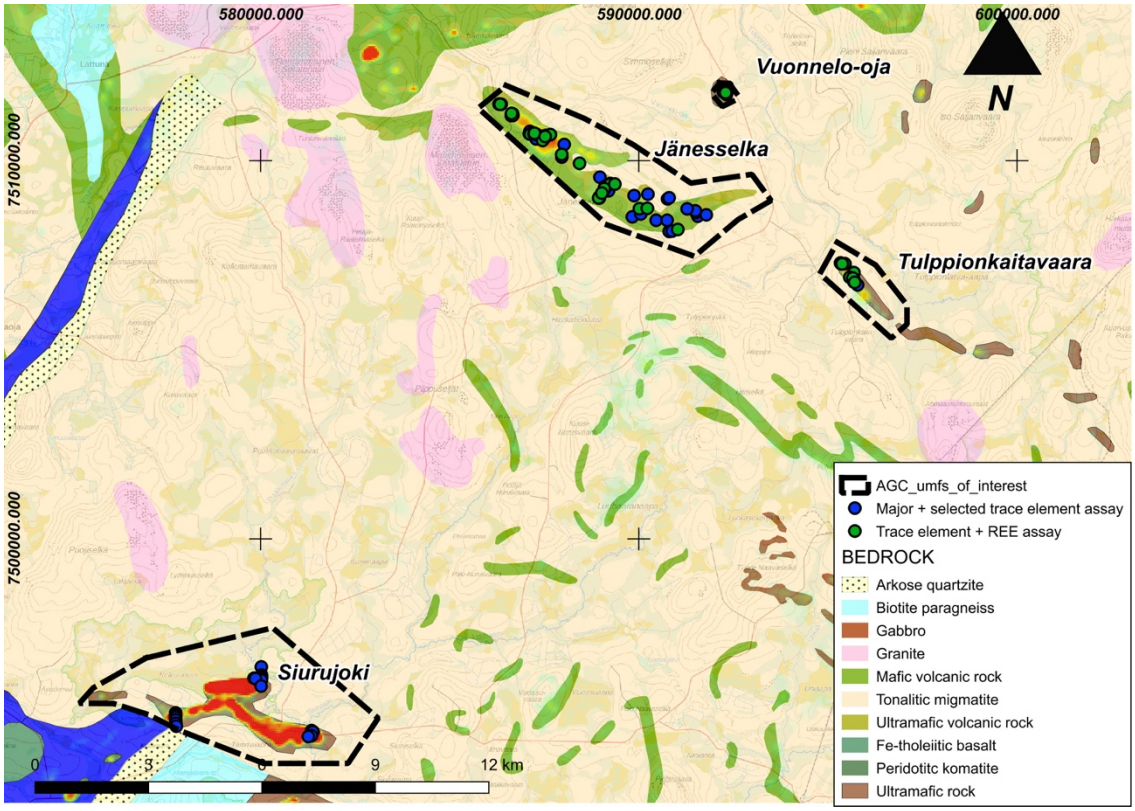

Figure 61. Major element and REE-assays performed from the komatiites of the Ahmatunturi granitoid complex

.

To briefly elaborate the major element chemistry of AGC presented in section 7.3: most of the targets have Al_2O_3/TiO_2 ca. 20, albeit in the Jänesselkä and Vuonnelo-oja some samples also show values up to 40. In the Siurujoki and Jänesselkä bodies minor individual samples also have Al_2O_3/TiO_2 close to 15. Distinct groups can be formed based

on MgO contents, as the Jänesselkä and Tulppionkaitavaara samples plot consistently at 25–32 wt.%, Siurujoki has a bit higher contents from at 35–40 wt.%, and Vuonnelo-oja has only samples with > 35 wt.%. Furthermore, the Jänesselkä and Tulppionkaitavaara bodies are the only ones containing samples with < 20 wt.% MgO samples.

Nickel contents range from 1000–1700 ppm in the Jänesselkä and Tulppionkaitaavaara bodies to 1500–2500 ppm in the Siurujoki and Vuonnelo-oja bodies. Ni-depleted samples are present in all of the bodies (Figure 62). Especially the Siurujoki and Vuonnelo-oja bodies show clear scatter in terms of Ni and plot mostly below the model line. Most of the Jänesselkä and Tulppionkaitavaara samples plot just below the model line, although anomalous depleted and enriched compositions are present in the Jänesselkä body. Nevertheless, Ni-enriched compositions are almost absent in all targets. As for other chalcophile elements, Cu contents are generally low (< 100 ppm), although some clearly elevated samples (> 150 ppm) are found in the Jänesselkä and Tulppionkaitavaara bodies. PGE (Pt+Pd) show relatively anomalous contents in all targets except for the Vuonnelo-oja body. PGE contents in Jänesselkä and Tulppionkaitavaara are between 10–20 ppb and the highest contents are observed in the Siurujoki body (20–35 ppb).

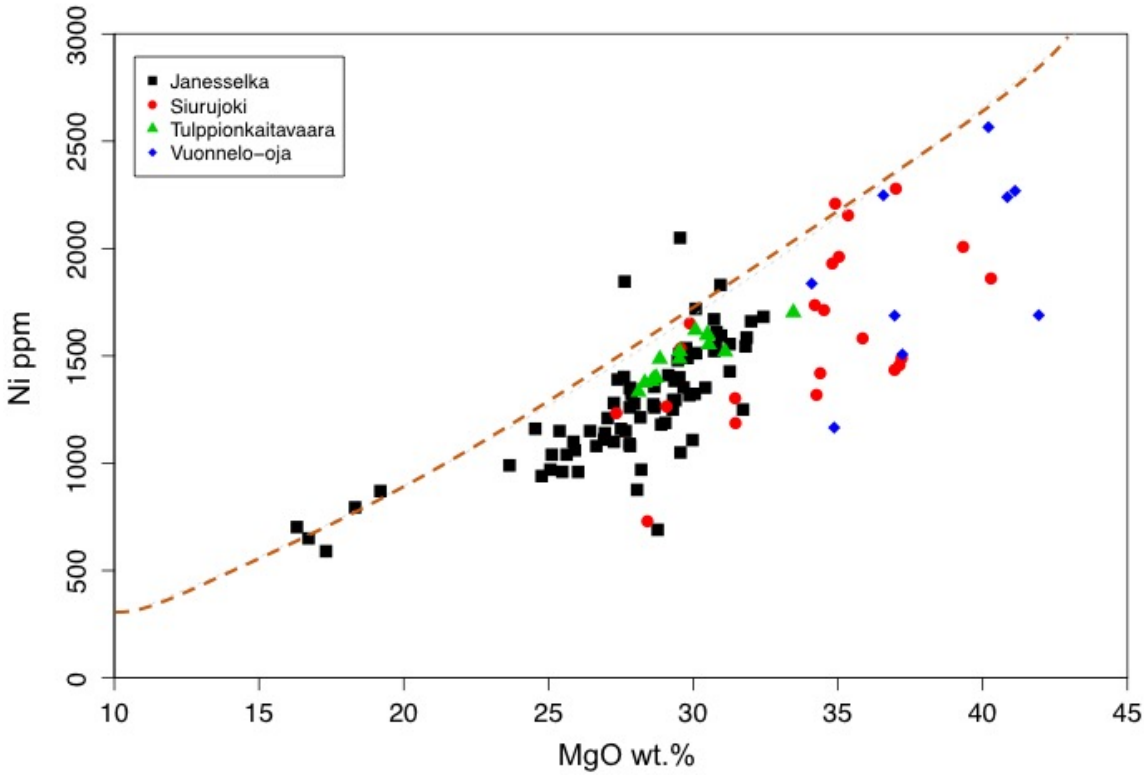

Figure 62. MgO vs. Ni plot of the Ahmatunturi granitoid complex komatiites. Samples plotting above the Ni-undepletion model line can be considered Ni-enriched, and those plotting below it can be considered Ni-depleted. The Ni-undepletion model line after Naldrett et al. 1984 and Makkonen et al. 2017.

High-MgO komatiites produced from Cr-undersaturated melts are almost non-existent except for some individual samples in the Siurujoki body, which barely plot inside the purple prospective samples circle in the Figure 63. However, being of lower MgO contents, the Jänesselkä and Tulppionkaitavaara bodies seem to have crystallized from Cr-saturated liquids, with a trend migrating towards the cotectic crystallization of olivine and chromite. This actually seems to be the case with all the targets, although Vuonnelo-oja forms a weak trend from cotectic crystallization trend towards the olivine-controlled (Cr-undersaturated) trends. Consequently, in the Ni vs. Cr plot (Figure 64) the Jänesselkä and Tulppionkaitavaara samples together with the Siurujoki samples plot in between olivine-chromite and olivine-cumulate fields with Vuonnelo-oja representing cotectic olivine-chromite compositions. Nevertheless, none of the targets trend towards the mineralized komatiite direction.

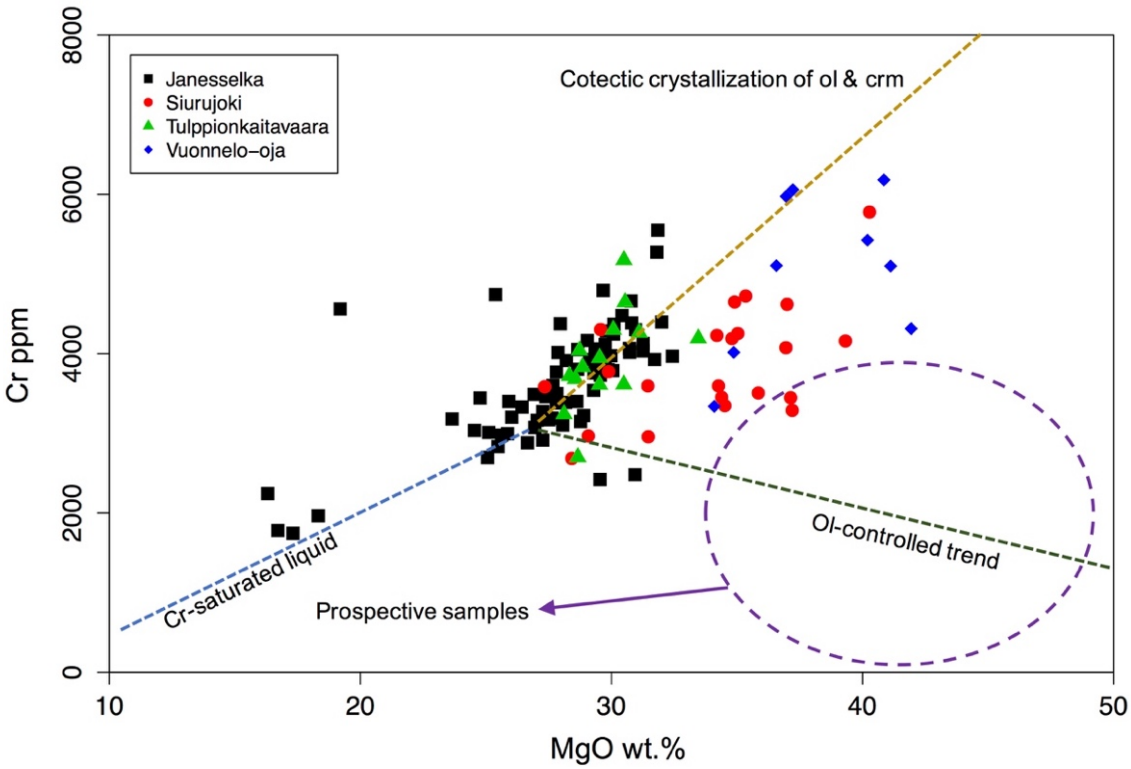

Figure 63. MgO vs. Cr plot of the Ahmatunturi granitoid complex komatiites. Globally, prospective samples plot in or in the proximity of the purple circle. Blue dashed line represents Cr-saturated liquid, in which solubility is controlled by chromite solubility (the low-MgO rocks). Yellow dashed line represents cotectic crystallization of chromite and olivine from Cr-saturated melt. Green dashed line represents olivine-controlled trend (olivine-liquid mixing, Cr-undersaturated melt), in which crystallization is controlled by olivine. Globally most of the komatiites plot in between the cotectic and ol-controlled trends. Lines after Barnes & Fiorentini (2012), prospective sample field after Konnunaho (2016). Ol = olivine, crm = chromite.

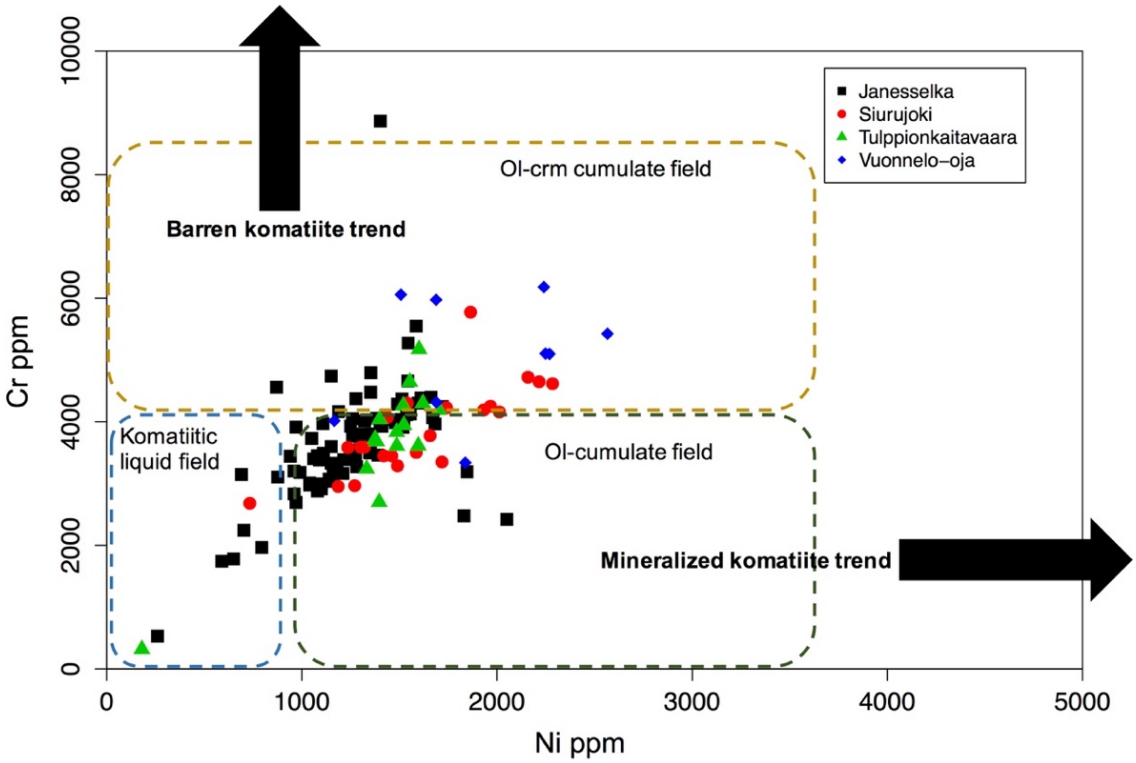

Figure 64. Ni vs. Cr plot of the Ahmatunturi granitoid complex komatiites. Samples with low Cr and high Ni represent mineralized komatiite trend, along which Ni sulfide abundance increases. Samples with high Cr and low to moderate Ni represent the barren komatiite trend, where ol-crm cumulates are produced and Ni typically partitions into silicates. The dashed fields represent theoretical ol-crm cumulates (yellow), ol-cumulates (green) and non-cumulus komatiites (blue). Trends and fields after Brand (1999). Ol = olivine, crm = chromite.

Sulfur contents range from generally low (< 300 ppm) contents of Vuonnelo-oja, Tulppionkaitavaara and Siurujoki to higher (from ca. 1000 ppm average up to 7000 ppm) contents in Jänesselkä (Figure 65). Notably, the Vuonnelo-oja samples show clear correlation in the S vs. Ni plot, although otherwise there is no clear correlation between sulfur and chalcophile elements. However, in the Jänesselkä body the highest S contents seem to correspond to Ni contents of around 1200–1500 ppm, most of which represent the highest MgO-fraction (27–30 wt.%) in there. This possibly demonstrates presence of sulfides that do not contain Ni, e.g., pyrite and pyrrhotite, in the Jänesselkä body. The anomalous Pt+Pd contents in Siurujoki are not either correlate with sulfur as uniform 20–25 ppm Pt+Pd abundances are found at S contents ranging from 80–800 ppm.

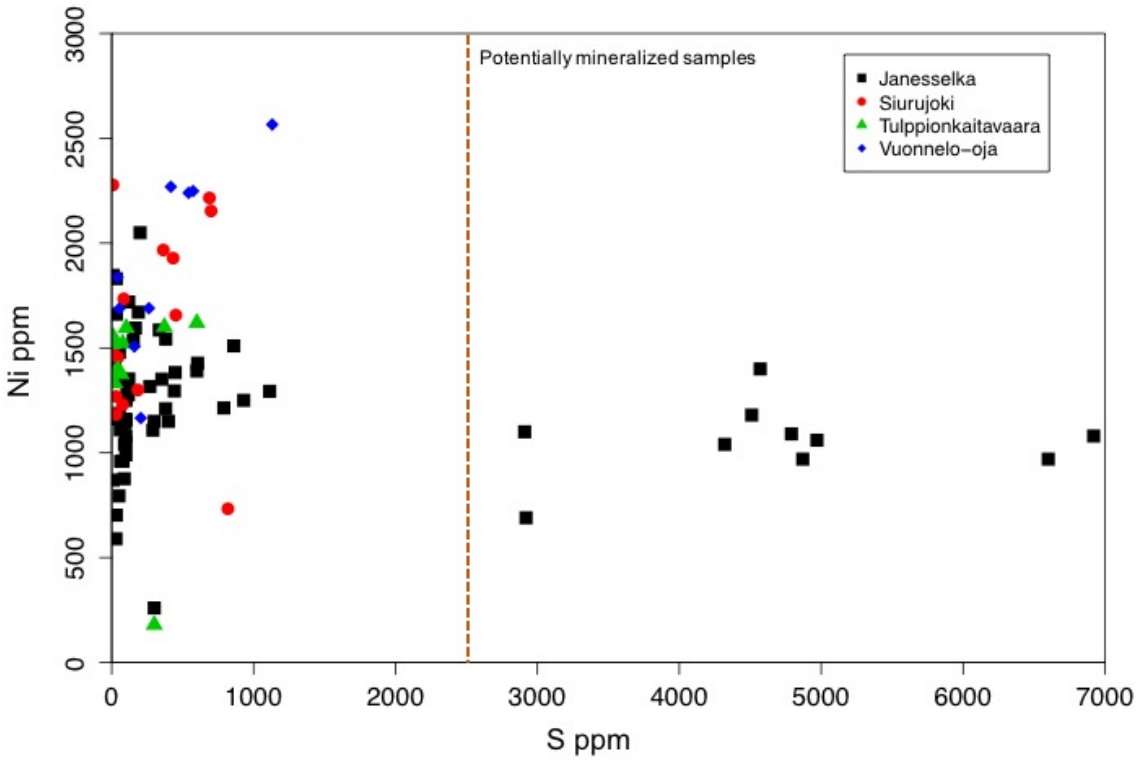

Figure 65. S vs. Ni plot of the Ahmatunturi granitoid complex komatiites. The yellow dashed line marks potentially mineralized samples.

The Jänesselkä and Tulppionkaitavaara bodies show very uniform REE-patterns (Figures 66A and 66B). Both have clearly elevated LREE (up to ten times primitive mantle values) with a drop in Eu and flat, relatively elevated HREE. Only one komatiitic basalt sample (JHTE-2017-35.2) lacks the Eu-anomaly, which is observed to be strongest in the komatiitic cumulate compositions. REE patterns of the Vuonnelo-oja body show depleted LREE and flat HREE, typically just below primitive mantle values (Figure 66C). Eu is below the detection limit in these samples. Furthermore, the Jänesselkä and Tulppionkaitavaara bodies have relatively high ca. 2.3 median $(La/Sm)_N$ values, whereas the Vuonnelo-oja body bears relatively low median value of ca. 0.67. All three targets have elevated $(Gd/Yb)_N$ values of ca. 1.4 (Figure 67). Notably, the Jänesselkä and Tulppiokaitavaara bodies form a clear linear positive trend between the ratios in this diagram.

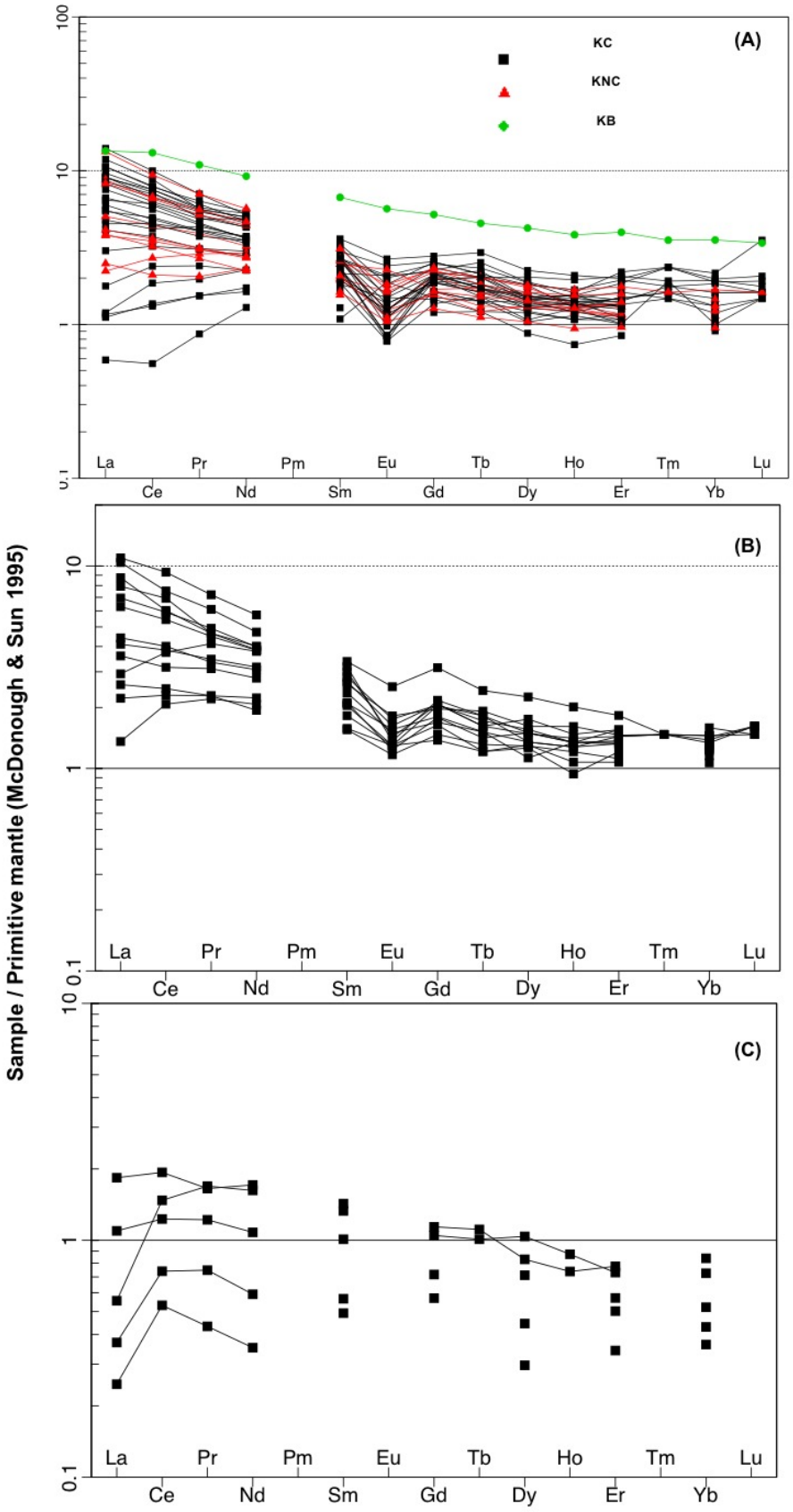

Figure 66. REE-patterns of the Ahmatunturi granitoid complex normalized to primitive mantle (Bulk Silicate Earth) after McDonough & Sun (1995). Gaps mean values below detection limit, Pm is an unstable element and was not determined. (A) Jänesselkä, (B) Tulppionkaitavaara, (C) Vuonnelo-oja. KC = komatiitic cumulate (MgO > 28 wt.%), KNC = komatiitic non-cumulate (28 < MgO > 18 wt.%), KB = komatiitic basalt (MgO < 18 wt.%).

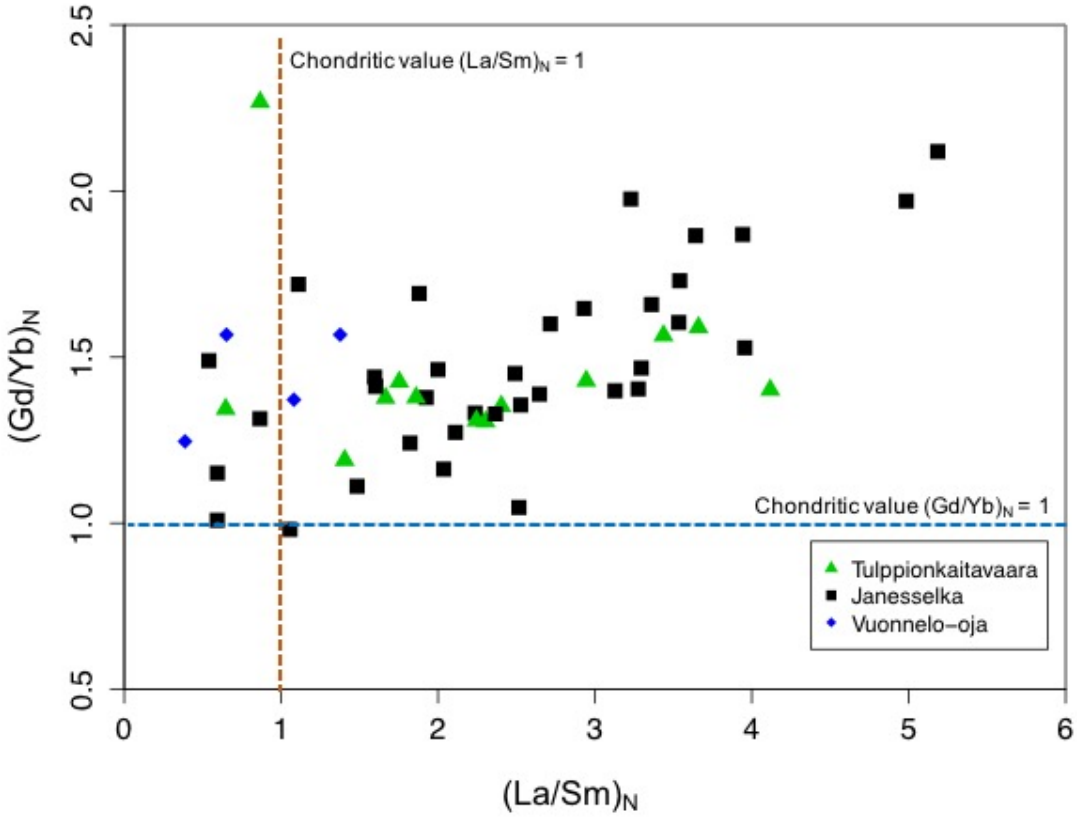

Figure 67. $(La/Sm)_N$ vs. $(Gd/Yb)_N$ plot of the Ahmatunturi granitoid complex komatiites. Enrichment in $(La/Sm)_N$ relative to $(Gd/Yb)_N$ have been in theory attributed to crustal contamination. Normalization values from REE C1 chondrite (McDonough & Sun 1995).

7.4.4 The Tuntsa metasedimentary belt komatiites

Five separate targets are studied within TSB: Kuskoiva, Moukavaara, Siriortsa, Torolehdontyvet-Muotkaselkä, and Värriöjoki (Figure 68). Altogether 305 samples, 91 with appropriate REE data, in the final processed data set are from these (Table 9).

Table 9. Distribution of samples between the studied targets in the Tuntsa metasedimentary belt. the Kuskoiva targets includes samples from the Kuskoivanpahka, Juntterivaara, Pirunkirkko, Takkaselkätunturi, Jäkälätunturi, and Alimmainen Nuolusoja subtargets. The Torolehdontyvet-Muotsalselkä target includes samples from the Torolehdontyvet, Muotkaselkä, and Marjavaaranharjut subtargets.

Target	Samples (with REE data)	Cumulates	Non-cumulates	Komatiitic basalts
Kuskoiva	36 (12)	23	8	5
Moukavaara	3 (2)	2	1	0
Siriortsa	2 (0)	0	2	0
Torolehdontyvet-Muotkaselkä	16 (7)	11	5	0
Värriöjoki, Leppäselkä	51 (39)	43	8	0
Värriöjoki, Liessijoki	18 (4)	17	1	0
Värriöjoki, Venehaara	26 (14)	23	1	2
Värriöjoki, Värriöjoki	153 (12)	150	1	2
In total	305 (91)	269	27	9

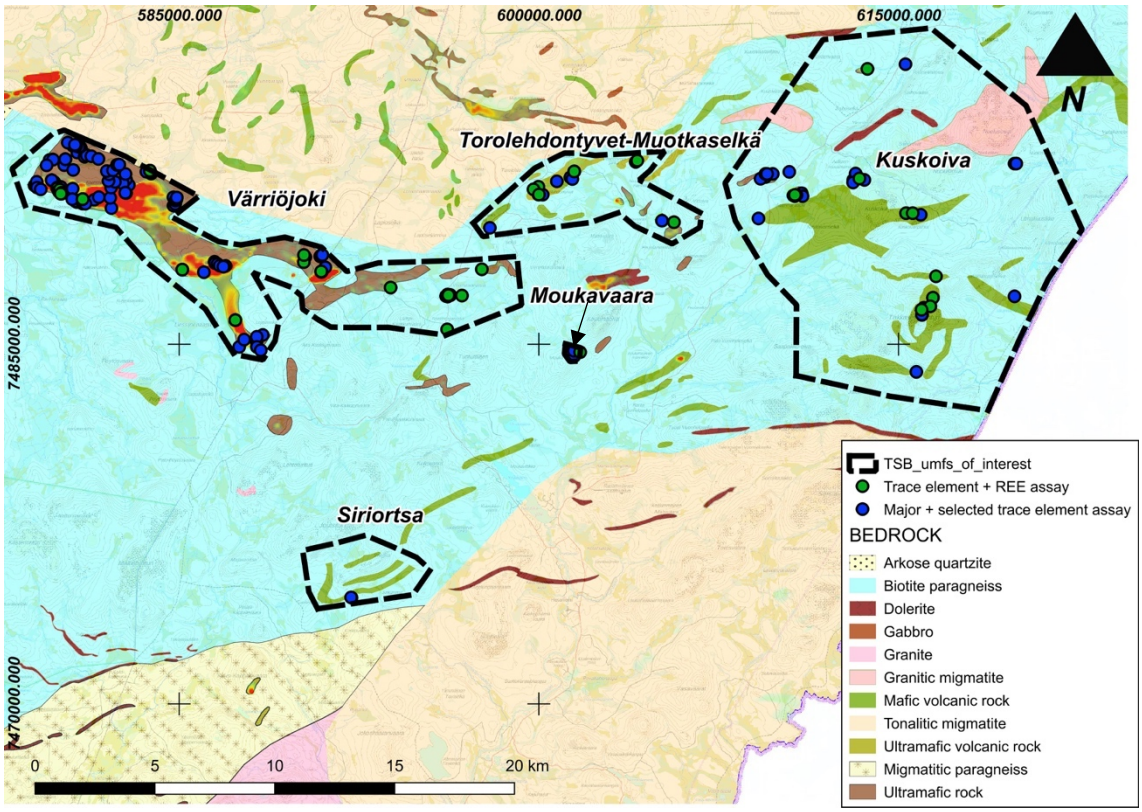

Figure 68. Major element and REE assays performed from the komatiites of the Tuntsa metasedimentary belt.

To briefly elaborate the major element chemistry of TSB presented in section 7.3, in Al_2O_3 vs. TiO_2 plot most of the Värriöjoki samples plot at values 15–20 with no detectable variation within the blocks. The Kuskoiva samples show scatter, but in general comprise two trends, one similar to that of Värriöjoki and another having ratios typical within ELAD (ca. 25–30). The Torolehdontyvet-Muotkaselkä, Moukavaara and Siriortsa samples also follow the latter trend. MgO contents in the Värriöjoki blocks range from ca. 25 up to ca. 50, mostly distributed between 40–50 wt.% MgO. The Kuskoiva samples show similar trend as Värriöjoki, except for they seem to lack samples with > 40 wt.% MgO. The Torolehdontyvet-Muotkaselkä has two distinct groups, one with > 40 wt.% MgO and other with ca. 25–32 wt.% of MgO corresponding to the values found in the Jänesselkä and Tulppionkaitavaara samples in AGC.

Nickel contents in The TSB komatiites range from ca. 1000 up to 4000 ppm, consistent with observations in ELAD in general. Nickel depletion is the most evident in the Värriöjoki body (Figure 69). Interestingly, scatter is particularly observed in the samples with the highest (40–50 wt.%) MgO. Furthermore, also a number of potentially mineralized samples plot above the model line. In addition, clear indication of Ni

depletion is observed in the Kuskoiva area komatiites, even though they principally follow the olivine-fractionation trend, as the other targets in TSB. As for the other chalcophile elements, Cu contents are generally low (< 100 ppm) in TSB but clearly anomalous samples exist, mainly in the Värriöjoki body (samples with 150–300 ppm Cu). Also, anomalous PGE (Pt+Pd) contents are found in the Värriöjoki and Kuskoiva (the Juntterivaara subtarget) targets with several samples showing values of 25–44 ppb (these lack only in the Venehaara block) and 51 ppb (JHTE-2017-17.1), respectively.

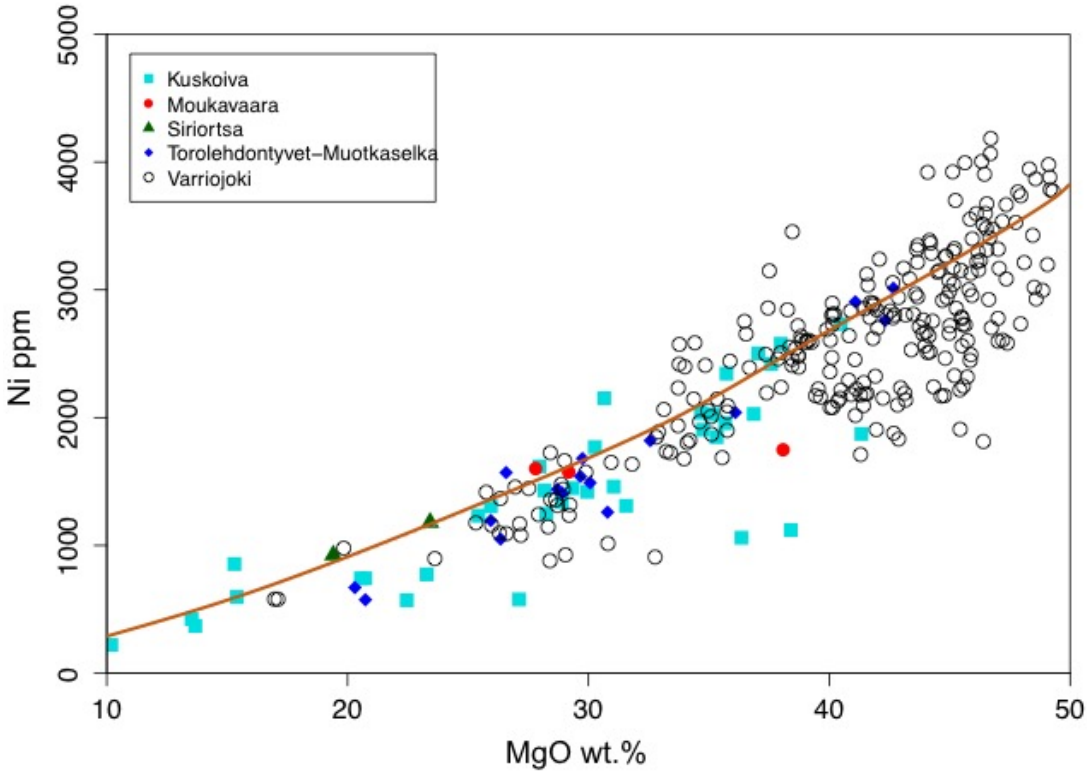

Figure 69. MgO vs. Ni plot of the Tuntsa metasedimentary belt komatiites. Samples plotting above the Ni-undepletion model line can be considered Ni-enriched, and those plotting below it can be considered Ni-depleted. The Ni-undepletion model line after Naldrett et al. 1984 and Makkonen et al. 2017.

Observations of high-MgO komatiites crystallized from Cr-undersaturated melt arouses curiosity even more in the case of the Värriöjoki body, as it comprises a clear group below the olivine-controlled fractionation (Cr-undersaturated) trend in the the Cr vs. MgO plot (Figure 70). Notably, the Värriöjoki melt seems to have been evolved in two directions, other following the cotectic crystallization of olivine and chromite, and the other following the olivine-controlled Cr-undersaturated trend. In addition, some samples from the Torolehdontyvet-Muotkaselkä, Kuskoiva and Moukavaara targets have crystallized from Cr-undersaturated melts. In addition, the Ni vs. Cr plot (Figure 71) displays the same

trends in the Värriöjoki body, in this case the other following the “barren komatiite”-trend and the other the “mineralized komatiite”-trend.

On the other hand, TSB is characterized by lack of S (Figure 72). Most of the samples have < 500 ppm of S, although higher clearly anomalous contents of 1000–3300 ppm are also observed. The highest anomalous S contents, however, are found in samples showing relatively high, 3000-4000 ppm Ni contents, although a clear correlation cannot be outlined. Nevertheless, the Värriöjoki samples comprise show a weak positive correlation (similar to Tulppio) in the S vs. Ni plot. As for the Cu and PGE (Pt+Pd) contents, the samples with anomalously high concentrations of these elements are not enriched in S.

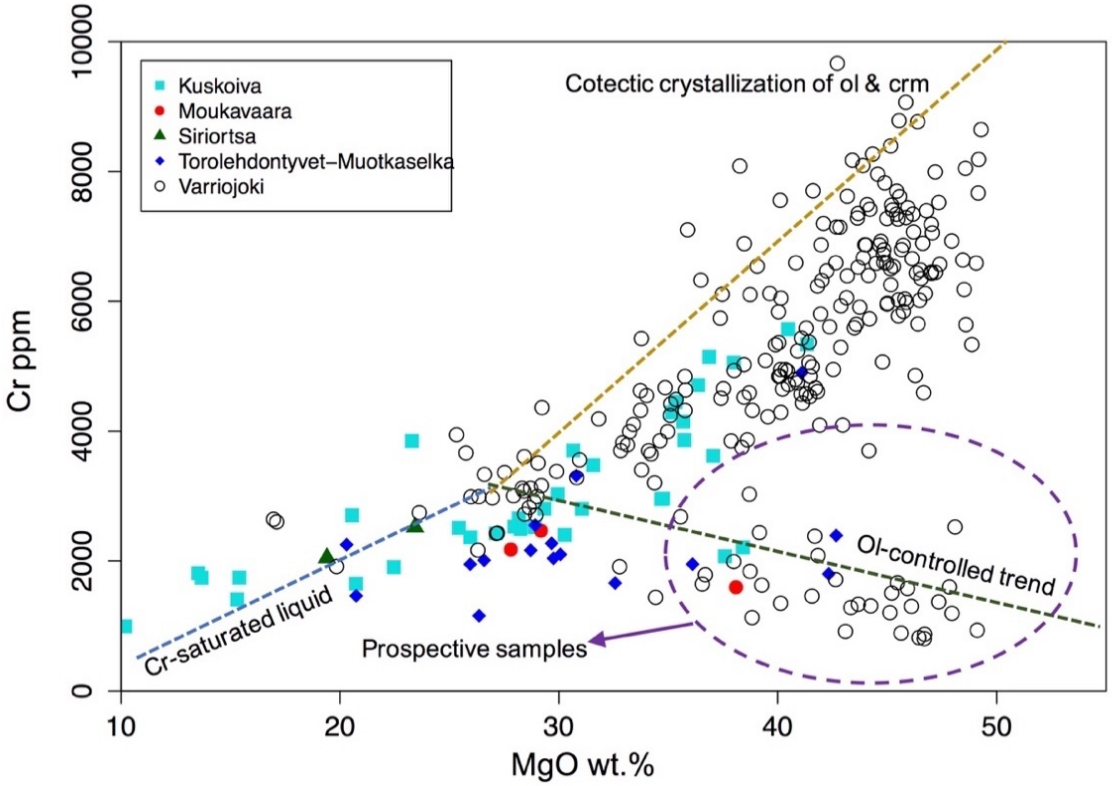

Figure 70. MgO vs. Cr plot of the Tuntsa metasedimentary belt komatiites. Globally, prospective samples plot in or in the proximity of the purple circle. Blue dashed line represents Cr-saturated liquid, in which solubility is controlled by chromite solubility (the low-MgO rocks). Yellow dashed line represents cotectic crystallization of chromite and olivine from Cr-saturated melt. Green dashed line represents olivine-controlled trend (olivine-liquid mixing, Cr-undersaturated melt), in which crystallization is controlled by olivine. Globally most of the komatiites plot in between the cotectic and ol-controlled trends. Lines after Barnes & Fiorentini (2012), prospective sample field after Konnunaho (2016). Ol = olivine, crm = chromite.

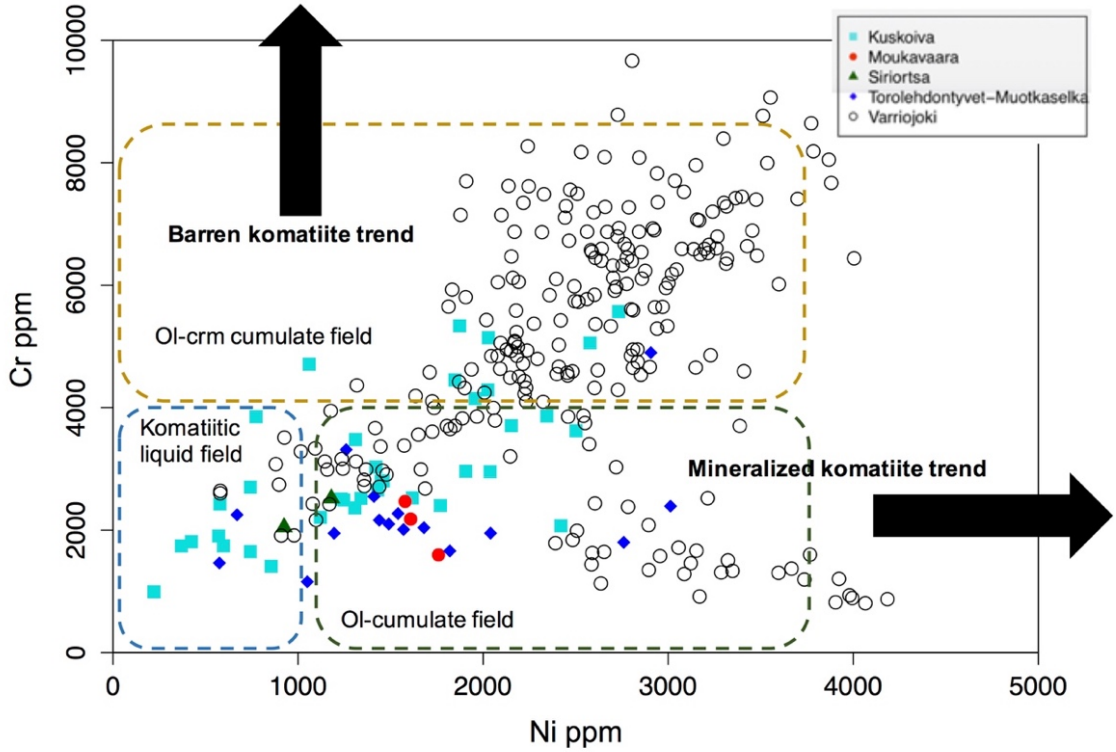

Figure 71. Ni vs. Cr plot of the Tuntsa metasedimentary belt komatiites. Samples with low Cr and high Ni represent mineralized komatiite trend, along which Ni sulfide abundance increases. Samples with high Cr and low to moderate Ni represent the barren komatiite trend, where ol-crm cumulates are produced and Ni typically partitions into silicates. The dashed fields represent theoretical ol-crm cumulates (yellow), ol-cumulates (green) and non-cumulus komatiites (blue). Trends and fields after Brand (1999). Ol = olivine, crm = chromite.

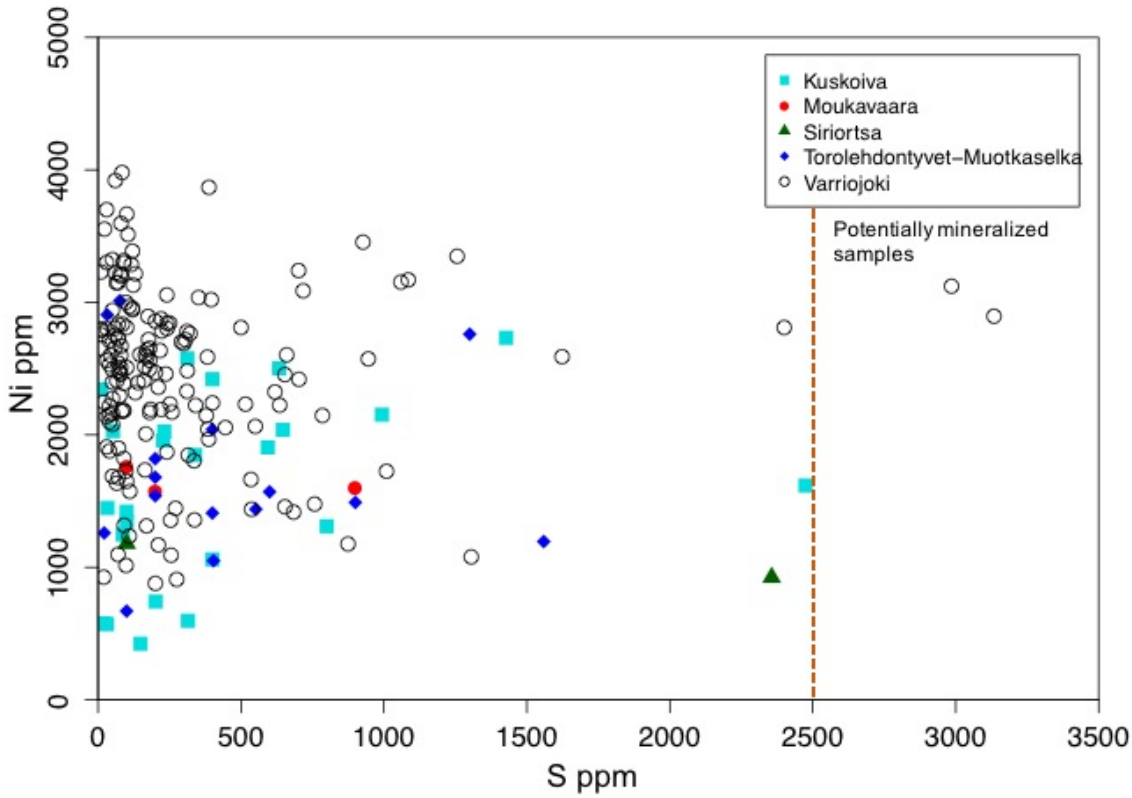

Figure 72. S vs. Ni plot of the Tuntsa metasedimentary belt komatiites. Enrichment in S is divided by primitive mantle sulfur content (250 ppm) from McDonough & Sun (1995).

REE patterns of the TSB komatiites show promising indications in terms of enriched LREE. In the Värriöjoki body, notably LREE-enriched (up to 20 times primitive mantle values) are observed in the Leppäselkä and Venehaara blocks (Figures 73A & 73B). The LREE-enriched samples are typically characterized by steep negative Eu anomalies, with respect to the general trends. Most of the LREE-enriched samples are from the DDH R25 (Leppäselkä block). In the main and the Liessijoki blocks similar degree of enrichment is not observed, although the patterns are still slightly LREE-enriched (Figures 73C & 73D). HREE are relatively depleted in all blocks. The Kuskoiva samples show flat REE patterns close to primitive values (Figure 74). The only clearly LREE-enriched komatiitic cumulate sample (PSHA-2017-15.1) with a weak negative Eu-anomaly is from the Pirunkirkko subtarget. The Torolehdontyvet-Muotkaselkä target has both LREE and HREE close to chondritic values, with MREE (middle REE) slightly enriched, which forms "hump-shaped" REE patterns (Figure 75). Negative Eu-anomalies are also present. Curiously, a sample from the Marjavaaranharjut subtarget (PSHA-2017-36.1) has very depleted LREE and HREE with La showing relative enrichment. From the Moukavaara body one sample (HMHO-2017-45.1) was analyzed for REE and it shows similar patterns to the Torolehdontyvet-Muotkaselkä target. Furthermore, the Värriöjoki body has median $(La/Sm)_N$ values around 2 (ranging from 1.8 in the Leppäselkä block to 2.7 in the Venehaara block) and $(Gd/Yb)_N$ values around 1.5. In the Kuskoiva target the median $(La/Sm)_N$ is ca. 1.5, whereas the Torolehdontyvet-Muotkaselkä target shows a relatively low median value of 0.75. All these targets, however, have $(Gd/Yb)_N$ close to 1 (Figure 75).

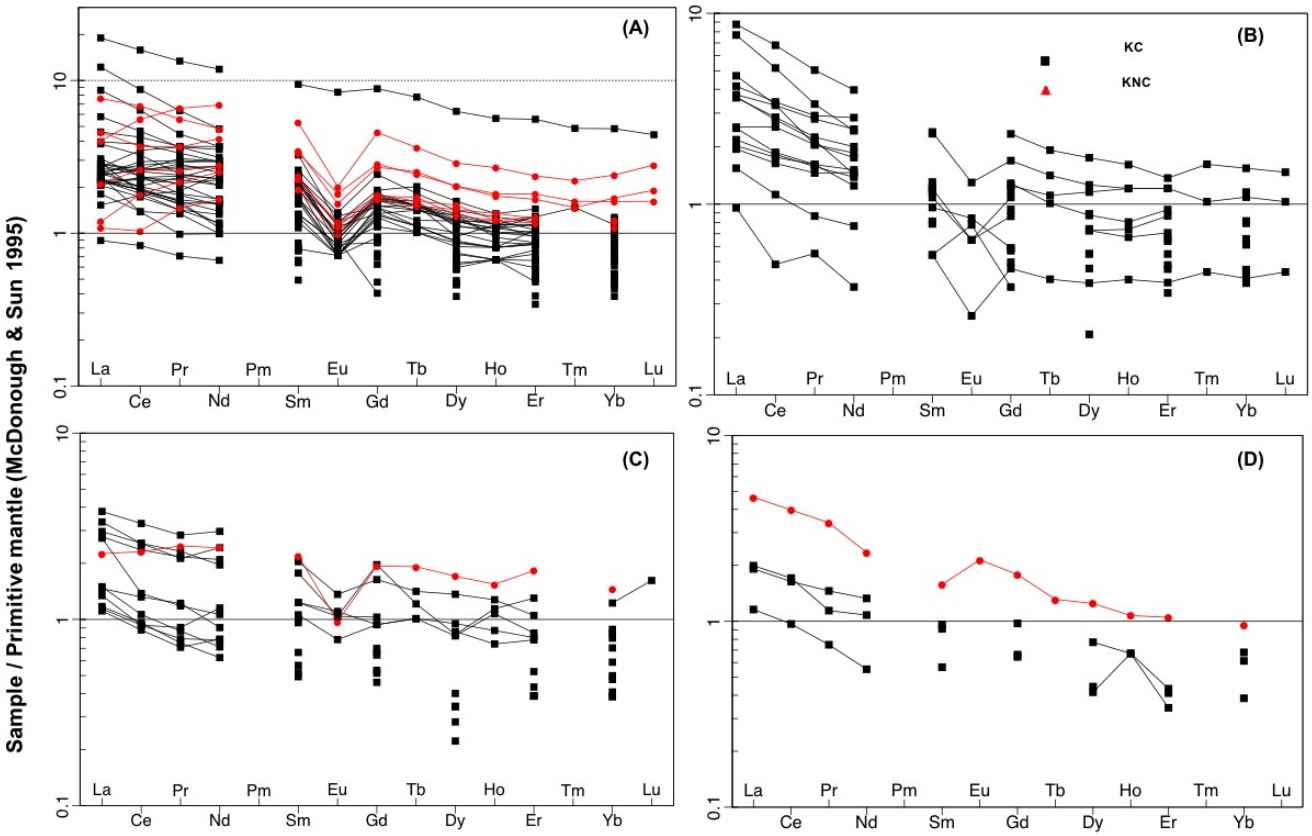

Figure 73. REE-patterns of the Värriöjoki blocks normalized to primitive mantle (Bulk Silicate Earth) after McDonough & Sun (1995). Gaps mean values below detection limit, Pm is an unstable element and was not determined. (A) Leppäselkä, (B) Venehaara, (C) Värriöjoki (main), (D) Liessijoki. KC = komatiitic cumulate (MgO > 28 wt.%), KNC = komatiitic non-cumulate (28 < MgO > 18 wt.%).

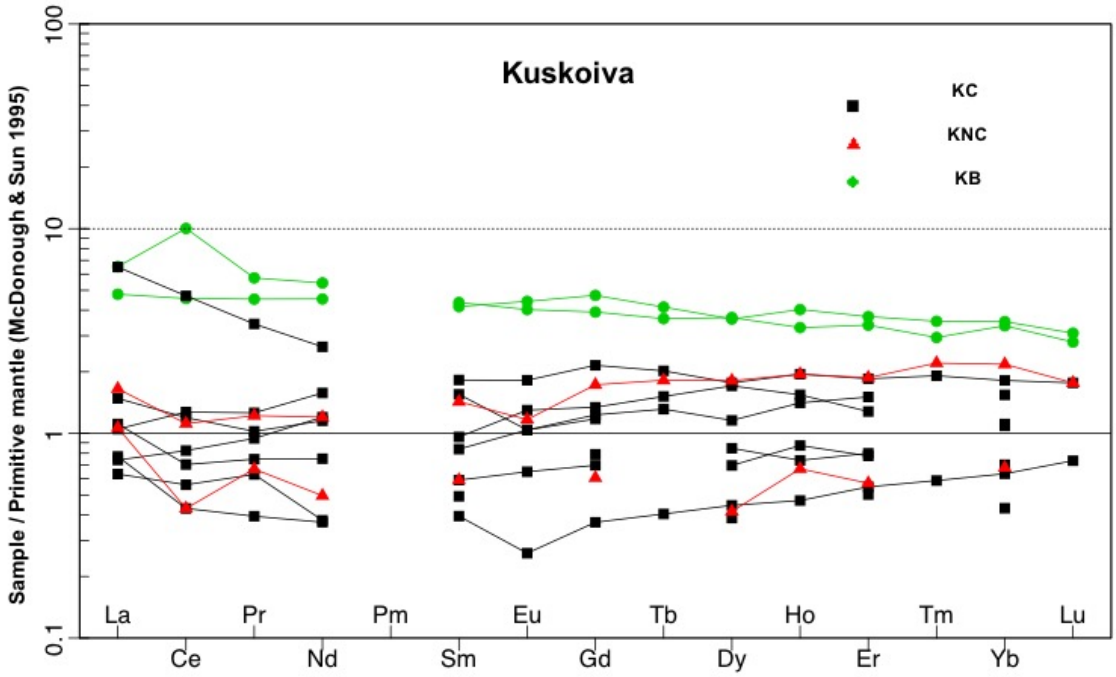

Figure 74. REE-patterns of the Kuskoiva area komatiites normalized to primitive mantle (Bulk Silicate Earth) after McDonough & Sun (1995). Gaps mean values below detection limit, Pm is an unstable element and was not determined. KC = komatiitic cumulate (MgO > 28 wt.%), KNC = komatiitic non-cumulate (28 < MgO > 18 wt.%), KB = komatiitic basalt (MgO < 18 wt.%).

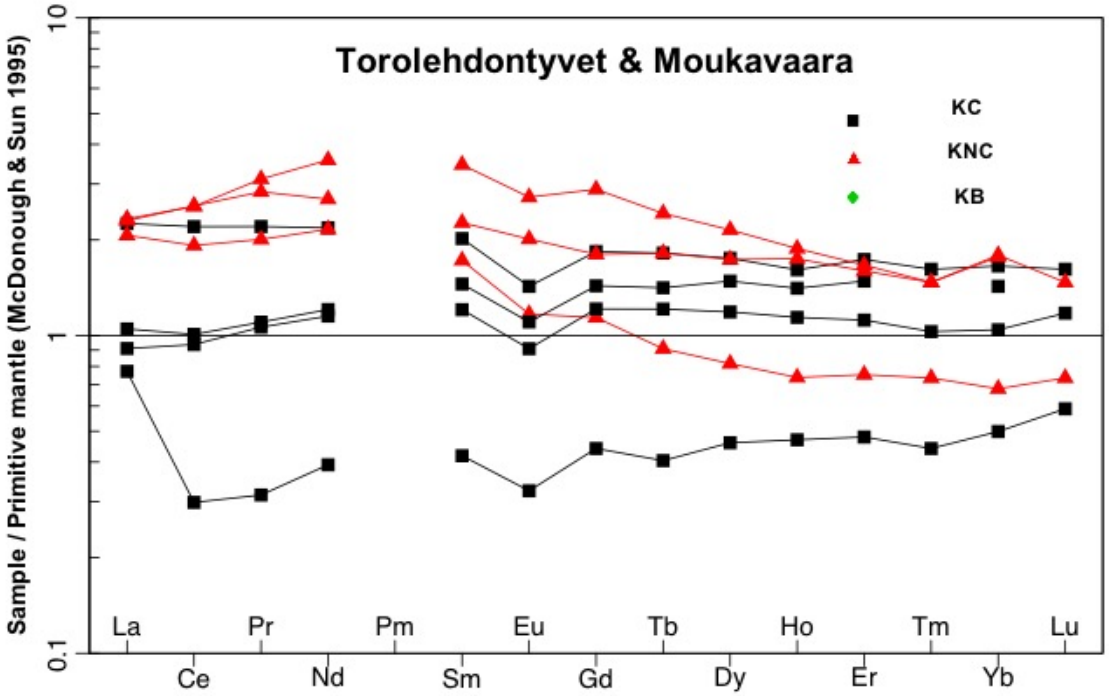

Figure 75. REE-patterns of the Torolehdontyvet-Muotkaselkä and Moukavaara komatiites normalized to primitive mantle (Bulk Silicate Earth) after McDonough & Sun (1995). Gaps mean values below detection limit, Pm is an unstable element and was not determined. KC = komatiitic cumulate (MgO > 28 wt.%), KNC = komatiitic non-cumulate (28 < MgO > 18 wt.%), KB = komatiitic basalt (MgO < 18 wt.%).

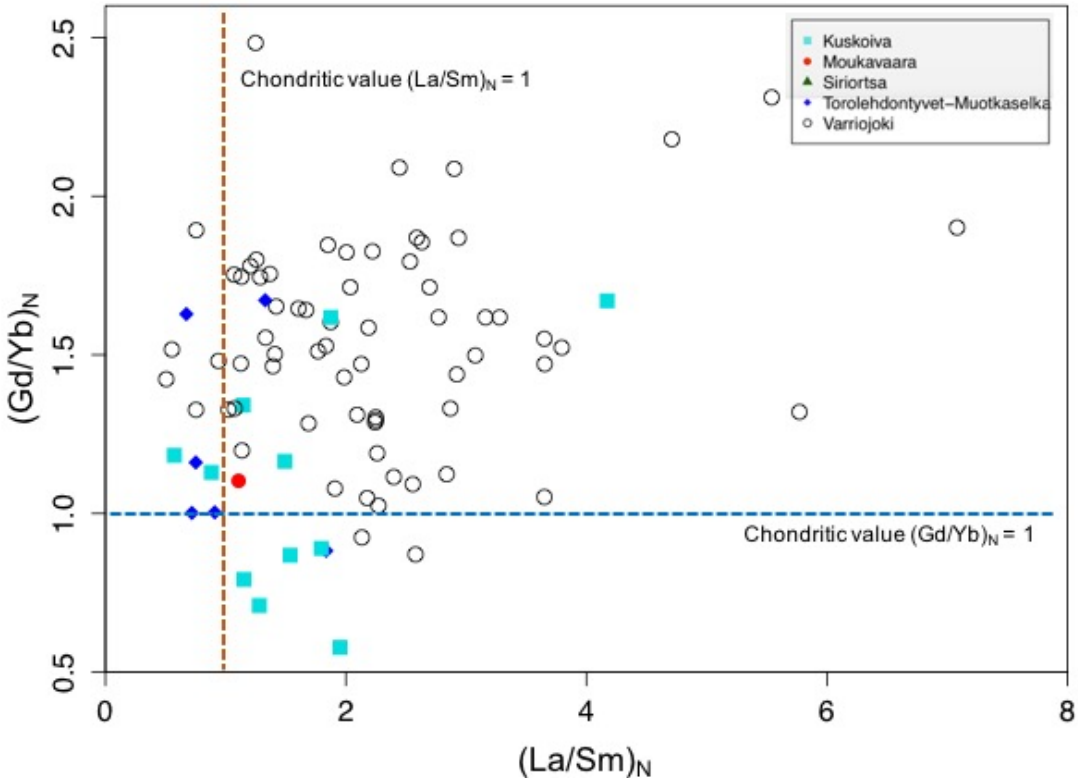

Figure 76. $(La/Sm)_N$ vs. $(Gd/Yb)_N$ plot of the Tuntsa belt komatiites. Enrichment in $(La/Sm)_N$ relative to $(Gd/Yb)_N$ have been in theory attributed to crustal contamination. Normalization values from REE C1 chondrite (McDonough & Sun 1995).

7.5 Mineral chemistry applied to Ni-Cu-PGE potential

7.5.1 Olivine

The analyzed olivines were divided into either magmatic or metamorphic type on the basis of petrography (Figure 77). Magmatic olivines were recognized only from the Tulppio and Värriöjoki (Venehaara) bodies. It is, however, important to note that "petrographically magmatic" does not strictly mean a confirmed magmatic origin. Petrographically magmatic olivines are typically subhedral to euhedral with relatively equal axis dimensions, bimodal in terms of grain size, and often lack inclusions. Petrographically metamorphic olivines are typically platy, large, broken, and full of inclusions (e.g., Cr-magnetite). Some are also characterized by intense serpentine veining. In many cases, olivines are interpreted metamorphic if the matrix shows a completely metamorphic assemblage, which cannot be observed in the olivine adcumulates regarded as magmatic. However, in some rocks with metamorphic olivine relict cumulate textures are still present, which makes the classification even more difficult (see Figures 77C, 77E, 77D).

Both magmatic and metamorphic olivine were analyzed from relatively unaltered clear parts of each grain. The analyzed olivine has forsterite contents of $Fo_{67\text{-}92}$ (Figure 78). The highest Fo contents are found in the Tulppio body, whereas the Jänesselkä body has the lowest contents. Interestingly, olivine grains from the Jänesselkä and Pirunkirkko targets form two distinct groups with high and low Fo contents, respectively, while the others make up homogeneous groups with no significant variation in their Fo content. In Jänesselkä the lower Fo contents (ca. Fo_{67}) are found in the southern edge of the body (sample PSHA-2017-26.1), where olivine grains are more broken and altered. The higher Fo contents (ca. Fo_{87}) are located in the middle parts of the body (sample HMHO-2017-20.1, Figure 77E), where olivine is much fresher. In Pirunkirkko, all olivine grains were analyzed from one thin section (PSHA-2017-14.1). The highest Fo contents (ca. Fo_{84}) were obtained from one unaltered and clean (possibly metamorphic) olivine, while the lower Fo contents (ca. Fo_{73}) were analyzed from the olivine grains displaying intense serpentine veining (Figure 77D).

Nickel contents of the olivine scatter respective to their Fo content (Figure 78). Highest Ni contents (> 0.4 wt.%) are found in the Heiniselkä and Tulppio areas. However, variation of Ni contents of the Heiniselkä olivine at given Fo content is quite notable, which reflects the metamorphic nature of the olivine. Theoretically, however, metamorphic olivine should be depleted in Ni, because Ni is released from magmatic olivine during serpentinization and consumed by the newly formed serpentine-magnetite-

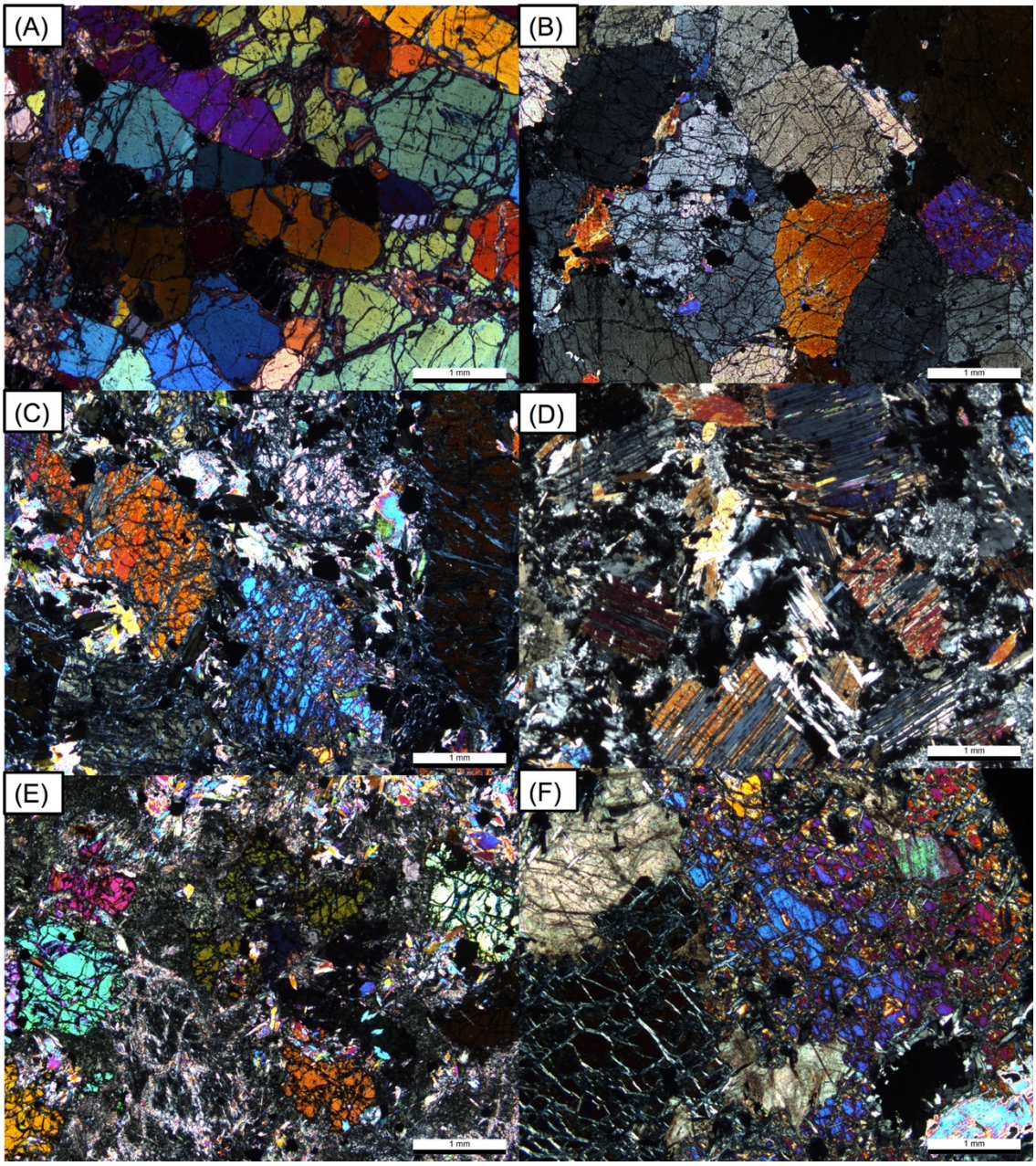

Figure 77. Photomicrographs of some of the analyzed olivines. (A) Magmatic olivines in olivine adcumulate (4723-2008-R0318-15.70) from Tulppio, (B) Magmatic olivines in olivine adcumulate (JHTE-2017-25.2) from the Venehaara block, Värriöjoki, (C) Broken and veined olivine grains in relict cumulate serpentine-tremolite-olivine rock (HMHO-2017-11.1) from Vuonnelo-oja, (D) Olivine grains with intense serpentine veining in relict cumulate olivine-tremolite-serpetine rock (PSHA-2017-14.1) from Pirunkirkko, (E) Olivine grains in a relict cumulate olivine-tremolite-chlorite rock (HMHO-2017-20.1) from Jänesselkä and (F) Large platy metamorphic olivines in olivine rock (HMHO-2017-17.1) from Heiniselkä. Scale bars in the down-right corners of the images are 1 mm.

brucite assemblage. This effect also makes metamorphic olivine more Mg-rich (increase in Fo) as Fe behaves in a similar manner with Ni. Nevertheless, many of the olivine grains have quite homogeneous Ni contents, such as the ones from Venehaara and Tulppio, but also from Vuonnelo-oja and Torolehdontyvet. Curiously, olivine from Tulppio, which were petrographically considered as metamorphic have higher Ni contents than the olivines that were petrographically considered magmatic. Also, the olivines from Jänesselkä and Pirunkirkko seems to have quite homogeneous Ni contents, even though they show variation in Fo content.

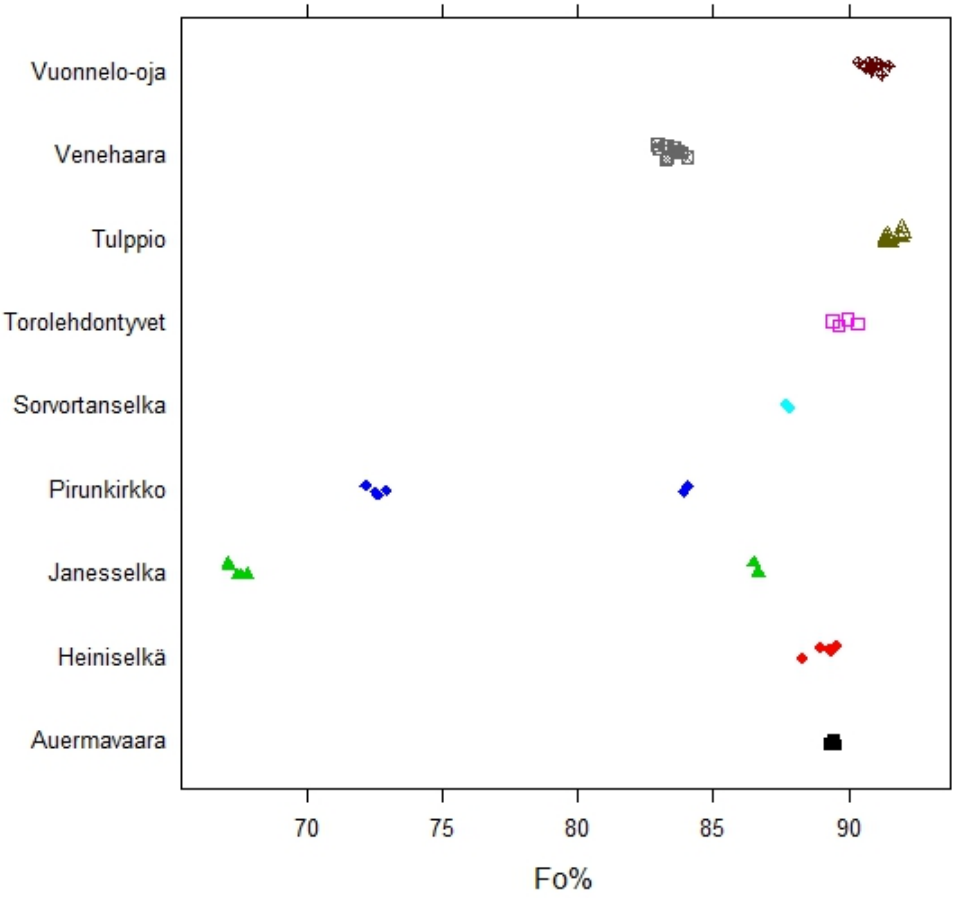

Figure 78. Fo% contents of the analyzed olivines in the Eastern Lapland Archean domain.

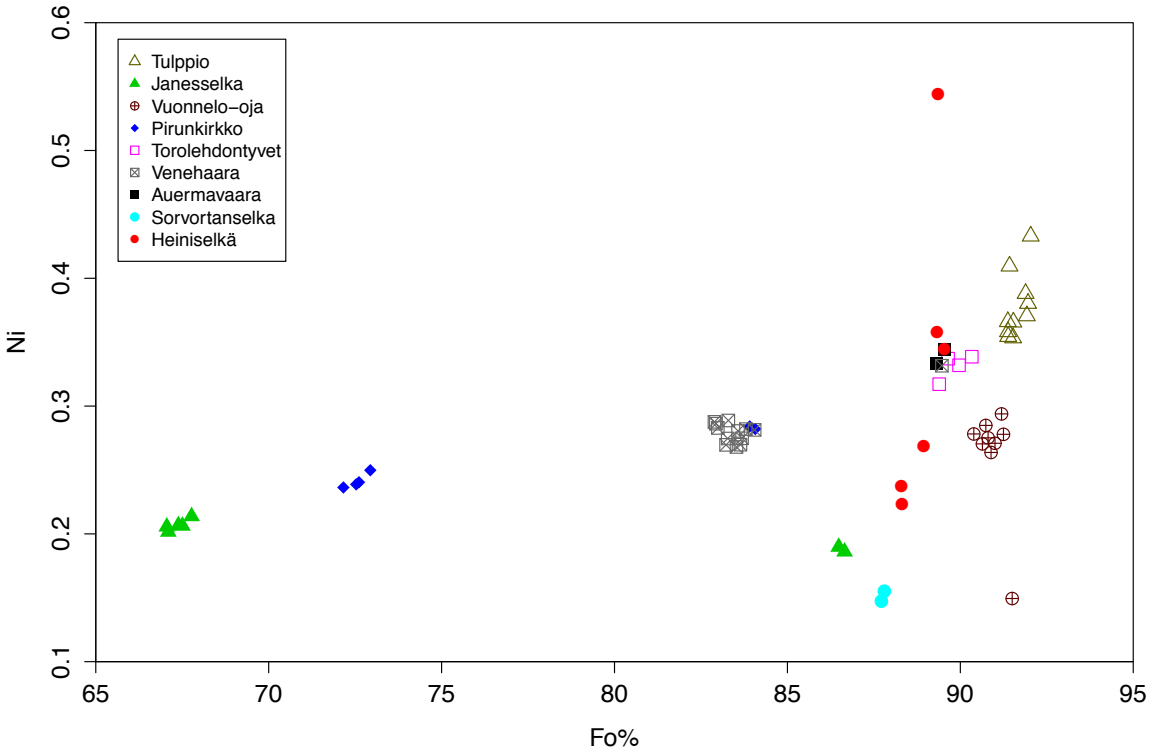

Figure 78. Fo% vs. Ni in olivine plot showing comparison of Ni contents (wt.%) of the analyzed olivines from the Eastern Lapland Archean domain.

Tulenheimo (1999) has studied olivine compositions in the Kellojärvi ultramafic complex in the Kuhmo greenstone belt in eastern Finland and evaluated magmatic and metamorphic origins based on constraints set by Blais (1989) in Fo vs. NiO and Fo vs. MnO plots (see Tulenheimo 1999, figs. 88 & 89). According to these criteria, olivine from Tulppio, Torolehdontyvet, Vuonnelo-oja, Auermavaara, Heiniselkä, as well as, the higher Fo olivine from Jänesselkä could be considered magmatic olivine in the Fo vs. NiO plot (Figure 79A). Furthermore, olivines from Venehaara, Pirunkirkko, Torolehdontyvet, Heiniselkä, and, in addition some olivines from Tulppio and Auermavaara, would display signs of magmatic origin in the Fo vs. MnO plot (Figure 79B).

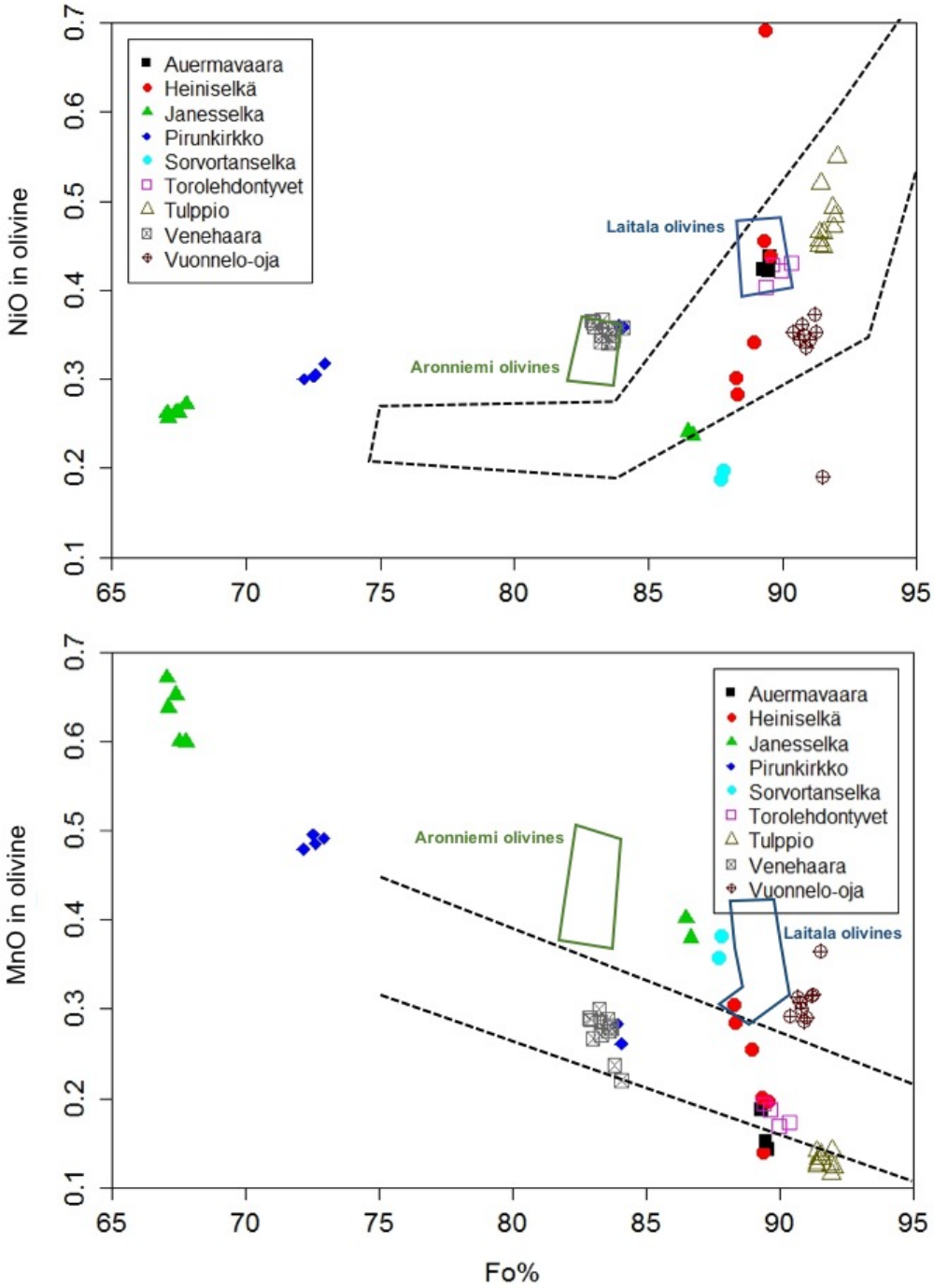

Figure 79. NiO wt.% (upper) and MnO wt.% (lower) data from the olivines of ELAD plotted against Fo. The areas between the dashed lines in both diagrams represent possibly magmatic olivine compositions after Blais (1989). The boxes illustrate olivine compositions from Aronniemi (green) and Laitala (blue) in the Kellojärvi ultramafic complex in the Archean Kuhmo greenstone belt, eastern Finland (Tulenheimo 1999).

As for exploration implications, Barnes et al. (2013) have studied olivine compositions from the type I Mirabela Ni-Cu-PGE deposit, Northeastern Brazil and the type II Betheno Ni-(Cu) deposit from Western Australia. Both of these deposits contain anomalously Ni-rich olivine associated within a Ni-Cu-PGE sulfide deposit. Comparison of ELAD compositios to their data shows that olivine from Tulppio, Torolehdontyvet and

Auermavaara (Marjavaaranharjut) plot on the sulfide-free komatiite field, albeit Tulppio has two olivine grains with clearly elevated Ni contents (Figure 80). The scattered Heiniselkä data has both depleted and enriched Ni contents. Olivine from Vuonnelo-oja and Sorvortanselkä are clearly depleted in Ni. On the other hand, the Venehaara olivines and some Pirunkirkko olivines plot to the field of layered intrusions without similar compositions to the Santa Rita ore zone in Mirabela. The Jänesselkä olivine shows very depleted Ni contents.

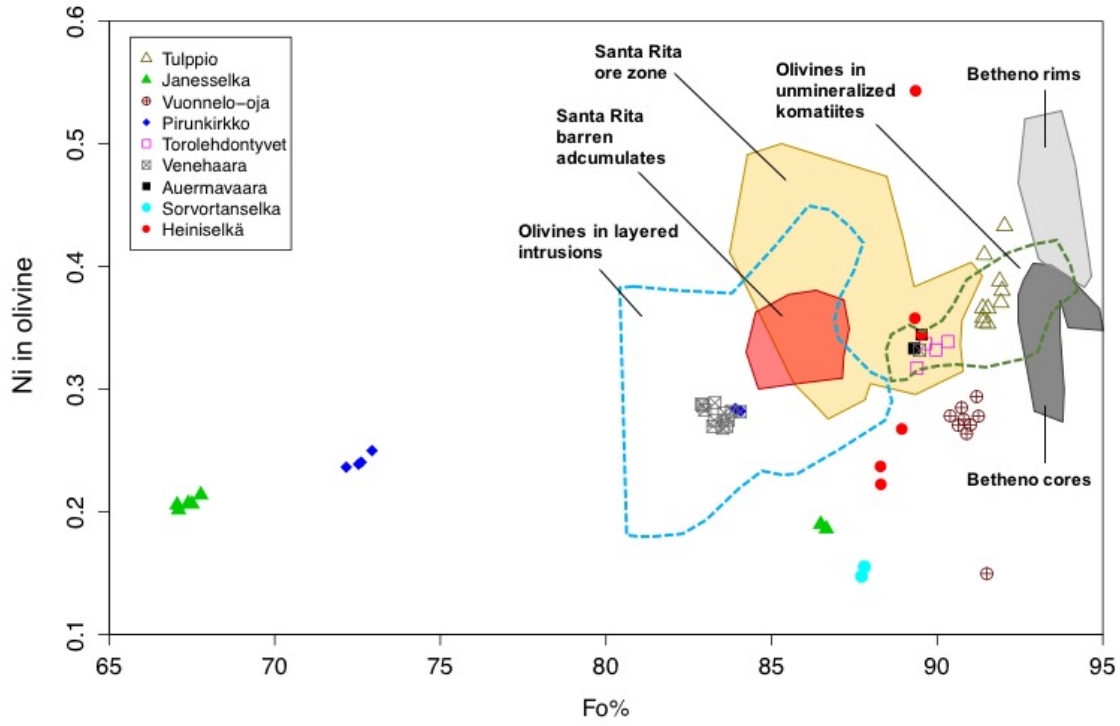

Figure 80. Comparison of olivine data from Mirabela and Betheno deposits from Barnes et al. (2013, see Figure 1) and olivine data from ELAD. Blue dashed field represents majority of olivine from layered intrusions, green dashed field is majority of olivine data from unmineralized komatiites. The grey fields represent olivine core compositions (dark grey) and olivine rim compositions (light grey) from the Betheno Ni-(Cu)-deposits. The yellow and red fields represent samples from the Santa Rita Ni-Cu-PGE ore zone (yellow) and sulfide-free adcumulates (red) from the the Mirabela deposit. All fields after Barnes et a. (2013). Ni in wt.%.

7.5.2 Cr-spinel

Cr-spinels (compositionally chromites and magnesiochromites) display varying crystal habits (Figure 81). Some of the grains have a clear zoning, with darker grey core and lighter grey rims, which is typical for Finnish komatiites (J.Konnunaho, personal communication). These Cr-spinel grains have typically euhedral to subhedral habit and they are restricted to the Tulppio, Värriöjoki (Venehaara block) and Pirunkirkko bodies

among the analyzed grains. Otherwise, Cr-spinel grains are not zoned, pale grey in color, and contain varying amount of inclusions. These grains vary from euhedral-subhedral to ragged and skeletal habits with irregular grain boundaries. Some of the Cr-spinel can be recognized as secondary due to them being situated in a fracture or in a vein. Otherwise, Cr-spinels are typically found enclosed in olivines, between olivines (in olivine cumulates) and within metamorphosed matrix.

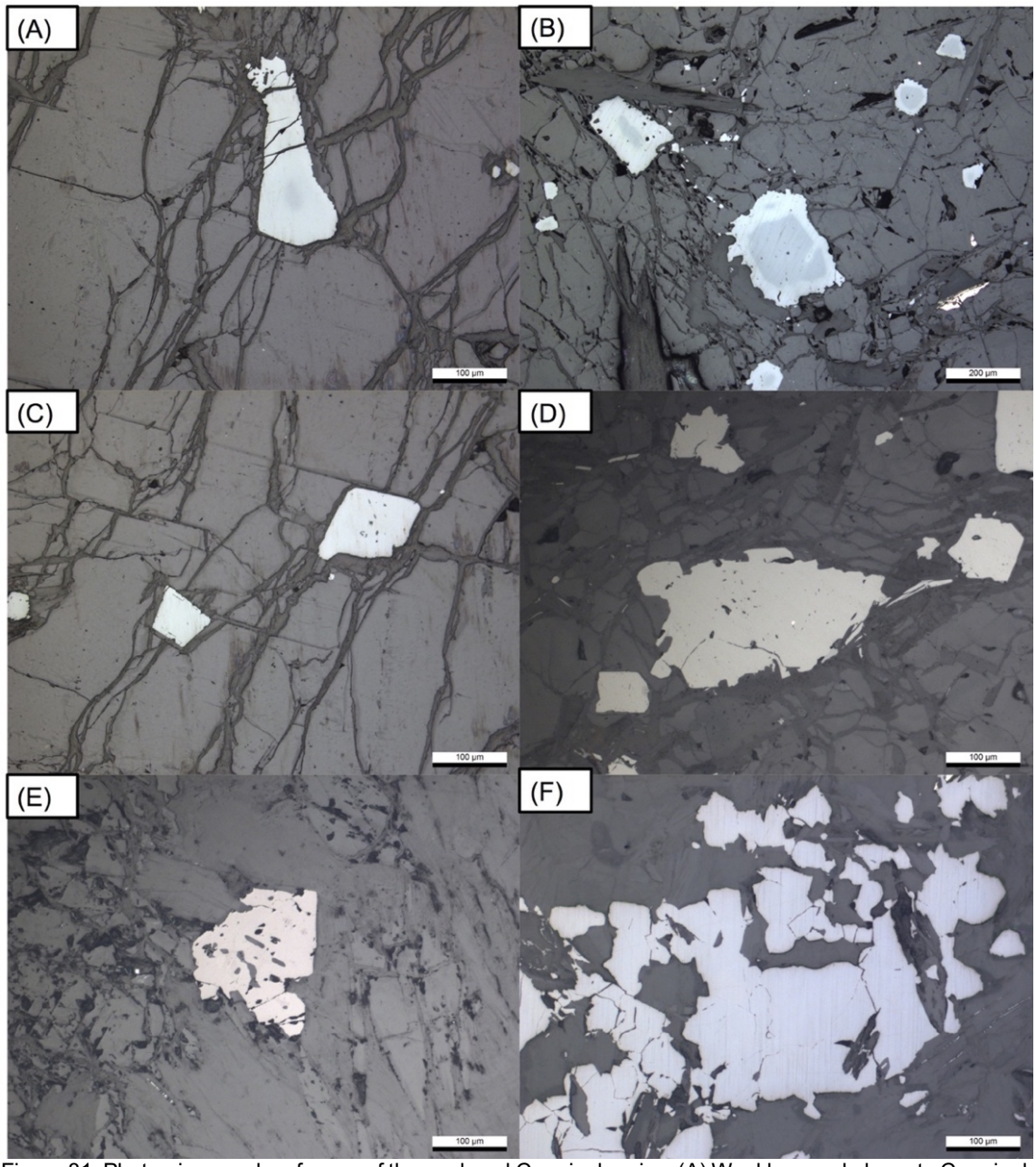

Figure 81. Photomicrographs of some of the analyzed Cr-spinel grains. (A) Weakly zoned elongate Cr-spinel with a relatively thick rim from Tulppio (4723-2008-R0318-15.70). (B) Zoned subhedral Cr-spinels from Venehaara block (Värriöjoki) (HMHO-2017-39.1). The core of the largest grain has been injected by rim material. (C) Euhedral non-zoned Cr-spinels from Tulppio (4723-2008-R0318-15.70). (D) Ragged Cr-spinel grains that contain abundant inclusions from Jänesselkä (PSHA-2017-26.1). (E) Subhedral skeletal Cr-spinel with inclusions from Torolhdontyvet (PSHA-2017-32.1) and (F) Secondary massive Cr-spinel accumulation from Sorvortanselkä (JHTE-2017-10.1). Scale bars are 100 μm, except for (B) 200 μm.

Cr-spinel grains were analysed systematically using four to ten analysis points from core to rim. In general, the cores are Cr-rich and contain more Al, Mg, V, and Zn compared to the rims. The rims, again, are more Fe-rich and contain larger amounts of Ni and Ti compared to the cores. Also, cores of the zoned Cr-spinel grains are much more Cr-rich (30–40 wt.%) than the non-zoned and secondary Cr-spinel grains, which have Cr contents ca. 3–15 wt.%.

In terms of data presented by Groves et al. (1977), the analyzed Cr-spinels are not Zn-rich (> 0.5 wt.% Zn), which can be outlined in a Cr vs. Zn plot (Figure 82). Only some zoned Cr-spinels from Tulppio and Pirunkirkko plot over the value.
However, as seen in the linear trends in the Jänesselkä, Vuonnelo-oja, Sorvortanselkä, and Heiniselkä targets, in addition to much higher concentrations in the cores of Cr-spinel from the Tulppio, Venehaara (Värriöjoki), Pirunkirkko, and Vuonnelo-oja targets, Zn can typically be added to Cr-spinel by diffusion reactions between the magnetitic rim and the chromite core during metamorphism (Barnes 2000).

Also, according to Barnes et al. (1996) Zn contents of the Cr-spinel are widely affected by metamorphism and not useful for exploration of komatiites. Nevertheless, in Venehaara, the rim compositions plot to the same group with the analyzed secondary (vein- and fracture-hosted) grains (low Cr and low Zn), which demonstrates the growth of the rims and diffusive cation exchange between the rim and the core during metamorphism. In Tulppio, this feature is not as clear as in Venehaara, as the rims are still very Cr-rich. This is possibly due to less intense effect of metamorphism in the Tulppio Cr-spinels, as also the rims of the non-zoned grains have preserved their high Zn and Cr contents. Notably, in Groves et al. (1977) mg vs. Zn plot (mg = 100*Mg/(Mg + Fe + Mn + Zn + Ni)) , the cores of the zoned Venehaara samples plot to the same group with unmineralized komatiitic units in selected domains metamorphosed in amphibolite facies (Figure 83).

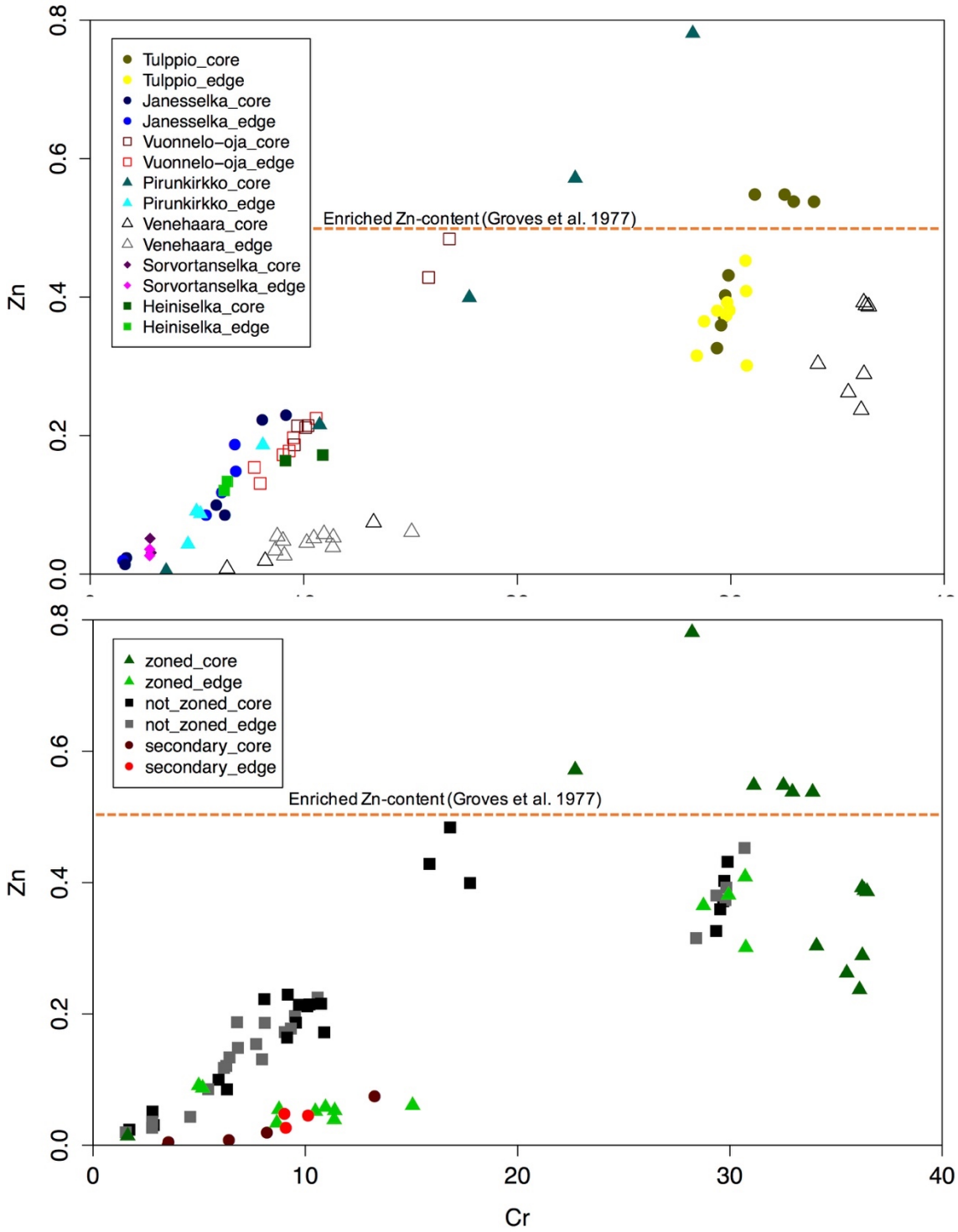

Figure 82. Cr vs. Zn plots of the analyzed Cr-spinel grains. Upper plot shows spinel compositions by location and also distinguishes between core and rim (edge in the diagrams) analyses. The lower plot shows same compositions, now divided into zoned, non-zoned and secondary spinels. Dashed orange line marks the limit for Zn enrichment as suggested by Groves et al. (1977). Both Cr and Zn as wt.%.

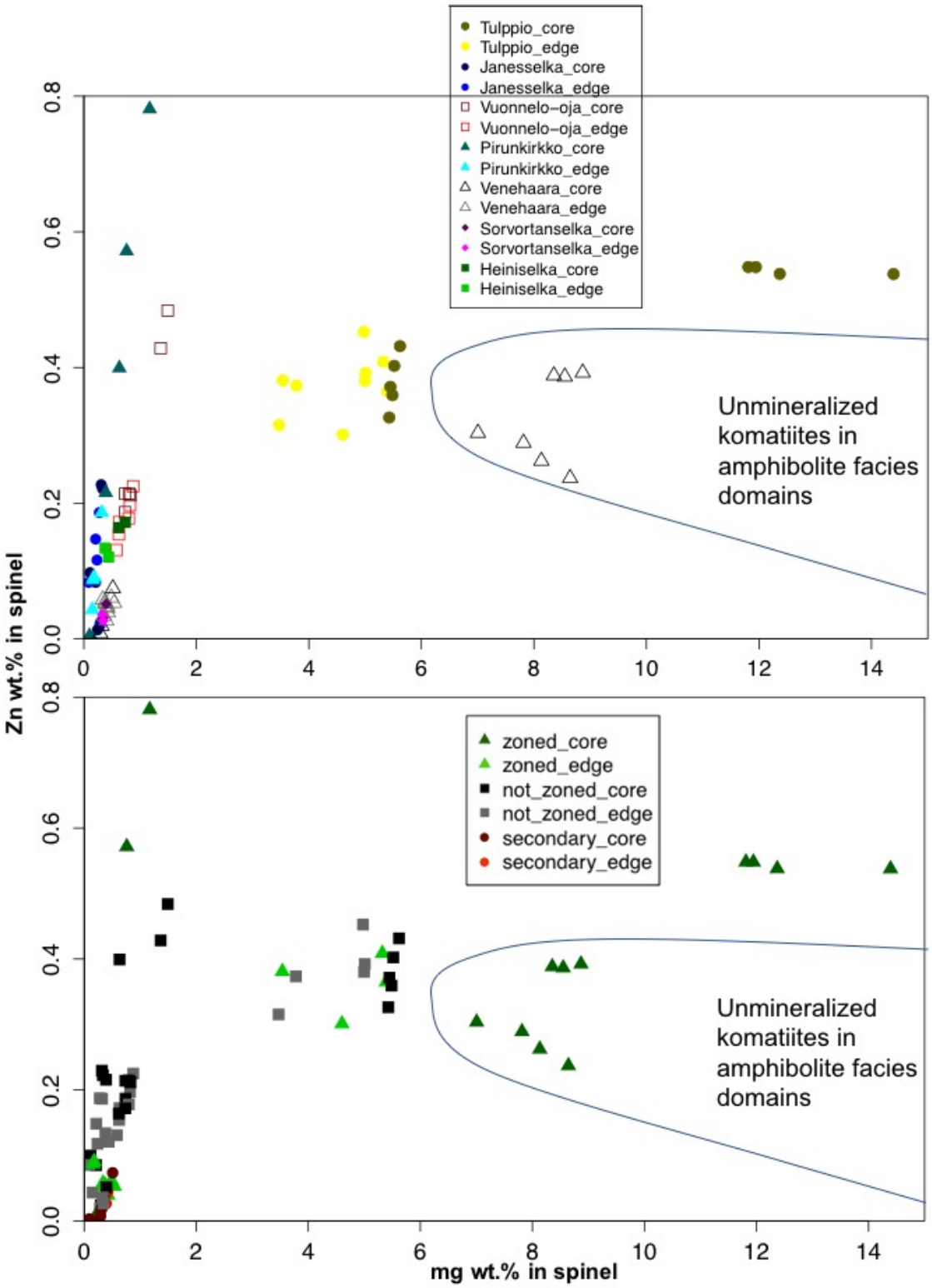

Figure 83. mg* vs. Zn in the analyzed Cr-spinels. The blue field marks compositions found typically in unmineralized komatiites from domains of dominant amphibolite facies metamorphism (Groves et al. 1977). mg = 100*Mg/(Mg + Fe + Mn + Zn + Ni), all wt.%.

Nickel content of the analyzed Cr-spinel is low in general (Figure 84). In the zoned grains, the Ni contents are < 0.1 wt.%in the cores but increase up to 0.2 wt.% in the rims, which

is a natural consequence of serpentinization as the released Ni from olivine partitions stronger to magnetite than Cr-spinel (Blais & Auvrey 1990, Barnes 2000). Also, non-zoned and secondary grains have clearly higher Ni contents (0.2–0.4 wt.%) compared to the zoned grains, regardless of location of the analysis point in rim or core. Interestingly, the zoned samples from Venehaara show much higher Ni contents in the rims than the zoned samples from Tulppio. This may be due to intensity of metamorphism, because during serpentinization Ni is released from olivine and it partitions more strongly to magnetite than serpentine. Curiously, on the basis of classification of Evans (2017) on chromites in the ultramafic intrusions of the East African nickel belt, the Venehaara Cr-spinels show the strongest Ni depletion (Figure 85).

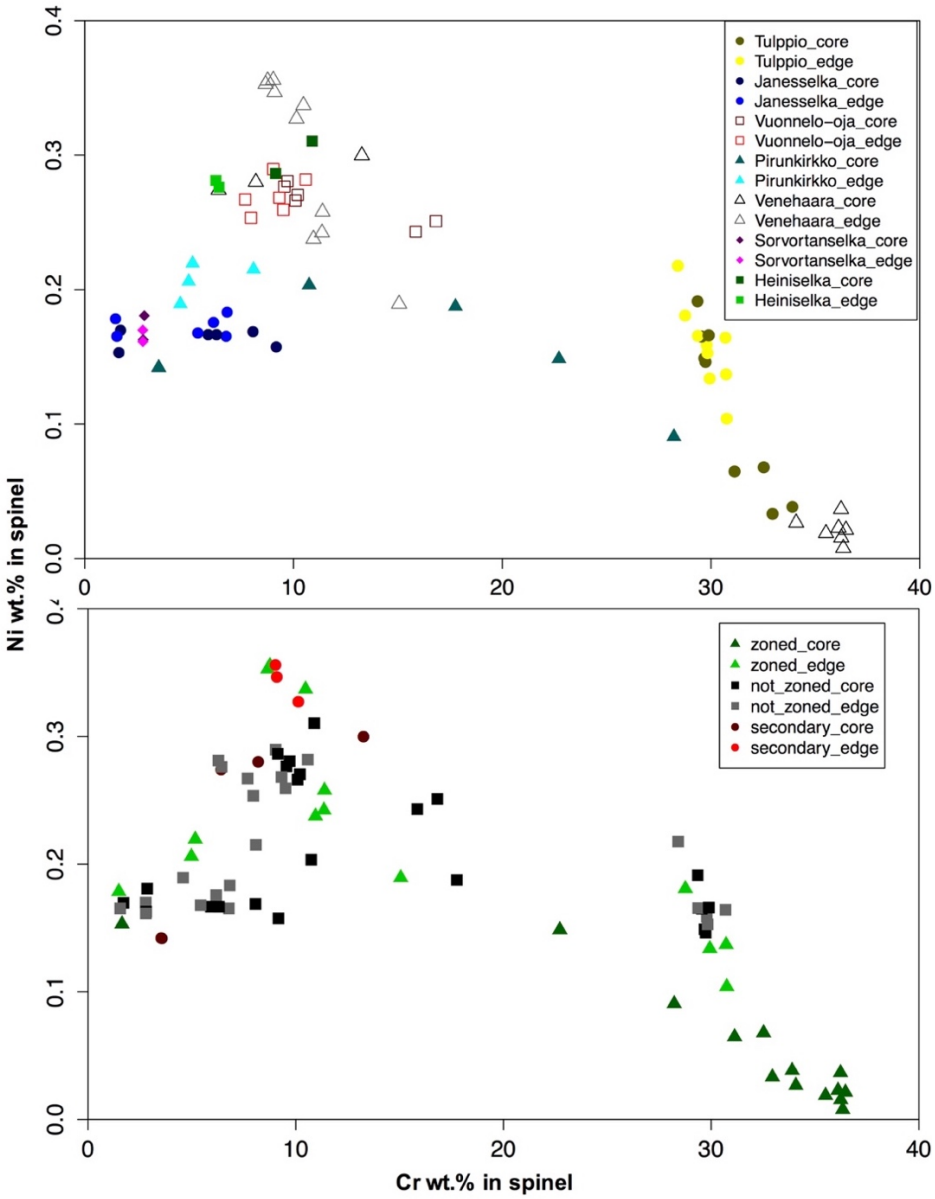

Figure 84. Cr vs. Ni plot of the analyzed Cr-spinels. Upper plot shows spinel compositions by location and also distinguishes between core and edge (rim) samples. The lower plot shows same composition by division of zoned, not zoned and secondary spinels. Cr and Ni in wt.%.

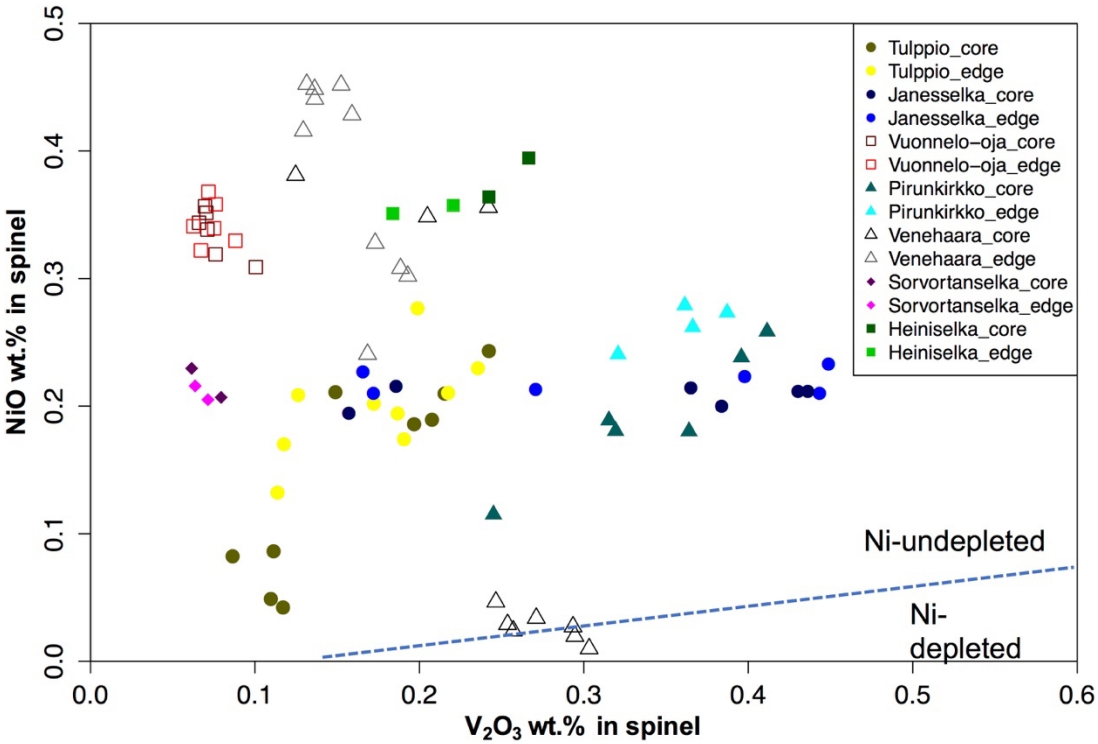

Figure 85. V_2O_3 vs. NiO plot of the analyzed spinels. The blue dashed line marks border between Ni-depleted and Ni undepleted samples in the East Arfican nickel belt after Evans (2017).

8. DISCUSSION

The aim of the following discussion is to focus on the key questions with respect to ore potential of komatiitic rocks in ELAD. Essential features of regional geology and petrology of komatiites are considered in light of prospectivity. Following this, geochemistry of komatiites concerning possible sulfide segregation and contamination features is discussed in detail, and vectoring towards potential environments is attempted.

8.1 General geology and stratigraphic constraints

ELAD is an Archean gneiss-granite-greenstone terrain, in which the presence of abundant komatiitic rocks, especially komatiitic cumulates, and proximity of sulfide-bearing country rocks undoubtly promote for potential of Ni-Cu-PGE ores. Komatiitic rocks are found within varying host rocks, including volcanic and sedimentary rocks of TVB, paragneisses and paraschists of TSB and granitoids of AGC and KVGC (see figure 6, 7, and 8). The precise age(s) of the komatiitic bodies in ELAD have no implications to ore potential, as both Archean and Paleoproterozoic komatiites are critical for Ni-Cu-PGE

ores in Finland. Also, considering the possible tectonic remobilization of Ni-Cu-PGE ores in ELAD, they may be contemporarily hosted by any lithology in the area due to the predominant thrust tectonics (e.g., Papunen et al. 1997), as seen for example in the case of the Peura-aho Ni-(Cu-PGE) deposit in the Suomussalmi greenstone belt, where a part of the ore has been transported to the adjacent schists (Konnunaho 2016).

The stratigraphic relationships between the komatiitic bodies and the surrounding lithologic units are not clear in all cases. As for possible gain of external sulfur from sulfide-bearing rock to komatiite melt, information of the stratigraphic relationships is important and should be investigated more closely in the future. Notably, possible sulfur sources may also be present deeper in the crust. Age determinations of the ELAD komatiites are only few. Furthermore, it seems likely that there are possibly three separate groups of Ni-Cu-PGE potential rocks present in the area: 1) Archean komatiitic rocks, 2) Paleoproterozoic komatiitic rocks, and 3) Paleoproterozoic layered intrusions. Below is outlined the current knowledge of the stratigraphic constaints in the light of ore potential.

Observations of crosscut relationships in the Tulppio metavolcanic belt indicate that the komatiites of the belt are crosscut by the adjacent granitoids. In addition, the volcanic sequence of the belt shows a discordant age determination (ca. 2.85 Ga, Juopperi & Vaasjoki 2001) measured from an interpreted felsic volcanic rock from the Rovaukonselkä area that implies an age older older than the surrounding ca. 2.8 Ga granitoids (Juopperi & Vaasjoki 2001) for TVB. Evidently, an analogue to ca. 2.9–2.85 Ga greenstone-paragneiss sequences in Belomoria and Kola can be considered. A contamination scenario for the TVB komatiites, however, would demand the presence of > 2.9 Ga crust, which has not been recognized in ELAD, but has, for instance, been identified in the Belomorian, as the 2.8–2.7 Ga orthogneisses there contain zircons with an age of ca. 3.0 Ga (Bibikova & Bogdanova 1993). Similar features are also found in the Karelia province in eastern Finland, where the uppermost sedimentary rocks in the Kuhmo-Suomussalmi-Tipasjärvi greenstone belts contain zircons older than 3.0 Ga (Lehtonen 2016) and in the Archean Rommaeno complex in western Lapland, where the orthogneisses underlying the Sarvisoaivi komatiite sequence yield ages of ca. 3.2 Ga (Karinen et al. 2015). Interestingly, however, similar lithologies to TVB association in the Kareka-Tundra area (Barkov, in press) on the Russian side of the border have been connected to Paleoproterozoic komatiitic magmatism. Also, considerations of the TVB

komatiites representing two separate age groups (Archean and Paleoproterozoic) have been suggested, as some of the rocks display geochemical similarity, e.g. “hump-shaped” REE patterns and Ti-enrichment, to the CLGB komatiites (e.g., Juopperi 1994, Papunen et al. 1997, Sorjonen-Ward & Luukkonen 2005). Features of both Paleoproterozoic and Archean komatiitic magmatism are observed in the Kuttusvaarat-Heiniselkä, Rovaukonselkä-Nivatunturi, Petäjä-Saijanvaara, and Iskemävaara-Pultoselkä areas (see figures 54, 56, 57, and 58).

Tepsell (2018) and Huhma et al. (2018) have obtained ages ca. 2.5 –2.44 Ga for the Jänesselkä and Värriöjoki bodies. The age determiantions are discordant to some degree, but they can be supported by each other and by the presence of the two relatively well-preserved representatives of the ca. 2.5–2.44 Ga layered intrusion magmatism: the Koulumaoiva and Peuratunturi intrusions. As most of the country rocks in ELAD span ages of 2.83–2.72 Ga (Juopperi & Vaasjoki 2001), contamination scenario with older sulfide-bearing country rocks by assimilation for these komatiitic bodies is possible. Furthermore, based on negative ε_{Nd}-values, a major LREE-enriched Archean component is present in the Värriöjoki komatiitic system (Huhma et al. 2018). This, together with the elevated $(La/Sm)_N$ values can be regarded as positive signatures for crustal contamination. Notably, the generally “hump-shaped” REE patterns with very low $(La/Sm)_N$ values (see Hanski et al. 2001, fig. 5), as well as, Ti enrichment typical for the Paleoproterozoic the CLGB komatiites, are not observed the Värriöjoki and Jänesselkä komatiites. Thus, they would rather be linked to either to ca. 2.45 layered intrusion magmatism (this should especially be considered in the case of Jänesselkä, see discussion in Haapala in preparation) or Archean komatiitic magmatism than Paleoproterozoic komatiite magmatism. However, especially, the case with the age and the origin of the Värriöjoki body is not straightforward, and a Paleoproterzoic komatiitic origin cannot be excluded. Nevertheless, to draw precise conclusions concerning the stratigraphy of ELAD, more research, in e.g., stabile isotopes is required.

8.2 Parental melt compositions and nature of komatiites

Due to the lack of primary magmatic textures in ELAD, komatiites that represent melt compositions, such as spinifex-textured rocks, chilled margins or sequence-top breccias,

are not available for determining parental melt compositions. Therefore, Haapala (in preparation) estimated them by using the whole-rock composition method introduced by Makkonen et al. (2017). The results show parental melts of 6.6, 12.5, and 17.8 wt.% MgO to the Jänesselkä, Värriöjoki and Tulppio bodies, respectively. By the same technique, the Kuttusvaarat-Heiniselkä komatiitic sequence also represents a product of similar parental melt with ca. 15 wt.% MgO. As for previous parental melt considerations, similar results have been obtained by Heikura et al. (2010), who have estimated a komatiitic (ca. 23 wt.% MgO) parental melt for the Tulppio body by linear regression line from whole-rock MgO vs. Al_2O_3 and MgO vs. TiO_2 plots. In contrast, Maier et al. (2013) argued that the Tulppio parental melt would be a komatiitic basalt corresponding to Fo_{87} olivine. Also, regarding the Värriöjoki body, Vuollo (1986) has calculated a 19.9 wt.% MgO komatiitic parental melt for it based on equilibrium with the olivine with the highest Fo content. Nevertheless, considering the uncertainty in the presence of magmatic olivine in these komatiitic bodies, the whole-rock parental melt calculations are regarded as the most reliable. Hence, cumulates in Jänesselkä body were derived from a Ti-poor basaltic parental melt, whereas cumulates in the Värriöjoki body and the Kuttusvaarat-Heiniselkä area are accumulations of komatiitic basaltic parental melts, and cumulates in the Tulppio body were derived from a low-MgO komatiitic/komatiitic basaltic parental melt. Therefore, it is likely that ELAD hosts cumulates derived from both low-MgO komatiitic and komatiitic basaltic parental melts. These kind of cumulates are critical particularly for PGE-rich Ni ores, as in contrast, cumulates of high-MgO komatiites are more linked to classical Ni±Cu ores. In the light of parental melt compositions, the Tulppio, Värriöjoki, and Kuttusvaarat-Heiniselkä komatiites could be correlated with e.g., the Archean Vaara, Sarvisoaivi, Tainiovaara, and Hietaharju deposits, as well as, the Paleoproterozoic Lomalampi and Sakatti deposits.

By magma type, the ELAD komatiites fall into three categories: 1) AUKs with Al_2O_3/TiO_2 ca. 18-20, 2) AUK with $Al_2O_3/TiO_2 > 20$, and 3) ADKs with Al_2O_3/TiO_2 ca. 10 (Figure 86). In Finland, most of the ore deposits are associated with AUK-type komatites, but in general both types can host Ni-Cu-PGE ores. The type 1 AUKs with have elevated median $(Gd/Yb)_N$ of ca. 1.5, whereas the type 2 AUKs have chondritic $(Gd/Yb)_N$ (ca. 1) as the median. The ADK komatiites also have enriched > 1.5 median value of $(Gd/Yb)_N$. Regarding the correlation between Al_2O_3/TiO_2 and $(Gd/Yb)_N$, komatiites of ELAD correspond to the classical source model by Nesbitt et al. (1979),

where ADK, typical for Archean greenstone belts (e.g. Barberton), would have been produced deeper at the mantle leaving behind a residual of garnet and olivine, and AUK would have been derived from shallower levels of the mantle with only olivine in the residual. Furthermore, presence of the Ti-enriched subgroups can be attributed to lower degree of partial melting and/or fertile source, which are typical for Paleoproterozoic komatiites. With respect to the komatiitic basaltic parental melt compositions, a relatively low-degree of mantle melting, and/or fertilized source region is likely. Anyhow, considering the scattered distribution of the petrogenetic types of komatiites, which are not significantly dependent by geography, the scenario of formation of these different magma types within a same mantle plume (see Sossi et al. 2016) or in varying tectonic settings would be supported.

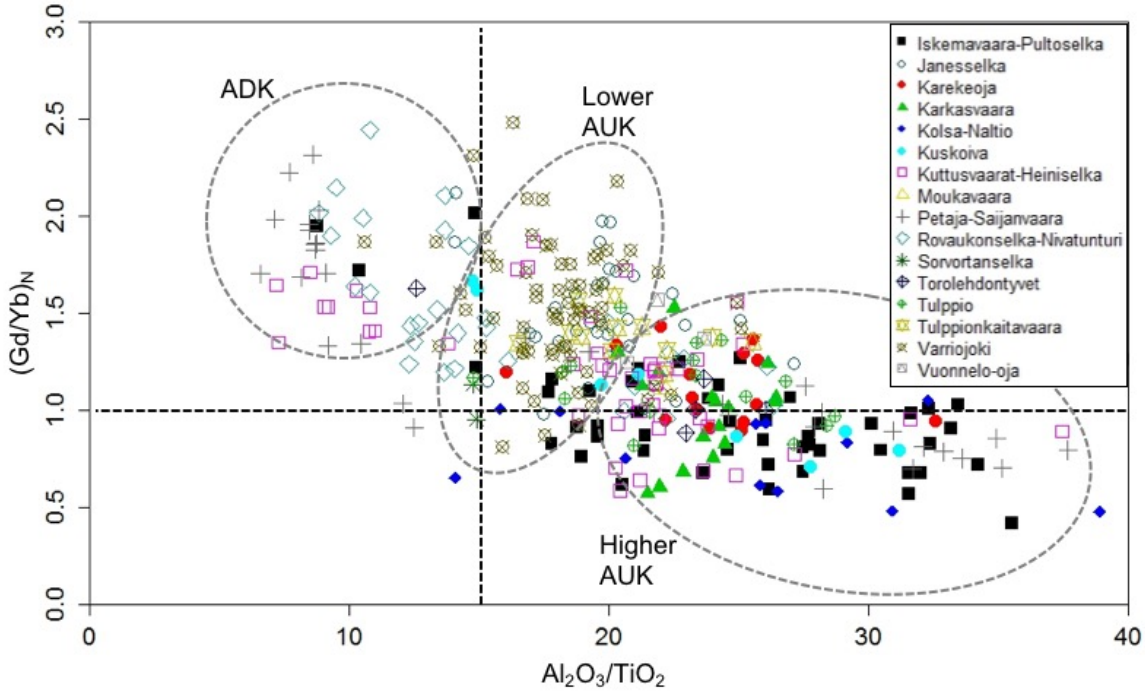

Figure 86. Al_3O_2/TiO_2 vs. $(Gd/Yb)_N$ plot of The ELAD komatiites. Outlined are the different magma types found in ELAD. ADK (aluminium-depleted komatiite) = Al_3O_2/TiO_2 ca. 8-15, $(Gd/Yb)_N$ > 1.5, Lower AUK (aluminium undepleted komatiite) = Al_3O_2/TiO_2 ca. 15-20, $(Gd/Yb)_N$ ca. 1.5, Higher AUK = Al_3O_2/TiO_2 ca. 20-35, (Gd/Yb)N ca. 1.0.

8.3 Komatiite geochemistry and ore potential

In terms of whole-rock geochemistry it is evident that some of the komatiites of ELAD display many generally favored features when it comes to their Ni-Cu-PGE potential. Ni depletion is clearly observed in the Tulppio, Värriöjoki, Kuskoiva, Vuonnelo-oja and Siurujoki targets (see figures 50, 62, and 69). Furthermore, according to Maier et al.

(2013), some of the TVB komatiites show moderate depletion of PGE. Also, relatively enriched Ni and PGE contents are present in some of the targets but as a negative feature, many of the targets are also characterized by lack of S (see figures 46, 53, 65, and 72). Also, noteworthy is that Ni data presented in this thesis also includes a lot of silicate Ni, meaning most of the Ni is mainly in olivine, especially if S contents are below ca. 2500 ppm. Regarding Cr, most of the ELAD komatiites have been derived from komatiitic basaltic and/or low-MgO komatiitic parental melts, both Cr-saturated. However, especially the Värriöjoki, Tulppio, Kolsa-Naltio, Kuskoiva, Kuttusvaarat-Heiniselkä, Iskemävaara-Pultoselkä and Petäjä-Saijanvaara targets also have compositions following the Cr-undersaturated trend (see figures 44, 51, and 70), which globally has been globally recognized as a prospective feature. As for contamination, enrichment of REE, especially LREE, has favorably been observed within ELAD, especially REE patterns in the Värriöjoki and Jänesselkä (+ Tulppionkaitavaara) (Figures 66 and 73) targets show clearly-enriched compositions. However, LREE might have been mobilized by metamorphism and may produce false trends indicating magmatic contamination.

8.3.1 Chromium content

Chromium content (or chromite contents) of komatiites especially komatiitic cumulates have been used to constrain favorable environments for exploration of Ni-Cu-PGE ores. Although, Cr itself does not play a role in sulfide segregation processes, in high-MgO (and low-MgO komatiitic) systems cumulates that crystallized from Cr-undersaturated melts are often associated with ore deposits (e.g., Lesher & Barnes 2008, Barnes & Fiorentini 2012, Konnunaho 2016). Using Cr contents for low-MgO komatiitic systems is not so useful, however, due to their initially Cr-saturated character.

Chromium is a sensitive indicator of temperature and fO_2 in komatiitic melts (e.g., Barnes 1998, Barnes & Fiorentini 2012). In general, Cr saturation (crystallization of chromite) is more intense under rising temperature and oxidizing conditions. Lower-MgO melts are more oxidized than higher-MgO melts, and hence typically Cr-saturated. Given the komatiitic basaltic/low-MgO komatiitic parental melts dominating in ELAD, most of the komatiites there are derived from Cr-saturated melts, which obscures the use of, e.g., MgO vs. Cr and Ni vs. Cr for prospective signals. However, also in Cr-saturated systems,

olivine cumulates that lack cumulus chromite are often present within mineralized bodies (Barnes & Fiorentini 2012). In ELAD, crystallization of chromite typically evolves from saturated compositions towards cotectic crystallization of olivine and chromite, representing typical relationship in komatiitic melts. However, despite the Cr-saturated origin, the Värriöjoki, Tulppio and Kuttuvaarat-Heiniselkä targets show also a number of compositions crystallized from Cr-undersaturated melts. Moreover, the Värriöjoki and Tulppio actually comprise two distinct trends from Cr-saturated melt, other evolving towards the cotectic trend, and the other towards the Cr-undersaturated trend. When applied to base metal behavior, low Cr compositions (Cr < 2000 ppm) clearly have elevated nickel contents (Figure 88), which is due to more intense crystallization of olivine but may demonstrate the relationship between prospective samples to and Cr-undersaturated compositions. This trend is particularly observed within the Värriöjoki, Tulppio and Kuttusvaarat-Heiniselkä targets (Figure 88).

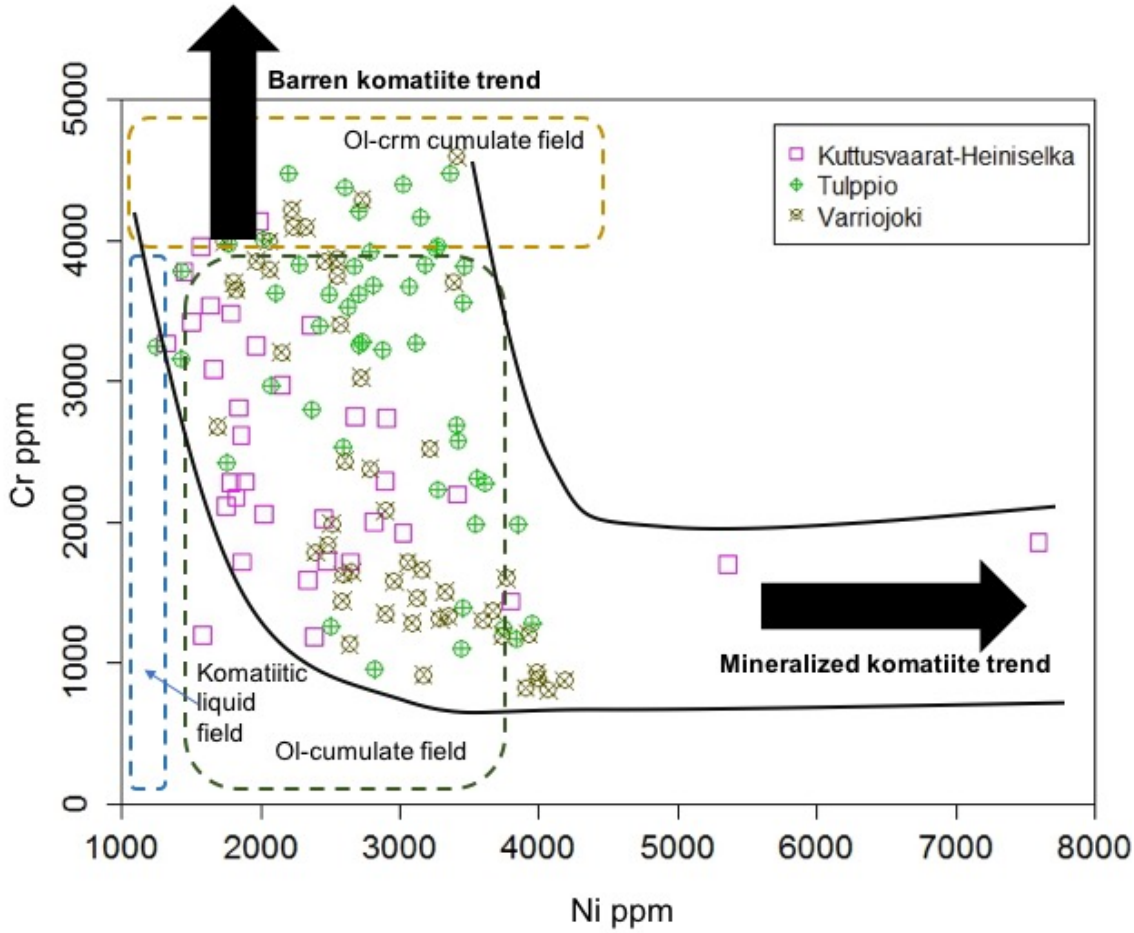

Figure 88. Ni vs. Cr plot showing the prospective trend (area defined by the black solid lines) in the Tulppio, Värrijoki and Kuttusvaarat-Heiniselkä komatiites. Fields and trends after Brand (1999).

8.3.2 Marks of sulfide segregation

The most significant controversy in tracing marks of sulfide segregation in ELAD is that the known komatiites in the area notably lack magmatic Ni-sulfides and S. However, proof of ore-forming processes taking place in the area is demonstrated by presence of Ni sulfides in komatiite boulders in the Kuttusoja area and by the two PGE-Ni-mineralized zones in the Tulppio komatiitic body. Also, positively varying correlations with nickel and sulfur, indicating precence of sulfidic nickel, has been observed in the Tulppio, Kuttusvaarat-Heiniselkä, Vuonnelo-oja, Siurujoki, and Värriöjoki targets. However, adequate Ni and S contents in terms of potentially mineralized rocks, are only present in the trends of Tulppio and Kuttusvaarat-Heiniselkä.

Depletions in Ni and PGE may be a cause of escape of metals from the komatiitic melt to sulfide melt and have together with enriched contents of these metals may linked to ore-forming event somewhere in the particular komatiitic sequence. Notably, significant crystallization of olivine and/or early sulfide segregation deep in the crust can also produce the Ni depletion features. Although Maier et al. (2013) has suggested a moderate PGE depletion occurring the Tulppio body, in the data set used in this thesis, PGE contents have no use in detecting depletion halos (see Heggie et al 2013, Fiorentini et al. 2010a) as the relatively high detection limits for Pt and Pd (5 ppb in most samples, 10 ppb in some older samples) restricts locating them. However, some relatively elevated abundances of PGE are found in ELAD (see figure 53 and the PGE content observations in text in section 7.4). Possible PGE depletion occurring in komatiitic cumulates produced by komatiitic basalt parental magmas that should bear high Pt- and Pd-tenors, can be regarded as a positive sign as for sulfide segregation. Furthermore, using mineral chemistry of olivine and Cr-spinel presented in this thesis for exploration implications, e.g., for detecting depletion halos, is fairly ambiguous. The insufficient data frequency on both minerals, and consequent difficulties in outlining metamorphic effects within the mineral chemistry data, would only end up in highly marginal interpretations. Therefore, PGE-depletion and mineral chemistry are not of valuable use in the consideration of potentially mineralized environments.

Altogether 645 samples within ELAD show marks of relative Ni depletion (= plot clearly under the Ni undepletion model line; see figures 43, 50, 62, and 69). The clearest Ni depletion trends are observed in the Värriöjoki, Tulppio and Kuskoiva targets. Moreover, slight Ni depletion is found in in, e.g., the Kolsa-Naltio, Kuttusvaarat-Heiniselkä, Petäjä-Saijanvaara, Siurujoki, Vuonnelo-oja and Jänesselkä targets. However, weakly enriched nickel contents (= plot above the Ni undepletion model line; see figures 43, 50, 62, and 69) are only observed within in the Tulppio, Värriöjoki and Kuttusvaarat-Heiniselkä targets. These enriched samples are only few (n = 40). Again, it must be highlighted that most of the Ni-depleted/enriched samples contain high amount of silicate Ni and are associated with seemingly unmineralized komatiites with low sulfur contents (< 2500 ppm), regardless of the depletion/enrichment feature (Figure 89). However, observations from the Kuttusvaarat-Heiniselkä (Figure 89B) and Tulppio (Heikura et al. 2010, see fig. 48) areas indicate that nickel has been affinitied to sulfur to some extent. Nevertheless, most of the samples in ELAD contain only Fe-rich and Ni-poor sulfides, if sulfides at all (Figures 89A and 89B).

Furthermore, to correlate between base metal signatures and possibly ore the critical samples representing Cr-undersaturated compositions, can be noted that Ni depletion often is found together with Cr-undersaturation. This is interesting, as these low-Cr olivine cumulate compositions should contain a relatively higher amount of olivine, and hence relatively a relatively higher amount of Ni than komatiites with Cr-saturated and cotectic olivine-chromite cumulate compositions. However, the currently known mineralized komatiites display either Ni-enriched (the Tulppio PGE-Ni zones) or Ni-enriched Cr-undersaturated compositions (the Kuttusoja boulders). In practice, samples displaying relatively enriched base metal contents that did not crystallize much chromite seem the most prospective in ELAD in terms of Ni-Cu-PGE ores. As examples, mineralized komatiites that crystallized from Cr-saturated parental melts host Ni-Cu-PGE deposit(s), in Raglan in northern Québec in Canada and in Petsamo (Pechenga) in the Kola Peninsula, NW Russia.

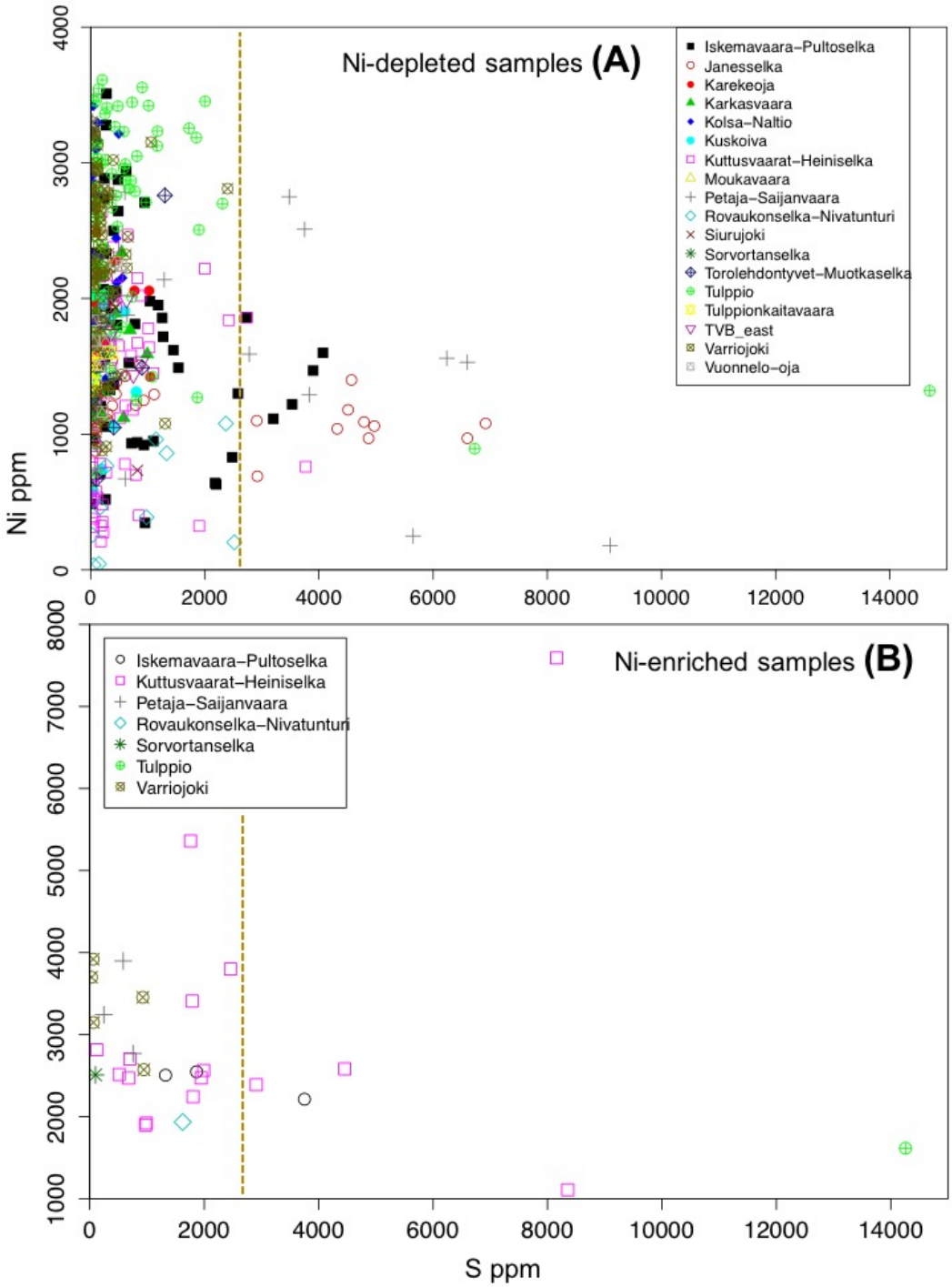

Figure 89. Ni vs. S plots of the Ni-depleted samples (A) and nickel-enriched samples (B), both relative abundances of each target defined by the Ni-undepletion model line (see Naldrett et al. 1984, Makkonen et al. 2017). The yellow dashed line illustrates the theoretical boundary between mineralized (S > 2500 ppm) and non-mineralized (S < 2500 ppm) samples.

8.3.3 Marks of contamination

The LREE-enriched REE patterns and especially LREE enrichment and general enrichment in HILE relative to MILE have been widely attributed to contamination of

komatiites by surrounding country rocks. However, as discussed by Jahn et al. (1980), Lesher et al. (2001) and Barnes et al. (2004) rocks with very high MgO and initially low HILE and MILE concentrations (namely adcumulates) are more susceptible for mobility of these elements during alteration. Therefore, komatiites that represent melt compositions should be used for detecting contamination in the first place. In addition, distinguishing between contamination and alteration effects is essential but not straightforward. Notably, contamination itself, however, is not a proof of ore formation, as not all possible contaminants contain adequate amount of sulfur to saturate the komatiite melt. Below, the mobility of contamination-critical elements in the ELAD komatiites is considered and signals of contamination are evaluated on the basis of results of the Monte Carlo simulations from the Western Australia komatiites by Barnes et al. (2004).

Elevated $(La/Sm)_N$ has been considered a strong indicator of crustal contamination (e.g., Jahn et al. 1980, Hanski et al. 2001, Lesher et al. 2001, Barnes et al. 2004). For example, Arndt et al. (2008) have emphasized that elevated $(La/Sm)_N$ values globally correspond to low isotopic ε_{Nd}-values, which suggest involvement of a crustal component in a magmatic system. In a wider view, elevated $(La/Sm)_N$ ratios (or elevated HILE in general) may be a combined result of source fertility, degree of melting, contamination, and/or post-magmatic modification by element exchange from surrounding host rocks by, e.g., metasomatism. In komatiites of ELAD, La shows mobility with respect to MgO and Al_2O_3, probably reflecting modification during post-magmatic processes. Samarium, on the other hand, shows a slight negative correlation with MgO and a slight positive correlation with Al_2O_3 indicating relatively less modified but more immobile behavior. However, the mobility of these elements varies among the targets, and, e.g., the Jänesselkä and Tulppionkaitavaara bodies, which show similar geochemical characteristics, show mobility in both La and Sm with respect to MgO and Al_2O_3. In contrast, the Värriöjoki, Tulppio, and Kolsa-Naltio bodies correlate quite well in terms of La and Sm vs. MgO and Al_2O_3 and suggest minimal mobility of these elements. Notably, Hanski et al. (2001) have suggested that due to Ti-enriched nature of the Paleoproterozoic komatiites of CLGB, La/Nb ratio could better reflect the effect of contamination than La/Sm ratio. However, in ELAD the Ti-enriched komatiites represent a minority and Sm actually behaves in a more immobile manner than Nb with respect to MgO and Al_2O_3. As for Nb, Lesher et al. (2001) have emphasized a negative Nb anomaly as an indicator of

crustal contamination. Promisingly, Nb anomalies are clearly present in the primitive mantle normalized patterns of the Jänesselkä, Kuskoiva, Kuttusvaarat-Heiniselkä, and Värriöjoki targets. In the latter three, the negative Nb-anomalies are also associated with positive Th and U anomalies, which could also be indicative for crustal contamination. As for MILE, $(Gd/Yb)_N$ is used to reflect the presence of garnet in the source of komatiite magma (Yb is more compatible to garnet than Gd). Both of these elements are incompatible to olivine but behave in a relatively immobile manner during magmatic processes and alteration. In ELAD, a negative correlation with MgO and a positive correlation with Al_2O_3 is observed with Gd and Yb, suggesting low mobility. Generally, ADK/Barberton-type/plume head-type komatiites have suprachondritic $(Gd/Yb)_N$ values (ca. 1.5) and AUK/Munro/distal-type komatiites have chondritic values of ca. 1 (e.g., Arndt et al. 2008). Nevertheless, as presented in the section 7.4, ELAD has a wide median range of $(La/Sm)_N$ from depleted (< 1) to very enriched (> 2), although their $(Gd/Yb)_N$ median values are somewhat constant, ranging from chondritic to suprachondritic (Figure 91). According to Lesher et al. (2001) and Barnes et al. (2004) depleted sources that have undergone prior melt extraction are depleted in HILE compared to MILE, and vice versa, sources that have undergone contamination/enrichment by incorporation of fertile material are enriched in HILE relative to MILE. By these means, many of the targets show potential features of crustal contamination, which are also indicated by LREE-enriched REE patterns shown in section 7.4 (see figures 47, 54-59, 66, and 73-75).

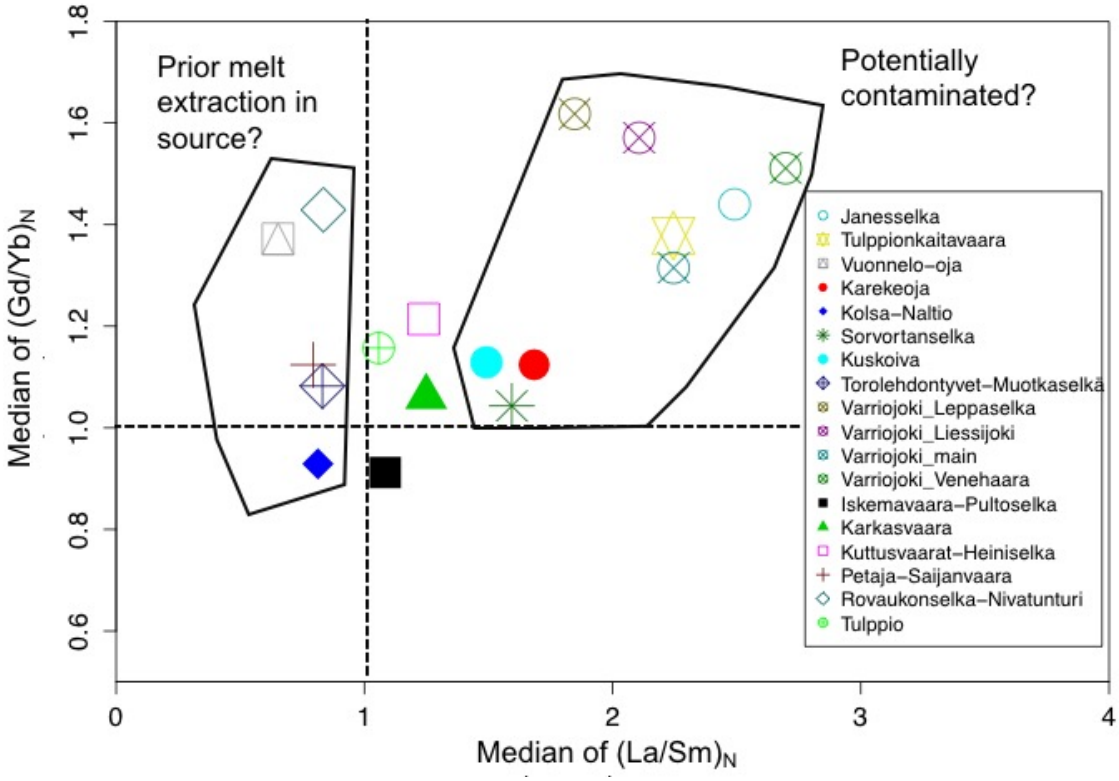

Figure 91. Median $(La/Sm)_N$ of the targets plotted against median $(Gd/Yb)_N$ values. Generally, enrichment in $(Gd/Yb)_N$ compared to $(La/Sm)_N$ indicates depleted source possibly due to prior melt extraction. Vice versa, enrichment in $(La/Sm)_N$ compared to $(Gd/Yb)_N$ indicates either fertile source or contaminant present in the system. Values normalized to C1 chondrite (McDonough & Sun 1995).

However, to argue if the elevated LREE and elevated HILE compared to MILE are due to contamination, effects of alteration must be considered. Barnes et al. (2004) suggested that lithophile and relatively immobile elements, e.g., Zr, Ti, and Y would behave as "ideal" incompatible elements in high-MgO komatiites. Hence, according to them, if alteration has caused the element signatures instead of magmatic processes, they should display negative correlation in ratios (e.g., Zr/Ti, Zr/Y) when plotted against, e.g., TiO_2 or Al_2O_3 (Barnes et al. 2004, see fig. 8A). However, rocks with high MgO are more vulnerable to modification of ratios of these elements than rocks with lower MgO due to low initial in Zr, Ti, and Y. Considering the ideality, ratios of these elements are useful as they should not vary due to alteration and fractionation and accumulation of olivine, chromite, and sulfide (Lesher et al. 2001, Barnes et al. 2004). As for ELAD, Ti and Y have negative correlation with MgO in general, but especially in the lower MgO (< 25 wt.%) compositions both show mobility. Similar behavior with positive correlation is also observed with respect to Al_2O_3. Zr behaves in a similar manner as Ti and Y with respect to MgO and Al_2O_3 and is comparable to typical trends in Munro-type (AUK) komatiites (see fig. 2.9, Arndt et al. 2008). Concerning the immobile behavior of Ti and Y in the

high-MgO rocks, it seems that Zr has preserved its magmatic signatures in these rocks, and also to some extent in the non-cumulus rocks.

To evaluate the usefulness of "ideal" incompatible elements for detecting contamination, Barnes et al. (2004) have produced models of alteration-dominant, alteration- and contamination-dominant, and contamination-dominant controls by "Monte Carlo" probability numerical simulations (see their figs. 8A, 8B, and 8C). Their model suggests that alteration-dominant control implies a strong rock type dependency of komatiitic cumulates and a bit weaker dependency in non-cumulates, seen as principal negative correlation on $(La/Al)_N$ vs. Al_2O_3 and $(Zr/Al)_N$ vs. Al_2O_3 plots (see Barnes et al. 2004, fig. 8A). In contrast, contamination-dominant control predicts the opposite: no correlation komatiitic cumulate and positive correlation non-cumulates (see Barnes et al. 2004, fig. 8C). When a similar plot is applied to ELAD komatiite compositions, a negative correlation with a weak scatter is observed within komatiitic cumulates and positive correlation within non-cumulates and komatiitic basalts (Figure 93). This data corresponds the best to model, where both alteration and contamination have modified the elements compositions (see Barnes et al. 2004, fig. 8C).

Furthermore, the ideal incompatible element ratios can be compared with HILE ratios (e.g., La/Sm), which may indicate contamination (see figure 91). Barnes et al. (2004) have produced a modelled theoretical mixing line between primitive komatiite (HILE-depleted) and a typical contaminant with a dacitic composition (HILE-enriched) (see their figure 9), to make further interpretations of possible contamination. On $(Zr/Ti)_N$ vs. $(La/Sm)_N$ plot, the ELAD komatiites plot on values indicating 0–30 % of contaminated material within (Figure 94). However, to argue for a contaminant component present in a komatiitic system, a correlation should be present with the model mixing line, which in the case of ELAD is principally absent. On the lithofacies-categorized plot (Figure 94A) plot the non-cumulate compositions actually correlate with the mixing line rather well, indicating 0–10 % of contamination present in the system. In contrast, cumulate compositions form two distinct trends, other showing no correlation with the model mixing line and the other, a minor trend, having a correlation with it. Interestingly, in the target-categorized plot (Figure 94B), correlation trend with the mixing line is principally produced by samples from the Värriöjoki and Jänesselkä, which also show contamination features on REE plots (see figures 66A and 73). By these means, cumulate compositions

with highly elevated Zr or La can be considered as crustal contamination signatures in ELAD, particularly in the Värriöjoki and Jänesselkä bodies. However, to truly confirm how much contamination has affected the concentrations of LREE, Zr, and other incompatible elements, isotopic data should be investigated.

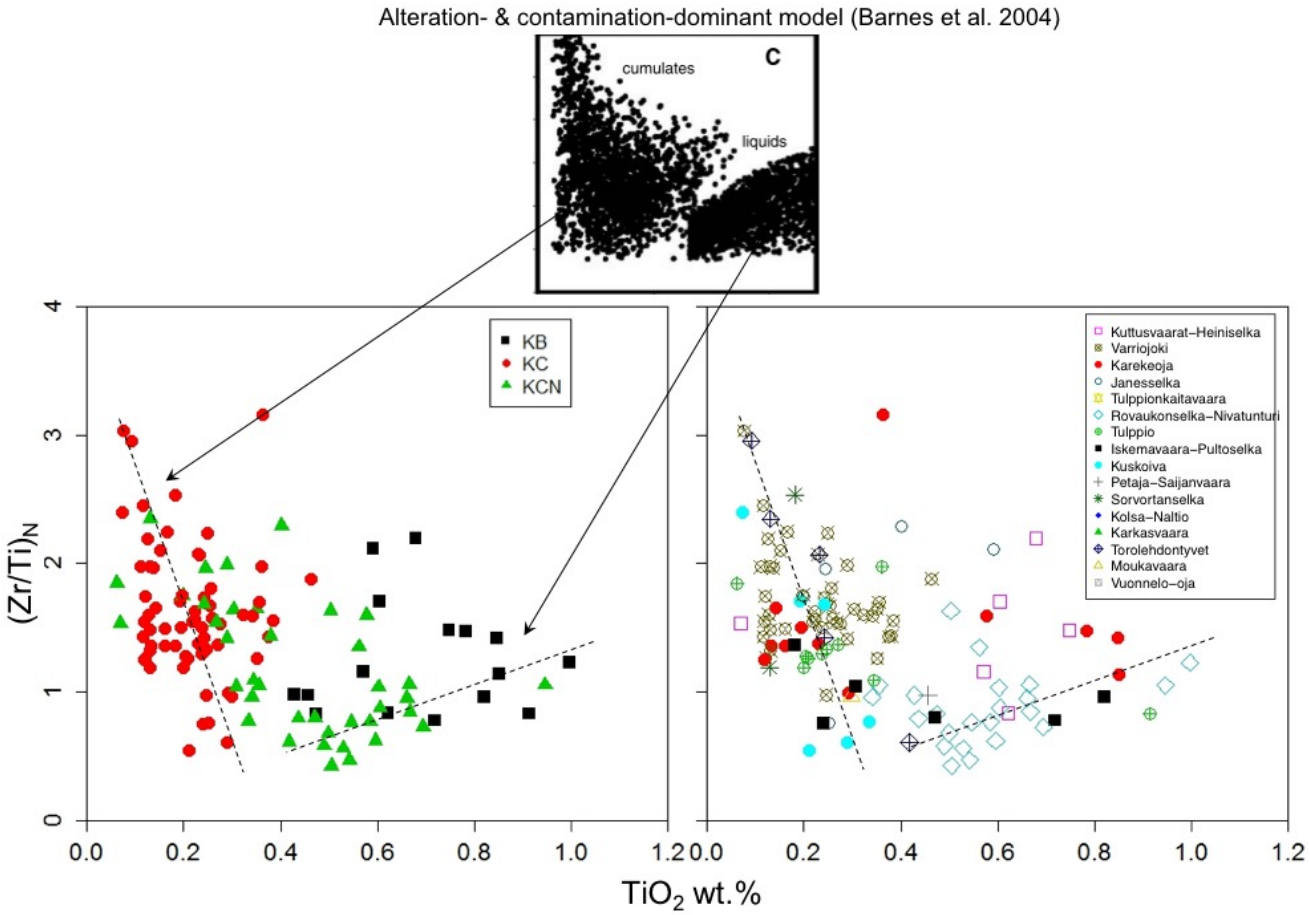

Figure 93. Comparison of The ELAD komatiites to Barnes et al. (2004) probability simulations of alteration- and contamination-controlled distribution within ideally incompatible elements such as Zr, Y, Ti and Al. In ELAD, TiO2 can be used instead of Al_2O_3 as their behavior with respect to MgO contents is similar. On the left The ELAD komatiites are categorized by lithofacies type and on the right by target. The dashed black lines illustrate the general trends. In general, the distributions have the best fit to the model showing both alteration- and contamination-controlled trends (uppermost image, after Barnes et al. 2004). The komatiitic cumulates show negative correlation with a minor scatter on the plot, indicating somewhat strong alteration dependency in their element compositions. The non-cumulates and komatiitic basalts, in contrast, show weaker dependency to alteration as they comprise a rather positive correlation trend with minor scatter. This implies that both alteration and contamination have modified the elements compositions of the ELAD komatiites.

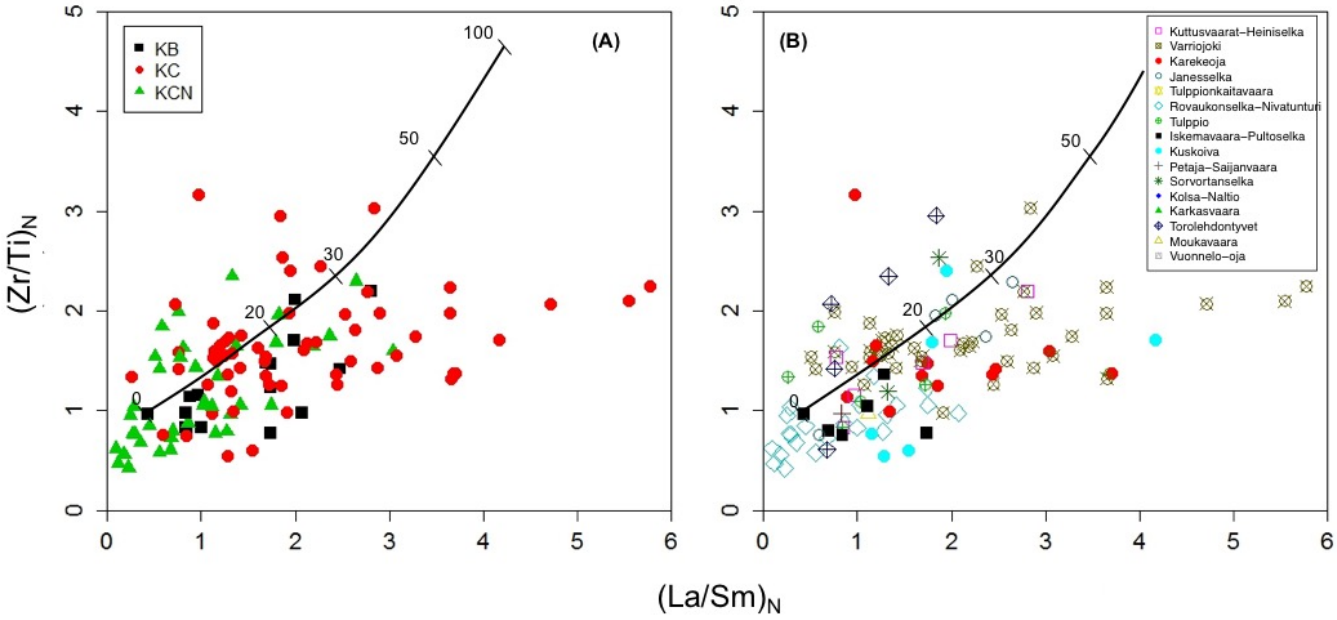

Figure 94. $(La/Sm)_N$ vs. $(Zr/Ti)_N$ plot of The ELAD komatiites. The black line with intervals represents a model mixing line between komatiite and dacite (from Barnes et al. 2004). The number display percentage of a dacitic (average contaminant) component in the komatiite melt.

9. CONCLUSIONS

The main results of this thesis are:

- The Eastern Lapland Archean domain (ELAD) has potential sulfur sources for komatiitic rocks to produce komatiite-hosted Ni-Cu-PGE deposits but their stratigraphy is not known in detail.

- Direct indications of Ni-Cu-PGE mineralizations in ELAD are restricted to the Ni-sulfide bearing komatiite boulders in the Kuttusvaarat-Heiniselkä area and two PGE-Ni-enriched zones in the Tulppio body.

- The majority of the komatiites of ELAD are komatiitic olivine cumulates derived from komatiitic basaltic/low-MgO komatiitic parental melts. These parental melts have generated extensive cumulate bodies, such as the Värriöjoki and Tulppio komatiitic bodies. This kind of extensive cumulate bodies are favorable

environments for Ni-Cu-PGE exploration. On the basis of parental magma composition, the low-MgO parental melts in ELAD are particularly critical for PGE-enriched komatiite-hosted Ni-Cu deposits.

- The ELAD komatiites are principally of the AUK-type, which seems to be favorable for komatiite-hosted sulfide deposits globally and also in Finland.

- Most of the ELAD komatiites were derived from Cr-saturated melts. However, also compositions indicating crystallization from Cr-undersaturated melts are present. These low-Cr cumulates show relatively high Ni, especially in the Värriöjoki, Tulppio and Kuttusvaarat-Heiniselkä targets and are critical in terms of exploration, as also shown in other parts of Finland.

- Ni depletion indicating possible sulfide segregation is most evidently observed in the Värriöjoki, Tulppio, Kuttusvaarat-Heiniselkä, Petäjä-Saijanvaara, and Siurujoki targets. Also, relatively elevated Ni and PGE (Pt + Pd) abundances are mainly present in the Tulppio, Värriöjoki, and Kuttusvaarat-Heiniselkä targets. However, as a negative feature, the known komatiitic bodies in ELAD are characterized by low S contents and lack of magmatic Ni sulfides.

- Evidently, both alteration and contamination have modified the incompatible element abundances (such as LREE & Zr) in ELAD. In the light of global trends, the strongest contamination indicative features are, however, found in the Värriöjoki and Jänesselkä bodies.

10. ACKNOWLEDGEMENTS

I want to thank Dr. Jukka Konnunaho and Dr. Tapio Halkoaho for introducing me to the world of komatiites. Jukka is also thanked for being the main instructor in my thesis and making me see things in new perspectives. Tapio is thanked for his useful comments, advice and his endless enthusiasm to answer my questions. Being a thesis worker in this GTK and University collaborative project has fully been a good experience. I want thank Professor Tapani Rämö for relying on me and giving me the chance to work with my thesis in this project. Also, I want to thank Dr. Aku Heinonen and Jussi S. Heinonen for always keeping their doors open for me, when I needed scientific advice. They are also thanked for very useful comments. Special thanks I want point to my "partners in crime", Pieti Haapala and Johanna Tepsell, with whom we spent two unforgettable summers in eastern Lapland, when mapping the ultramafic bodies. Thanks for the memorable moments and solidarity. Also, I want to present my warmest regards to our hosts at the Kemihaara field base, Helena and Juhani († 2018) Peltoniemi and to Saija, the keeper of the Tulppio pub. Ville Järvinen is thanked for useful practical hints and guidance with geochemical plotting. Dr. Jouni Vuollo is thanked for fruitful discussions in the field and at the coffee table. Radek Michallik is thanked for helping with sample preparation. Dr. Tuomo Törmänen is thanked for his useful help when processing the preceding data sets. Lassi Pakkanen and Bo Johanson at the GTK EPMA lab are thanked for their contribution to our mineral chemistry analyses. Pertti Telkkälä is thanked for company on the extraordinary trip to the remote areas of the Urho Kekkonen National Park. Heimo Tolonen is thanked for field preparations. The past years as a student at the Department Geosciences and Geography in the University of Helsinki have been the time of my life. For this, thanks goes to the lovely staff of the department, but also to my fellow students, with whom I have made lifelong friendships. Lastly, I want to thank my parents Anita and Pasi, my sister Heini and our dog Hugo for supporting me during the writing of this thesis. Finally, the warmest hugs and kisses to my love, Salla, for solidarity and bearing with my absence at home.

11. REFERENCES

Aitken, B.G. & Echeverría, L.M. 1984. Petrology and geochemistry of komatiites and tholeiites from Gorgona Island, Colombia. Contributions to Mineralogy and Petrology 86, 94-105.

Allégre, C.J. 1982. Genesis of Archean komatiites in a wet ultramafic subducted plate. In Arndt, N.T., Nisbet, E.G. (eds.) 1982. Komatiites, 495–500, George Allen & Unwin Ltd.

Arndt, N.T. 1977. Ultrabasic magmas and high–degree melting of the mantle. Contributions to Mineralogy and Petrology 64, 205–221.

Arndt, N.T., Lesher C.M. & Barnes S.J 2008. Komatiite. 467 p. Cambridge University Press.

Barkov, A.Y., Nikiforov, A.A., Korolyuk, V.N. & Halkoaho, T.A.A. in press. A suite of ultramafic rocks of Mount Kareka-Tundra, Serpentinite belt, Kola Peninsula, Russia (Running title: Ultramafic rocks of Mount Kareka-Tundra, Kola Peninsula). 14 p.

Barnes, S.J. 1998. Chromite in Komatiites, I. Magmatic Controls on Crystallization and Composition. Journal of Petrology 39, 1689–1720.

Barnes, S.J. 2000. Chromite in komatiites, II. Modification during greenschist to mid-amphibolite facies metamorphism. Journal of Petrology 41, 387-409.

Barnes, S.J. 2006. Nickel Deposits of the Yilgarn Craton: Geology, Geochemistry, and Geophysics Special Publication 13, Society of Economic Geologists, 13 –119.

Barnes, S.J. & Hill, R.E.T 1995: Poikilitic chromite in komatiitic cumulates. Mineralogy and Petrology 54, 85-92.

Barnes, S.J. & Roeder, P.L. 2001. The range of Spinel Compositions in Terrestrial Mafic and Ultramafic Rocks. Journal of Petrology 42, 2279-2302.

Barnes, S.J. & Fiorentini, M.L. 2012. Komatiite magmas and sulfide nickel deposits: A comparison of variably endowed Archean terranes. Economic Geology 107, 755–780.

Barnes, S.J., Coats, C. J. A. & Naldrett, A. J. 1982. Petrogenesis of a Proterozoic nickel sulphide-komatiite association: the Katiniq Sill, Ungava, Quebec. Economic Geology 77, 413–429.

Barnes, S.J., Wells, M.A. & Verrall, M.R. 2009. Effects of magmatic processes, serpentinization, and talc-carbonate alteration on sulfide mineralogy and ore textures in the Black Swan disseminated nickel sulfide deposit, Yilgarn Craton. Economic Geology and the Bulletin of the Society of Economic Geologists 104, 539-562.

Barnes, S.J., Halkoaho, T., Papunen, H. & Perring, C. 1996. Chromite in komatiites: A comparative study of chromite in komatiites from the Forrestania Greenstone belt, Western Australia, and the Pulju and Kuhmo greenstone belts, Finland. CSIRO Australia, Exploration and Mining Report 273R prepared for Outokumpu Finnmines Oy. 84 p.

Barnes, S.J., Hill, R.E.T., Perring, C.S. & Dowling, S.E. 2004. Lithogeochemical exploration for komatiite-associated Ni sulfide deposits: Strategies and limitations. Mineralogy and Petrology 82, 259-293.

Barnes, S.J, Godel, B., Gürer, D., Brenan, J.M., Robertson, J. & Paterson, D. 2013. Sulfide-olivine Fe-Ni exchange and the origin of anomalously ni rich magmatic sulfides. Economic Geology, 108, 1971-1982.

Barnes, S.J., Cruden, A.R., Arndt, N.T, Saumur, B.M. 2016. The mineral system approach applied to magmatic Ni–Cu–PGE sulphide deposits. Ore Geology Reviews 76, 296-316.

Barnes, S-J. & Often, M. 1990. Ti-rich komatiites from northern Norway. Contributions to Mineralogy and Petrology 105, 42-54.

Barnes, S-J., Naldrett, A. J. & Gorton, M. P. 1985. The origin of the fractionation of the platinum-group elements in terrestrial magmas. Chemical Geology 53, 303–323.

Bekker, A., Barley, M.E., Fiorentini, M.L., Rouxel, O.L, Rumble, D. & Beresford, S.W. 2009. Atmospheric Sulfur in Archean Komatiite-Hosted Nickel Deposits. Science 326, 1086-1089.

Beswick, A.E. 1982. Some geochemical aspects of alteration, and genetic relations in komatiitic suites. In Arndt, N.T. & Nisbet, E.G (eds.). Komatiites, 283–308.

Blais, S. 1989. Les ceintures de roched ve4rtes archéennes de Finlande Orientale: Géologie, pétrologie, geóchimie et evolution géodynamique. Mémoires et Documents du Centre Armoricain d'Étude Structurale des Socies 22, 256 p. Université de Rennes. (in French)

Blais, S. & Auvray, B., 1990. Serpentinization in the Archean komatiitic rocks of the Kuhmo greenstone belt, eastern Finland. The Canadian Mineralogist 28, 55-66.

Bogdanova, S.V., Bibikova E.V. and Kirnozova, T.I. 1990. The "Saamian" of the Belomorian mobile belt: fiction or reality? Abstracts of the 2nd Symposium on the Baltic Shield, Lund, Sweden, June 5-7. 18-19.

Bogdanova, S.V. & Bibikova E.V. 1993. The "Saamian" of the Belomorian Mobile Belt: new geochronological constraints. Precambrian Research 64, 131-152.

Boutroy, E., Dare, S., Beaudoin, G., Barnes, S-J. & Lightfoot, P.C. 2014. Magnetite composition in Ni-Cu-PGE deposits worldwide: Application to mineral exploration.

Brooks, C. & Hart, S.R. 1974. On the significance of Komatiites. Geology 2, 107-110. Geological Society of America.

Brand, N.W. 1999. Element ratios in nickel sulphide exploration: Vectoring towards ore environments. Journal of Geochemical Exploration 67, 145-165.

Brenan, J.M., 2003. Effects of fO_2, fS_2, temperature, and melt composition on Fe-Ni exchange between olivine and sulfide liquid: Implications for natural olivine–sulfide assemblages. Geochimica et Cosmochimica Acta 67, 2663-2681.

Brownscombe, W., Ihlenfeld, C., Coppard, J., Hartshorne, C., Klatt, S., Siikaluoma, J.K. & Herrington, R.J. 2015. The Sakatti Cu-Ni-PGE Sulfide Deposit in Northern Finland. In Maier, W.D., Lahtinen, R. & O'Brien, H. (eds.): Mineral Deposits of Finland. 211-252. Elsevier.

Campbell, I. H. & Naldrett, A.J. 1979. The influence of silicate: Sulfide ratios on the geochemistry of magmatic sulfides. Economic Geology and the Bulletin of the Society of Economic Geologists 74, 1503-1506.

Campbell, I.H., Griffiths, R.W. and Hill, R.I. 1989. Melting in an Archean mantle plume: heads it's basalts, tails it's komatiites. Nature 339, 697–697.

Dare, S. Barnes, S-J. & Beaudoin, G. 2012. Variation in trace element content of magnetite crystallized from a fractionating sulfide liquid, Sudbury, Canada: Implications for provenance discrimination. Geochimica et Cosmochimica Acta 88, 27-50.

Dare, S., Barnes, S-J., Beaudoin, G., Méric, J., Boutroy, E. & Potvin-Doucet, C. 2014. Trace elements in magnetite as petrogenetic indicators. Mineralium Deposita 49, 785-796.

Davies, R. 1996. Report of Investigation, Jää 73. Report 5857/1. 4 p. Glenmore Highland Inc.

Bedrock of Finland – DigiKP. Digital map database, Geological Survey of Finland, visited on 8.12.2018, http://gtkdata.gtk.fi/Kalliopera/index.html

Donaldson, C.H. 1976. An experimental study of olivine morphology. Contributions to Mineralogy and Petrology 57, 187–213.

Donaldson, C.H. 1982. Spinifex –textured komatiites: a review of textures, mineral compositions, and layering. In Arndt, N.T., Nisbet, E.G. (eds.) 1982. Komatiites, 211–244.

Dupuis, C. & Beaudoin, G. 2011. Discriminant diagrams for iron oxide trace element fingerprinting of mineral deposit types. Mineralium Deposita 46, 319-335.

Duuring, P., Bleeker, W., Beresford, S.W. & Hayward, N. 2010. Towards a volcanic–structural balance: Relative importance of volcanism, folding, and remobilisation of nickel sulphides at the Perseverance Ni–Cu–(PGE) deposit, Western Australia. Mineralium Deposita 45, 281-311.

Echeverría, L.M. 1980. Tertiary or Mesozoic komatiites from Gorgona Island, Colombia: Field realtions and geochemistry. Contributions to Minrealogy and Petrology 73, 253-266.

Evans, D. 2017. Chromite compositions in nickel sulphide mineralized intrusions of the Kabanga-Musongati-Kapalagulu Alignment, East Africa: Petrologic and exploration significance. Ore Geology Reviews 90, 307-321.

Faure, F., Arndt, N.T. & Libourel, G. 2006. Formation of spinifex texture in komatiites: An experimental study. Journal of Petrology 47, 1591-1610.

Fiorentini, M.L., Barnes, S.J., Lesher, C.M., Heggie, G.J., Keays, R.R. & Burnham, O.M. 2010a. Platinum group element geochemistry of mineralized and nonmineralized komatiites and basalts. Economic Geology 105, 795–823.

Fiorentini, M. L., Beresford, S. W., Rosengren, N., Barley, M. E. & McCuaig, T. C. 2010b. Contrasting komatiite belts, associated Ni–Cu–(PGE) deposit styles and assimilation histories. Australian Journal of Earth Science 57, 543-566.

Gaál, G. & Gorbatschev, R. 1987. An outline of the Precambrian evolution of the Baltic Shield. Precambrian Research 35, 15-52.

Grove, T.L. & Parman, S.W. 2004. Thermal evolution of the Earth as recorded by komatiites. Earth and Planetary Science Letters 219, 173-187.

Groves, D.I., Barrett, F.M., Binns, R.A. & McQueen, K.G. 1977. Spinel phases associated with metamorphosed volcanic-type iron–nickel sulfide ores from Western Australia. Economic Geology 72, 1224–1244.

Haapala, P.S. in preparation. Petrological and geochemical comparison of the ultramafic rocks of Tulppio, Jänesselkä and Värriö. Unpublished M.Sc. thesis. University of Helsinki.

Haapala, P.S., Höytiä, H.M.A. & Tepsell, J.H.M. 2018. Origin, exploration potential, and metallogeny of komatiitic suites of Eastern Lapland. In Skyttä, P. & Eklund, O. (eds.): 4th National Colloquium of Geosciences, Turku, 14–15 March 2018, Abstract Book. Geological Survey of Finland (GTK), 77 p.

Hanski, E.J. 1992. Petrology of the Pechenga ferropicrites and cogenetic, Ni–bearing gabbro wehrlite intrusions, Kola Peninsula, Russia. Academic dissertation, Bulletin of the Geological Survey of Finland 367, 192p.

Hanski, E., Huhma, H., Rastas P. & Kamenetsky, V.S. 2001. The Paleoproterozoic Komatiite Picrite Association of Finnish Lapland. Journal of Petrology 42, 855–876.

Hanski, E., Walker, R.J., Huhma, H., Polyakov, G.V., Balykin, P.A., Tran Trong Hoa & Ngo Thi Phuong 2004. Origin of the Permian-Triassic komatiites, northwestern Vietnam. Contributions to Mineralogy and Petrology 147, 453–469.

Hanski, E. & Huhma, H. 2005. Central Lapland greenstone belt. In: Lehtinen, M., Nurmi, P.A. & Rämö, O.T. (eds.) Precambrian Geology of Finland – Key to the Evolution of the Fennoscandian Shield. Elsevier B.V., Amsterdam, 139-194

Heggie, G.J., Barnes, S.J. and Fiorentini, M.L., 2013. Application of lithogeochemistry in the assessment of nickel-sulphide potential in komatiite belts from northern Finland and Norway. Bulletin of the Geological Society of Finland 85, 107-126.

Heikura, P., Törmänen, T., Iljina, M., & Salmirinne, H. 2010. Tutkimustyöselostus Savukosken kunnassa valtausalueilla Tulppionkariste 1-5 (kaivosrekisterinumerot 8246/1-5) suoritetuista nikkeli- & PGE-malmitutkimuksista vuosina 2005 – 2008, Claim Report M06/4723/2009/68, Geological Survey of Finland, Rovaniemi, Finland, 72 p. (In Finnish)

Heikura, P., Sarapää O., Törmänen, T., Iljina, M., Salmirinne, H. & Sarala, P. 2011. Tutkimustyöselostus Savukosken kunnassa Ketunkangas 1 (kaivosrekisterinumero 8247/1) & Kuttusoja 1-4 (kaivosrekisterinumero 8410/1-4) –nimisillä valtausalueilla vuosina 2006-2009 suoritetuista nikkeli-, PGE- & kultatutkimuksista. Archive report M06/4721/2009/67, Geological Survey of Finland (GTK), 73 p. (In Finnish)

Herzberg, C. 1992. Depth and Degree of Melting of Komatiites. Journal of Geophysical Research 97, 4521–4540. American Geophysical Union.

Herzberg, C.T. & Ohtani, E. 1988. Origin of komatiite at high pressures. Earth and Planetary Science Letters 88, 321-329.

Hill, R.E.T, Barnes, S.J., Gole, M.J. & Dowling, S.E. 1995. The volcanology of komatiites as deduced from field relationships in the Norseman–Wiluna greenstone belt, Western Australia. Lithos 34, 159–188.

Hill, R.E.T, 2001. Komatiite volcanology, volcanological setting and primary geochemical properties of komatiite-associated nickel deposits. Geochemistry: Exploration, Environment, Analysis 1, 365-381.

Huhma, H., Mänttäri, I., Peltonen, P., Kontinen, A., Halkoaho, T., Hanski, E., Hokkanen, T., Hölttä, P., Juopperi, H., Konnunaho, J., Layahe, Y., Luukkonen. E., Pietikäinen. K., Pulkkinen, A., Sorjonen-Ward, P., Vaasjoki, M. & Whitehouse, M. 2012. The age of the Archaean greenstone belts in Finland. Geological Survey of Finland Special Paper 54, 74−175.

Huhma, H., Hanski, E., Kontinen, A., Vuollo, J., Mänttäri, I. & Lahaye, Y. 2018. Sm–Nd and U–Pb isotope geochemistry of the Palaeoproterozoic mafic magmatism in the eastern and the northern Finland. Bulletin of Geological Survey of Finland 405, 150 p.

Huppert, H.E. & Sparks, R.S. 1984. Komatiites I: Eruption and flow. Journal of Petrology 26, 694-725.

Hölttä, P., Heilimo, E., Huhma. H., Juopperi, H., Kontinen, A., Konnunaho, H., Lauri, L., Mikkola, P., Paavola, J. & Sorjonen-Ward, P. 2012. Archeaean Complexes of the Karelian province in Finland. In: Hölttä, P. (ed.) The Archaean of the Karelia Province in Finland. Geological Survey of Finland, Special Paper 54, 9−20.

Hölttä, P. & Heilimo, E. 2017. Metamorphic map of Finland. In: Nironen, M. (ed.) Bedrock of Finland at the scale 1:1 000 000 – Major stratigraphic units, metamorphism and tectonic evolution Guide to the Geological Map of Finland – Bedrock 1:1 000 000. Geological Survey of Finland, Special Paper 60, 75-126.

Idman, H. 1980. Lapin ultramafiittien oksidifaasista. Unpublished M.Sc. thesis, University of Turku, Department of Geology, 147 p. (In Finnish)

Iljina, M. 2003. Pohjois-Suomen Kerrosintruusiot 1996-2002, 2106001 Final Report, M10.4/2003/4, Geological Survey of Finland (GTK), Rovaniemi, Finland. 36 p. (In Finnish)

Iljina, M. 2009. Hanke 2901007, Pohjois-Suomen emäksisten magmakivien malmivarojen kartoitus 2003-2008. Archive report M10.4/2009/49, Geological Survey of Finland (GTK). 32 p. (In Finnish)

Jahn, B-M., Auvray, B., Blais, S., Capdevila, R., Cornichet, J., Vidal, F. & Hameurt, J., 1980. Trace element geochemistry and petrogenesis of Finnish greenstone belts. Journal of Petrology 21, 201-244.

Jahn, B–M., Gruau, G. & Glickson, A.Y. 1982. Komatiites of the Onverwacht Group, South Africa; REE geochemistry, Sm/Nd age and mantle evolution. Contributions to Mineralogy and Petrology 80, 25–40.

Janoušek, V., Farrow, C. M. & Erban, V. 2006. Interpretation of whole-rock geochemical data in igneous geochemistry: introducing Geochemical Data Toolkit (GCDkit). Journal of Petrology 47, 1255-1259.

Jolly, W.T. 1982. Progressive metamorphism of komatiites and related Archean lavas of the Abitibi area, Canada. In Arndt, N.T., Nisbet, E.G. (eds.) 1982: Komatiites. George Allen & Unwin Ltd. 247–266.

Juopperi, H. 1983. Tuntsa-muodostumasta & sen vulkaniiteista. Archive report, Geological Survey of Finland (GTK), Rovaniemi, 2 p. (In Finnish)

Juopperi, H. 1988. Tuntsa. In Manninen, T., Hanski, E. & Kesola, R. Lapin vulkaniittiprojekti vuosikertomus 1987. Archive report K/1988/1. Geological Survey of Finland (GTK), 23-27. (In Finnish)

Juopperi, H. 1994. Arkeeinen kallioperä Itä-Lapissa. 13102 Final report K/21.42/94/9. Geological Survey of Finland (GTK), Rovaniemi, Finland, 17 p. (In Finnish)

Juopperi, H. 2002. Pohjois-Suomen arkeeiset alueet. 2105001 Final Report, M10.4/2002/1, Geological Survey of Finland (GTK), Rovaniemi, Finland, 24 p. (In Finnish)

Juopperi, H. 2005. Project 2105002 Archaean terranes in the northern Finland II. Final report M10.4/2005/1, Geological Survey of Finland (GTK), Rovaniemi, Finland. 37 p.

Juopperi, H., & Veki, A. 1988. The Archaean Tuntsa Supergroup in the Nuolusvaara area, area, the norththe eastern Finland. In: Marttila, E. (ed.) Archaean Geology of the Fennoscandian Shield, Proceedings of a Finnish - Soviet Symposium in Finland on July 28-August 7, 1986. The Committee for Scientific and Technical co-operation between Finland and the Soviet. Geological Survey of Finland, Special Paper 4, 145-151.

Juopperi, H. & Vaasjoki, M. 2001. U-Pb mineral age determinations from Archean rocks in the eastern Lapland. In Vaasjoki (ed.) Radiometric age determinations from Finnish Lapland and their bearing on the timing of Precambrian volcano-sedimentary sequences. Special Paper 33, Geological Survey of Finland (GTK), 209-227.

Kauniskangas, E. 1987. Savukosken koillisosan Arkeeisten liuskeiden petrografia & geokemia. M.Sc. thesis, Arkeeisten alueiden malmiprojekti 25, University of Oulu, Department of Geology, 90 p. (In Finnish)

Karinen, T., Lepistö, S., Konnunaho, J., Lauri, L.S., Manninen, T. & Huhma, H. 2015. Yksikkökuvausraportti Enontekiö, Käsivarsi. Archive report 66/2015. The Geological Survey of Finland (GTK). 39 p. (In Finnish, English abstract).

Kerr, A.C. & Arndt, N.T. 2001. A note on the IUGS reclassification of the high–Mg and picritic volcanic rocks. Journal of Petrology 42, 2169–2171.

Kivisaari, T. 2008. Tuntsan metasedimenttivyöhykkeen metamorfoosi. Unpublished M.Sc. thesis, University of Helsinki, Department of Geology, 53 p. (In Finnish)

Koistinen, T.J. 1987a. Alustava tutustuminen: Savukosken koillisosa 10.-11.6.1986. Memorandum 3.2.1987, Outokumpu Oy Exploration Reports, 6 p. (In Finnish)

Koistinen, T.J. 1987b. Muistio, Savukoski 11-15.6.1987. Memorandum 22.6.1987, Outokumpu Oy Exploration Reports, 18 p. (In Finnish)

Konnunaho, J. 2016. Komatiite-hosted Ni-Cu-PGE deposits in Finland: Their characterization, PGE content, and petrogenesis. Academic dissertation, Geological Survey of Finland, Espoo. 38 p.

Konnunaho, J., Halkoaho, T., Hanski, E. & Törmänen, T. 2015. Komatiite-hosted Ni-Cu-PGE Deposits In Finland. In Maier, W.D., Lahtinen, R. and O'Brien, H. (eds.): Mineral Deposits of Finland. 93-128. Elsevier.

Konnunaho, J., Hanski, E., Wing, B., Bekker, A., Lukkari, S. & Halkoaho, T. 2016. The Hietaharju PGE-enriched komatiite-hosted sulfide deposit in the Archean Suomussalmi greenstone belt, eastern Finland. Ore Geology Reviews 72, 641-658.

Konnunaho, J., Hanski, E., Bekker, A., Halkoaho, T., Hiebert, R. & Wing, B. 2013. The Archean komatiite-hosted, PGE-bearing Ni–Cu sulfide deposit at Vaara, eastern Finland: Evidence for assimilation of external sulfur and post-depositional desulfurization. Mineralium Deposita, 48 967-989.

Lahti, I., Salmirinne, H., Törmänen, T. & Iljina, M. 2007. Värriöjoen ultramafisen intruusion geofysikaaliset tutkimukset vuosina 2002 – 2006. Q19/4712/2007/77, Geological Survey of Finland (GTK), Rovaniemi, Finland, 38 p. (In Finnish)

Lahtinen, J. 2003. Tutkimustyöselostus Tuntsan arkeeisella vihreäkivivyöhykkeellä valtauksilla "Kuttusoja 1-3" suoritetuista malmitutkimuksista. Report of Investigation 080/4721/JJL/03, Outokumpu Oy. 18 p. (In Finnish)

Le Bas, M.J. 2000. IUGS Reclassification of the High–Mg and Picritic Volcanic Rocks. Journal of Petrology 41, 1467–1470.

Le Maitre, R.W. (ed.), Streckeisen, A., Zanettin, B., Le Bas, M.J., Bonin, B., Bateman, P., Bellieni, A., Dudek, A., Efremova, S., Keller, J., Lameyre, J., Sabine, P.A., Schmid, R., Sorensen, H. & Wolley, A.R. 2002. Igneous rocks A Classification and Glossary of Terms, 2nd edition. Cambridge University Press, Cambridge. 236 p.

Le Vaillant, M., Barnes, S.J., Fisher, L., Fiorentini, M.L. & Caruso, S. 2014. Use and calibration of portable X-ray fluorescence analysers; application to lithogeochemical exploration for komatiite-hosted nickel sulphide deposits. Geochemistry - Exploration, Environment, Analysis, 14(3), pp. 199-209.

Le Vaillant, M., Fiorentini, M.L & Barnes, S.J. 2016. Review of lithogeochemical exploration tools for komatiite-hosted Ni-Cu-(PGE) deposits. Journal of Geochemical Exploration 168, 1-19.

Lehtonen E. 2016. Painting the volcanic landscape of early Fennoscandia – Geochronology of the Meso- and Neoarchaean Suomussalmi-Kuhmo-Tipasjärvi greenstone complex, Karelia Province, Finland. Academic dissertation, University of Helsinki, 40 p.

Lehtonen, M., Airo, M.-L., Eilu, P., Hanski, E., Kortelainen, V., Lanne, E., Manninen, T., Rastas, P., Räsänen, J. & Virransalo, P., 1998. Kittilän vihreäkivialueen geologia. Lapin vulkaniittiprojektin raportti. Summary: The stratigraphy, petrology and geochemistry of the Kittilä greenstone area, the northern Finland. A report of

the Lapland Volcanite Project. Geological Survey of Finland (GTK), Report of Investigation 140, 1–144.

Lesher, C.M. 1989. Komatiite-associated nickel sulfide deposits. In: J. A. Whitney & A. J. Naldrett (eds.) Ore Deposition Associated with Magmas, 45–102.

Lesher, C.M. & Keays, R.R. 2002. Komatiite-associated Ni-Cu-(PGE) deposits: geology, mineralogy, geochemistry and genesis. In: Cabri, L.J. (ed.). The Geology, Geochemistry, Mineralogy and Mineral Beneficiation of Platinum-Group Elements. Canadian Institute of Mining and Metallurgy, Special Volume 54, 579–619.

Lesher, C.M. & Barnes, S.J. 2008. Komatiite-associated Ni–Cu–PGE deposits. In Arndt, N.T., Lesher C.M. & Barnes S.J 2008 (eds.). Komatiite, 295-327. Cambridge University Press.

Lesher, C.M., Burnham, O.M., Keays, R.R. & Hulbert, L. 2001. Trace-element geochemistry and petrogenesis of barren and ore-associated komatiites. Canadian Mineralogist 39, 673–696.

Li, C., Xu, Z., de Waal, S.A., Ripley, E.M. & Maier, W.D., 2004. Compositional variations of olivine from the Jinchuan Ni–Cu sulfide deposit, western China: implications for ore genesis. Mineralium deposita 39, 159-172.

Li, C., Naldrett, A.J. & Ripley, E.M., 2007. Controls on the Fo and Ni Contents of Olivine in Sulfide-bearing Mafic/Ultramafic Intrusions: Principles, Modeling, and Examples from Voisey's Bay. Earth Science Frontiers 14, 177-183.

Li, C., Ripley, E.M., Tao, Y. & Mathez, E.A., 2008. Cr-spinel/olivine and Cr-spinel/liquid nickel partition coefficients from natural samples. Geochimica et Cosmochimica Acta 72, 1678-1684.

Lowrey, J.R., Ivanic, T.J., Wyman, D.A. & Roberts, M.P. 2017. Platy Pyroxene: New Insights into Spinifex Texture. Journal of Petrology 58, 1671–1700.

Luukas, J., Kousa, J., Nironen, M & Vuollo, J. 2017. Major stratigraphic units in the bedrock of Finland, and an approach to tectonostratigraphic division. In: Nironen, M. (ed.) Bedrock of Finland at the scale 1:1 000 000 – Major stratigraphic units, metamorphism and tectonic evolution. Special Paper 60, Geological Survey of Finland, 9-39.

Maier, W. D., Peltonen, P., Halkoaho, T. & Hanski, E. 2013. Geochemistry of komatiites from the Tipasjärvi, Kuhmo, Suomussalmi, Ilomantsi and Tulppio greenstone belts, Finland: Implications for tectonic setting and Ni sulphide prospectivity. Precambrian Research 228, 63-84.

Manninen, T., Hanski, E. & Kesola, R. (eds.) 1988. Lapin vulkaniittiprojekti vuosikertomus 1987. Archive report K/1988/1. Geological Survey of Finland (GTK), 49 p. (In Finnish)

Mattila, H. 1979. Sähköisten anomalioiden tutkimukset Soklin länsipuolella 1978-1979. Rautaruukki Oy, Report of Investigation RO 16/79, 001/4712, 4721/HM/79. 49 p. (In Finnish)

Mavrogenes, J.A. & O'Neill, H.S.C. 1999. The relative effects of pressure, temperature and oxygen fugacity on the solubility of sulfide in mafic magmas. Geochimica et Cosmochimica Acta 63, 1173-1180.

McCutcheon, S.R. 2011. "Durchbewegung" texture: what is it and does it occur in massive sulphide deposits of the Bathurst Mining Camp? AGS Abstracts– 37th Annual Colloquium & Annual General Meeting 2011. Atlantic Geology 47.

McDonough, W.F. & Sun, S.-s. 1995. The composition of the Earth. Chemical geology 120, 223-253.

Mikkola, E. 1936. Bedrock map of Tuntsajoki, 1:400 000. Maps of Pre-Quarternary rocks D7, Map sheet 47. The Geological Survey of Finland. (In Finnish)

Mikkola, E. 1941. Muonio-Sodankylä-Tuntsajoki general geological map 1:400 000, explanation to the map of rocks. Suomen Geologinen Toimikunta, 278p. (In Finnish)

Mikkola, P. 1979. Slingram-magneettiset & gravimetriset mittaukset Sorvortanjoella talvella 1979. Rautaruuki Oy reports, 040/4721/SMOY/79. 48 p. (In Finnish)

Mudd, G.M. & Jowitt, S.M. 2014. A Detailed Assessment of Global Nickel Resource Trends and Endowments. Economic Geology 109, 1813-1841.

Naldrett, A.J., 1966. The role of sulphurization in the genesis of iron-nickel sulfide deposits of the Porcupine district, Ontario. Canadian Institute of Mining and Metallurgy Transactions 69, 147-155

Naldrett, A.J., Duke, J.M., Lightfoot, P.C. & Thompson, J.F.H. 1984. Quantitative modelling of the segregation of magmatic sulfides: an exploration guide. Canadian Mining and Metallurgical Bulletin 77, 45-56

Nesbitt, R.W. 1971. Skeletal crystal forms in the ultramafic rocks of the Yilgarn block, Western Australia: Evidence for an Archean ultramafic liquid. Geological Society Special Publication 3, 331-350.

Nesbitt, R.W. & Sun, S.–s. 1976. Geochemistry of Archaean spinifex–textured peridotites and magnesian and low–magnesian tholeiites. Earth and Planetary Science Letters 31:433:453.

Nesbitt, R.W., Sun, S.–s. & Purvis A.C. 1979. Komatiites: Geochemistry and Genesis. Canadian Mineralogist 17, 165–186.

Nironen, M., 2017. Guide to the Geological Map of Finland – Bedrock 1:1 000 000. In: Nironen, M. (ed.) Bedrock of Finland at the scale 1:1 000 000 – Major stratigraphic units, metamorphism and tectonic evolution Guide to the Geological Map of Finland – Bedrock 1:1 000 000. Geological Survey of Finland, Special Paper 60, 40-74.

Nisbet, E.G. & Walker, D. 1982. Komatiites and the structure of the Archaean mantle. Earth and Planetary Science Letters 60, 105-113.

Nuutilainen, J. 1980a. Heinivuotso 1:n tutkimukset. Rautaruukki Oy, Report of Investigation 405/460/79. 9 p. (In Finnish)

Nuutilainen, J. 1980b. Sorvorta 1-3 tutkimukset. Rautaruukki Oy, Report of Investigation 333/460/79. 9 p. (In Finnish)

Papunen, H. 1976. Lapin ultramafiittien geologiset, petrologiset, geokemialliset & mineralogiset datat. Lapin nikkeliprojektin dokumenttikokoelma PSMT-P11-76-2. 1836 p.

Papunen, H., Idman, H., Ilvonen, E., Neuvonen, K.J., Pihia&, P. and Taivitie, J. 1977. Lapin ultramafiiteista. Summary: The ultramafics of Lapland. Geological Survey of Finland, Report of investigation 23, 87 p.

Papunen, H. (ed.), Halkoaho, T., Kilpeläinen, T., Lepistö, S., Liimatainen, J., Lyons, K., Tulenheimo, T. & Välimaa, J. 1997. Savukosken Tulppio alueen kartoitukset kesällä 1997. Technical Report, Integrated technologies for mineral exploration pilot project for nickel ore deposits, University of Turku, Department of Geology, 50 p. (In Finnish)

Peltoniemi, H. 1984. Savukosken koillisosan proterotsooiset kivet. Project on Archean areas report 17. University of Oulu, Department of Geology. 52 p. (In Finnish)

Piirainen, T., Virransalo, P. & Kauniskangas, E. 1985. Savukosken osaprojektin tutkimusalueen geologia. In: Piirainen, T. (ed.) Arkeeisten alueiden malmiprojektin

loppuraportti. Arkeeisten alueiden malmiprojekti 25, University of Oulu, Department of Geology, 140-178. (In Finnish)

Pyke, D.R., Naldrett, A. & Eckstrand, O. 1973. Archean Ultramafic Flows in Munro Township, Ontario. Geological Society of America Bulletin 84, 955-977.

Ripley, E. M. & Li, C. 2013. Sulfide saturation in mafic magmas; is external sulfur required for magmatic Ni-Cu-(PGE) ore genesis? Economic Geology and the Bulletin of the Society of Economic Geologists 108,45-58.

Robb, L. 2005. Introduction to ore-forming processes. Blackwell, 368 p.

Roos, S. 1983. Värriojoen syväkairaus 1982-1983. Lapin Malmi Oy, Report of Investigation 030/4712/SIR/83/13. 47 p. (In Finnish)

Ross, J.R. & Hopkins, G.M.F., 1975. Kambalda nickel sulphide deposits. Economic Geology of Australia and Papua New Guinea 1, 100-121.

Saverikko, M. 1985. The pyroclastic komatiite complex at Sattasvaara in northern Finland. Bulletin of the Geological Society of Finland 57, 55-87.

Shore, M. and Fowler, A.D. 1999. The origin of spinifex texture in komatiites. Nature 397, 691–693.

Slabunov, A. I. & Bibikova, E. V. 2001. The meso- and neo-Archaean of the Karelian and Belomorian provinces, Baltic Shield (geology, isotope geochemistry and geodynamic reconstructions). In: Cassidy, K.F., Dunphy, J.M., Kranendonk van, M.J. (eds.): 4th International Archaean Symposium 2001, Perth, The western Australia, Extended Abstracts. Australian Geological Survey record 37, 359-363.

Slabunov, A. I., Lobach-Zhuchenko, S. B., Bibikova, E. V., Balagansky, V. V., Sorjonen-Ward, P., Volodichev, O. I., Shchipansky, A. A., Svetov, S. A., Chekulaev, V.P., Arestova, N. A. & Stepanov, V. S. 2006a. The Archean of the Baltic Shield: Geology, Geochronology, and Geodynamic settings. Geotectonics 40, Pleiades Publishing, 409-433.

Slabunov, A. I., Lobach-Zhuchenko, S. B., Bibikova, E. V., Sorjonen-Ward, P., Balagansky, V. V., Volodichev, O. I., Shchipansky, A. A., Svetov, S. A., Chekulaev, V.P., Arestova, N. A. & Stepanov, V. S. 2006b. The Archaean nucleus of the Fennoscandian (Baltic) Shield. In Gee, D.G. & Stephensov, R.A. (eds.) 2006. European Lithosphere Dynamics, Geological Society of London, Memoir 32, 627-644.

Sorjonen-Ward, P. & Luukkonen, E.J. 2005. Archean rocks. In: Lehtinen, M., Nurmi, P.A. & Rämö, O.T. (eds.) Precambrian Geology of Finland – Key to the Evolution of the Fennoscandian Shield. Developments in Precambrian Geology 14, 19-99.

Sossi, P.A., Eggins, S.M., Nesbitt, R.W., Nebel, O., Hergt, J.M., Campbell, I.H., O'Neill, H.S.C., Van Kranendonk, M. & Davies, D.R., 2016. Petrogenesis and geochemistry of Archean komatiites. Journal of Petrology 57, 147-184

Stenar, M. M. 1972. Tectonic development of the Archean complex in Karelia (Belomorides of the western White Sea region). Geotectonics, 279-284.

Stone, W.E & Archibald, N.J. 2004. Structural controls on nickel sulphide ore shoots in Archaean komatiite, Kambalda, WA: The volcanic trough controversy revisited. Journal of Structural Geology, 26, 1173-1194.

Stone, W.E., Crocket, J.H. & Fleet, M.E. 1993. Sulfide-poor platinum-group mineralization in komatiitic systems: Boston Creek Flow, layered basaltic komatiite, Abitibi Belt, Ontario. Economic Geology 88, 817–836.

Sun, S.–s. & Nesbitt, R.W. 1978. Petrogenesis of Archean ultrabasic and basic volcanics: evidence from the rare elements. Contributions to Mineralogy and Petrology 65, 301–325.

Tepsell, J.H.M. 2018. Itä-Lapin komatiittien rikki-kupari isotoopit & geokronologia. (Sulphur-copper isotopes and geochronology of the komatiites of the eastern Lapland). Unpublished M.Sc. thesis. University of Helsinki. (In Finnish, English abstract).

Tukiainen, T. & Mattila, H. 1979. Geologinen kartoitus Ruuvaojan-Sotataipaleen-Kuttusvaarojen-Sorvortanjoen alueella 1978. Rautaruukki Oy, Report of Investigation RO 6/79. 27 p. (In Finnish)

Tulenheimo, T., 1999. Kuhmon Kellojärven kerroksellinen ultramafinen muodostuma. Unpublished M.Sc. Thesis, Department of Geology, University of Turku. 199 p.

Törmänen, T., Iljina, M., Heikura, P. & Salmirinne, H. 2007. Tutkimustyöselostus Savukosken kunnassa valtausalueilla Värriö 1-6 (Kaivosrekisterinumerot 7910/1-7910/6) suoritetuista tutkimuksista. Mineral exploration report M064712/2007/10/75, Geological Survey of Finland (GTK), Rovaniemi, Finland. 30 p. (In Finnish)

Törmänen, T., Iljina, M. & Heikura, P. 2009. Petrological characteristics of the ultramafic (komatiitic) formations in the Savukoski area. In: Mitrofanov, F., Iljina & M., Zhirov, D. (eds.). An Interreg-Tacis Project: Strategic Mineral Resources of Lapland - Base for the Sustainable Development of the north. Project Publication II, Apatity Russia, 65-70.

Törmänen, T., Konnunaho, J., Hanski, E., Moilanen, M. & Heikura, P. A. 2016. The Paleoproterozoic komatiite-hosted PGE mineralization at Lomalampi, Central Lapland Greenstone Belt, northern Finland. Mineralium deposita 51, 411-430.

Vartiainen, H 1980. The petrography, mineralogy and petrochemistry of the Sokli carbonatite massif, the northern Finland. Bulletin of the Geological Survey of Finland 313. 126 p.

Vartiainen, H. & Woolley, A. R. 1974: The age of the Sokli carbonatite, Finland, and some relationships of the north Atlantic alkaline igneous province. Bulletin of Geological Society of Finland 46, 81-91.

Vihreäpuu, U. 2001. Kaivoslain 19§:n mukainen tutkimustyöselostus Kettukangas 1 & 2. Outokumpu Oy reports, 080/4721/07/UMV/2001. 3 p. (In Finnish)

Viljoen, M.J. & Viljoen, R.P. 1969a. The geology and geochemistry of the Lower Ultramafic Unit of the Onverwacht Group and a proposed new class of igneous rocks. Geological Society of South Africa Special publication 2, 55–85.

Viljoen, M.J. & Viljoen, R.P. 1969b. Evidence for the existence of a mobile extrusive peridotite magma from the Komati Formation of the Onverwacht Group. Geological Society of South Africa Special Publication 2, 87–112.

Virransalo, P., 1985. Savukosken koilliosan kallioperän stratigrafia, rakenne & metamorfoosi, M.Sc. thesis, Arkeeisten alueiden malmiprojekti 24, University of Oulu, Department of Geology, 81 p. (In Finnish)

Vuollo, J. 1986. Värriojoen ultraemäksisen intruusion petrografia, mineralogia & geokemia. M.Sc. thesis, University of Oulu, Department of Geology, 110 p. (In Finnish)

Vuollo, J., Piirainen, T., & Huhma, H., 1992. Two Early Proterozoic tholeiitic diabase dyke swarms in the Koli-Kaltimo area, eastern Finland - their geological significance. Bulletin of the Geological Survey of Finland 363. 30p.

Vuotovesi, T. 1983a. Moreenin raskasmineraalitutkimus, Savukoski, Värriöjoki. Lapin Malmi Oy, report of investogation 060/4712/TV/83/3. 22p. (In Finnish)

Vuotovesi, T. 1983b. Kaivoslain 19 §:n mukainen tutkimustyöselostus valtausalueelta Kuttusvaara 1/kaiv.rek.no. 2865/1. Lapin Malmi Oy, Report of Investigation 080/4721/TV/83/6. 6 p. (In Finnish)

Vuotovesi, T. 1984. Kaivoslain 19 §:n mukainen tutkimustyöselostus valtausalueilta Värriöjoki l/kaiv.rek.no 2866/1, Värriöjoki S vs. kaiv.rek.no 3395/1. Report of Investigation 080/4712/TV/84/2, Lapin Malmi Oy. 8 p. (In Finnish)

Vuotovesi, T. 1985. Kaivoslain 19 §:n mukainen tutkimustyöselostus valtausalueelta Kiimavaara 1/kaiv.rek.no 3180/1. Report of Investigation 080/4714/TV/85/4, Lapin Malmi Oy. 13 p. (In Finnish)

Wager, L.R., Brown, G.M. & Wadsworth, W.J. 1960. Types of igneous cumulates. Journal of Petrology 1, 73-85.

APPENDIX 1

Thin section ID	Rock type	Subtarget	Laboratory
HMHO-2017-1.1	ol-serp-tre rock	Iskemävaara	TS lab, FRA
HMHO-2017-11.1	serp-tre-ol rock	Vuonnelo-oja	TS lab, FRA
HMHO-2017-13.1	ol-talc-serp-tre rock	Tulppionkaitavaara	TS lab, FRA
HMHO-2017-14.1	hb-plg rock	Tulppionkaitavaara	TS lab, FRA
HMHO-2017-17.1	ol-rock/dunite	Heiniselka	TS lab, FRA
HMHO-2017-20.1	ol-tre-chl rock	Jänesselkä	GTK lab
HMHO-2017-22.1	talc-tre-chl rock	Jänesselkä	GTK lab
HMHO-2017-24.1	chl-rock	Jänesselkä	GTK lab
HMHO-2017-38.2	ol-tre-chl rock	Venehaara	GTK lab
HMHO-2017-39.1	ol-adcumulate/dunite	Venehaara	TS lab, FRA
HMHO-2017-45.1	ol-tre rock	Moukavaara	TS lab, FRA
HMHO-2017-46.1	ol-serp-tre rock	Moukavaara	TS lab, FRA
HMHO-2018-12.2	ol-serp-tre rock	Kärkäsvaara	TS lab, FRA
HMHO-2018-14.1	serp-ol rock	Kärkäsvaara	TS lab, FRA
HMHO-2018-16.1	ol-tre-serp rock	Pultoselkä	TS lab, FRA
HMHO-2018-16.2	hb-plg-opx roxk	Pultoselkä	TS lab, FRA
HMHO-2018-17.1	ol-chl-tre rock	Sotajokilatvat	GTK lab
HMHO-2018-4.1	hb-plg-qt rock	Suurkovanselkä	TS lab, FRA
HMHO-2018-5.1	ol-adcumulate/dunite	Lakijänkä	TS lab, FRA
JHTE-2017-10.1	talc-tre-ol-serp rock	Sorvortanselka	TS lab, FRA
JHTE-2017-17.1	tre-chl rock	Juntterivaara	TS lab, FRA
JHTE-2017-18.1	ol-talc-serp rock	Juntterivaara	TS lab, FRA
JHTE-2017-25.1	ol-adcumulate/dunite	Venehaara	TS lab, FRA
JHTE-2017-25.2	ol-adcumulate/dunite	Venehaara	TS lab, FRA
JHTE-2017-28.1	chl-tre rock	Siriortsa	TS lab, FRA
JHTE-2017-35.2	hb-plg rock	Jänesselkä	GTK lab
JHTE-2017-36.1	chl-tre rock	Jänesselkä	GTK lab
JHTE-2017-8.1	talc-tre-serp rock	Sorvortanselka	TS lab, FRA
JHTE-2018-4.1	ol-serp rock	Siurujoki	TS lab, FRA
PS_vaara_1	tre-ol rock	Petäjä-Saijanvaara	TS lab, FRA
PSHA-2017-14.1	ol-tre-serp rock	Pirunkirkko	TS lab, FRA
PSHA-2017-15.1	ol-talc-serp-tre rock	Pirunkirkko	TS lab, FRA
PSHA-2017-16.1	tre-serp-ol rock	Pirunkirkko	TS lab, FRA
PSHA-2017-18.1	chl-tre rock	Jänesselkä	GTK lab
PSHA-2017-19.1	chl-serp-tre rock	Jänesselkä	GTK lab
PSHA-2017-2.1	hb-plg rock	Kontioselka-S	TS lab, FRA
PSHA-2017-20.1	tre-chl rock	Jänesselkä	GTK lab
PSHA-2017-24.2	chl-serp-tre rock	Jänesselkä	GTK lab
PSHA-2017-25.1	ol-chl-tre rock	Jänesselkä	GTK lab
PSHA-2017-26.1	ol-chl-tre rock	Jänesselkä	GTK lab

Thin section ID	Rock type	Subtarget	Laboratory
PSHA-2017-27.1	chl-tre schist	Jänesselkä	GTK lab
PSHA-2017-29.1	serpentinite	Sorvortanselka	TS lab, FRA
PSHA-2017-3.1	serp-tre-chl rock	Jänesselkä	GTK lab
PSHA-2017-32.1	tre-serp-ol rock	Torolehdontyvet	TS lab, FRA
PSHA-2017-32.2	serp-tre rock	Torolehdontyvet	TS lab, FRA
PSHA-2017-33.2	ol-serp-tre rock	Muotkaselka	TS lab, FRA
PSHA-2017-34.1	talc-chl-tre rock	Muotkaselkä	TS lab, FRA
PSHA-2017-36.1	ol-tre-serp rock	Auermavaara	TS lab, FRA
PSHA-2017-39.1	chl-plg-tre rock	Auermavaara	TS lab, FRA
PSHA-2017-40.1	ol-serp-chl-tre rock	Veneenvetojanka	TS lab, FRA
PSHA-2017-42.1	ol-serp-chl-tre-rock	Hannu Ollin vaara	TS lab, FRA
PSHA-2017-7.1	ol-rock/dunite	Iskemävaara	TS lab, FRA
PSHA-2018-11.2	tre-chl schist	Sotajokilatvat	GTK lab
PSHA-2018-12.1	tre-chl schist	Sotajokilatvat	GTK lab
PSHA-2018-5.1	tre-chl rock	Jänesselkä	GTK lab
PSHA-2018-7.1	tre-chl rock	Jänesselkä	GTK lab

APPENDIX 2

Sample ID	Field name	Location	176X	705P	705U	811L	308M
HMHO-2017-1.1	Tremolite rock	Iskemävaara	X	X		X	
HMHO-2017-13.1	Serpentinite	Tulppionkaitavaara	X	X		X	
HMHO-2017-14.1	Gabbro	Tulppionkaitavaara	X	X		X	
HMHO-2017-17.1	Serpentinite	Heiniselkä	X	X		X	X
HMHO-2017-18.1	Tremolite-chlorite rock	Heiniselkä	X	X		X	
HMHO-2017-20.1	Serpentinite	Jänesselkä	X	X		X	X
HMHO-2017-22.1	Tremolite-serpentine rock	Jänesselkä	X	X		X	
HMHO-2017-24.1	Melagabbro	Jänesselkä	X	X		X	
HMHO-2017-38.1	Ultramafic rock	Venehaara	X	X		X	X
HMHO-2017-39.1	Ultramafic rock	Venehaara	X	X		X	
HMHO-2017-44.1	Talc-serpentine schist	Moukavaara	X	X		X	
HMHO-2017-45.1	Ultramafic volcanic rock	Moukavaara	X	X		X	X
HMHO-2017-46.1	Serpentinite	Moukavaara	X	X		X	
JHTE-2017-10.1	Serpentinite	Sorvortanselkä	X	X		X	X
JHTE-2017-17.1	Chlorite-tremolite schist	Juntterivaara	X	X		X	
JHTE-2017-18.1	Serpentinite	Juntterivaara	X	X		X	X
JHTE-2017-24.1	Ultramafic rock	Venehaara	X	X		X	X
JHTE-2017-25.1	Ultramafic rock	Venehaara	X	X		X	
JHTE-2017-25.2	Ultramafic rock	Venehaara	X	X		X	
JHTE-2017-28.1	Tremolite-chlorite schist	Siriortsa	X	X		X	
JHTE-2017-35.2	Leucogabbro	Jänesselkä	X	X		X	X
JHTE-2017-36.1	Serpentinite	Jänesselkä	X	X		X	
JHTE-2017-7.1	Serpentinite	Sorvortanselkä	X	X		X	X
JHTE-2017-8.1	Serpentinite	Sorvortanselkä	X	X		X	
JHTE-2017-9.1	Serpentinite	Sorvortanselkä	X	X		X	
PSHA-2017-12.1	Amphibolite	Iskemävaara	X	X		X	
PSHA-2017-13.1	Tremolite rock	Iskemävaara	X	X		X	
PSHA-2017-14.1	Augite-olivine rock	Pirunkirkko	X	X		X	
PSHA-2017-15.1	Olivine rock	Pirunkirkko	X	X		X	X
PSHA-2017-16.1	Ultramafic rock	Pirunkirkko	X	X		X	
PSHA-2017-18.1	Amphibolite	Jänesselkä	X	X		X	
PSHA-2017-19.1	Tremolite-serpentine rock	Jänesselkä	X	X		X	

Sample ID	Field name	Location	176X	705P	705U	811L	308M
PSHA-2017-2.1	Komatiitic basalt	Kontioselkä	X	X		X	
PSHA-2017-20.1	Tremolite-serpentine rock	Jänesselkä	X	X		X	X
PSHA-2017-24.2	Serpentinite	Jänesselkä	X	X		X	
PSHA-2017-25.1	Serpentinite	Jänesselkä	X	X		X	
PSHA-2017-26.1	Serpentinite	Jänesselkä	X	X		X	X
PSHA-2017-27.1	Talc-chlorite schist	Jänesselkä	X	X		X	
PSHA-2017-29.1	Serpentinite	Jänesselkä	X	X		X	
PSHA-2017-3.1	Augite-olivine rock	Jänesselkä	X	X		X	X
PSHA-2017-32.1	Ultramafic rock	Torolehdontyvet	X	X		X	
PSHA-2017-32.2	Ultramafic rock	Torolehdontyvet	X	X		X	X
PSHA-2017-33.1	Tremolite rock	Muotkaselkä	X	X		X	
PSHA-2017-33.2	Serpentinite	Muotkaselkä	X	X		X	X
PSHA-2017-34.1	Tremolite rock	Muotkaselkä	X	X		X	
PSHA-2017-35.1	Serpentinite	Auermavaara	X	X		X	
PSHA-2017-36.1	Serpentinite	Auermavaara	X	X		X	X
PSHA-2017-39.1	Gabbro	Auermavaara	X	X		X	
PSHA-2017-40.1	Serpentinite	Veneenvetojänkä	X	X		X	X
PSHA-2017-42.1	Tremolite-serpentine rock	Hannu Ollin vaara	X	X		X	
PSHA-2017-7.1	Duniitti	Iskemävaara	X	X		X	
PSHA-2017-8.1	Serpentinite	Tahkomännikkö	X	X		X	
HMHO-2017-38.2	Ultramafic rock	Venehaara	X		X	X	X
HMHO-2018-12.2	Tremolite-serpentine rock	Kärkäsvaara	X		X	X	X
HMHO-2018-12.4	Tremolite-serpentine rock	Kärkäsvaara	X		X	X	
HMHO-2018-14.1	Tremolite rock	Kärkäsvaara	X		X	X	
HMHO-2018-15.1	Tremolite-serpentine rock	Pultoselkä	X		X	X	
HMHO-2018-16.1	Tremolite-serpentine rock	Pultoselkä	X		X	X	X
HMHO-2018-17.1	Ultramafic volcanic rock	Pultoselkä	X		X	X	
HMHO-2018-4.1	Gabbro	Suurkovanselkä	X		X	X	
HMHO-2018-5.1	Dunite	Lakijänkä	X		X	X	X
HMHO-2018-9.1	Talc-serpentine rock	Jänesselkä	X		X	X	
PSHA-2018-11.1	Serpentine-tremolite rock	Sotajokilatvat	X		X	X	X
PSHA-2018-11.2	Chlorite-tremolite rock	Sotajokilatvat	X		X	X	X
PSHA-2018-12.1	Serpentine-tremolite rock	Sotajokilatvat	X		X	X	

Sample ID	Field name	Location	176X	705P	705U	811L	308M
PSHA-2018-3.1	Serpentine-tremolite rock	Kärkäsvaara	X		X	X	
PSHA-2018-5.1	Melagabbro	Jänesselkä	X		X	X	X
PSHA-2018-6.1	Melagabbro	Jänesselkä	X		X	X	
PSHA-2018-7.1	Chlorite-tremolite schist	Jänesselkä	X		X	X	X
PSHA-2018-8.1	Chlorite-tremolite schist	Jänesselkä	X		X	X	